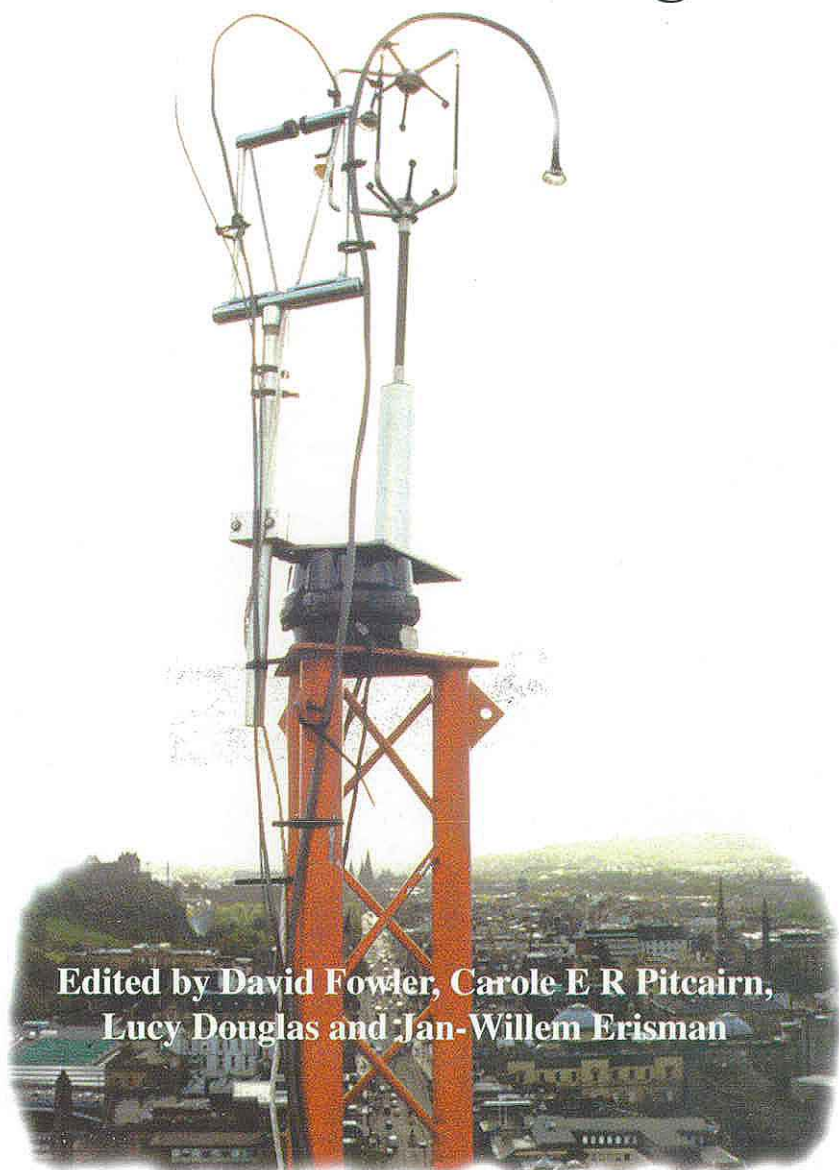


AIR-SURFACE EXCHANGE OF GASES AND PARTICLES:

Poster Proceedings



Edited by David Fowler, Carole E R Pitcairn,
Lucy Douglas and Jan-Willem Erisman

Poster papers from the Sixth International Conference on
Air-Surface Exchange of Gases and Particles,
Edinburgh 3-7 July 2000



Centre for
Ecology & Hydrology

NATURAL ENVIRONMENT RESEARCH COUNCIL

Copyright: Centre for Ecology and Hydrology, Edinburgh, 2001
Air-Surface Exchange of Gases and Particles – Poster Proceedings

ISBN: 1 870393 59 7

Published by:

Centre for Ecology and Hydrology, Edinburgh
Bush Estate
Penicuik
Midlothian
EH26 0QB
UK

Technical Enquiries to:

Professor David Fowler
Centre for Ecology and Hydrology, Edinburgh
Bush Estate
Penicuik
Midlothian
EH26 0QB
UK

Foreword

The Sixth International Conference on Air-Surface Exchange of Gases and Particles, held in Edinburgh in July 2000, brought together the 'pollutant deposition' science community, largely from Europe and North America, for the first time in a decade. With the rapid progress in instrumentation, models and methods, a substantial divergence in approach has developed during the 10 year gap and the discussions at the conference provided a valuable opportunity to compare experiences and results. This period was also a time of considerable change in emissions and deposition of sulphur, and to a lesser extent, nitrogen oxides. The underlying scientific understanding developed considerably during this period and many of the processes simplified in long-range transport models of the 1970s as a single fixed parameter have been shown to require models of their own to simulate the temporal and spatial variability. Such changes are entirely expected, and conferences of this type, which are focussed on a relatively narrow field, provide an excellent opportunity to review progress and identify the major gaps in understanding.

The conference provided a forum for presentation and discussion of 55 oral papers, which are published in the international literature as a special issue of the journal *Water, Air and Soil Pollution*. The informal sessions at the conference also provided ample discussion around the 28 poster presentations covering a broad range of gases and surface-atmosphere exchange processes. This proceedings brings together the poster papers from the conference in a single volume. As such, it provides a valuable reference volume for the delegates from the conference. The volume also provides contact details of the conference delegates.

David Fowler, Carole Pitcairn, Lucy Douglas and Jan-Willem Erisman

Centre for Ecology & Hydrology
Library Service
Monks Wood, Abbots Ripton
Huntingdon
Cambs PE28 2LS

9.08.33-50013

CENTRE FOR
ECOLOGY & HYDROLOGY
LIBRARY SERVICE

30 NOV 2001

OVERSIZE

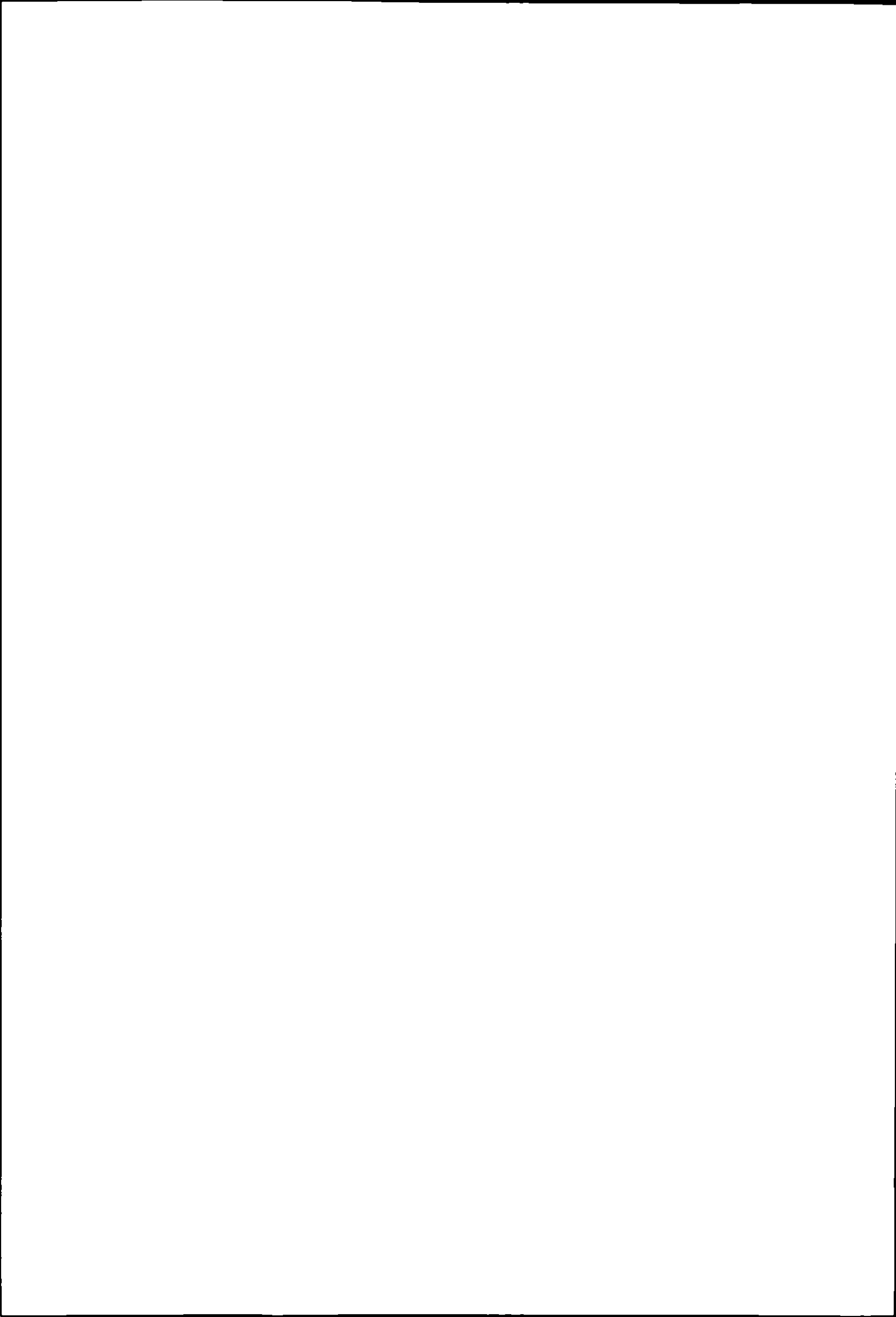
MO

614.71

Contents

Page No.

S.D. SARGENT, I.G. BOGOEV, AND B.D. TANNER Compact Sampling Systems for Measuring Atmospheric Trace Gas Profiles	
R.L. STORETON-WEST, D. FOWLER, I.D. LEITH, K.J. HARGREAVES & T.D. MURRAY Trends in Ozone, Sulphur Dioxide and Nitrogen Oxides at a Semi-Rural Site in South East Scotland	9
LEIMING ZHANG AND JEFFREY R. BROOK Estimation of site-specific dry deposition velocity from a regional model output considering sub-grid variations of land types	13
PAUL A. ROELLE, VINEY P. ANEJA AND JEFFREY PEIRCE Nitric Oxide Emissions from Soils Amended with Municipal-Waste Biosolids	18
J. S. WARLAND, G. DIAS, C. WAGNER-RIDDLE AND G. W. THURTELL Field Tests of a Micrometeorological System for Ammonia Flux Measurements Using TDL Technology	22
P. HOFSCHEUDER Modelling Short-Range Dispersion of Pollution	25
LÁSZLÓ HORVÁTH, JOSEPH PINTO AND TAMÁS WEIDINGER Estimate of the Dry Deposition of Atmospheric Nitrogen and Sulfur Species to Spruce Forest	31
S.C. PRYOR, R.J. BARTHELMIE, B. JENSEN, M.L. DAVIS, K.C. HIRZY, J.T. SCHOOF AND L.L. SØRENSEN Bidirectionality of Ammonia Fluxes: Observations over a Deciduous Forest	36
M.A. SUTTON, C. MILFORD, E. NEMITZ, M.R. THEOBALD, P.W. HILL, D. FOWLER, J.K. SCHJØRRING, M.E. MATTSSON, K.H. NIELSEN, J.W. ERISMAN, R. OTJES, A. HENSEN, J. MOSQUERA, P. CELLIER, B. LOUBET, M. DAVID, S. GENERMONT, A. NEFTEL, A. BLATTER, B. HERRMANN, S.K. JONES, L. HORVATH, T. WEIDINGER, R. MESZAROS, J. RASO, C., MANTZANAS K., KOUKOURA Z., M. GALLAGHER, M. FLYNN AND M. RIEDO Exchange of atmospheric ammonia with European grasslands	42
Y.S. TANG, U. DRAGOSITS, M.R. THEOBALD, D. FOWLER AND M.A. SUTTON Sub-grid variability in ammonia concentrations and dry deposition in an upland landscape	48
M. COYLE, D. FOWLER, R. STORETON-WEST Ozone deposition at a polluted site in the English Midlands	58



NURIA ALTIMIR Ozone flux monitoring by shoot chambers	61
J. PLAZA, J.M. FERNÁNDEZ, D. DE LA TORRE, A. GONZÁLEZ, B.S. GIMENO AND B. ARTIÑANO Ozone dry deposition measurements over wheat in Central Spain	65
THOMAS E. PIERCE, ELLEN J. KINNEE AND CHRISTOPHER D. GERON Development of a 1-km Vegetation Database for Modeling Biogenic Fluxes of Hydrocarbons and Nitric Oxide	72
J BECK, C AMMANN, U RUMMEL, F X MELXNER, M O ANDREAEE, G HELAS Aerosol Particle Flux Measurements over the Rainforest of Amazonia	76
F CHOUBEDAR, D BRANFORD, K J WESTON, D FOWLER, E NEMITZ AND K GOULDING Direct Measurements of the Long-Term Enhancement of Aerosol Deposition onto Woodland using a ²¹⁰ Pb Tracer Method	80
J.R. DORSEY, E.G. NEMITZ, M.W. GALLAGHER, K.N. BOWER, P.I. WILLIAMS AND D. FOWLER Eddy Correlation Measurements of Urban Aerosol Fluxes	84
LEONARD LEVIN, STEVE LINDBERG AND MAE SAXAUER GUSTIN Uncertainties in Mass Balance of US Atmospheric Mercury Emissions	87
G. SPINDLER, TH. GNAUK, H. HERRMANN, K. MÜLLER AND U. TEICHMANN Size Dependent Particle Concentration And Deposition Measurements With Filterpacks - A Five Year Study In Germany	93
I.D. LEITH, D. FOWLER, B. REYNOLDS, A.J. DORE, T.W. CHOULARTON, M. MOUSAVI, J.A.H. LOWE, D. NORRIS AND M. J. ROSSALL Validation Experiments for Wet Deposition Estimates at 5 km x 5 km in Complex Topography	99
C. WAGNER-RIDDLE, H. A. BROWN, G.W. THURTELL AND R. WENZEL N ₂ O Flux from a Solid Dairy Manure Pile Determined with a Micrometeorological Mass Balance Technique	103
ULRICH DAMMGEN AND CATHLEEN FRÜCHAUF Stochastic Properties of Micrometeorological Parameters	108
R.L. DESJARDINS, J.I. MACPHERSON, C.R. FLECHARD, E. PATTEY, T. ZHU, R. RIZNEK AND D. DOW Sharpening the Regional Picture of N ₂ O Emissions from Agricultural Land	113
C.R. FLECHARD, R.L. DESJARDINS, E. PATTEY, W.S. REID, A.S. DENNING, P.J. SELLERS AND J.A. BERRY CO ₂ Fluxes At Regional Scales From Profile Measurements Through The Convective Boundary Layer	116

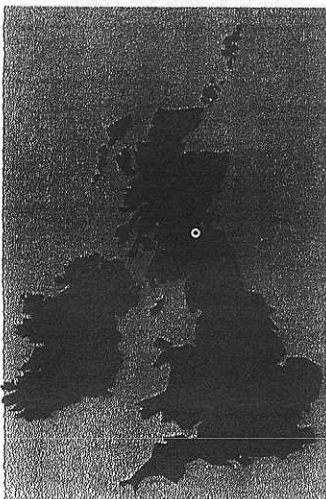
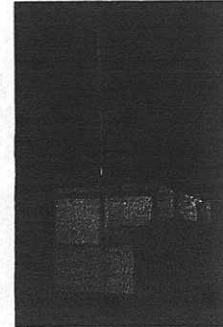


Trends in Ozone, Sulphur Dioxide and Nitrogen Oxides at a Semi-Rural Site in South East Scotland

R.L. STORETON-WEST, D. FOWLER, I.D. LEITH, K.J. HARGREAVES & T.D. MURRAY

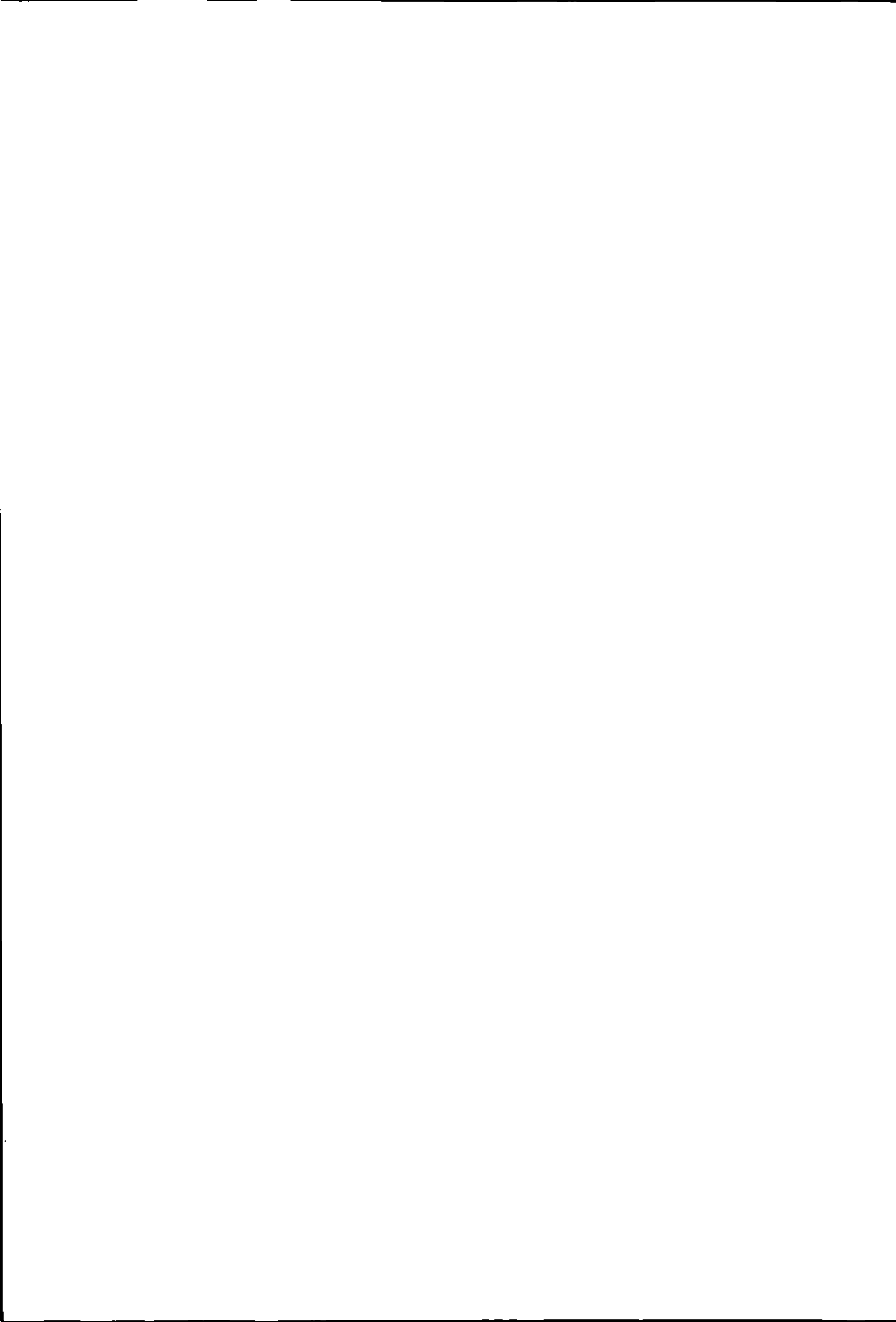
Centre for Ecology and Hydrology (Institute of Terrestrial Ecology), Edinburgh, Bush Estate, Penicuik, Midlothian, UK. EH26 0QB

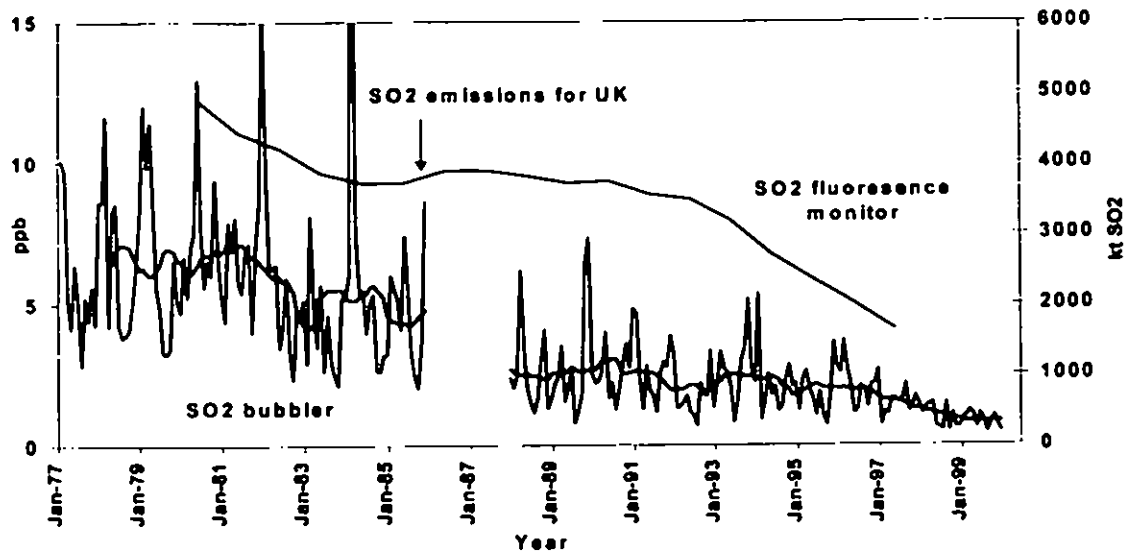
Continuous long-term measurements of ozone (O_3), nitric oxide (NO), nitrogen dioxide (NO_2), sulphur dioxide (SO_2) and meteorological parameters were made at a site in a semi-rural location at the foot of the Pentland Hills, 12 km south of the city of Edinburgh. The site is part of the UK National Air Quality Network. Twenty-one years of SO_2 data have been obtained. Ozone and nitrogen oxides (NO_x) have been measured since 1988.



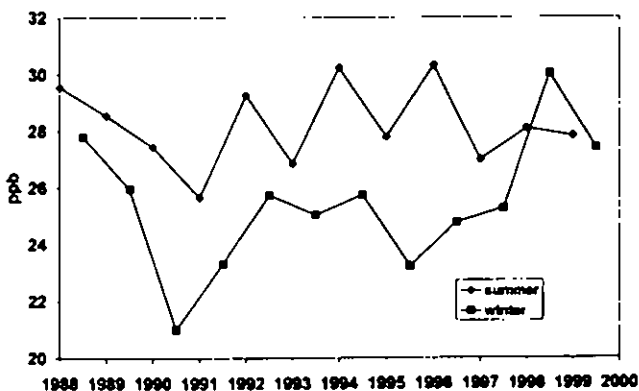
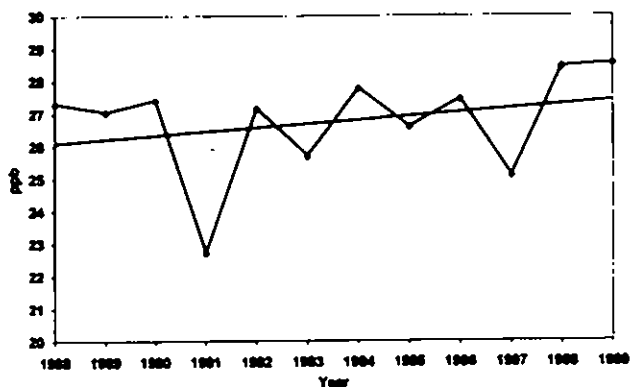
Reduction in sulphur dioxide (SO_2) concentrations 1977 to 1999 is mainly the result of a reduction in coal burning, flue gas desulphurisation of power stations and reduced sulphur in vehicle fuels. Total UK emissions have fallen from 4910 kt SO_2 in 1980 to 1656 kt SO_2 in 1997. Annual average SO_2 concentrations have fallen from 6 ppb in 1977 to less than 1 ppb by 1999. Peak values of SO_2 have also reduced as both local sources and continental long range transported air has become less polluted.





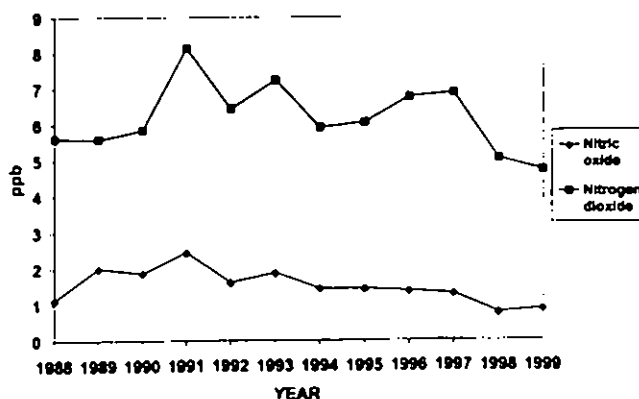


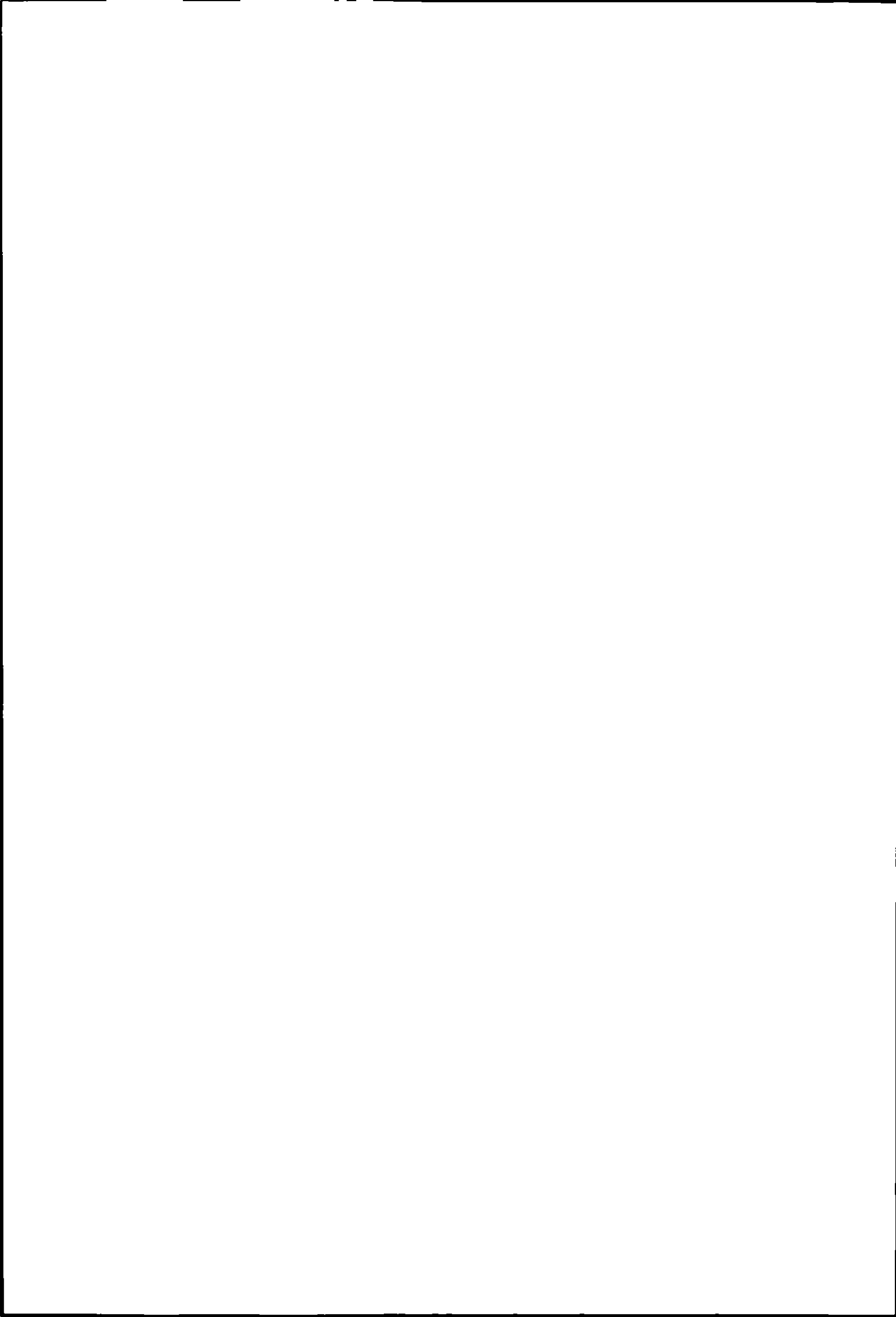
Annual average ozone concentrations show a very small upward trend but this is insignificant by comparison with the inter-year variation. The Bush Estate is in a semi-rural location such that the measurements are affected by the City of Edinburgh and other local sources. Nitric oxide from these local sources reduces annual mean ozone concentrations compared to more remote rural sites.

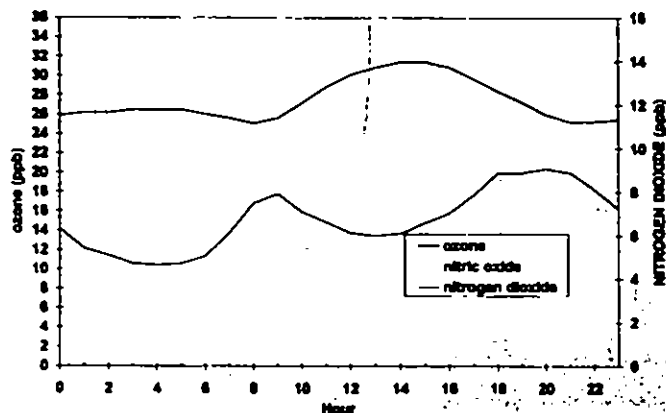


Mean summer ozone concentrations are higher than those observed in winter. Long day-lengths shift the photostationary state (assuming an absence of competing interconversion reactions) towards ozone production because NO_2 is photolysed to NO by sunlight with consequent regeneration of ozone.

Annual mean concentrations of nitric oxide and nitrogen dioxide peaked in the early 1990's (2.5 and 8.1 ppb respectively in 1991) before the introduction of catalysts on new petrol-engined vehicles during 1993. Concentrations of both species at Bush Estate are now at their lowest since measurements began with an annual mean in 1999 of 0.9 and 4.7 ppb respectively.

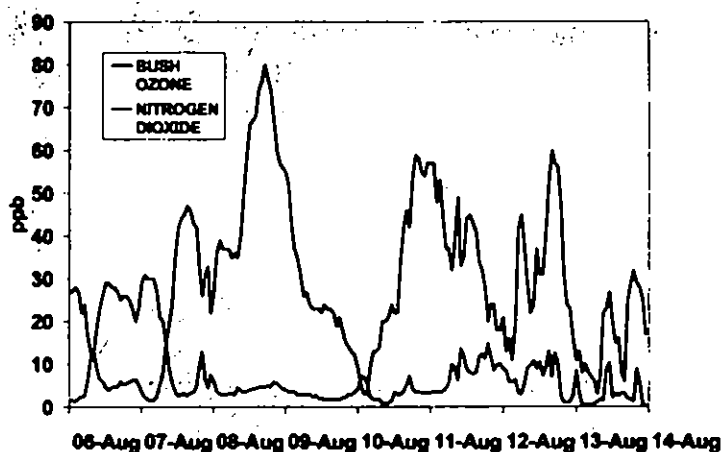




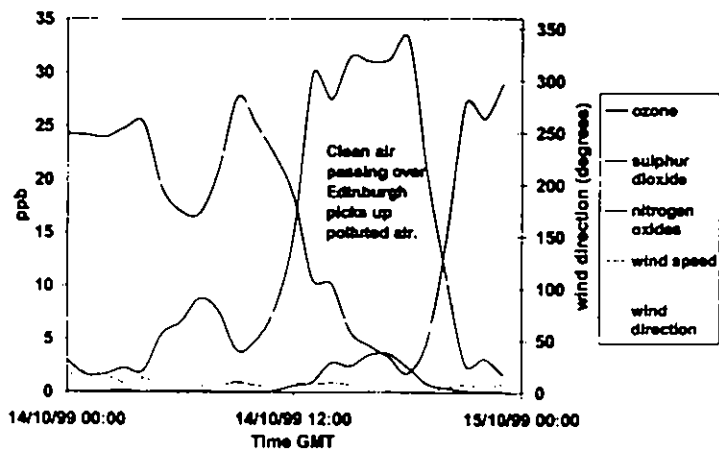


The annual mean diurnal cycle of ozone and nitrogen dioxide for 1996 shows a characteristic pattern. The morning "rush hour" is evident centred around 08:30 with the reduction in ozone due to the $\text{NO} + \text{O}_3$ reaction producing elevated concentrations of NO_2 . During the midday period, greater mixing of air during daylight hours enhances ozone concentrations before a rather more prolonged evening traffic peak when ozone is depleted again.

Ozone concentrations can be abnormally high in air originating from Europe and southern England. These peak concentrations occur in the summer months by the long-range transport of polluted air, trapped for several days under a high pressure system. August 1997 was the second hottest on record (since 1659) with higher than average sunshine figures.



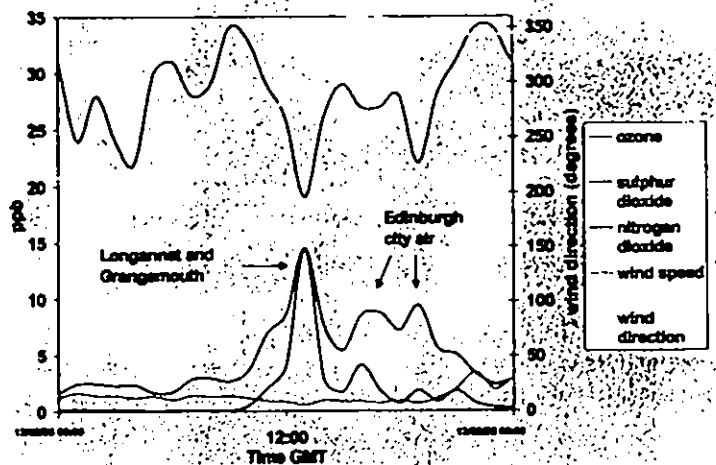
In the case shown, between 6 and 14 August 1997, high concentrations of ozone built up during the day under the influence of sunlight and photochemical production, despite rapid deposition to terrestrial surfaces. During the night, ozone was deposited to the ground as wind speed fell and a temperature inversion formed, separating air near the ground from the well-mixed air above.



A high pressure system centred over the British Isles on 14 October 1999 bringing clean arctic air down from the north over the city of Edinburgh and across the Bush Estate. Ozone concentrations, which are normally around 20 to 30 ppb dropped to below 5 ppb and NO_2 concentrations reached over 30 ppb. The plume from the city shows ozone is reacted with nitric oxide in the city to produce NO_2 .



Predominant south-west winds normally bring background (clean air) concentrations of pollutants over the measurement site. When the wind direction is in northerly directions plumes can be seen from local sources such as the Longannet coal fired power station, the Grangemouth oil refinery and the city of Edinburgh. Air from Longannet and Grangemouth refineries contains proportionally more sulphur dioxide than city air

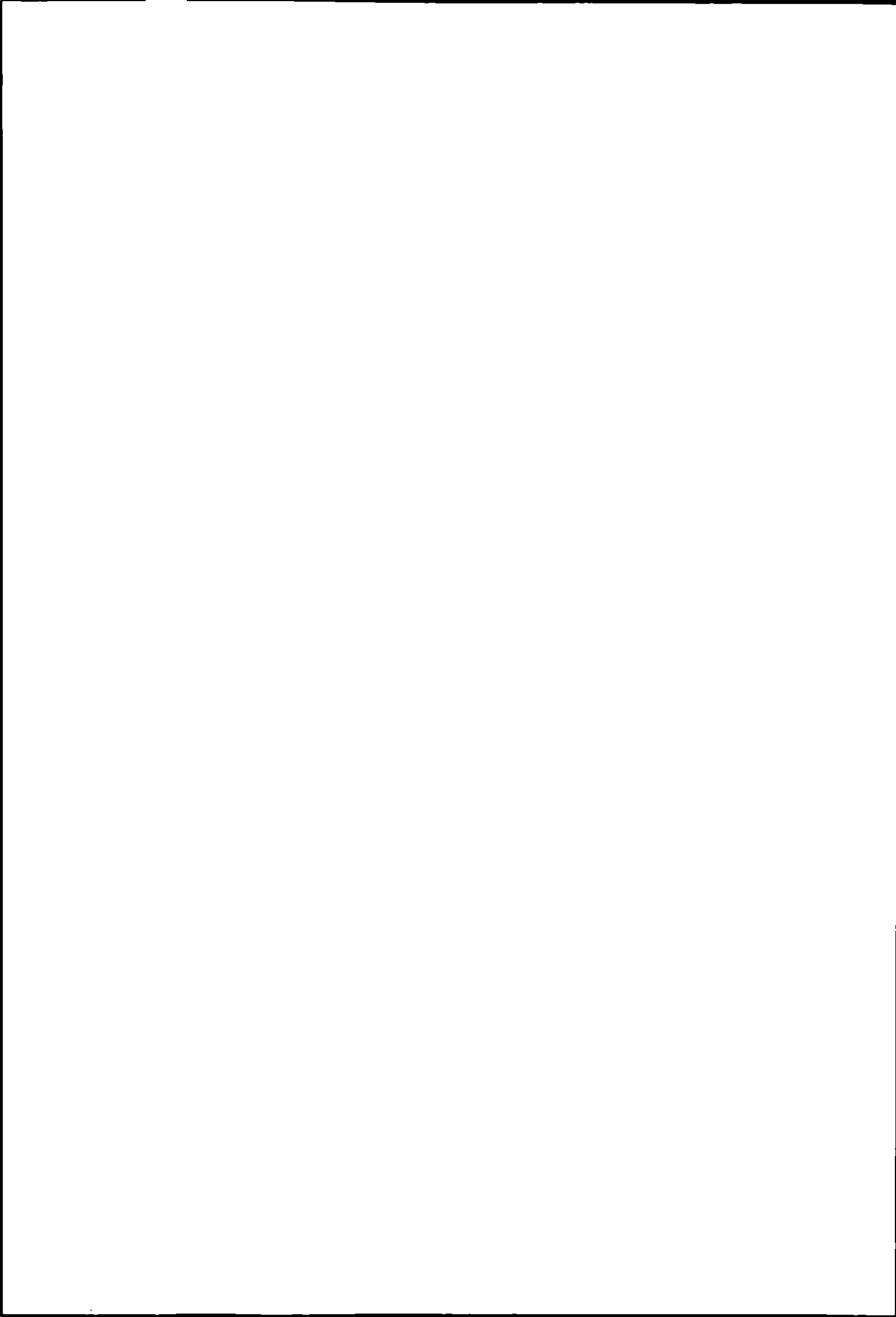


where the reduction in the sulphur content of automotive fuels has reduced concentrations in recent years.

Longannet power station emissions are presently the largest power station emissions in Scotland (48.8 kt a⁻¹ SO₂ and 19.2 kt a⁻¹ NO₂). Further reductions in sulphur dioxide emissions will be possible with the introduction of desulphurisation equipment scheduled for 2005. New limit values for sulphur content of petrol (150mg/kg) and diesel (350mg/kg) came into force on 1st January 2000 and these limits are to be further tightened in 2005 (50mg/kg for both petrol and diesel).

References

- State of the Environment Air Quality Report, Scottish Environment Protection Agency, June 2000
- Ozone in the United Kingdom, Fourth Report of the Photochemical Oxidants Review Group, 1997, Published by DETR, London
- The Co-operative Programme for Monitoring and Evaluation of the Long Range Transmission of Air Pollutants in Europe Website at www.emep.int/index.html



Estimation of site-specific dry deposition velocity from a regional model output considering sub-grid variations of land types

LEIMING ZHANG¹ AND JEFFREY R. BROOK²

¹ Rumble Research, 18 Plaisance Rd., Richmond Hill, Ontario, Canada L4C 5B5

² Meteorological Service of Canada, 4905 Dufferin St, Toronto, Ontario, Canada M3H 5T4

Abstract

A method for deriving the site-specific wind speed and friction velocity from regional model output is developed. The "subgrid velocity scale" is introduced to account for generation of turbulent fluxes by subgrid motions. The grid vector averaged wind speed is adjusted by adding the "subgrid velocity scale". The assumption of $u_* = \text{constant}$ is then applied within a model grid area to obtain wind speed for specific sites. Using this method, the site-specific wind speed and friction velocity can be estimated from grid averaged model output. In addition, more realistic air pollutant dry deposition velocities for specific locations can be calculated. Deposition velocities calculated using this approach can be 30% different (larger or smaller) for HNO_3 and sulphate and about 10% different for SO_2 and O_3 compared to values calculated by the more traditional method, which assumes a constant wind speed over the whole model grid area.

Introduction

Atmospheric models produce results for discrete grid points, which are the average conditions within a given volume, or horizontally, over a given area (i.e., grid boxes). A problem arises when model output is needed for specific locations near the surface because in reality there is heterogeneity within grid areas due to variations in surface characteristics. This problem is experienced when model results are to be compared to point measurements (e.g., model validation), when model estimates are required for a specific location (e.g., forecasting) and when surface interactions are to be estimated from model output. In this study, a method for estimating subgrid variations of wind speed, friction velocity is described. This method is adopted in RDM (Routine Deposition Model, Brook et al., 1999) to provide more realistic air pollutant dry deposition velocity (V_d) estimates at specific locations.

Methods

The spatial average of the local wind speed is usually larger than the spatially vector averaged wind speed, especially when spatially vector averaged wind speed is small and when different land or surface types exist within the spatial averaging area (Mahrt and Sun, 1995). For a grid area in a regional model domain, this relation can be expressed as: $|\mathbf{V}| < \sum V_i f_i$. \mathbf{V} is the model predicted grid-averaged wind vector, V_i is the wind vector for the sub-grid areas and f_i is the area fraction of the sub-grids. Figure 1 is an example of the wind flow produced from MC2 (Mesoscale Compressible Community model, Benoit et al., 1997) with a 3km x 3 km horizontal resolution for an area equivalent to one coarse grid area of MC2 with 35km x 35 km horizontal resolution. Note the subgrid converging flow pattern. Consequently, the wind vector for this particular coarse grid area determined by MC2 is under 1 m s^{-1} . In contrast, Figure 2 shows that the wind speeds at many subgrid (fine grid) locations, as determined by MC2 for the same time, are around 2-3.5 m s^{-1} . This demonstrates the difference between the spatially averaged wind vector (\mathbf{V}) and the spatial



average of the local time-averaged speed (u_{la}). Figure 2 compares the modelled surface momentum flux values for one selected coarse grid ($35 \times 35 \text{ km}^2$) to the corresponding averaged subgrid values (around 136 subgrids of $3 \times 3 \text{ km}^2$). The momentum fluxes averaged from subgrids are systematically greater than that from the coarse grid, which suggests that grid squares with more than one land type may have a subgrid velocity that cannot be neglected. Based upon the nested grid MC2 calculations it is clear that subgrid fluxes exist and are usually positive. The relative importance of the subgrid flux is greater when the grid-average fluxes are small. In many cases the subgrid fluxes were more than 50% larger than the grid-averaged fluxes.

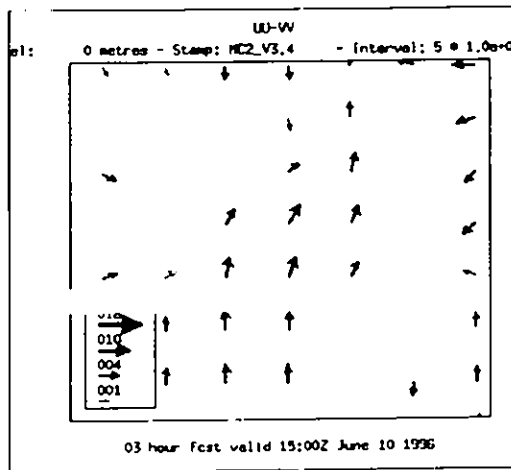


Figure 1. Example of converging flow from MC2 output with $3 \times 3 \text{ km}$ resolution covering one coarse grid of $35 \times 35 \text{ km}$

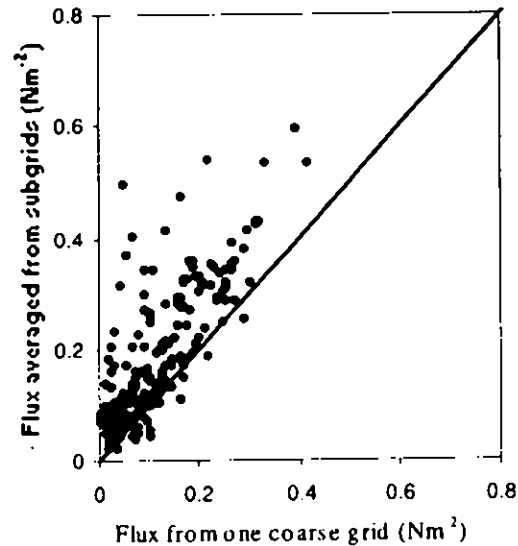


Figure 2. Comparison of momentum fluxes from one $35 \times 35 \text{ km}$ grid and averaged fluxes from nested $3 \times 3 \text{ km}$ grids. An example of converging flow from MC2 3 km run

To address this problem, the "subgrid velocity scale" was introduced to account for generation of turbulent fluxes by subgrid motions. Based on Mahrt and Sun (1995), the "subgrid velocity scale" is parameterized as:

$$V_{sg}(\Delta T, |V|, \Delta x) = C_0 \exp\left(-\frac{|V|}{V_{crit}}\right) \left(\frac{g}{T_0} \Delta T \Delta x\right)^{\frac{1}{2}} + C_1 \left(\frac{\Delta x}{5} - 1\right)^{\frac{1}{2}}$$

where ΔT is the variability of surface temperature within the grid, Δx is the grid size, T_0 is the grid-averaged temperature, g is the acceleration of gravity, V_{crit} is an empirical constant representing the critical wind speed, below which the subgrid wind speed becomes important, and C_0 and C_1 are empirical constants. To study the "sub-grid velocity scale" in more detail using the MC2 output, all coarse grids were sorted into 3 categories. Category I represents grids with only one land type defined in RDM. Category II corresponds to grids with more than one land type, but without a water surface. Category III contains grids with more than one land type with at least one of them being a water surface. Examinations of temperature from MC2 results, ΔT is given 0.5, 3 and 8°C for category I, II and III, respectively. Based on the discussion in Mahrt and Sun (1995) and the ΔT data from MC2, the first term on the right hand side of the above equation should have a strong influence on V_{sg} in grid squares belonging to categories II and III and the second term is important to V_{sg} in all grid types. Based on ΔT data and the available V values from MC2 for the coarse grid and subgrids,



separate best-fit estimates for C_0 , C_1 and V_{crit} were derived for each grid category. The resulting values were $V_{crit}=4 \text{ m s}^{-1}$ and $C_0=0.01$ for all three grid categories, and $C_1=0, 0.01$ and 0.02 for Grid category I, II and III, respectively. The "subgrid velocity scale" is added to the model predicted wind speed $|V|$ to get the spatial average of local wind speed u_{la} ($u_{la}=|V|+V_{sg}$). The friction velocity corresponding to u_{la} is calculated as $u_{*la}=u_* \cdot u_{la}/|V|$.

Figure 3 compares the fluxes for the same grid shown in Figure 2, but with coarse grid fluxes replaced by using revised friction velocity, u_{*la} . It is seen that the modified fluxes agree better with averaged subgrid fluxes compared to the original results in Figure 2. The tendency to underestimate fluxes is reduced considerably.

The other concern is that wind speed for different land types with different roughness length existing within one model grid area may be different. To solve this problem, Walcek et al. (1986) assumed that the product of wind speed and friction velocity is approximately constant ($u_i u_{*i} = \text{constant}$) among varying surfaces, or land-use types, i , within a model grid. This assumption is based upon the common observations that wind speed is usually smaller over rougher surfaces and larger over smoother surfaces within an averaging area (a model grid here). Walcek et al. (1986) demonstrated that using this assumption was better in estimating V_d than assuming a constant wind speed within one model grid. The same approach is used here, but the model predicted $|V|$ and u_* are replaced by u_{la} and u_{*la} , yielding $u_i u_{*i} = u_{la} u_{*la}$. Using this relation and the above equations, wind speed and friction velocity for each individual land type existing within one grid are solved.

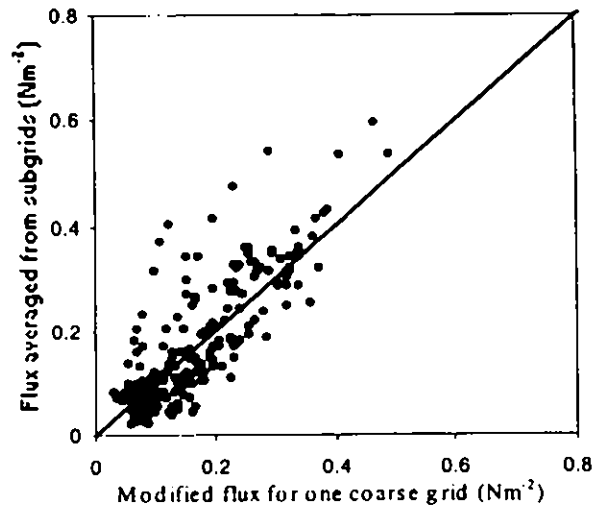


Figure 3, same as Figure 2 except using revised u_{*la} to replace u_* for the coarse grid

Comparison of dry deposition velocities using two different methods

Within the context of the RDM, the main application for the modified method is to determine more realistic V_d values at specific sites where concentrations are available. Monthly average V_d values using this approach were calculated for two CAPMoN sites, Egbert and Algoma, which are located in southern and northern Ontario, respectively. These values are compared to results obtained using the old method, which assumes a constant wind speed over the whole model grid area. In addition to site-specific u_i and u_{*i} values, temperature (T) and humidity (RH) representative of the site conditions were also needed. However these values were not available and instead, the grid-averaged values (i.e., model output) of T and RH were used. V_d values were computed using land type information pertaining to an area within 1 km of the sites and GEM (Global Environmental Multiscale model, Cote et al., 1998) output. Agricultural land occupies 75% of the area surrounding Egbert and the remaining area is covered with broadleaf trees. In contrast, within the 35 km GEM grid that includes Egbert there is 30% broadleaf trees, 56% agricultural land and 14% other land types. For Algoma, 100% of the area within a 1 km radius is mixed forest and in the corresponding GEM grid there is 67% mixed forest, 27% water area and a small area of other surface types.



Figure 4 shows that compared to the old method the monthly averaged V_d values from modified method are smaller for Egbert and larger for Algoma. This can be explained by the differences in the land types within the local area and within the 35km x 35 km GEM grid covering the site. At Algoma for example, there is a significant amount of water surfaces within the 35 km grid area, which usually leads to a large subgrid wind speed. This likely explains the larger V_d values from the modified method. As shown above, the differences in V_d between the two methods were relatively small for SO_2 and O_3 (~10%) and noticeably larger for HNO_3 and sulphate (~30%). For both examples shown in Figure 4 (i.e., Egbert and Algoma), the dominant land type in the smaller (1 km radius) and larger (35 km grid) areas are the same. For sites where the land types for its 1 km circular area differs from the dominant land type within the corresponding GEM model grid area, the change in V_d when the modified method is applied is likely to be larger. This is because that if the land type of a site is different from the dominant land type of the corresponding model grid, the wind speed at the site calculated from the assumption of $u, u_* = \text{constant}$ can deviate significantly from the grid-averaged value $|V|$.

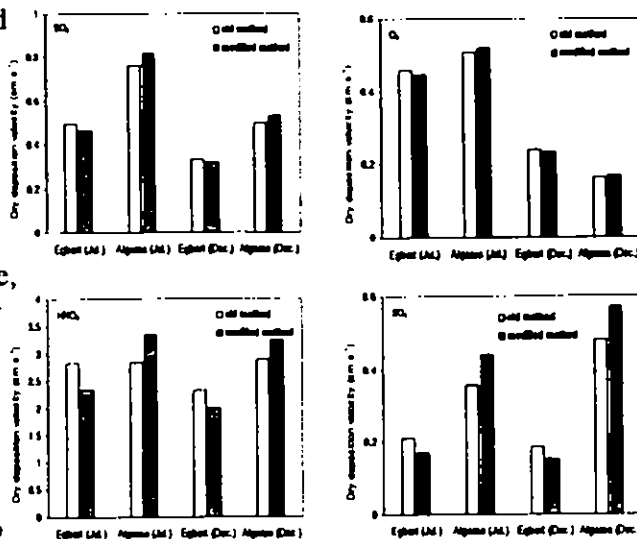


Figure 4, Monthly averaged V_d for July and December 1998 for two sites using modified and old method

Conclusions

The subgrid velocity scale is important for grids having land types with different roughness length and surface temperature. The larger the grid size and the weaker the grid averaged wind speed, the more important the subgrid velocity scale becomes. For specific sites where the surrounding land type differs from the dominant land type within the corresponding model grid, the change in V_d resulting from the modified method can be relatively large compared to the simple assumption of constant $|V|$ in the grid.

The assumption of $u, u_* = \text{constant}$ may need to be revised by including the stability and plane boundary height. Method on how to estimate the temperature and humidity variation within one model grid is needed. More information on the appropriate values for the empirical constants versus different types of grids would also be valuable.

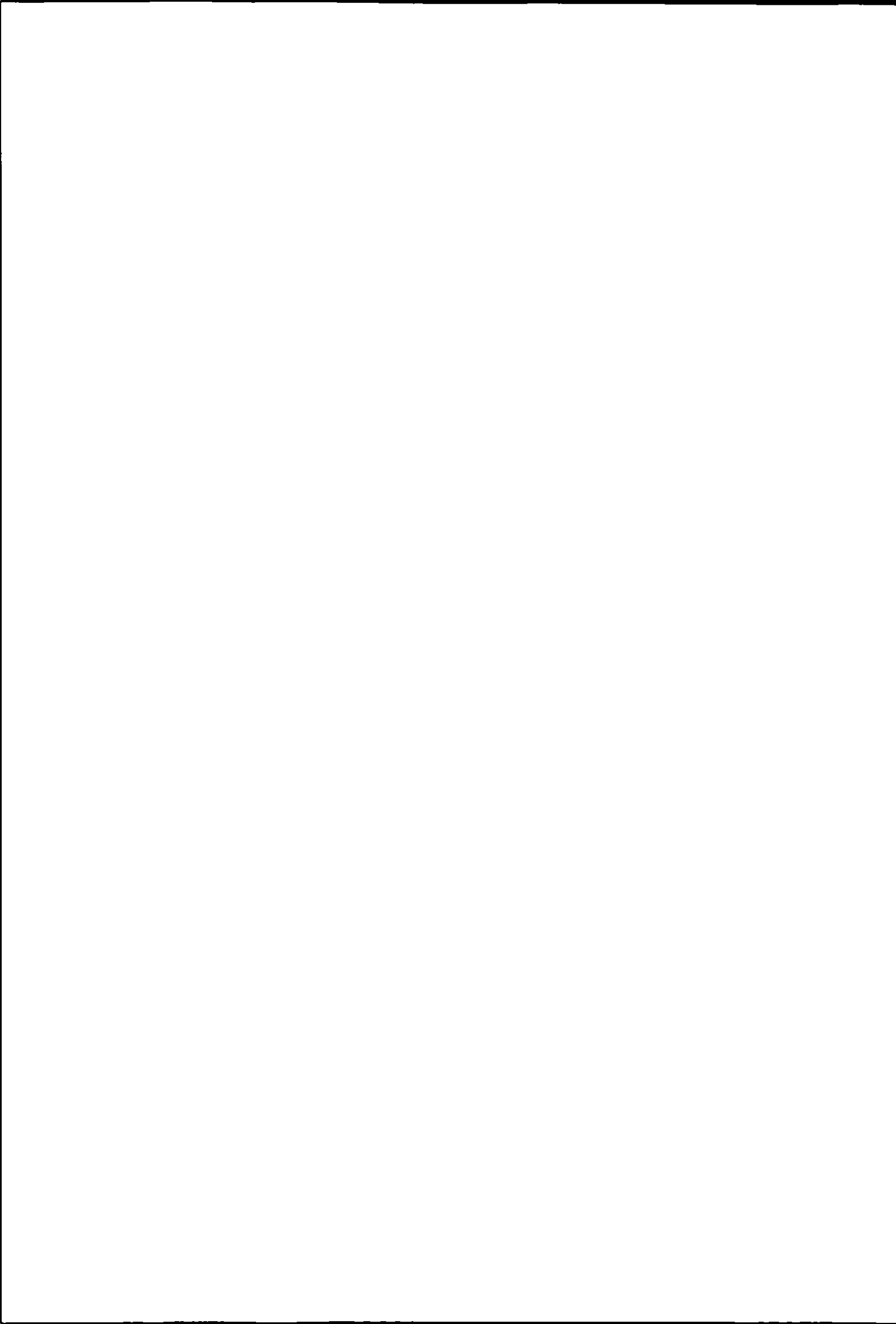
Acknowledgements

The authors greatly appreciate the MERMOZ group for providing MC2 data, Dr. J. Pudykiewicz for some initial ideas on this subject and comments from Drs. Jacob Padro and Jianmin Ma.



References

- Benoit R., Desgagne M., Pellerin P., Pellerin S., Chartier Y. and Desjardins S. (1997) *Mon. Wea. Rev.*, **125**, 2382-2415.
- Brook J., Zhang L., Digiovanni F. and Padro J. (1999) *Atmos. Environ.* **33**, 5037-5051.
- Cote J., Desmarais J. G., Gravel S., Methot A., Patoine A., Roch M. and Staniforth A. (1998a) *Mon. Wea. Rev.*, **126**, 1373-1395.
- Mahrt L. and Sun J. (1995) *Mon. Wea. Rev.*, **123**, 3032-3401.
- Walcek C. J., Brost R., A. and Chang J. S. (1986) *Atmos. Environ.* **20**, 949-964.



Nitric Oxide Emissions from Soils Amended with Municipal-Waste Biosolids

PAUL A. ROELLE*¹, VINEY P. ANEJA¹ AND JEFFREY PEIRCE²

¹*Department of Marine, Earth and Atmospheric Sciences, North Carolina State University, Raleigh, NC 27695-8208, USA*

**Corresponding Author: Telephone Number: 919.515.3690, Fax Number: 919.515.7802, e-mail: paroelle@unity.ncsu.edu*

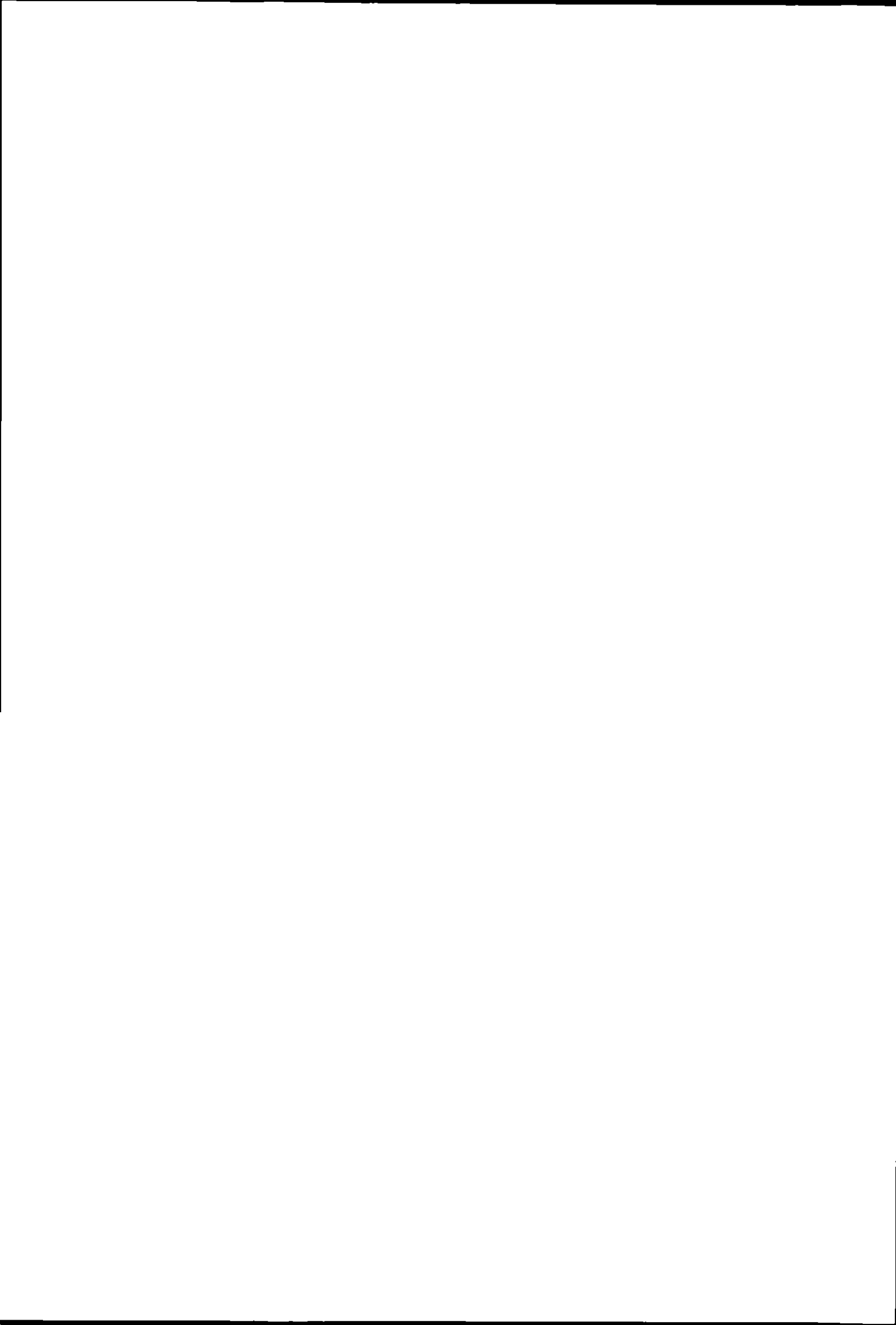
²*Department of Civil and Environmental Engineering, Duke University, Durham, NC 27708-0287, USA*

Abstract

Land spreading nitrogen-rich municipal waste biosolids (NO_3^- -N < 256 mg-N/kg dry weight, NH_3 -N ~23,080 mg-N/kg dry weight, Total Kjeldahl N ~ 41,700 mg-N/kg dry weight, to human food and non-food chain land is a practice followed throughout the US. This practice may lead to the recovery and utilization of the nitrogen by vegetation, but it may also lead to emissions of biogenic nitric oxide (NO), which may enhance ozone pollution in the lower levels of the troposphere. Recent global estimates of biogenic NO emissions from soils are cited in the literature, which are based on field measurements of NO emission from various agricultural and non-agricultural fields. However, biogenic emissions of NO from soils amended with biosolids are lacking. Utilizing a state-of-the-art mobile laboratory and a dynamic flow-through chamber system, in-situ concentrations of nitric oxide (NO) were measured during the Summer/Fall of 1999 and Winter/Spring of 2000 from an agricultural soil which is routinely amended with municipal waste biosolids. The average NO flux for the entire time period prior to a biosolids application (9 June 1999- 3 September 1999) was $57.8 \pm 34.6 \text{ ng NO-N m}^{-2} \text{ s}^{-1}$. Biosolids were applied during September 1999 and the field site was sampled again during Winter 2000 (28 February - 9 March 2000), during which the average flux was $3.6 \pm 3.9 \text{ ng NO-N m}^{-2} \text{ s}^{-1}$. Field experiments were conducted which indicated that the application of biosolids increase the emissions of NO. Soil temperature and % Water Filled Pore Space (%WFPS) were observed to be significant variables for predicting NO emissions, however %WFPS was found to be most significant during high soil temperature conditions. In the range of pH values found at this site (5.8 ± 0.3), pH was not observed to be a significant parameter in predicting NO emissions.

Introduction

NO plays an important role in tropospheric photochemistry. Increasing NO emissions, in the presence of hydrocarbons and sunlight, are thought to be the cause of increased regional levels of tropospheric ozone and other photochemical oxidants [Logan, 1983]. Yienger and Levy [1995] developed an empirically based model to estimate soil NO_x emissions on a global scale. They have reported that anthropogenic land use is having a significant impact on global soil NO_x emissions and that soil emissions can account for up to 75% of the total NO_x budget depending on location and time of year.



Methods and Materials

Dynamic Flow-Through Chamber and Flux Calculation

A dynamic flow-through, as described by *Roelle et al.*, 1999, was used to measure NO concentrations emitted from the soil. Zero grade air, which is used as a carrier gas, is passed through the chamber at a constant flow rate (approximately 5 lpm), via a flow controller located on top of the chamber (Gilmont Shielded Industrial Flowmeter, Accuracy $\pm 5\%$). The NO fluxes were calculated from the following mass balance equation:

$$\frac{dC}{dt} = \left(\frac{q[C_{air}]}{V} + \frac{JA}{V} \right) - \left(\frac{LA'}{V} + \frac{q}{V} \right) [C] - R \quad (1)$$

where J = emission flux per unit area; L = loss term by chamber wall per unit area assumed first order in [NO]; q = flow rate through the chamber; V = volume of the chamber; C = NO concentration in the chamber; C_{air} = NO concentration in the ambient air immediately adjacent to the chamber (the inlet of the chamber); R = chemical production/destruction rate in the chamber; A = surface area covered by the chamber; A' = surface area of the chamber walls. The total loss in the chamber was estimated to be 0.02 ± 0.007 cm second⁻¹ from the average of 5 experiments conducted at different times throughout the measurement period [*Kaplan et al.*, 1988; *Roelle et al.*, 1999]. This value of (L') ($=0.02$ cm second⁻¹) agrees with that found by *Kim et al.*, [1994].

Results

Soil Temperature and Soil Water Content

The relationship between emissions of NO and soil temperature is confounded by the dependence of NO emissions on soil moisture content. Researchers have found that nitrification is optimized for moisture contents between 30 and 65% WFPS [*Davidson et al.*, 1986; *Linn and Doran*, 1984; *Parton et al.*, 1988]. Recent laboratory experiments conducted by *Ormechi et al.*, [1999] found that this range for maximum NO emissions occurred between 20-45%.

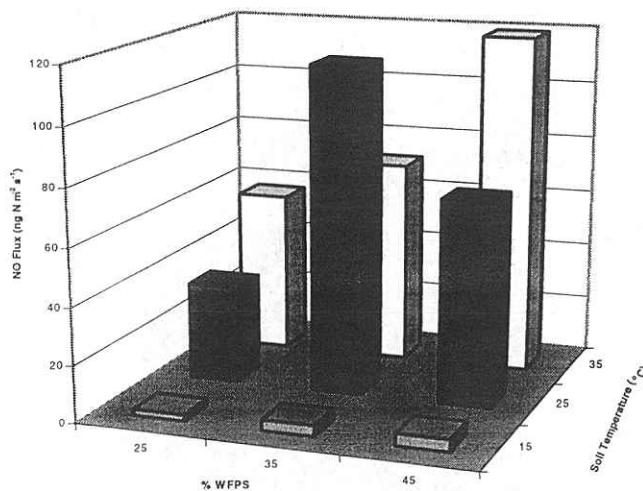
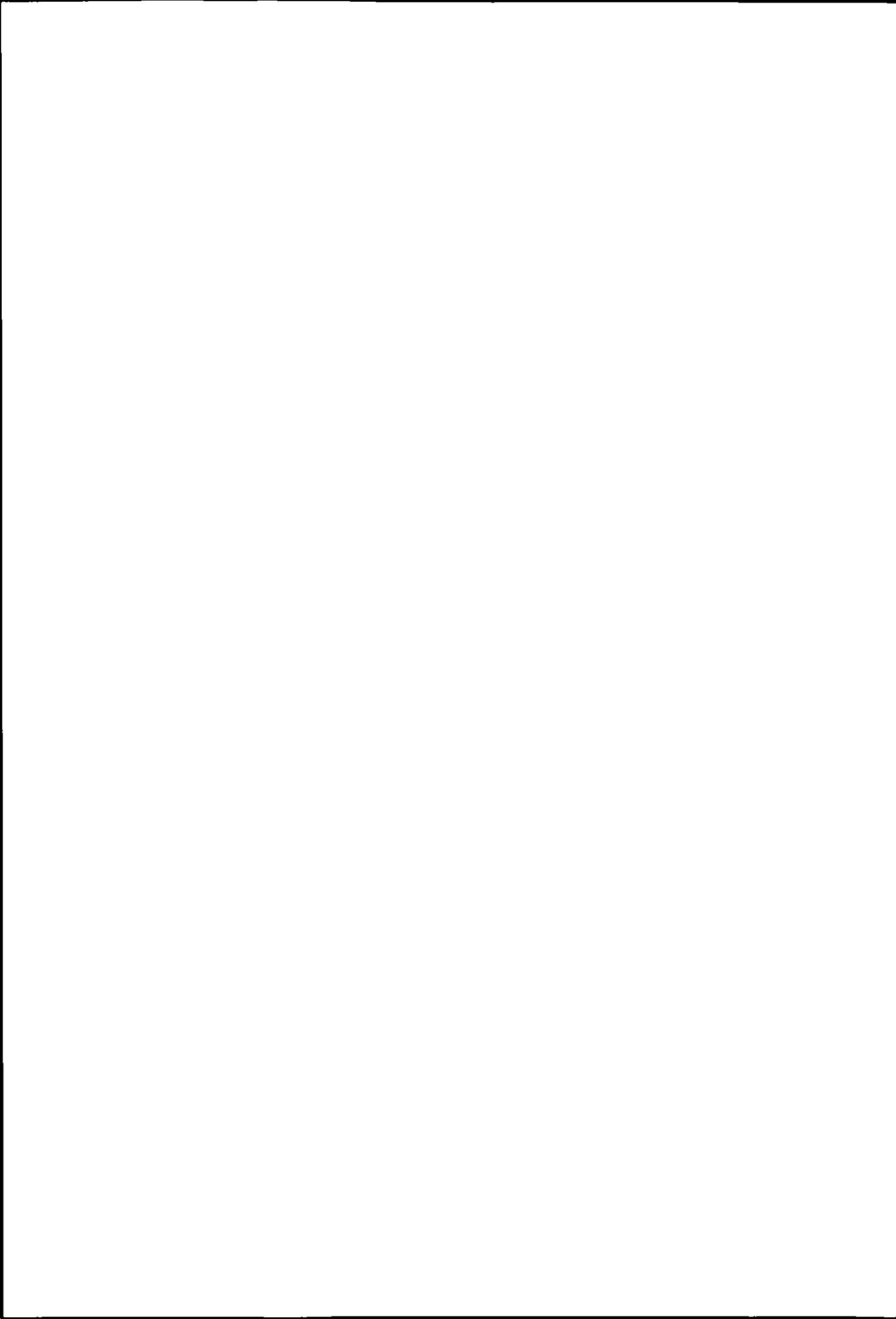


Figure 1. NO flux plotted versus % Water Filled Pore Space (WFPS) and Soil Temperature. %WFPS data have been binned into values of 25, 35 and 45, while soil temperature data have been binned into values of 15, 25 and 35 $^{\circ}\text{C}$.



In Figure 1, the data is binned into values of % WFPS of 25, 35 and 45 and soil temperatures of 15, 25, 35. NO flux follows a general trend of increasing emissions as % WFPS increases within a given soil temperature. Likewise, within a given % WFPS, NO emissions increase as soil temperatures increase. The highest average NO flux occurred at 45% WFPS and 35 °C soil temperature ($119.3 \text{ ng N m}^{-2} \text{ s}^{-1}$), which is expected when considering the temperature dependence alone. However, relatively equivalent the NO flux values occurring at 35% WFPS and 25 °C ($114.3 \text{ ng N m}^{-2} \text{ s}^{-1}$) seems to indicate that these conditions may also be an optimum condition for maximum NO production from this biosolid amended field site.

Conclusions

NO emissions from fields amended with biosolids were studied during Summer 1999 and Winter 2000, in order to examine how NO emissions might be affected by biosolid applications. Soil temperature ($R^2 = 0.89$) and %WFPS were both found to be significant parameters for predicting NO emissions, however %WFPS was only significant during high ($T=35 \text{ °C}$; $R^2=0.46$) and low ($T=15 \text{ °C}$; $R^2=.21$) soil temperatures. The average NO emissions from this small grain field were a factor of 22 higher than what the EPA's currently used biogenic emissions model would predict for similar field conditions.

In North Carolina, approximately 1.44 million dry tons of biosolids are applied to 42,000 acres annually [NCDENR, 1999]. This practice serves as an economical means to dispose of the biosolids while saving farmers the expense of purchasing chemically-derived fertilizers. In North Carolina, biosolid amended soils are applied in localized areas and represent a small fraction of total crop land soils (<1%), and therefore will likely represent only a small fraction of the total biogenic NO budget. However, these biosolid amended soils may act as significant sources of localized O₃ production, especially during the hot and stagnant periods of the summer when biogenic NO emissions and photochemical activity are at a maximum. Therefore future work should consist of a modeling study to examine the localized effects biosolid amended soils has on O₃ production.

Acknowledgements

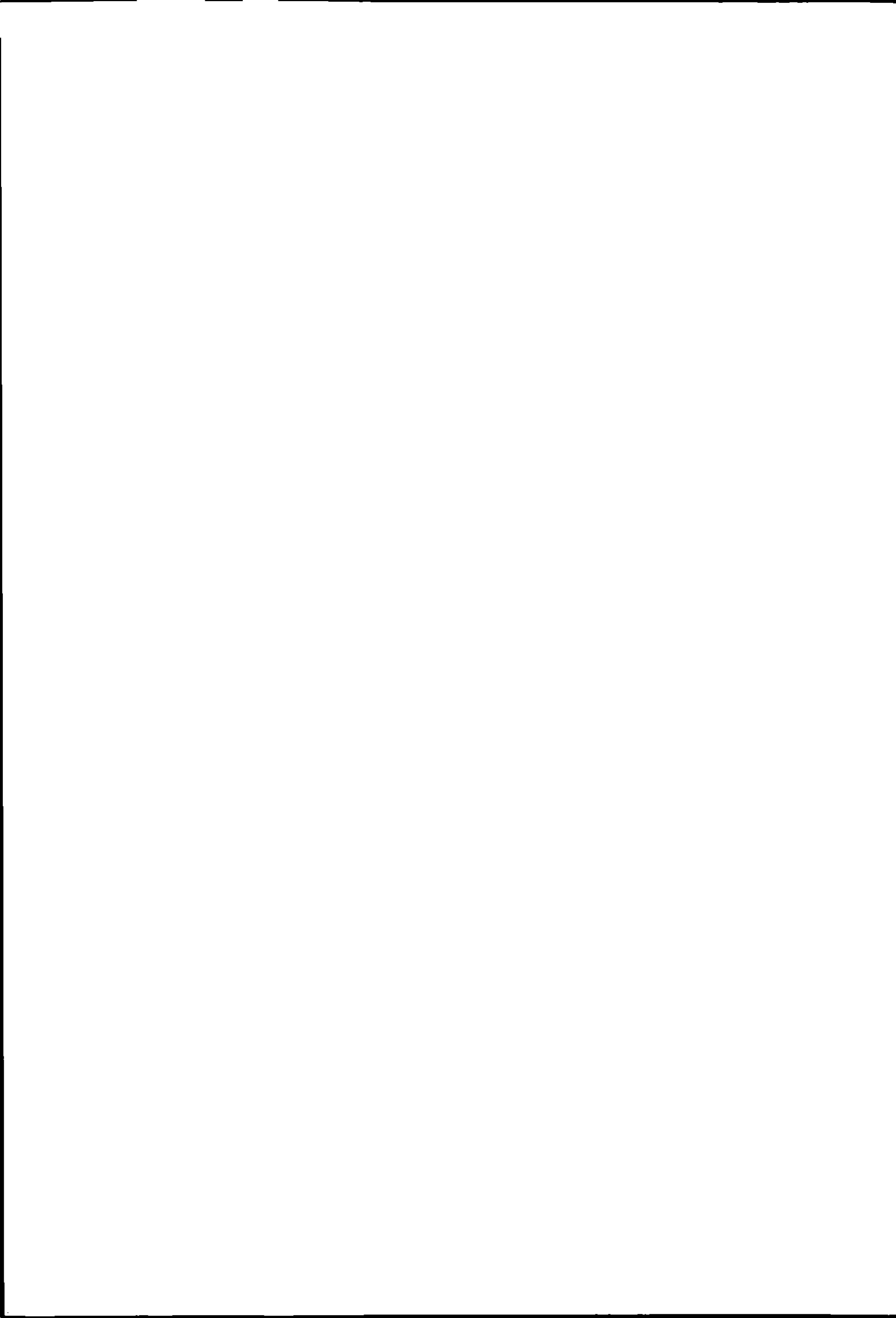
This research was funded by the National Science Foundation Grant (atm-9420610) and the National Science Foundation Grant (99-sc-nsf-1019) via Duke University. We sincerely acknowledge members of the North Carolina State University Air Quality Research Group for the technical discussions and review of the manuscript and R. Tabachow of Duke University for assistance with site preparation and selected calculations. Financial support does not constitute an endorsement of the views expressed in the article/report, nor does mention of trade names of commercial or noncommercial products constitute endorsement or recommendation for use.

References

- Davidson, E.A., and Swank, W.T.: 1986, 'Environmental parameters regulating gaseous-N losses from two forested ecosystems via nitrification and denitrification', *Appli. Environ. Microbiol.* **52**, 1287-1292.



- Kaplan, W.A., Wofsy, S.C., Keller, M. and Costa, J.M.D.: 1988, 'Emission of NO and deposition of O₃ in a tropical forest system', *J. Geophys. Res.* **93**, 1389-1395.
- Kim D.-S., Aneja, V.P. and Robarge, W.P.: 1994, 'Characterization of nitrogen oxide fluxes from soil of a fallow field in the central piedmont of North Carolina', *Atmos. Environ.* **28**, 1129-1137.
- Linn, D.M. and Doran, J.W.: 1984, 'Effect of water-filled pore space on carbon dioxide and nitrous oxide production in tilled and nontilled soils', *Soil Sci. Soc. Am. J.* **48**, 1267-1272.
- Logan J.A.: 1983, 'Nitrogen oxides in the troposphere; Global and regional budgets', *J. Geophys. Res.* **88**, 10785-10807.
- North Carolina Department of Environment and Natural Resources, Division of Water Quality, Non-Discharge Compliance/Enforcement Unit, Annual Report, 1999.
- Ormeci, B, Sanin, S.L. and Peirce, J.J.: 1999, 'Laboratory study of NO flux from agricultural soil: Effects of soil moisture, pH, and temperature', *J. Geophys. Res.* **104**, 1621-1629.
- Parton, W.J., Mosier, A.R. and Schimel, D.S.: 1988, 'Rates and pathways of nitrous oxide production in a shortgrass steppe', *Biogeochemistry*, **6**, 45-58.
- Roelle, P.A., Aneja, V.P., O'Connor, J., Robarge, W., Kim, D.-S. and Levine, J.S.: 1999, 'Measurement of nitrogen oxide emissions from an agricultural soil with a dynamic chamber system', *J. Geophys. Res.* **104**, 1609-1619.
- Yienger, J.J., Levy II H.: 1995, 'Empirical model of global soil-biogenic NO_x emissions', *J. Geophys. Res.* **100**, 11,447-11,464.



Field Tests of a Micrometeorological System for Ammonia Flux Measurements Using TDL Technology

J. S. WARLAND, G. DIAS, C. WAGNER-RIDDLE AND G. W. THURTELL

Department of Land Resource Science, University of Guelph, Canada

Abstract

A tunable diode laser trace gas analyser system (TDLTGAS) was built for continuous monitoring of ammonia fluxes over four plots. The system measures the concentration difference between two heights over each plot and relates the gradient to a flux using the aerodynamic method. Field testing of the system took place in October-November 1998 using three different manure applications to bare soil. Liquid swine manure, incorporated and unincorporated, and solid dairy manure (unincorporated) were applied to 1 ha plots and flux measurement begun immediately upon application. Mean gradients were output every 15 min to provide high temporal resolution of fluxes and monitoring continued for 10 days following application. Tests of the system showed that adsorption of ammonia to tubing walls was negligible. The system proved capable of continuous monitoring and provided a high-quality data set with fine temporal resolution. Results showed cumulative 10 day losses of applied nitrogen to be 73%, 10% and 43% from the unincorporated swine manure, the incorporated swine manure and the unincorporated dairy manure, respectively.

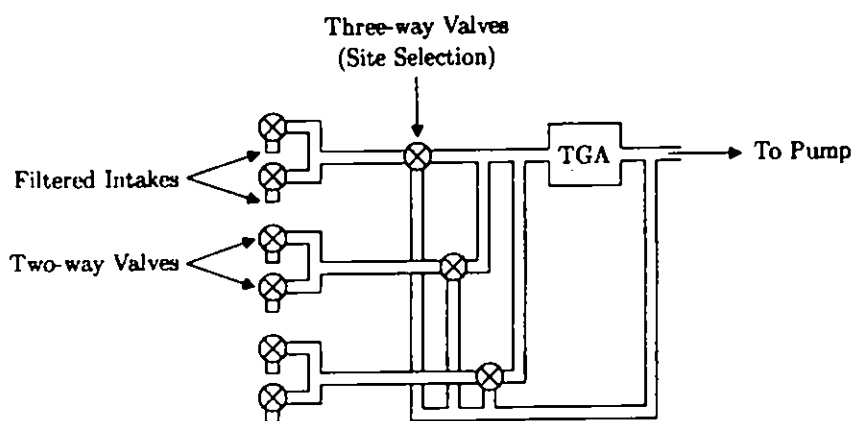
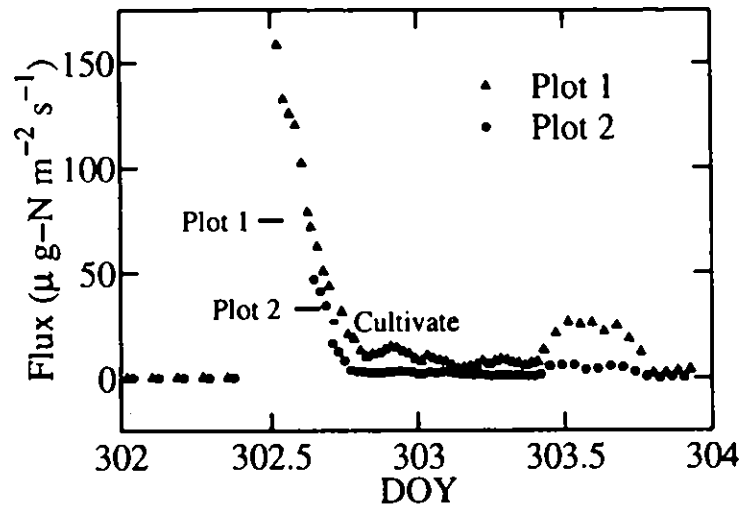


Figure 1. Schematic diagram of TDLTGAS system for monitoring fluxes from 3 field plots. At any time one three-way valve was opened to the analyzer to select that site and one two-way valve was open to permit sampling. This kept all tubing evacuated when not sampling to avoid water (and consequently ammonia) adsorption to the tubing walls. Not to scale.

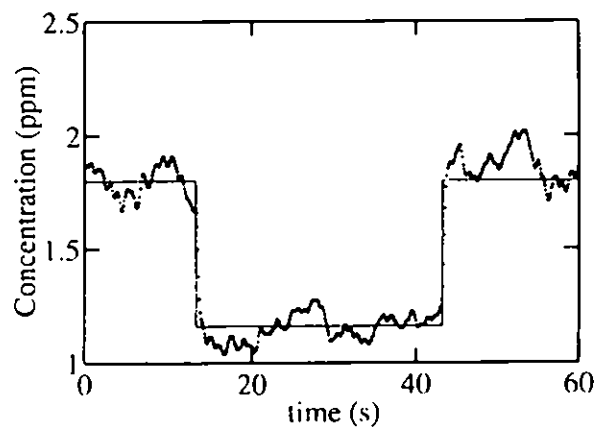
The TDLTGAS (Model TGA100, Campbell Scientific Inc., Logan, Utah) uses infra-red absorption spectroscopy to determine ammonia concentration in an air sample from the ratio of transmittance of the sample to a reference gas of known concentration. The laser used in this system operated in the region of 966 cm^{-1} at a temperature of $\sim 95\text{ K}$ and current of $\sim 300\text{ mA}$. Pressure in the system was maintained at approximately 45 mb.



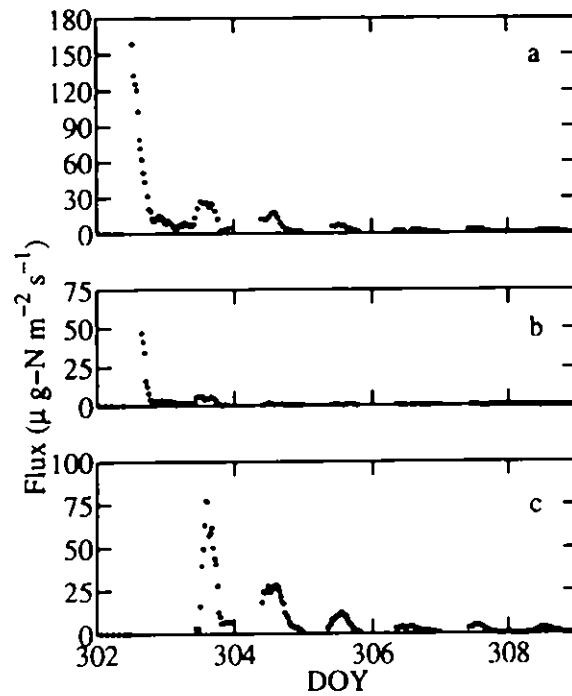


Detail of NH_3 fluxes from Plots 1 and 2 during first 2 days of experiment. Plot 1 received unincorporated liquid swine manure and Plot 2 received incorporated liquid swine manure. Lines show duration of applications and cultivation, as labelled.

Concentration measurements averaged over each point in the cycle for 2-h. Line shows mean reported concentrations (from the average concentration after 15-s equilibration period), representing the ideal square wave response. The noise in the signal is due to the natural variability in ammonia concentration, but quick response of the system can still be seen, indicating that adsorption problems were not present.







Hourly NH_3 fluxes from Plots 1--3 (respectively a-c) during first week of experiment. Plot 1: unincorporated swine manure, Plot 2: incorporated swine manure, Plot 3: unincorporated dairy manure. The ability of the system to measure both large and small fluxes can be seen.

Plot	Treatment	Applied N (kg)	Cumulative emissions as % applied N after 10 days	after 6 h
1	liquid, swine	47.5	73	37
2	liquid, swine, incorporated	47.5	10	6
3	solid, dairy	62.0	43	10

Table 1: Summary of emissions from the three plots 10 days after application and 6 h after application. Emissions expressed as percent of applied total ammoniacal nitrogen.



Modelling Short-Range Dispersion of Pollution

P. HOFSCHEUDEF

*Meteorology and Air Quality Group, Wageningen University, Duivendaal 2,
6701 AP Wageningen, the Netherlands, tel. +31-317-482104, fax. +31-317-482811,
e-mail: Peter.Hofschreuder@user.metair.wag-ur.nl*

Abstract

Experiments on short-range dispersion of the tracer gas SF₆ in the Flevo polder under neutral to unstable conditions showed systematic differences in measured and modelled concentrations. The modelled concentrations were strongly dependent on the parameterisation scheme that was chosen. Extension of the model comparison to unstable and stable conditions using Prairie Grass and Hanford data shows a large discrepancy in modelling results for lateral dispersion in unstable conditions and for dispersion in height for neutral and stable conditions.

Keywords: Dispersion, tracer, short range, model, parameterisation.

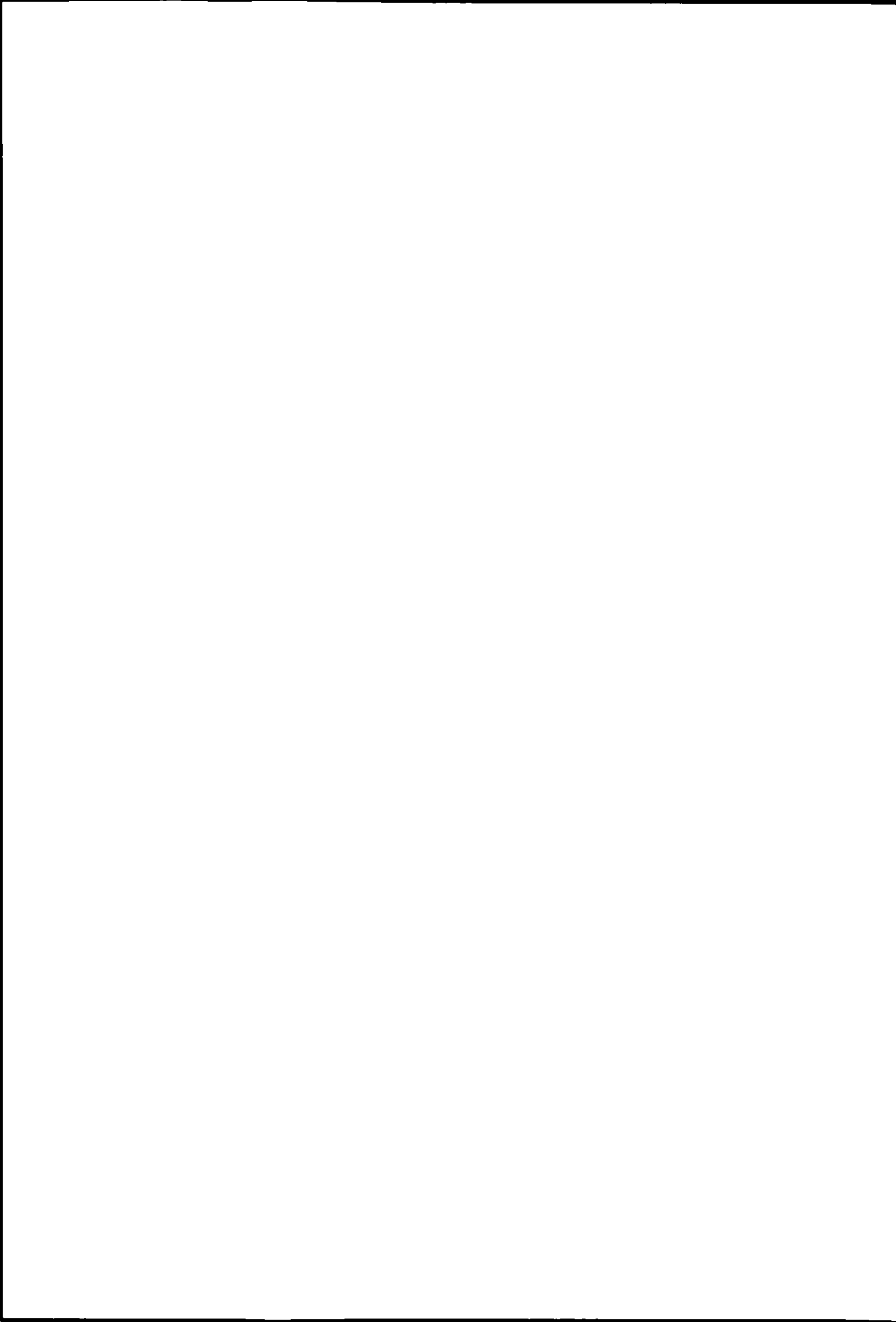
Introduction

Modelling the dispersion of air pollution on a national scale or larger provides results for year average concentrations within uncertainties of about 30-40% (v. Jaarsveld, 1995). The results will strongly depend on proper estimation of the mixing height. When we want to model dispersion of air pollution on a smaller scale or for a short averaging time, uncertainty will increase. There will be less averaging in meteorological conditions for turbulent transport, more local parameters influencing dispersion, and the parameterisation of the dispersion parameters σ_y and σ_z play a more important role.

Why look at this scale? We need short range modelling for estimation of local air quality for vegetation and mankind close to low sources, provided the background concentration is low. Another application for local modelling is the estimation of pollution source strength by inverse modelling, after measuring concentrations. The third application is trend evaluation for the emissions of low sources of pollution as is done for NH₃ in the Netherlands by RIVM.

Common practice for calculations of short-range dispersion is the use of a Gaussian plume model with the source strength, wind speed and dispersion parameters σ_y and σ_z as main (Doran and Horst, 1985). A modified approach is the use of a Gaussian plume model with effective plume rise for low sources (v. Jaarsveld, 1995). This takes the distortion of a Gaussian plume due to the wind velocity profile into account. The third type of model is the K-model, allowing for a shape factor for the vertical concentration profile depending on meteorological conditions. Horizontal dispersion is again considered to be Gaussian (Gryning et al, 1987). Less commonly used methods like LaGrange or Monte Carlo modelling will not be discussed here.

There are three methods available for the parameterisation of both the horizontal and vertical dispersion parameters. For σ_y we have the methods of Hanna (1981), Gryning et al., (1987) and KNMI (1979). For σ_z we have the methods of Hanna (1981), van Jaarsveld (1995) and Gryning et al. (1987).



All methods exhibit small variations in parameters by other authors.

The mentioned parameterisations were compared to measurements of the dispersion of a tracer gas in the Flevo polder. The spread in simulated concentrations appeared to be so large that further interpretation and use of data sets for more stable and more unstable situations was prompted. The only information available is from the Prairie Grass experiments in 1958 (van Ulden, 1978) and Hanford experiments (Doran and Horst, 1985). The drawback of these experiments is that primary description of the experiments is not easy to obtain. The information provided by the mentioned authors is thorough, but only provides crosswind-integrated concentrations. This prevents comparison with individual data.

Theory

Details on the theory in estimating σ_y and σ_z are provided by Hanna, (1981), van Ulden, (1978), Gryning et al., (1987) and van Jaarsveld, (1995). Essential parameters for estimation of σ_y and σ_z are the standard deviation of the wind speed perpendicular to the mean wind direction (σ_v) and in height σ_w , or the standard deviation of the horizontal fluctuations of the wind speed σ_θ and elevation σ_e . When this information is not available, values can be estimated when the mixing height (h) is known. This mixing height can be estimated using the equation of Nieuwstadt (1978) for stable and neutral conditions. For unstable conditions the method of Garrat (1992) can be used. This asks for a continuous record of the sensible heat flux from sunrise to the hour of the experiments. The mixing height is also essential in estimating the turbulent LaGrange time scales T_L^u , T_L^v and T_L^w . These time scales also play a role in turbulent dispersion.

Gryning et al. recommend the use of a turbulent time scale T_L^v of 200 seconds for low sources and all meteorological conditions. This indeed provides better simulations compared to other simulations and compared to the only available individual data of the Flevo experiments, than the use of actual time scales. Actual time scales of this order of magnitude are only encountered in unstable conditions for low sources. In neutral and stable conditions the actual time scale T_L^v is in the order of a few seconds.

The Flevo experiments

The Flevo experiments are fully described in Hofschreuder et al. (1999). The terrain is a flat open polder with only farmhouses at distances of more than 1.5 kilometres. The fields were covered with sugar beet at the time of the experiments. The roughness length was estimated to be 0.15 m. The energy balance and latent heat flux were monitored continuously with a sonic anemometer, a fast Krypton vapour sensor, devices for incoming and outgoing short wavelength and long wavelength radiation, temperature profile measurements in air and soil and heat flux sensors in the soil. The tracer gas SF₆ was released from a gas cylinder equipped with flowcontroller and flowmeter to control source strength.

The source strength was 0.152 g s⁻¹ during the first two experiments and 0.286 g s⁻¹ during the following ten experiments. The gas was sampled during 45 minutes in glass jars fitted with a hypodermic needle to control the outflow of water (and the sampling of SF₆ containing air). The glass entrance tube protruded deep into the jar to maintain constant atmospheric pressure on the hypodermic needle for constant volumetric sampling. Analysis was done using a gas chromatograph fitted with ECD detector. The sampling sites were projected along



a road approximately perpendicular to the mean wind direction. The average distance between source and receptor point varied between about 200 and 700 m depending on wind direction. Source height and measuring height was 2 m. At one location, depending on the expected wind direction, a tower was placed for measurements at 2, 5, 10, 15 and 20 m height.

Primary data and results are available in Hofschreuder et al. (1999) (in Dutch). They are still subject to interpretation because interpretation was hampered by the unexpected spread in results of the different parameterisations. Interpretation was therefore first focussed on these parameterisations. An indication of the results is presented in Figures 1 and 2.

No data on measured results are introduced in Table 1, as the measuring sites hardly ever form a line perpendicular to the mean wind direction. They are preferably compared to simulated data for the same site. The use of cross wind integrated concentrations is not preferred as this makes it possible to compensate errors in horizontal dispersion by errors in vertical dispersion.

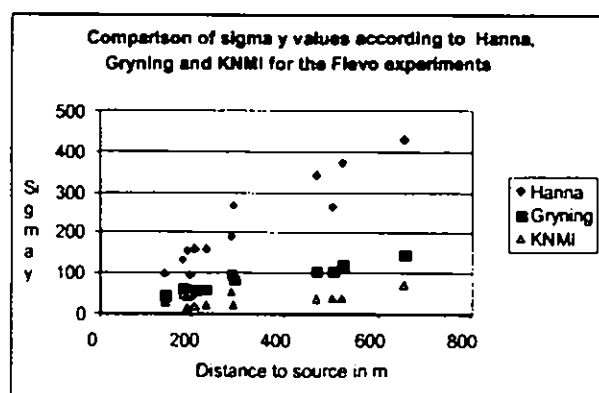


Figure 1. Comparison of measured horizontal concentrations with modeled data using the parameterization of Hanna (1981) for σ_y and the parameterization of Gryning et al. (1987) for σ_z .

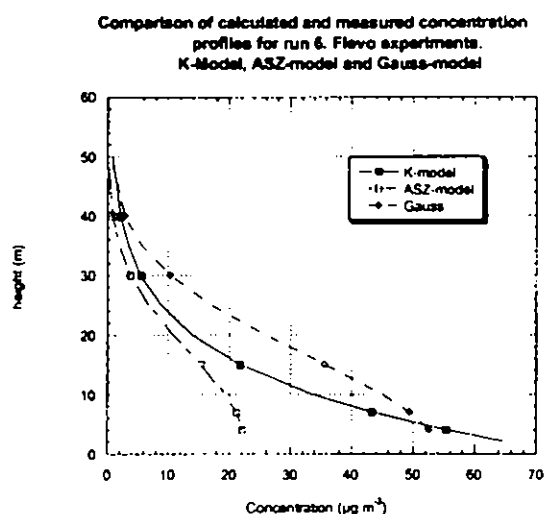


Figure 2. Comparison of measured vertical concentrations with modeled data using the parameterization of Hanna (1981) for σ_y and the parameterization of Gryning et al. (1987) for σ_z .



A comparison of measured and calculated concentrations with horizontal modelling according to Hanna in vertical modelling according to Gryning et al. is presented in Figure 1. With regard to the total ensemble of Flevo experiments, the combination of modelling the horizontal dispersion according to Hanna and vertical dispersion according to Gryning et al. gives the best comparison with the measured results. The spread in results is nevertheless large.

The spread in the vertical profile (Figure 2) is less, mainly because of locating the tower near the estimated centre of the plume, with high concentrations. In this case the comparison is less prone to large differences because of a slight misalignment of the plume. Especially with a narrow plume a little shift in plume axis will give rise to large differences between measured and modelled concentrations on the large gradient at the side of the plume. The results indicate that many experiments are needed before one can judge the value of a parameterisation.

Comparison of results of different parameterisations

The interpretation of the results of the Flevo experiments indicated differences in modelling results and dependence of these results from atmospheric stability. The only information on local scale dispersion experiments known to the author are the Prairie Grass and Hanford experiments. A drawback is that no primary data could be obtained. Calculations with the parameterisations mentioned before are only possible based on secondary (condensed) information from van Ulden (1978) and Doran and Horst (1985). The mixing height for neutral and stable conditions was calculated according to Nieuwstadt (1978). From this σ_v , σ_w , σ_θ , and σ_c , and T_L^v and T_L^w could be derived.

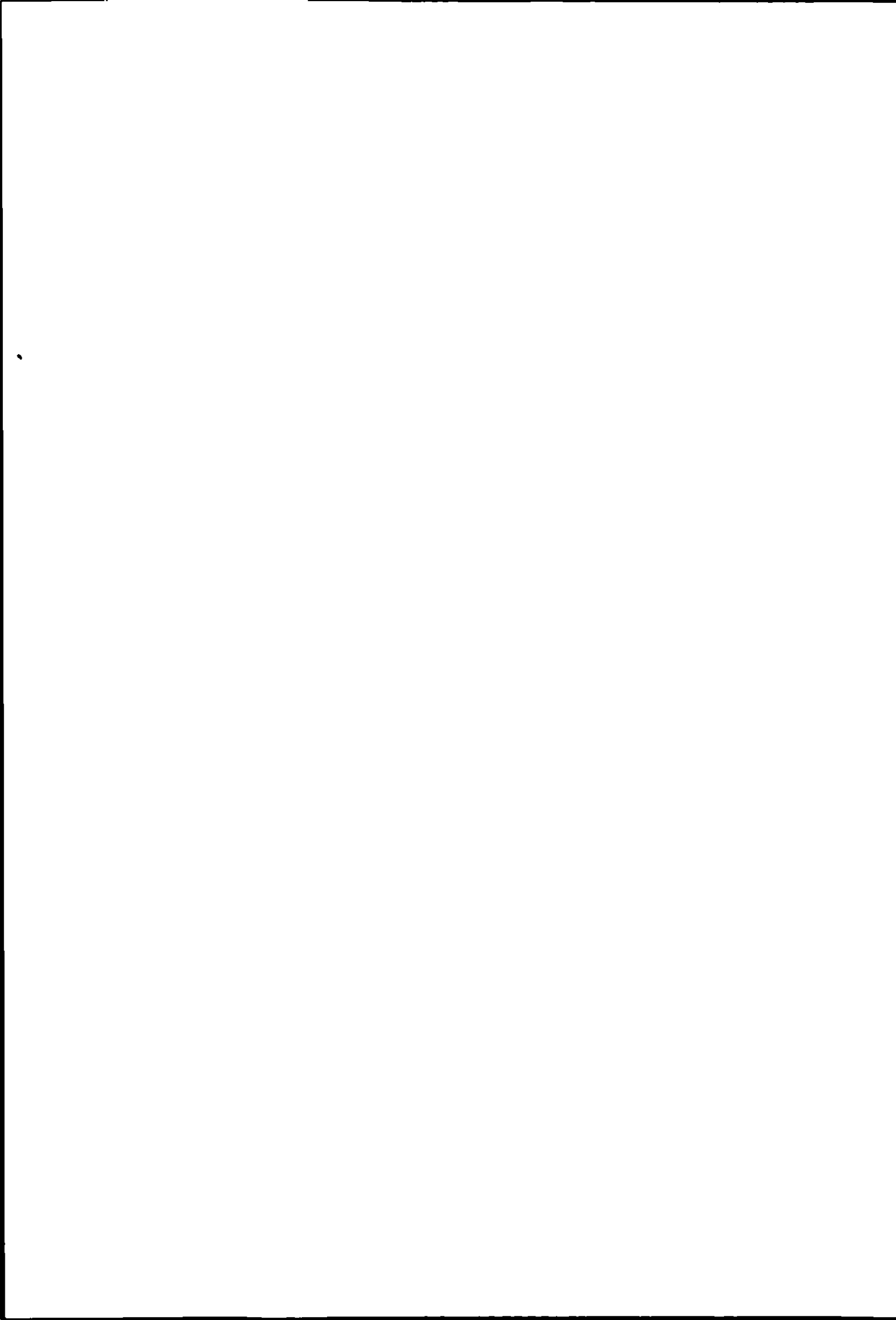
Lack of information on the sensible heat flux since sunrise prevented calculation of h for the unstable experiments in the Prairie Grass data. Arbitrarily the value of h was set at 800 m when $-0 < H < -100$ ($W m^{-2}$) and 1100 m when $H < -100$ ($W m^{-2}$). For the Flevo experiments, the measured standard deviations of the wind speed were used. Mixing height was calculated according to Garrat (1992).

The total ensemble of experiments was classified in three sets of data: unstable situation ($z/L < -0.02$), neutral situation ($-0.02 < z/L < 0.02$) and stable situation ($z/L > 0.02$).

Two parameterisations were tried for the horizontal dispersion parameter σ_y , Hanna (1981) and Gryning et al. (1987) with T_L^v fixed at 200 s (recommended). The parameterisation according to KNMI (1979) was not used, as no data on cloud cover for the Pasquill classification were available other than for the Flevo experiments.

Three parameterisations were tried for the vertical dispersion parameter Hanna (1981), van Jaarsveld (ASZ) (1995) and the K-model of Gryning et al. (1987).

For vertical dispersion Hanna uses source height as height for axis of the (Gaussian) plume. Van Jaarsveld does the same but calculates σ_z in an iterative procedure for a larger effective plume height due to the existing wind velocity profile close to the ground. Gryning et al. calculate the cross wind integrated concentration distribution using a stability dependent shape factor and subsequently assume a horizontal Gaussian distribution. The vertical profile is then defined by an effective plume height and the profile of the crosswind integrated concentrations.



A comparison of results is made adding source height and σ_z for Hanna and ASZ (van Jaarsveld) and adding calculating the height at which the cross wind integrated concentration according to Gryning et al. reaches 67% of the value at the effective plume height at that place. The results are expressed in the ratio (parameterisation by Hanna/other parameterisation in Table 1.

Table 1. Ratio of σ_y and (source height + σ_z) according to Hanna, divided by the other parameterisations for the Prairie Grass, Hanford and Flevo experiments, classified in unstable (n=30), neutral (n=26) and stable (n=22) conditions.

	distance	50	100	200	800	1600
σ_y	unstable Han./Gryn.	0.99	0.99	0.99	0.99	0.99
	neutral Han./Gryn.	0.99	0.89	0.94	0.96	0.91
	stable Han./Gryn.	1.10	1.20	1.20	1.30	1.60
σ_z	unstable Han./Gryn.	0.85	1.14	1.09	0.94	0.86
	unstable Han./ASZ	1.04	0.84	0.60	0.20	0.09
	neutral Han./Gryn.	0.75	0.71	0.62	0.43	0.34
	neutral Han./ASZ	0.90	0.81	0.71	0.49	0.41
	stable Han./Gryn.	equation Gryning explodes				
	stable Han./ASZ	1.01	1.03	1.04	1.10	1.15

Conclusions

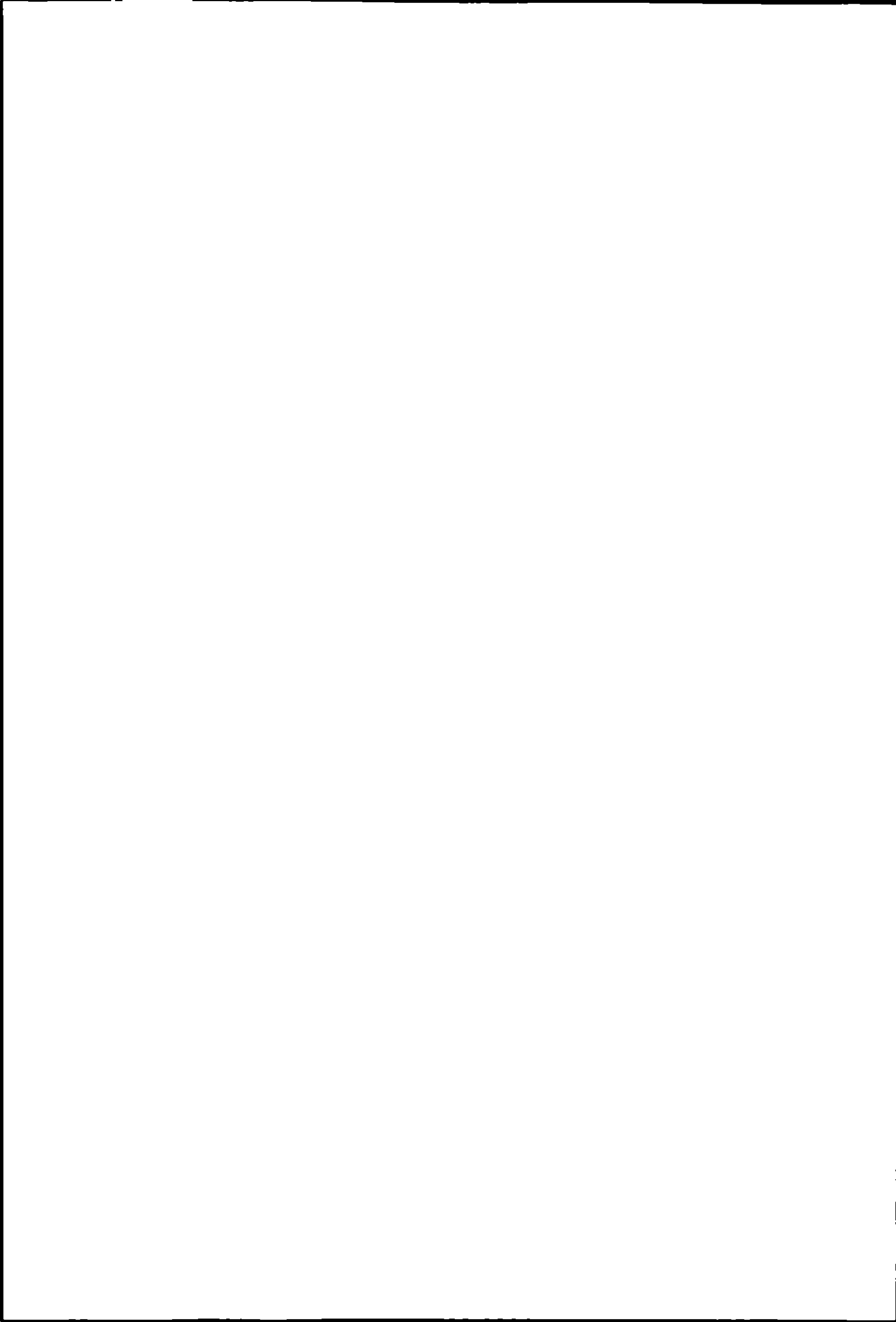
There is a large discrepancy in the parameterisation of short-range dispersion of pollutants, especially for horizontal dispersion in stable conditions and vertical dispersion in neutral and unstable conditions.

Data for validation of parameterisations are scarce and for the Flevo experiments only available in vertical profiles.

Future experiments need detailed information on the meteorological situation.

References

- Doran, J.C., Horst, T.W.: 1985, 'An evaluation of Gaussian plume depletion models with dual-tracer field measurements', *Atmospheric Environment*, **19**, 6, 939-951.
- Garrat J.R.: 1992, *The atmospheric boundary layer*. Chapter 6. Cambridge atmospheric and space science series, 145-192.
- Gryning, S.E., Holtslag, A.A.M., Irwin, J.S., Sivertsen, B.: 1987, 'Applied dispersion modelling based on meteorological scaling parameters'. *Atmospheric Environment* **21**, 1, 79-89.



- Hanna, S.R.: 1981, *Applications in air pollution modelling*. in Atmospheric turbulence and air pollution modelling (Nieuwstadt, F.T.M, Van Dop, H eds.). p 275-310.
- Hofschreuder, P, Vonk, A.W, Heeres, P.: 1999, 'Tracer gas experiments in the Flevo polder; Comparison of measured concentrations with simulated concentrations using a Gauss model, the ASZ model and a K-type model'. (in Dutch). Wageningen University, Meteorology and Air Quality, Report R 835.
- Jaarsveld J.A. van.: 1995, 'Modelling the long-term atmospheric behaviour of pollutants on various spatial scales', *Ph.D. Thesis*, University of Utrecht. 235 pp. ISBN 90-393-0950-7.
- KNMI: 1979, *Luchtverontreiniging en weer*. (Air Quality and weather)(in Dutch). Staatsuitgeverij/KNMI. ISBN 90-12-02444-7.
- Nieuwstadt, F.: 1978, 'The computation of the friction velocity u_* and the temperature scale T_* from temperature and wind velocity profiles by least-square methods'. *Boundary-Layer Meteorology*, **14**, 235-246.
- Ulden, A.P. van.: 1978, 'Simple estimates for vertical diffusion from sources near the ground'. *Atmospheric Environment* **12**, 2125-2129.



Estimate of the Dry Deposition of Atmospheric Nitrogen and Sulfur Species to Spruce Forest

LÁSZLÓ HORVATH¹, JOSEPH PINTO² AND TAMÁS WEIDINGER³

¹*Hungarian Meteorological Service, 1181 Budapest, Gilice tér 39, Hungary, E-mail: horvath.l@met.hu*

²*U.S. Environmental Protection Agency, Research, Triangle Park, NC 27711, USA*

³*Eötvös Loránd University, Department of Meteorology, 1117 Budapest, Pázmány sétány 1, Hungary*

Introduction

Knowledge of the dry deposition flux of different nitrogen and sulfur containing species is necessary for estimating the nitrogen and sulfur balance in forest ecosystems. However, there are substantial differences among the few existing data sets caused in part by differences in climatic conditions during the collection of the data.

Field studies carried out mostly during the last decade have derived dry deposition velocities for gaseous ammonia ranging typically between 0.8 and 4.5 cm sec⁻¹ (Andersen et al., 1993; Erisman et al., 1995; Duyzer et al., 1994; Wyers et al., 1995). In some cases emission was reported (Andersen et al., 1999). Dry deposition velocities for nitric acid determined in field studies are much higher (Janson and Granat, 1997) than had been estimated on the basis of theoretical and field studies (Baldocchi et al., 1992) due to the low canopy resistance of these species.

In the case of sulfur dioxide the dry deposition velocity measured over forests ranges between 0.05-3 cm s⁻¹ (Mennen, 1995). For aerosol particles, recent but limited field studies (Erisman, 1995; Wyers, 1995) have obtained systematically higher deposition velocities than there were determined by theoretical calculations and wind tunnel experiments (Ruijgork et al., 1993 and Borrell et al., 1997).

The aim of this paper is to provide data set for dry deposition velocities of these compounds, to increase the available data based on experimental investigations.

Measurements and Calculations

Gradient flux measurements were carried out in the Mátra Mountains, Hungary (Nyírjes station) in a Norway Spruce forest, during a field campaign in May 1998. Characteristics of the measuring site are: latitude = 47°54'N, longitude = 19°57'E, altitude = 560 m asl., type of vegetation: Norway Spruce (50 ha), surroundings: Pine, Beech, average height: 16 m, age 26 years, leaf area index (LAI): 3.3.

Concentrations of gaseous and aerosol species were measured with parallel three stage filter packs, located at heights of 13 and 23 meters on an instrumented tower for 8 hour sampling periods, during day and night (corresponding to unstable and stable conditions). Since the average calculated displacement height was 12 m, the lower height (13 m) is also above the canopy layer, therefore the turbulent motions are not disturbed by the canopy between the two measuring heights. A total of 18 measurements were carried out partly during daytime,



partly in the night. A Teflon filter collected particles on the first stage of the filter packs, and on the second and third stages Whatman filters with basic and acid coatings collected acidic (nitric acid, sulfur dioxide) and alkaline (ammonia) gases, respectively. Concentrations of ammonium ions were determined spectrophotometric method using the indophenol-blue method, while nitrate and sulfate ions were determined by ion chromatography. The bulk precision of sampling and analysis was determined by parallel sampling at the same (23 m) level. The results of 10 measurements show that the mean relative error of sampling and measurements for all components is around $\pm 5\%$.

The eddy-diffusivity of heat was calculated from the measured wind and temperature profiles on the basis of the Monin-Obukhov similarity theory (Horváth et al., 1998; Weidinger et al., 2000). The Monin-Obukhov length was calculated using the Richardson-number derived from profile measurements and the universal functions for momentum and heat transfer (for details see Horváth et al., 1998). It was assumed that the average bulk eddy-diffusivity for the trace materials is same as for the eddy-diffusivity of momentum and heat transfer. The values of K_T were calculated on the basis of profile-flux relationship using the measured wind and temperature profiles. During the evaluation of the profile measurements the similarity theory provides the more appropriate estimations for the calculation of turbulent momentum and heat flux and hence for the calculation of the eddy-diffusivity (Weidinger et al., 2000).

The eddy-diffusivity depends on the surface roughness as well as on meteorological conditions in the surface layer, especially the stratification. During stable conditions (mostly during nighttime) the rate of exchange is generally lower, when the eddy-diffusivity is generally lower ($0.3 \text{ m}^2\text{s}^{-1}$) by a factor of three as compared to unstable conditions ($0.9 \text{ m}^2\text{s}^{-1}$ as an average, daytime). The eddy-diffusivity of the heat was considered as the measure of the turbulent exchange for all species. Stable and unstable cases were separated by the sign of the *Richardson*- number.

Results and Discussion

Dry deposition velocities of gases were calculated according to the gradient method. Concentration gradients of gases were multiplied by eddy-diffusivities. Eddy-diffusivities and gradients were determined separately for unstable (mainly daytime) and stable (nighttime) conditions. Concentration differences between the two sampling heights ranged between 4 and 82 per cent as shown in Table 1. The precision of concentration measurements was determined to be about ± 5 per cent in field and laboratory tests.

According to Table 1, in the case of nitric acid the deposition velocities for both unstable and stable conditions are similar, indicating substantial cuticular uptake. These figures are in the range of the deposition velocities collected by Baldocchi (1992), $0.5\text{-}5.0 \text{ cm s}^{-1}$ for deciduous forests on the basis of model calculations compared to experimental results. The deposition velocity provided by Janson and Granat (1997), 7 cm s^{-1} for coniferous forest, is substantially higher, suggesting that canopy resistance is higher than it was expected by these authors.

For ammonia, where the stomatal uptake is the dominant deposition process, the deposition velocity figure (Table 1) is about three times higher when stomata are open (daytime) than during nighttime. These figures are in a good agreement with other field measurements above forests: Andersen et al., 1993: 2.6 cm s^{-1} or 4.5 cm s^{-1} in the intensive vegetation period; Duyzer et al., 1994: $2\text{-}3 \text{ cm s}^{-1}$; Erisman et al. 1995: 2.5 cm s^{-1} ; Wyers et al., 1995: $1.5\text{-}4.3 \text{ cm s}^{-1}$ at night, $0.8\text{-}4.0 \text{ cm s}^{-1}$ in daytime, however the last authors did not found any



difference between the deposition velocities during day and night hours. Andersen et al. (1999) pointed out the importance of ammonia emission from the forest, demonstrating that deposition dominates in the net flux when the ammonia concentration exceeds the compensation point.

compound	period	mean deposition velocity (cm s^{-1})	mean concentration (nmol m^{-3})		mean concentration difference (%)
			23 m	13 m	
HNO_3	day	1.9 ± 0.4	11	8.1	27
	night	1.3 ± 0.1	2.7	0.5	82
NH_3	day	3.7 ± 0.4	28	18	35
	night	1.1 ± 0.1	16	8.2	47
SO_2	day	0.6 ± 0.4	134	124	8
	night	0.3 ± 0.1	59	49	18
NO_3	day		6.9	4.8	30
	night		12	7.6	37
NH_4^+	day	<0.4	68	72	6
	night	<0.1	82	78	4
SO_4^{2-}	day	<0.4	54	51	6
	night	<0.1	81	49	5

Table 1. Deposition velocities, mean concentrations and mean differences of gases and aerosols

The deposition velocity of sulfur dioxide is lower than that of nitric acid and ammonia during both stable and unstable conditions (Table 1). The sulfur dioxide deposition rate determined for forests ranges two orders of magnitude (Mennen, 1995: $0.05\text{-}3 \text{ cm s}^{-1}$; Erisman, 1995: 1.5 cm s^{-1} ; Horváth, 1997: $0.6\text{-}1.6$ and $0.2\text{-}0.34 \text{ cm s}^{-1}$, during unstable and stable conditions, respectively).

As to the nitrate particles, annular denuder system (ADS) (cyclone, denuder tubes, filter pack) measurements made in parallel with the filter pack measurements show that nitrate particles are found mainly in the coarse fraction (Table 2). Therefore, the gradient method for determining the dry deposition of nitrate flux needs correction for the effects of gravitational settling.



phase	nitrate/nitric acid	ammonium/ammonia
coarse particles $d > 2.5 \mu\text{m}$	18	<2
fine particles $d < 2.5 \mu\text{m}$	<2	188
gas	12	26

Table 2. Share of nitrogen compounds in different phases in nmol m^{-3}

In contrast, ammonium particles were found solely in the fine fraction ($d < 2.5 \mu\text{m}$). The majority of the total nitrogen, consisting of ammonia gas, nitric acid, and particulate nitrate and ammonium, was contained in the form of ammonium fine particles. The molar ratio of ammonium to sulfate in the samples was close to equal, i.e. sulfuric acid has been neutralized by ammonia to ammonium bisulfate. Because ammonium bisulfate was present mainly in the fine fraction, the gradient method is applicable provided gravitational settling can be neglected.

However, the average concentration difference between the upper and lower levels was between 4 and 6 per cent for ammonium and sulfate during both unstable and stable conditions. Considering the precision in sampling and measuring the concentrations with the filter pack method (about 5 per cent), a deposition velocity for ammonium and sulfate could not be determined. Table 1 shows lower limits for dry deposition velocities of ammonium and sulfate. According to the measurements concerning forests the dry deposition velocity of these compounds are: 2.4 cm s^{-1} for sulfate (Sánchez, 1993); $1.2\text{-}1.5 \text{ cm s}^{-1}$ for ammonium particles over $0.8 \mu\text{m}$ size (Wyers et al., 1995); $1\text{-}2 \text{ cm s}^{-1}$ for fine and 5 cm s^{-1} for coarse sulfate and ammonium particles (Erisman et al., 1995). Different research groups agree with the high uncertainty of these figures (Lopez, 1994). Borrell (1997) suggests over 1 cm s^{-1} deposition velocity of particles according to the re-evaluation of theoretical, wind tunnel and field estimations (Ruijgork et al., 1993). Our results contrast with these studies where relatively high ammonium deposition velocities were found suggesting that generalization of particle dry deposition field measurements is limited.

Acknowledgements

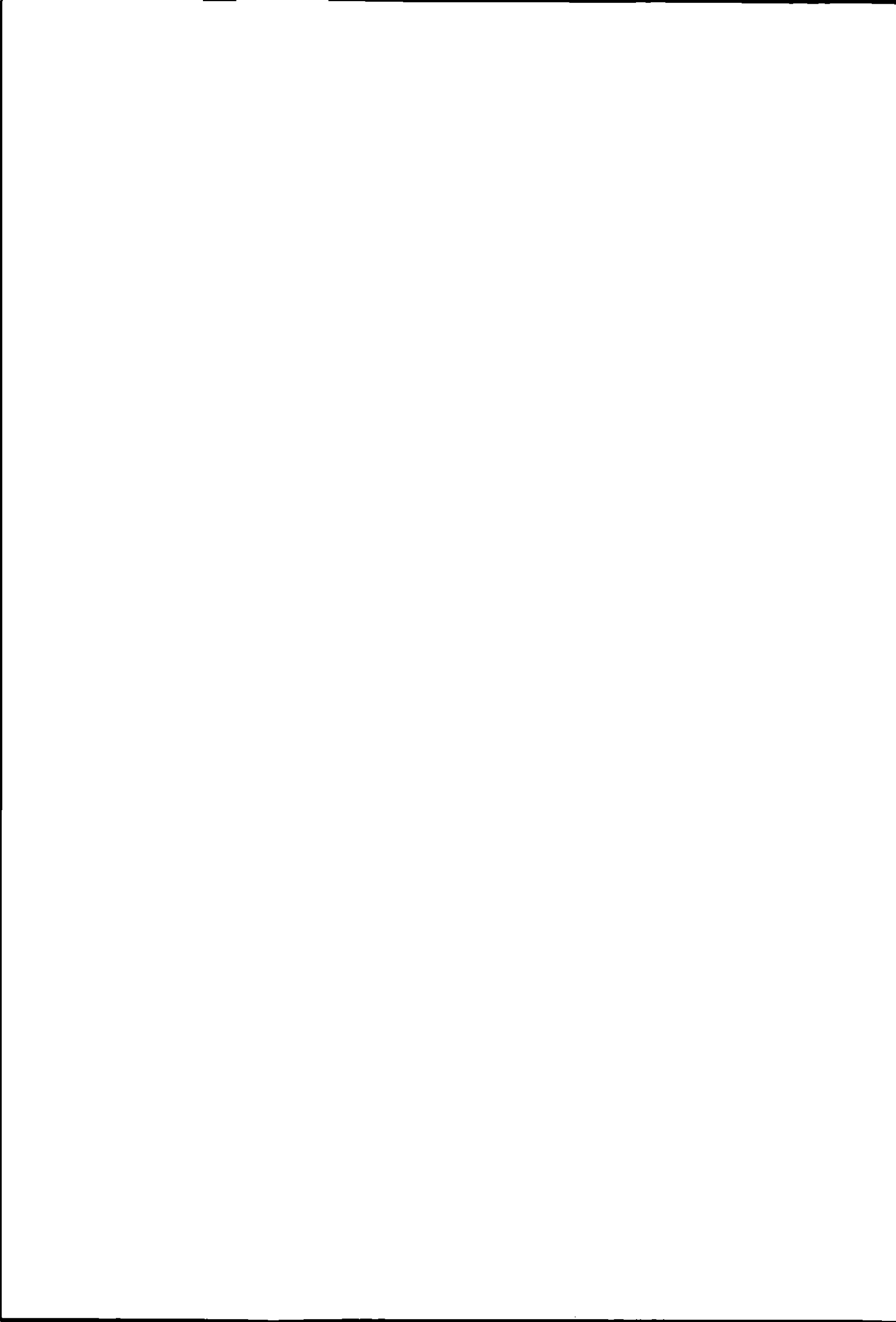
Investigations were funded by the US-Hungarian Research Joint Fund, No. 503. The authors would like to acknowledge the valuable technical assistance provided by Lilla Váradi throughout the measurement program.

References

- Andersen, H.V., Hovmand, M.F., Hummelshøj, P. and Jensen, N.O. 1993. Measurements of ammonia flux to a Spruce stand in Denmark. *Atmospheric Environment* **27A**, 189-202.
- Andersen, H.V., Hovmand, M.F., Hummelshøj, P. and Jensen, N.O., 1999. Measurements of ammonia concentrations, fluxes and dry deposition velocities to a spruce forest 1991-1995. *Atmospheric Environment* **33**, 1367-1384.
- Baldocchi, D.B. 1992. On estimating HNO_3 deposition to a deciduous forest with a Lagrangian random-walk model. *Precipitation Scavenging and Atmosphere-Surface*



- exchange (2) (eds. S.E. Schwartz and W.G.N. Slinn) Hemisphere Publishing Corporation, Washington, Philadelphia, London, p. 1081.
- Borrell, P., Builtjes, J.H., Grennfelt, P. and Hov, O. (eds.), 1997. *Transport and chemical transformation of pollutants in the troposphere. Vol. 10*. Photo-oxidants, acidification and tools: policy applications of EUROTRAC results. Springer, p. 116.
- Duyzer, J.H., Verhagen, H.L.M. and Weststrate, J.H., 1994. The dry deposition of ammonia onto a Douglas fir forest in the Netherlands. *Atmospheric Environment* **28**, 1241-1253.
- Erisman, J.W., Draaijers, G., Duyzer, J., Hofschreuder, P., van Leeuwen, N., Römer, F., Ruijgork, W. and Wyers, P., 1995. Particle deposition to forests. *Acid rain research: do we have enough answers? Studies in Environmental Science* **64** (eds. Heij, G.J. and Erisman, J.W.). Elsevier, Amsterdam, Lausanne, New York, Oxford, Shannon, Tokyo, p. 115.
- Horváth, L., Nagy, Z., Weidinger, T. and Führer, E., 1997. Measurement of dry deposition velocity of ozone, sulfur dioxide and nitrogen oxides above pine forest and low vegetation in different seasons by the gradient method. *Proceedings of EUROTRAC Symposium '96*. (eds. Borrell, P.M., Cvitas, T. Kelly, K. and Seiler, W.), Computational Mechanics Publications, Southampton, p. 315.
- Horváth, L., Nagy, Z. and Weidinger, T., 1998. Estimation of dry deposition velocities of nitric oxide, sulfur dioxide and ozone by the gradient method above short vegetation during the TRACT campaign. *Atmospheric Environment* **32**, 1317-1322.
- Janson, R. and Granat, L., 1997. Dry deposition of HNO₃ to the coniferous forest. *Proceedings of EUROTRAC Symposium '96*. (eds. Borrell, P.M., Cvitas, T. Kelly, K. and Seiler, W.), Computational Mechanics Publications, Southampton, p. 351.
- Lopez, A., 1994. Biosphere atmosphere exchanges: ozone and aerosol dry deposition velocities over a pine forest. *EUROTRAC Annual Report part 4, BIATEX, EUROTRAC ISS, Garmisch-Partenkirchen*, p. 80.
- Mennen, M.G., Hogenkamp, J.E.M., Ywart, H.J.M.A. and Erisman, J.W., 1995. Monitoring dry deposition fluxes of SO₂ and NO₂: analysis of errors. *Acid rain research: do we have enough answers? Studies in Environmental Science* **64** (eds. Heij, G.J. and Erisman, J.W.). Elsevier, Amsterdam, Lausanne, New York, Oxford, Shannon, Tokyo, p. 41.
- Ruijgork, W., Nicholson, K.W. and Davidson, C.I., 1993. Dry deposition of particles. *Models and methods for the quantification of atmospheric input to ecosystems. Nordiske Seminar og Arbejdsrapporter 1993*: 573. Nordic Council of Ministers, Copenhagen, pp 145-161.
- Sánchez, M.L., Domínguez, J., Sanz, F. and Rodríguez, R., 1993. Preliminary study of dry deposition. *Air Pollution Research Report* **47**. (eds. Slanina, J., Angeletti, G. and Beilke, S.) CEC, p. 65.
- Wyers, G.P., Veltkamp, A.C., Geusebroek, M., Wayers, A. and Möls, J.J., 1995. Deposition of aerosol to coniferous forest. *Acid rain research: do we have +enough answers? Studies in Environmental Science* **64** (eds. Heij, G.J. and Erisman, J.W.). Elsevier, Amsterdam, Lausanne, New York, Oxford, Shannon, Tokyo, p. 127.
- Weidinger, T., Pinto, J. and Horváth, L., 2000: Effects of uncertainties in universal functions, roughness length, and displacement height on the calculation of surface layer fluxes. *Meteorologische Zeitschrift* **9**, 139-154.



Bidirectionality of Ammonia Fluxes: Observations over a Deciduous Forest

S.C. PRYOR*, R.J. BARTHELMIE^{*/†}, B. JENSEN[†], M.L. DAVIS^{*}, K.C. HIRZY^{*}, J.T. SCHOOF^{*},
L.L. SØRENSEN[†]

**Atmospheric Science Program, Department of Geography, Indiana University,
Bloomington, IN47405, USA*

*†Department of Wind Energy and Atmospheric Physics, Risø National Laboratory, DK-4000
Roskilde.*

*†Department of Atmospheric Environment, National Environmental Research Institute, DK-
4000 Roskilde.*

Abstract

We present measurements of ammonia (NH_3) over a deciduous forest in southern Indiana collected during spring and winter field campaigns. Ammonia concentrations measured continuously using Wet Effluent Diffusion Denuders indicate mean concentrations of $0.6 - 1.2 \mu\text{g m}^{-3}$ during the spring and $0.1 - 0.3 \mu\text{g m}^{-3}$ during the winter. On average the forest acts as a sink of NH_3 , with a representative daily deposition flux of $1.8 \text{ mg-NH}_3 \text{ m}^{-2}$ during the spring. However, on some days during the spring inverted concentration gradients of NH_3 were observed resulting in an upward flux of nearly $0.2 \text{ mg-NH}_3 \text{ m}^{-2} \text{ hr}^{-1}$. Analyses suggest that this apparent emission flux may be due to canopy emission but evaporation of ammonium nitrate particles may also be partly responsible for the observed inverted concentration gradients.

Key Words: Gas-particle conversion, vertical gradients, time scales, atmosphere-surface exchange

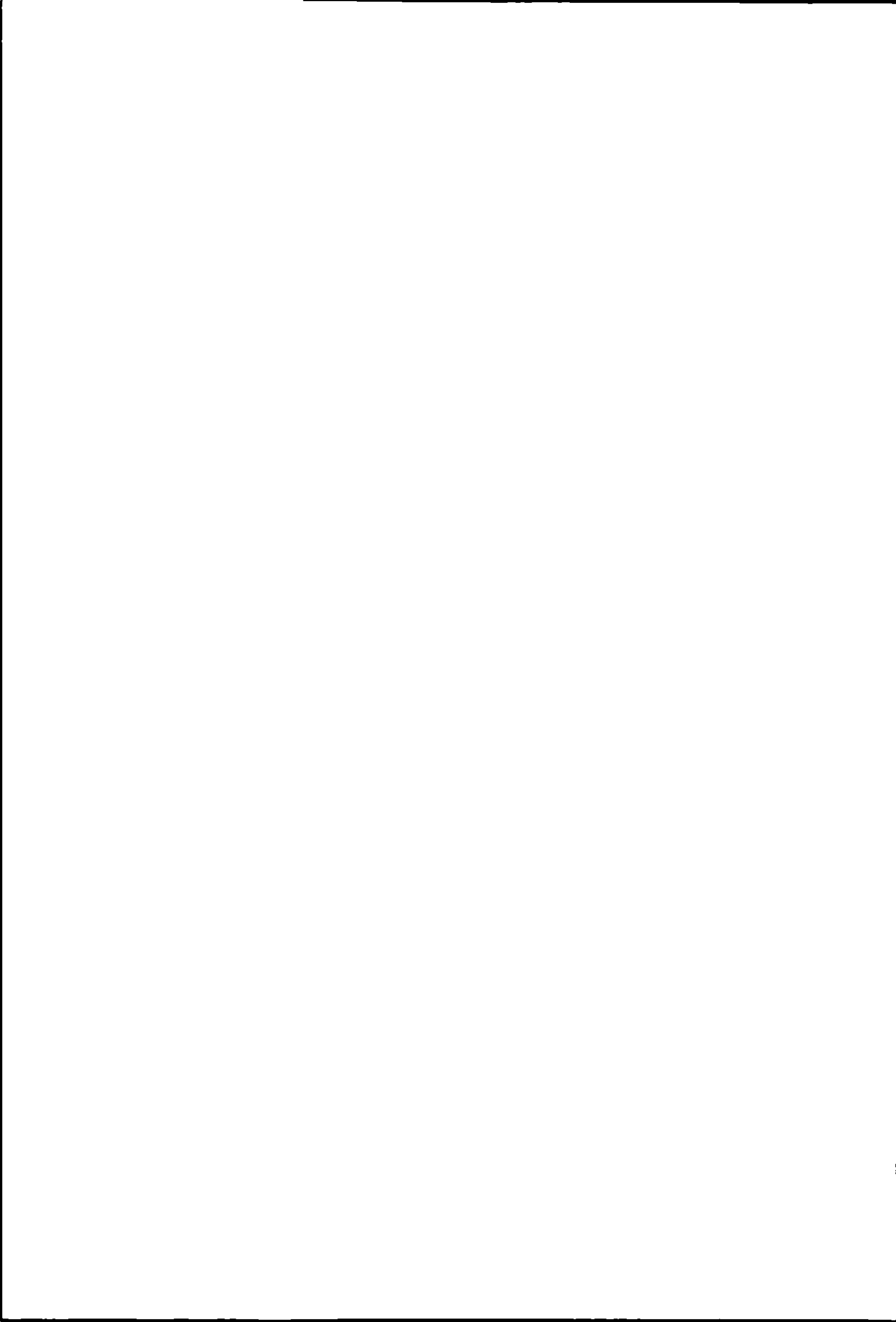
Introduction

Inverted concentration gradients of ammonia (NH_3) have been previously observed over forests (Langford and Fehsenfeld, 1992), however, observations of inverted vertical concentration gradients can not be conclusively attributed to emission from the plant stomata, since other potential sources of apparent upward fluxes of NH_3 exist. For example, evaporation of ammonium nitrate (NH_4NO_3) particles (Kramm and Dlugi, 1994) or drying of leaf surfaces (Wyers and Erisman, 1998). Here we present data showing inverted NH_3 gradients over natural deciduous forest and document analyses to investigate causes of apparent emission fluxes.

Ammonia concentrations and fluxes at MMSF

The experimental site

This paper presents results of above canopy measurements of NH_3 at the AmeriFlux tower in Morgan-Monroe State Forest (MMSF), southern Indiana (at $39^\circ 19' \text{ N } 86^\circ 25' \text{ W}$) (Figure 1). MMSF is located in the Ohio River Valley, a region characterised by high emissions of nitrogen and sulphur oxides, and increasing NH_3 emissions due to animal husbandry. MMSF is a secondary successional broadleaf forest with a spatially consistent canopy at 25 m. Data collected during four field campaigns are presented here. Two campaigns were conducted in spring during the period from bud-break to near complete leaf out; April 19 - May 5, 1998



and April 20 - May 5, 1999. The winter field campaigns were conducted during January 8 - 19, 1999 and February 25 - March 2, 2000. An overview of nitrogen measurements conducted at MMSF is given in Table 1.

	Instrumentation	Sampling	Heights (m)	Notes
HNO ₃	NaCl coated denuders	8-16 hour integrated	25, 37.7, 45.7	3-14 samples, 2-4 blanks per height
NH ₃	Oxalic acid coated denuders	8-16 hour integrated	25, 37.7, 45.7	3-14 samples, 2-4 blanks per height
NH ₃	Wet Effluent Diffusion Denuders (WEDD)	Continuous (2 min. av.)	25, 37.7, 45.7	
Particle size/composition	MOUDIs (analysis by IC)	8-24 hour av.	25, 39.6	10 stages.
Particle size distribution	TSI APS 3320 & AEROCHEM wet-dry	10 second av.	39.6	Dp < 0.524 - 19.81 μm
Wet dep. throughfall		Event basis	25 m, below canopy	

Table 1. Nitrogen measurements at MMSF.

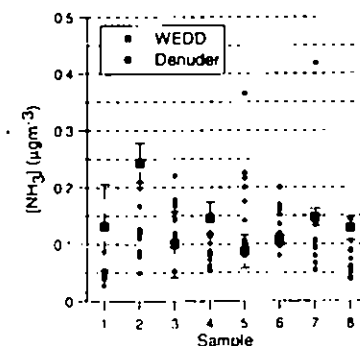
Measurement technique

Filter packs or active denuders (e.g. Andersen et al., 1993, Sutton et al., 1993) require long averaging times, have high analytical demands and typically have relatively low precision which limits their utility for quantifying vertical gradients of NH₃. Here we report continuous measurements of NH₃ made using WEDD systems designed after Soerensen *et al.* (1994). WEDDs use a similar concept to denuders, but water is used to collect the gas of interest and concentrations are measured in situ. Gas calibrations are not currently practical for field operation, so the systems were calibrated daily in the field using three to six liquid standards and a zero point and indicate linear response in the range of anticipated atmospheric concentration (Pryor *et al.*, 1999b). Two WEDD systems were co-located and independently calibrated at Indiana University during September 1999. Over 90% of the two minute mean NH₃ concentrations showed a difference of < ± 8 % for concentrations in the range 0.4 - 4 μg m⁻³. Also co-located measurements at MMSF conducted during February 2000 indicate good correspondence between 8-14 hour average NH₃ concentrations (blank corrected) measured using 12 denuders and mean and standard deviation WEDD concentrations averaged to the same time interval (Figure 2).

Figure 1. Location of the MMSF tower (marked by the asterisk).



Figure 2. Comparison of denuder and mean and standard deviation WEDD concentrations.



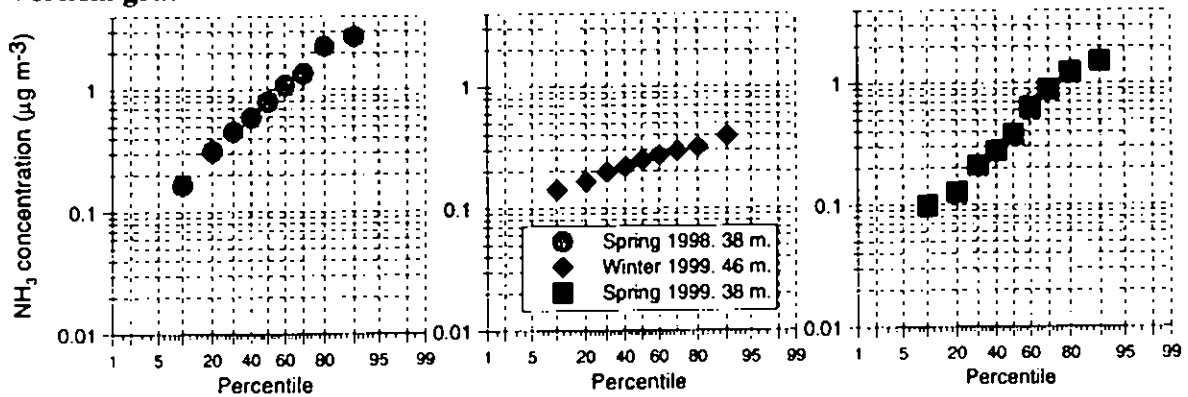


Ammonia concentrations at MMSF

Figure 3 presents example NH_3 concentration probability distributions for the spring 1998, winter 1999 and spring 1999 field campaigns. As shown, data from each campaign conform to a log-normal distribution. As shown in Figures 2 and 3, NH_3 concentrations were considerably lower during the winter measurement campaigns than during the spring campaigns. Observed concentrations during all campaigns seldom dropped below $0.1 \mu\text{g m}^{-3}$ indicating that this may be a regionally representative background concentration.

Figure 3. Example probability distributions of NH_3 concentrations from field campaigns conducted during April 19th - May 5th, 1998, January 8th - 19th, 1999 and April 20th - May 5th, 1999

Vertical gradients of ammonia concentrations at MMSF



During three of the seventeen sampling days during April-May 1999 an inverted vertical gradient of NH_3 was observed above the canopy (e.g. Figure 4). When inverted gradients were observed, the lower WEDD system exhibited higher concentrations than at 46 m during the daytime and lower concentrations during the previous and subsequent night. This observation is in accord with Wyers and Erisman (1998) and laboratory studies which suggest a temperature dependence of the NH_3 compensation point. Assuming the inverted vertical gradients observed are due to canopy emission of NH_3 (either via surface drying and evaporation of NH_3 or stomatal release), the flux of NH_3 may be calculated from (Andersen *et al.*, 1993):

$$F_c = -u_* c_* \quad (1)$$

Where: u_* = friction velocity (\propto momentum flux) calculated from a sonic anemometer located at 45.7 m (where, $u_*^2 = \sqrt{u'w'^2 + v'w'^2}$). c_* = flux concentration gradient (\propto concentration gradient) determined from:

$$c_* = \frac{\kappa(C_2 - C_1)}{\ln\left(\frac{z_2 - d}{z_1 - d}\right) - \left[\Psi_C\left(\frac{z_2 - d}{L}\right) - \Psi_C\left(\frac{z_1 - d}{L}\right)\right]} \quad (2)$$

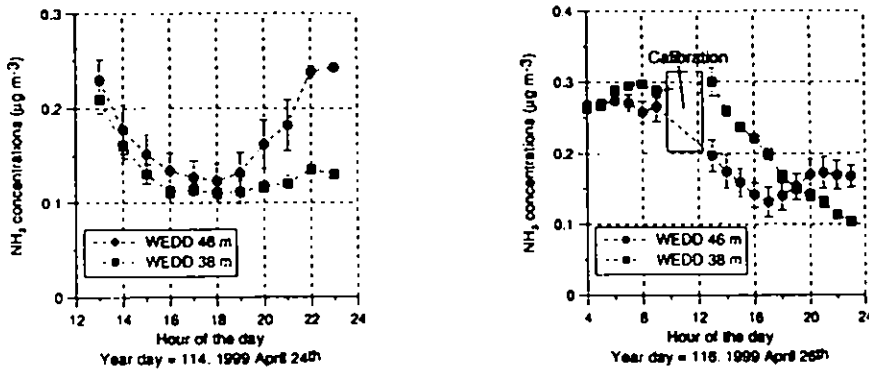
Where: C_x = concentration at height x . z_x = height. Ψ_C = stability correction. d = displacement height. L = Monin-Obhukov length.

Using (1) and (2) the net NH_3 flux over year day 116 (April 26th) of 1999 (for near-neutral conditions) is equivalent to a net emission for the day of $1 \text{ mg } \text{NH}_3 \text{ m}^{-2}$ with a peak hourly averaged (apparent) emission flux of $0.055 \mu\text{g m}^{-2} \text{ s}^{-1}$. On day 114 (April 24th) conditions



were also near-neutral, and the more common situation of lower concentrations at 38 m height resulted in a cumulative deposition flux of $1.8 \text{ mg NH}_3 \text{ m}^{-2}$.

Figure 4. NH_3 concentrations at 38 and 46 m for two days during the Spring 1999 field campaign. Data are shown for April 24th 1999 (left) and April 26th 1999 (right). All times are local.



There are several possible sources of the apparent emission flux of NH_3 at MMSF other than loss of NH_3 from the stomata. One possibility is loss of NH_3 from soils. However, the pH in de-ionised water of the upper 10 cm of the soils at MMSF is 5.4 (with a range of 3.5-6.5) which would tend to preclude a large soil efflux. Evaporation of moisture on the foliage surfaces may also be the cause of NH_3 fluxes from the surface since NH_3 is known to deposit on moist leaf surfaces, particularly in the presence of sulphur dioxide (Sutton *et al.*, 1993). Surface wetness was not measured during April 1999, but humidity measurements do not support volatilization due to evaporation of surface moisture. Finally, gas-particle exchange can cause inverted concentration gradients. Due to the differing deposition velocities for NH_3 , HNO_3 and particle ammonium nitrate (NH_4NO_3), dis-equilibrium between NH_4NO_3 and NH_3 and HNO_3 may arise in the surface layer leading to evaporation or condensation of NH_4NO_3 (Kramm and Dlugi, 1994). To examine the potential for chemically induced flux divergence as a source of the apparent emission of NH_3 the response time of chemical processes (τ_c) may be compared to the response time (τ_d) of diffusive transfer. Where $\tau_d/\tau_c \sim 1$ chemical time scales are of the same order as transport time scales and hence chemical processes can significantly modify the transfer of NH_3 to/from the canopy. τ_d and τ_c , may be estimated using:

$$\tau_c = \frac{1}{3D \int_0^\infty \frac{m(R_p)dR_p}{\left(1 + \frac{\lambda}{\alpha R_p}\right) R_p^2 \rho_p}} \quad (3) \quad \tau_d = \frac{\kappa(z+z_0)}{1.56u_*} \quad (4)$$

Where; D = molecular diffusivity. α = accommodation coefficient. $m(R_p)$ = mass distribution. R_p = particle radius. λ = mean free path of molecules. ρ_p = particle density (Wexler and Seinfeld, 1992). κ = von Karman constant. z_0 = roughness length. u_* = friction velocity (De Arellano and Duynkerke, 1992).

Particle and HNO_3 measurements are not available for spring 1999, so to investigate whether chemically induced flux divergence may be occurring at MMSF we analysed data from spring 1998. Evidence of NH_4NO_3 dis-equilibrium can be obtained by comparing the equilibrium dissociation constant (K_e) for solid NH_4NO_3 .

$$\ln K_e = 84.6 - \frac{24220}{T} - 6.1 \ln \left(\frac{T}{298} \right) \quad (5)$$



Where: T = absolute temperature (mean T for the duration of HNO_3 sampling).

with the dissociation constant for the observed gas phase concentrations (K_p) calculated as the product of the measured HNO_3 and NH_3 samples:

$$K_p = p_{\text{NH}_3} \cdot p_{\text{HNO}_3} \quad (6)$$

Where: p_{NH_3} and p_{HNO_3} (ppb) are the partial pressures for 1 atmosphere (Seinfeld and Pandis, 1998).

The results suggest dis-equilibrium conditions favouring evaporation of NH_4NO_3 (defined as $K_p < K_e \cdot 0.5$) for six of the eleven periods for which HNO_3 and NH_3 measurements are available from spring 1998. Although K_e from (5) is strictly applicable only for solid NH_4NO_3 , and relative humidities above the deliquescence relative humidity for NH_4NO_3 were observed at the site, this analysis suggests the potential for NH_4NO_3 dissociation.

In order to calculate τ_d and τ_c for the spring 1998 data we made the following assumptions; all ammonium and nitrate is present as NH_4NO_3 giving an upper bound on the NH_4NO_3 size distribution, the particle radius of each stage of the MOUDI is adequately characterised by the 50% cut point (adjusted for flow variability as in Pryor *et al.* (1999a)), the accommodation coefficient of NH_3 is 0.1 (Wexler and Seinfeld, 1992), and the diffusive time scale can be estimated using a sample mean u . τ_d was calculated using $z+z_0$, and $z+z_0+d$, where d is the displacement height ($d = 3/4$ canopy height, (Jensen and Hummelshoj, 1995)) to bound the possible effects of canopy v. sub-canopy deposition. As shown in Figure 5, for ten of the 15 time integrated particle composition samples τ_d calculated including the displacement height is within an order of magnitude of τ_c implying potential for flux divergence of NH_3 due to evaporation of NH_4NO_3 particles and release of NH_3 . The average concentration of NH_4NO_3 particles approximated as outlined above is $3 \mu\text{g m}^{-3}$, hence if evaporation of NH_4NO_3 is responsible for addition of $0.1 \mu\text{g m}^{-3}$ NH_3 at the lower sampling height (as observed on April 16th) this equates to evaporation of 1/6 of the NH_4NO_3 mass.

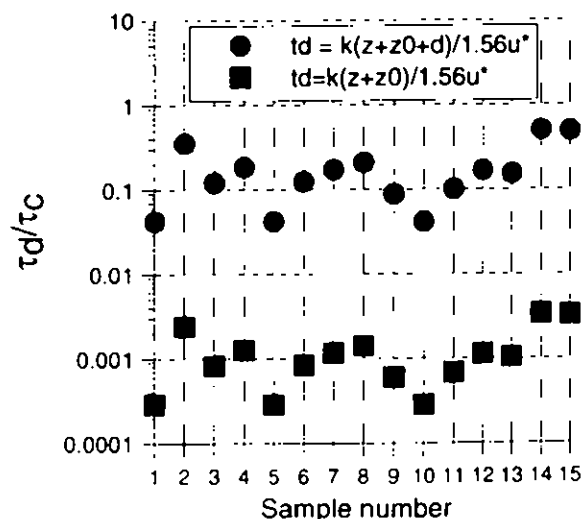


Figure 5. Sample average diffusive and chemical time-scales for NH_4NO_3 during the spring 1998 field campaign. The duration of the sample periods is variable between 8 and 16 hours.

Summary and conclusions

Ammonia concentrations measured at a regionally representative location over a deciduous forest during spring and winter field campaigns indicate mean concentrations of 0.6-1.2 and



0.1-0.3 $\mu\text{g m}^{-3}$, respectively. Observed concentrations seldom dropped below 0.1 $\mu\text{g m}^{-3}$ indicating that this may be a regionally representative background concentration.

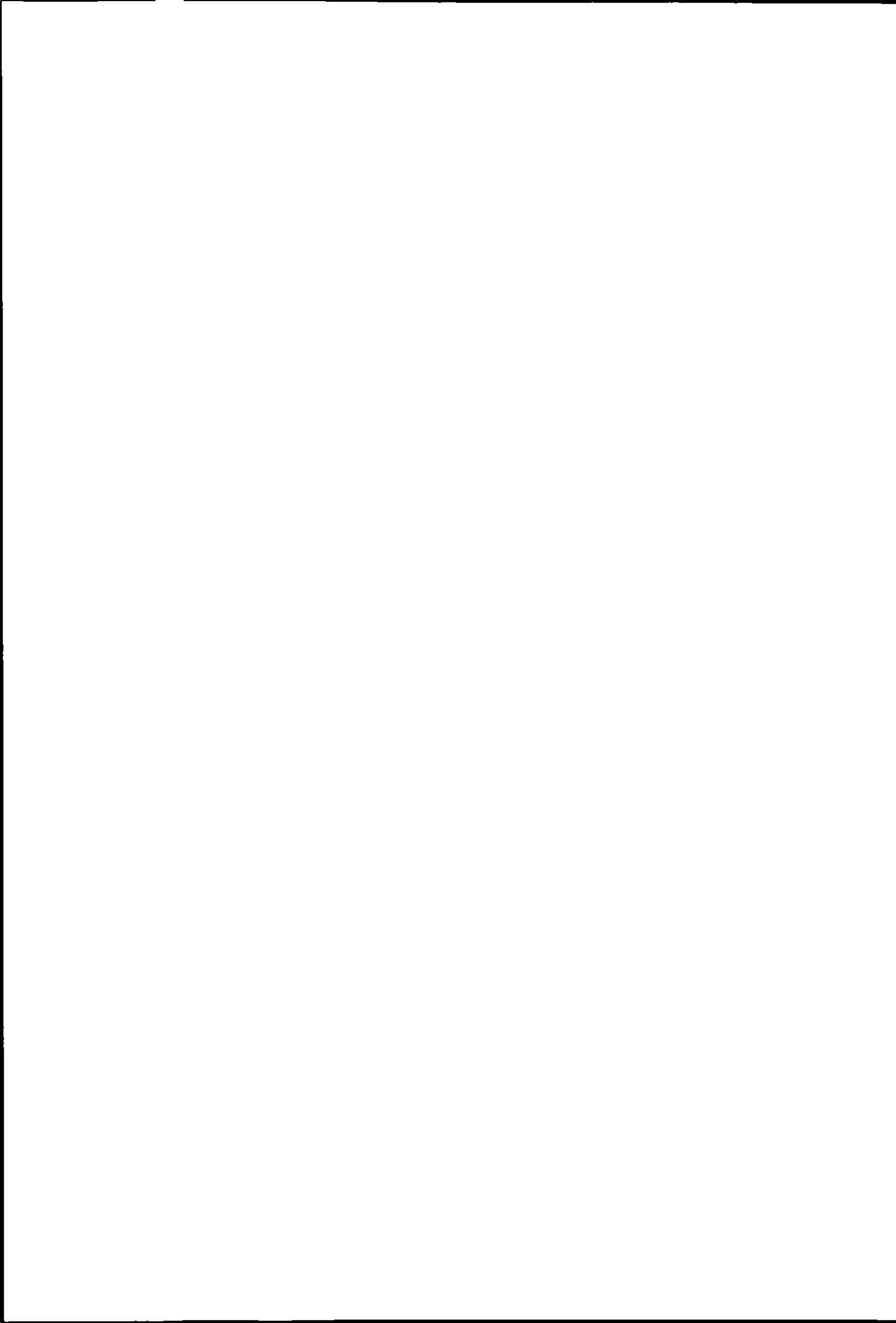
On average the forest acts as a sink of NH_3 , with a representative daily deposition flux of 1.8 $\text{mg-NH}_3 \text{ m}^{-2}$ during the spring. However, on three of the seventeen days of intensive sampling during April and May 1999 inverted concentration gradients of NH_3 were observed during daylight hours. The maximum hourly average vertical gradient between 46 - 38 m was - 0.1 $\mu\text{g m}^{-3}$ resulting in an upward flux of nearly 0.2 $\text{mg-NH}_3 \text{ m}^{-2} \text{ hr}^{-1}$ (approximately 3 $\text{nmol m}^{-2} \text{ s}^{-1}$) leading to a net emission flux for the day. If this apparent emission flux is solely generated by canopy emission this flux is at the upper limit of cuvette measurements of stomatal release from oil seed rape presented in Asman *et al.* (1998). However, there is evidence that the inverted vertical gradient of NH_3 may be due to evaporation of NH_4NO_3 particles.

Acknowledgements

The authors acknowledge financial support from NIGEC Midwestern Regional Center (grant 901214-IND) and the National Science Foundation (grant ATM-9977281). Thanks to Nicole Welch for soil pH data, Deb Backhus for laboratory space, Ford Cropley and Sue Grimmond for meteorological data and the Danish National Environmental Research Institute for chemical analysis of the 1998 samples.

References

- Andersen, H., Hovmand, M., Hummelshoj, P. and Jensen, N., 1993: *Atmospheric Environment*, **27A**, 189-202.
- Asman, W.A.H., Sutton, M.A. and Schjorring, J.K., 1998: *New Phytologist*, **139**, 27-48.
- De Arellano, J. and Duynkerke, P., 1992: *Boundary-Layer Meteorology*, **61**, 375-387.
- Jensen, N.O. and Hummelshoj, P., 1995: *Agricultural and Forest Meteorology*, **73**, 339-352.
- Kramm, G. and Dlugi, R., 1994: *Journal of Atmospheric Chemistry*, **18**, 319-357.
- Langford, A.O. and Fehsenfeld, F.C., 1992: *Nature*, **253**, 581-583.
- Pryor, S.C., Barthelmie, R.J., Geernaert, L.L.S., Ellermann, T. and Perry, K., 1999a: *Atmospheric Environment*, **33**, 2045-2058.
- Pryor, S.C., Barthelmie, R.J. and Jensen, B., 1999b: *Geophysical Research Letters*, **26**, 691-694.
- Seinfeld, J. and Pandis, S., 1998: *Atmospheric chemistry and physics: from air pollution to climate change*. Wiley-Interscience, 1326 pp.
- Soerensen, L.L., Granby, K., Nielsen, H. and Asman, W.A.H., 1994: *Atmospheric Environment*, **28**, 3637-3645.
- Sutton, M.A., Pitcairn, C. and Fowler, D., 1993: *The exchange of ammonia between the atmosphere and plant communities*, Advances in Ecological Research. Academic Press, pp. 301-393.
- Wexler, A. and Seinfeld, J., 1992: *Atmospheric Environment*, **26**, 579-591.
- Wyers, G.P. and Erisman, J.W., 1998: *Atmospheric Environment*, **32**, 441-451.



Exchange of atmospheric ammonia with European grasslands

M.A. SUTTON¹, C. MILFORD¹, E. NEMITZ¹, M.R. THEOBALD¹, P.W. HILL¹, D. FOWLER¹,
J.K. SCHJØRRING², M.E. MATTSSON², K.H. NIELSEN², J.W. ERIJSMAN³, R. OTJES³,
A. HENSEN³, J. MOSQUERA³, P. CELLIER⁴, B. LOUBET⁴, M. DAVID⁴, S. GENERMONT⁴, A.
NEFTEL⁵, A. BLATTER⁵, B. HERRMANN⁵, S.K. JONES⁵, L. HORVATH⁶, T. WEIDINGER⁶, R.
MESZAROS⁶, J. RASO⁶, C., MANTZANAS K.⁷, KOUKOURA Z.⁷, M. GALLAGHER⁸, M. FLYNN⁸
AND M. RIEDO^{1,5}

¹ CEH Edinburgh, Bush Estate, Penicuik, Midlothian, EH26 0QB, Scotland, UK.

² Royal Veterinary and Agricultural University (RVAU), Copenhagen, Denmark.

³ Netherlands Energy Foundation (ECN), Petten, The Netherlands.

⁴ National Institute for Agronomic Research (INRA), Thiverval-Grignon, France.

⁵ Institute of Environmental Protection and Agriculture (IUL), Bern-Liebefeld, Switzerland.

⁶ Forest Research Institute (FRI), Eotvos Lorand University and Inst. Atmos. Physics,
Budapest, Hungary

⁷ School of Agronomy, Aristotle University of Thessaloniki (AUT), Thessaloniki, Greece

⁸ University of Manchester Institute of Science and Technology (UMIST), Manchester, UK.

A new European scale programme has been established to address the biosphere-atmosphere exchange of ammonia (NH_3) with grasslands. GRAMINAE (GRassland AMmonia INteractions Across Europe) has set up a transect of six field sites from Scotland to Hungary and Greece to measure NH_3 fluxes using micrometeorological methods. At each site measurements are made to interpret fluxes in relation to atmospheric conditions, grassland management, sward characteristics and soil chemistry. These measurements are supported by laboratory and field studies of NH_3 exchange and bioassays of the NH_3 'stomatal compensation point' (χ_s). The aerodynamic gradient method (AGM), applying sensitive continuous NH_3 detectors, provides the core micrometeorological approach. Relaxed eddy accumulation (REA) is also being applied to enable flux measurements at one height; this is relevant to help address flux divergence due to gas-particle inter-conversion or the presence of local sources in a landscape.

Both the field and laboratory measurements demonstrate the bi-directional nature of NH_3 fluxes, with typically daytime emission and small nocturnal deposition. They also confirm the existence of enhanced NH_3 emissions following cutting of intensively managed swards. Further increased emissions follow fertilization), although in both cases most of the emission appears to be due to foliar emissions from the remaining sward. Measurements using REA support these patterns. However, the advantage of measuring at one height is partly offset by a requirement for greater analytical precision than with the AGM.

The results are being used to develop resistance models applying a 'canopy compensation point' approach to reproduce the bi-directional NH_3 fluxes. Key applications of the work include the incorporation of the resistance models in wider models of local and regional NH_3 dispersion and to assess scenarios of global change.

Introduction

Ammonia (NH_3) occurs naturally in the atmosphere, but most of the European emission (>90%) is of anthropogenic origin. The largest source is volatilization from livestock wastes with a significant fraction from fertilized agricultural land. NH_3 is important since:

- with emissions of SO_2 and NO_x , it contributes to long-range pollutant transport and acidic deposition - "acid rain",



- with emissions of NO_x it causes eutrophication of sensitive N-poor ecosystems - changing species composition of threatened habitats.
- atmospheric reaction of NH_3 produces ammonium aerosol (NH_4^+), which contributes to a negative global warming potential.

While NH_4^+ may be transported for >1000 km, deposition of NH_3 is largest in source areas. Hence relict natural habitats in intensive agricultural landscapes are particularly at risk.

Policy context

The 1979 Geneva Convention on Long-Range Transboundary Air Pollution (CLRTAP) was established under the auspices of the UNECE to tackle European air pollution as an international problem. In 1984 the first Sulphur Protocol ("30% club") was signed, and this was followed in 1991 by the NO_x Protocol, and in 1994 with the Second Sulphur (Oslo) Protocol. The agreements have now shifted from simple % cuts, to an effects-based approach minimizing the European exceedance of deposition over ecosystem sensitivity thresholds ('critical loads').

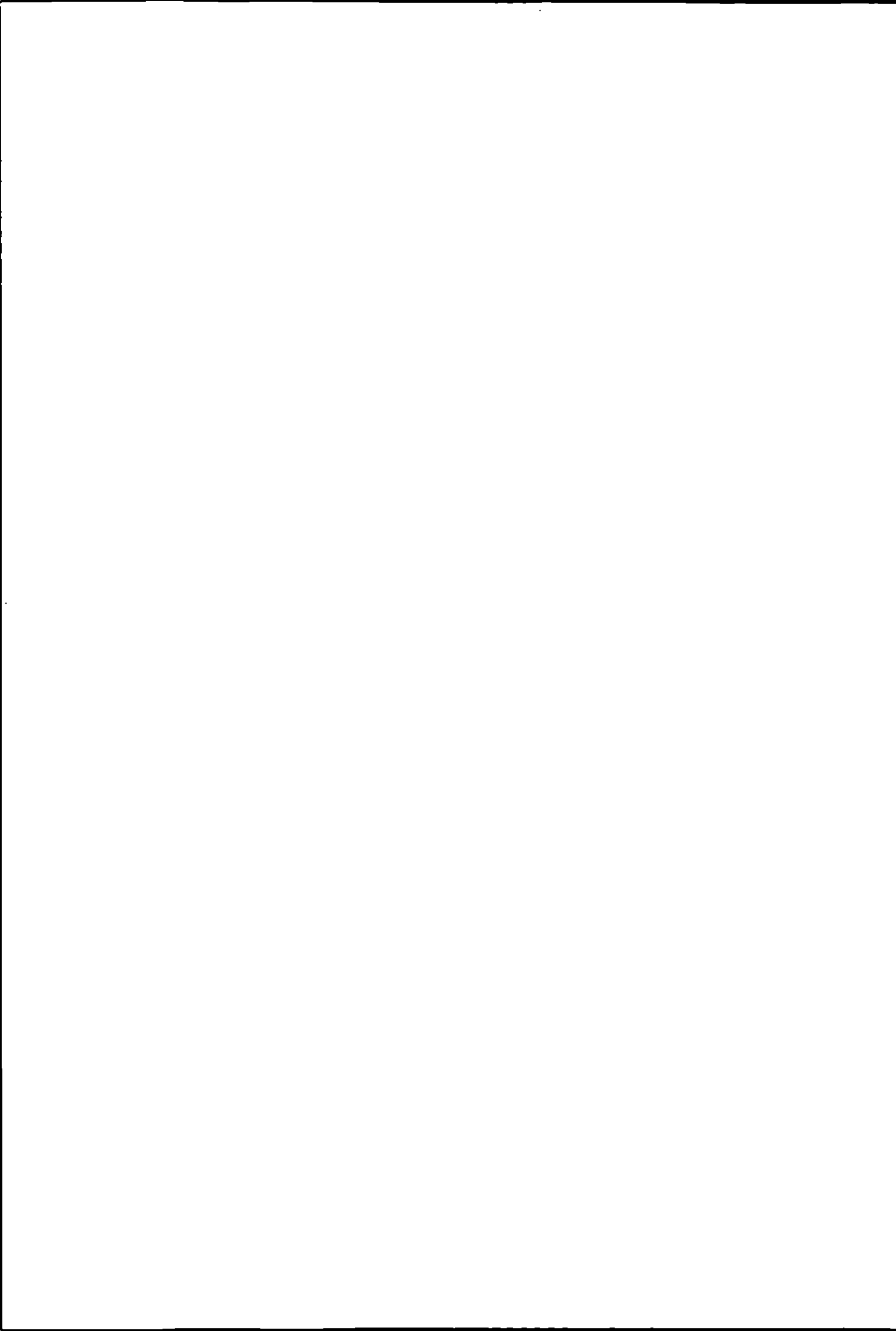
Since 1994, the Convention has been negotiating revision of the NO_x protocol and to deal with the linked issues is taking a multi-pollutant, multi-effect approach, including effects of NO_x , NH_3 , SO_2 and VOCs. Hence, international abatement of NH_3 is being negotiated for the first time, with the protocol expected to be finalized in late 1999.

In parallel, the EC has developed its Acidification Strategy, which will lead to the National Emissions Ceilings (NEC) Directive, again including SO_2 , NO_x , NH_3 and VOCs.

Objectives

GRAMINAE is a 2nd tranche TERI project running between 1998 and 2001 that has been designed to address these issues. It is widely recognized that there are major uncertainties in the quantification of the atmospheric NH_3 cycle. A key element is the biosphere-atmosphere exchange process. Data on this aspect are essential to parametrize the European transboundary models used in both the UNECE and EC negotiations. With this in mind, GRAMINAE has the following objectives:

- to quantify emissions from different sources (including land area sources such as intensive agricultural land)
- to quantify the rates of NH_3 deposition to receiving ecosystems
- to understand & quantify the biospheric controls on these processes
- to understand the controls on NH_3 - NH_4^+ dynamics
- to develop models both to explain the processes and for incorporation in the European policy models used in the negotiations.



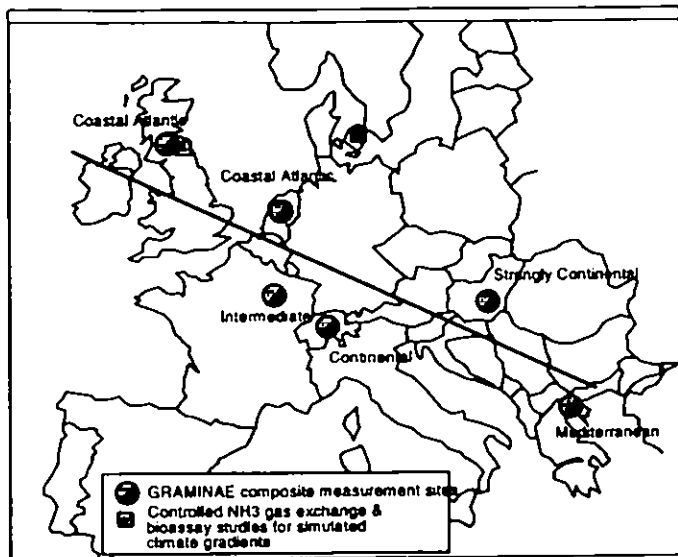


Figure 1: GRAMINAE experimental transect across Europe to address the effect of increasing continentality. It is hypothesized that biospheric controls result in longer atmospheric residence times of NH_3 in continental than in oceanic climates. This has implications for modelling the transboundary transport of NH_3 for example in estimating polluter-receptor 'blame matrices' for different European countries.

Approaches

The objectives of GRAMINAE are being achieved through:

1. Applying state-of-the-art technology to measure NH_3 fluxes with European grasslands using micro-meteorological methods.
2. Exploiting the TERI transect approach to quantify interactions with climate, particularly continentality (Figure 1).
3. Considering both I) intensive grasslands as these impact on the atmosphere (through emissions), II) semi-natural grasslands as these are impacted by the atmosphere (deposition).
4. Making complementary laboratory & interpretative measurements to understand the exchange processes.
5. Developing quantitative process based models of both I) biosphere-atmosphere exchange and II) grassland ecosystem functioning.
6. Providing the models to European policy modellers to underpin the negotiations for revision of the UNECE N Protocol, and EC NEC.
7. Engaging in the UNECE and EC negotiations on the potential for and difficulties in NH_3 abatement across Europe.

Novel scientific elements in the project include: Europe-wide analysis of NH_3 exchange with grasslands; linking of micromet approach with laboratory cuvette analysis and plant bioassays; new flux sampling methods (Relaxed Eddy Accumulation, REA) for NH_3 ; Assessment of gas-aerosol flux interactions; Assessment of biospheric controls on atmospheric NH_3 concentrations; Development of dynamic ecosystem- NH_3 flux models able to consider management practice.

Modelling ammonia fluxes

Ammonia exchanges in relation to a compensation point (χ_s) which is the concentration at equilibrium with $[\text{H}^+]$ & $[\text{NH}_4^+]$ in the apoplastic solution. Models being developed under GRAMINAE, describe the different component fluxes in relation to Ohm's Law: 'Voltage = Current x Resistance' transposes to ' $(\chi_1 - \chi_2) = \text{Flux} \times \text{Resistance}$ ' (Figure 3).



The resistances are: R_a , R_b , atmospheric transfer; R_w , uptake to leaf cuticles; R_s , stomatal transfer; R_{ac} , R_{bl} , in-canopy transfer (for the 3-layer model), while the subscripts p and f denote upper and lower canopy parts. χ is air concentration, with χ_l and χ_c the litter and canopy compensation point, respectively.

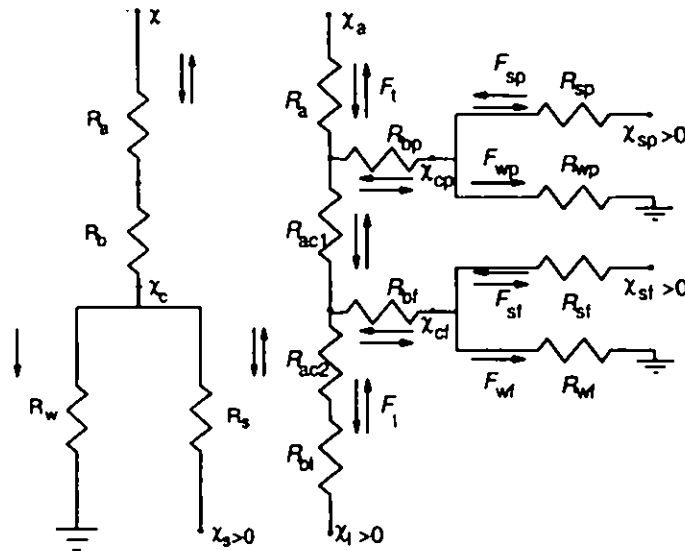


Figure 2: Example NH_3 models under development in GRAMINAE showing a 1-layer and 3-layer model. See text for explanation of concentration (χ), flux (F) and resistance (R) subscripts.

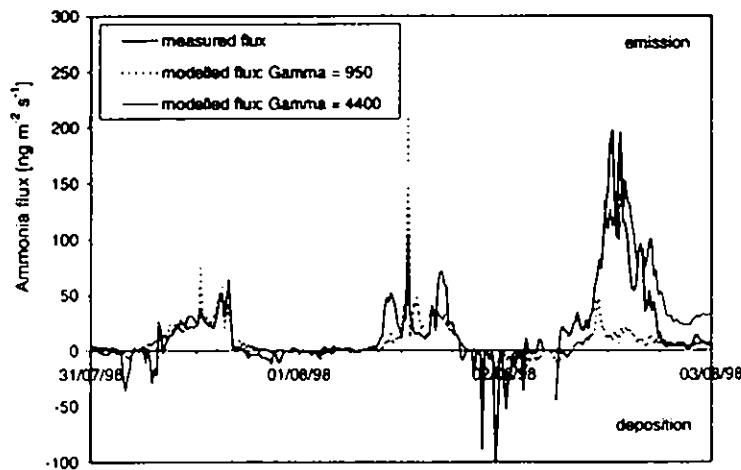
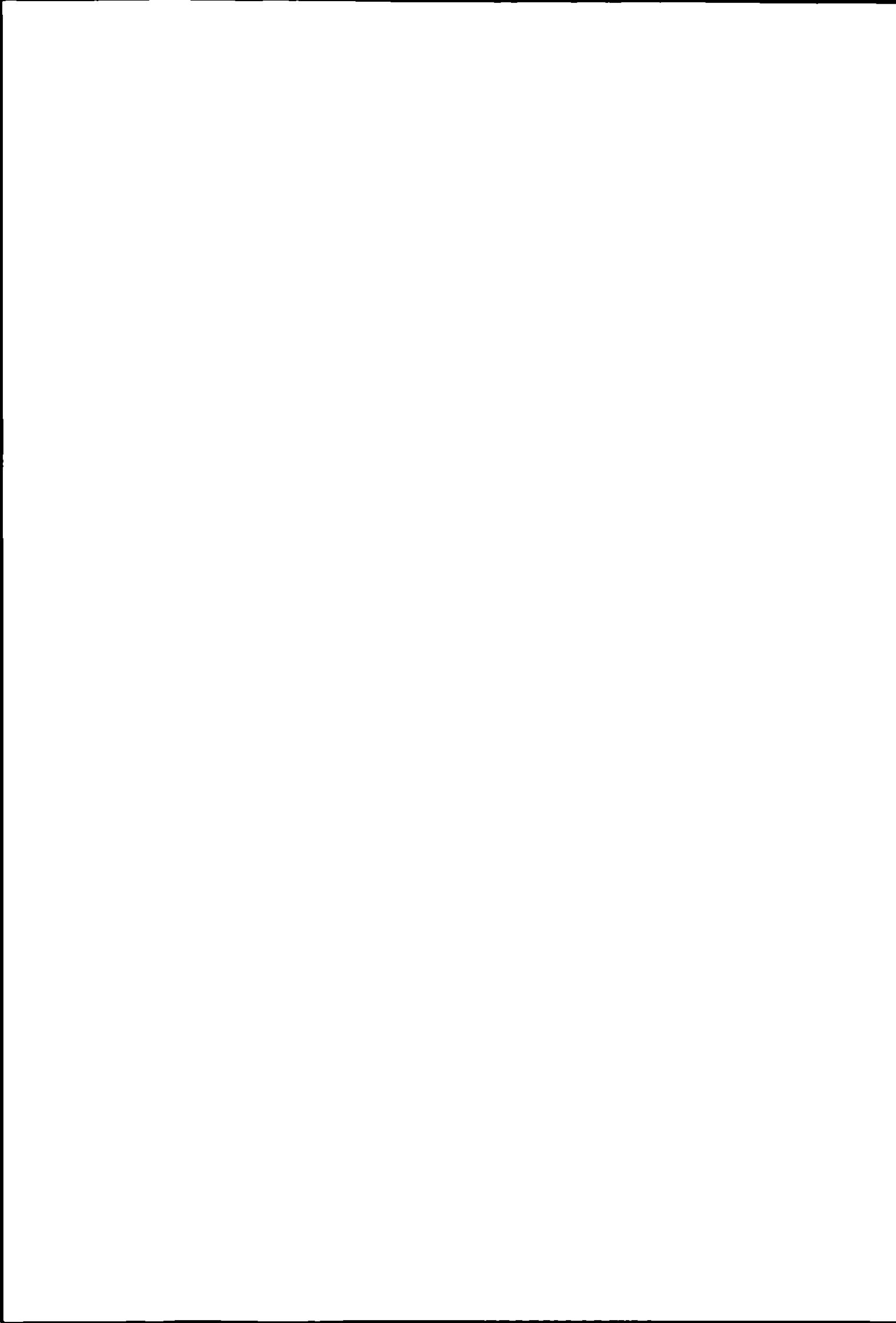


Figure 3: Example NH_3 models under development in GRAMINAE showing a 1-layer and 3-layer model. The one layer model is applied to grassland in the right hand graph.

The measurements shown in Figure 3 are for the Scottish GRAMINAE site. The period is after the second cut of the field, but before fertilization, with the grass being lifted on 2 August. The model (see Figure 2 – one layer model) is parametrized with $R_w = 30 \exp^{100 \cdot \%RH/7}$ (s m^{-1}) with the ratio of apoplastic $[\text{NH}_4^+]/[\text{H}^+] = \Gamma = 950$. The emissions following lifting of the grass would be consistent with $\Gamma > 4000$.

These results demonstrate both the close coupling of NH_3 fluxes to N turnover in the grassland, and the performance of the 1-layer model in rapidly changing conditions. A key challenge is to generalize these results for scaling up in time and for different European grasslands. In this respect GRAMINAE are coupling the NH_3 resistance modelling approaches, with dynamic grassland ecosystem models in order to develop a functional prediction of NH_3 fluxes in relation to C and N cycling.



Current policy debate - the 'Ammonia Gap'

As Europe moves towards NH_3 emissions abatement for the first time, it is important to ensure that the investment will result in environmental benefits. To do this, it is necessary to show the link between changing emissions and monitored deposition of NH_3 and NH_4^+ .

Over the last century the link is clear, with deposition estimates more than doubling at remote locations (e.g. ice cores, long-term precipitation chemistry).

However, NH_3 emissions should already have been reduced in two cases:

- *Eastern Europe* (e.g. Hungary), due to the collapse of the agricultural sector (reduced animal numbers and fertilizer consumption).
- *The Netherlands*, due to the implementation of an NH_3 abatement policy.

In both cases, analyses by GRAMINAE partners in the Netherlands, Hungary & UK have shown that the expected reductions are difficult to observe.

This has important implications for the policy negotiations, as it indicates uncertainty in our understanding of the controls on NH_3 levels. In recent discussions for the UNECE Protocol (5/1999) it was agreed that countries should proceed with caution using a selection of well established abatement techniques, but that further measurements are essential to investigate these issues.

One of the messages of GRAMINAE, is that a feedback exists (via the NH_3 'compensation point') where ecosystems can control NH_3 concentrations as well as being impacted by NH_3 deposition. In a further linkage it needs to be recognized that NH_3 abatement will be much less effective if N inputs to the system are also not reduced. Together with interactions with SO_2 chemistry, inter-annual variation and possible reduced efficiency of some abatement measures, this may go some way to explaining the ammonia gap.

Acknowledgements

We are grateful for funding of GRAMINAE through the EC TERI programme under contract ENV4-CT98-0722, for the UK, NL, DK and FR, under the EC International Co-operation Programme for HU (INCO-IN20-CT98-00118), and the Swiss National Research Foundation (SNRF) for CH. National funding is provided by Ministries of Environment and Research in the UK, NL and FR. M. Riedo is supported under a two-year TMR Fellowship (1999-2000) from the SNRF linked to GRAMINAE, MEGARICH and MAGEC.

For further details see the following example publications:

Fowler D., Coyle M., Flechard C., Hargreaves K.J., Nemitz E., Storeton-West R., Sutton M.A., Erisman J.W. (2001). Advances in micrometeorological methods for the measurement and interpretation of gas and particle nitrogen fluxes. *Plant and Soil* **228** (1):117-129.

Nemitz E., Milford C. and Sutton M.A. (2001) A two-layer canopy compensation point model for describing bi-directional biosphere/atmosphere exchange of ammonia. *Q. J. Roy. Meteor. Soc.* **127**, 815-



- Spindler G., Teichmann U. and Sutton M.A. (2001) Ammonia Dry Deposition over Grassland: Micrometeorological Flux Gradient Measurements and Bi-directional Flux Calculations using an Inferential Model. *Q. J. Roy. Meteor. Soc.* **127**, 795-814.
- Sutton M.A., Milford C., Nemitz E., Theobald M.R., Hill P.W., Fowler D., Schjoerring J.K., Mattsson M.E., Nielsen K.H., Husted S., Erisman J.W., Otjes R., Hensen A., Mosquera J., Cellier P., Loubet B., David M., Genermont S., Neftel A., Blatter A., Herrmann B., Jones S.K., Horvath L., Führer E., Mantzanas K., Koukoura Z., Gallagher M., Williams P., Flynn M. and Riedo M. (2001) Biosphere-atmosphere interactions of ammonia with grasslands: experimental strategy and results from a new European initiative. *Plant and Soil* **228** (1):131-145.
- Sutton M.A., Asman W.A.H., Ellerman T., van Jaarsveld J.A., Acker K., Aneja V., Duyzer J.H., Horvath L., Paramonov S., Mitosinkova M., Tang Y.S., Achermann B., Gauger T., Bartnicki J., Neftel A. and Erisman J.W. (2001). Establishing the link between ammonia emission control and measurements of reduced nitrogen concentrations and deposition. In: *UNECE Ammonia Expert Group (Berne 18-20 Sept 2000) Proceedings* (Eds: Menzi H. and Achermann B.) pp 57-84 Swiss Agency for Environment, Forest and Landscape (SAEFL), Bern.



Sub-grid variability in ammonia concentrations and dry deposition in an upland landscape

Y.S. TANG^{*}, U. DRAGOSITS, M.R. THEOBALD, D. FOWLER AND M.A. SUTTON

Centre for Ecology and Hydrolog (Edinburgh), Penicuik, Midlothian, Scotland, UK.

Abstract

Ground level atmospheric ammonia (NH₃) concentrations and dry deposition are spatially very variable, due to the large range of NH₃ emissions in the rural landscape, as well as large NH₃ dry deposition velocities. In the UK National Ammonia Monitoring Network, NH₃ concentrations are compared with estimates from an emission inventory and atmospheric transport model at 5 km grid resolution. However, it is recognised that mapping of NH₃ concentration and deposition at a national scale using monitoring and atmospheric transport models need to consider the extent of sub-grid variability and the representativity of sampling points.

In the present study, spatially detailed NH₃ monitoring is reported across an example upland 5 km grid square containing one of the National Network sites. This is compared with the national inventory and a local-scale dispersion model at a sub-1 km level to assess the extent to which the monitoring location is representative.

The National Network site selected (Glenshee: annual mean 2.6 µg m⁻³) was located at the side of a valley in the Scottish Highlands. Sampling for 8 months was made at 12 sites over the surrounding 5 km grid, including both valley and hill sampling locations, using a high sensitivity passive sampling method. The results demonstrate concentrations typically a factor of 4 larger in the valley than on the hills; monthly concentrations were in the range 0.15 – 2.01 µg m⁻³ and were closely correlated with the output from the local transport model. The analysis supports the performance of the 1 km emissions inventory in this landscape and provides a means to identify sampling locations representative of the 5 km grid square.

Introduction

The UK National Ammonia Monitoring Network operated by CEH (formerly ITE) on behalf of the Department of Environment, Transport and the Regions (DETR) has been running since 1996. Data from the network confirm the high spatial variability in NH₃ concentration and dry deposition across the country, reflecting the large regional variability in NH₃ emissions, and rapid rates of NH₃ dry deposition (Sutton *et al.*, 1998b).

The network currently estimates the national UK concentration field for ammonia from 90 sites and is combined with the CEH deposition model (Smith *et al.*, 2000) to provide estimates of NH₃ dry deposition. Monitored concentrations from the network (Sutton *et al.*, 1998b) are also compared with estimates from an atmospheric transport model (FRAME) at a 5 km grid resolution (Singles 1996, Singles *et al.*, 1998). The underlying NH₃ emission inventory is modelled at a 1 km resolution, using agricultural census and land cover data, and is subsequently aggregated to a 5 km grid (Dragosits *et al.*, 1998, Dragosits 1999) for input to the dispersion model.



Substantial variability in NH_3 concentration and deposition is expected even at the sub-5 km level (Dragosits *et al.* 2001). For this reason, it is important that the extent of sub-grid variability and the representativity of sampling sites in the network are considered.

In the present study, a detailed local variability study was conducted across one 5 km x 5 km grid square in an upland landscape (Glenshee in NE Scotland). The results are compared with the 5 km resolution estimates for the UK national model, and a local scale dispersion model at 250 m and 500 m grid resolution (LADD model, Hill 1996, Sutton *et al.*, 1998a). This allows the performance of the national NH_3 emission model of Dragosits *et al.* (1998) to be tested and an assessment of the representativity of the existing monitoring network site to be made.

Methods

Local scale modelling of NH_3 emissions

Ammonia emissions for the 5 km x 5 km study area were modelled at a 1 km resolution, using the CEH Landcover data and agricultural census data from 1988. Although the model of Dragosits *et al.* (1988) is also available for 1996, the 1988 estimates were used due to sensitivity of confidentiality with the data for 1996. Comparison of the two datasets for Glenshee however showed no major difference in emissions between the two years. Sheep and cattle grazing emissions are the dominant NH_3 sources within the grid square, occurring mainly within the more intensively managed valley, whereas most of the 5 km square is upland moorland (Figure 1).

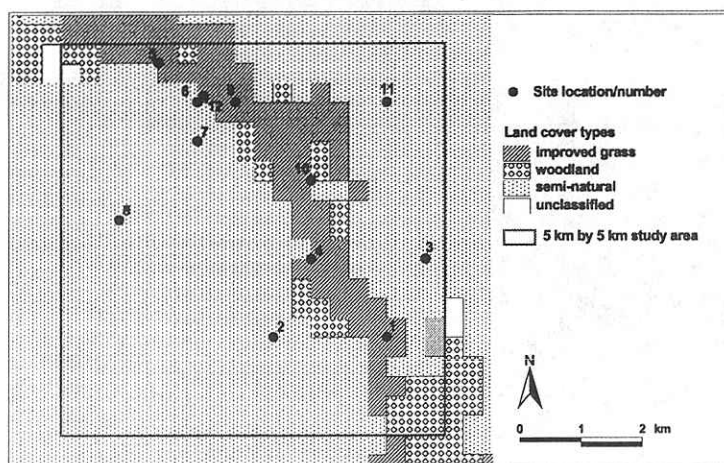


Figure 1: Land cover map of the Glenshee study area at a 250 m grid resolution, showing sampling locations with site numbers.

A model for the spatial distribution of NH_3 emission sources applied to the whole of the UK provided weighted allocations of emissions to different land cover types at Glenshee at the 1 km level (Dragosits *et al.*, 1998). This approach results in a large proportion of the emissions being realistically located in the intensively farmed areas, and only small sources of livestock grazing on the extensive upland areas. In Figure 1, land cover at 250 m grid resolution is shown, which allows a greater precision in the model analysis.



Local scale modelling of NH₃ concentrations and deposition

The LADD model (Hill 1998, Sutton *et al.* 1988a) was used to simulate atmospheric NH₃ concentration and dry deposition at 250 m and 500 m grid resolutions within the 5 km x 5 km grid. LADD is a multi-layer Lagrangian model, which utilises statistical meteorology and straight line trajectories. Information from the local scale emissions inventory at the 1 km level, plus meteorological data (obtained from Aboyne automatic weather station: 57.08 ° latitude, -2.84° longitude) are incorporated as input to the model. The concentration field output is coupled with land-use dependent deposition velocities (V_d) to provide a detailed dry deposition field. Land cover information at matching scales (250 m and 500 m resolution) is included within the model, so that the values of V_d can be varied according to land-use in the grids. Different estimates of ecosystem specific surface roughness (z_0) and canopy resistances (R_c) (Sutton *et al.*, 1998a) similar to those adopted by Singles *et al.* (1998) in FRAME are used to calculate ecosystem specific V_d , which should give improved estimates of deposition, allowing the distinction to be made between the semi-natural upland areas and agricultural lands in the valley.

Field measurements of NH₃ concentrations

The national NH₃ network site selected is located at the side of a valley in the Scottish Highlands (56.81 ° latitude, -3.45° longitude). The local variability measurements began in April 1999 and sampling for 8 months was conducted at 12 sites, including both valley and hill sampling locations (Figure 1). NH₃ concentrations were measured using a new improved high sensitivity diffusion sampler with 3 replicate samplers at each site at 1.5 m above ground (Sutton *et al.*, 1998b, Tang *et al.*, 2001). The average reproducibility of replicate samples in the field was 6 % (RSD) and the detection limit (3 µ of blanks) was 0.02 µg m³ for a one month exposure period.

Results and Discussion

Ammonia emissions map

A high degree of variability in NH₃ concentrations within the 5 km grid area was expected on the basis of the emission estimates at a 1 km resolution, as shown in Figure 2.

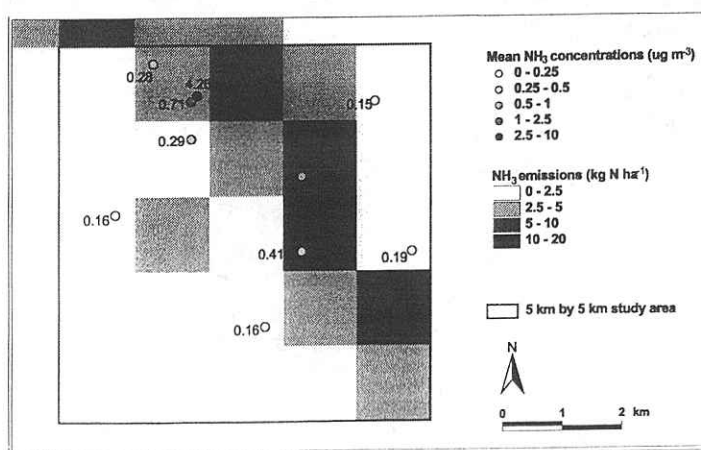
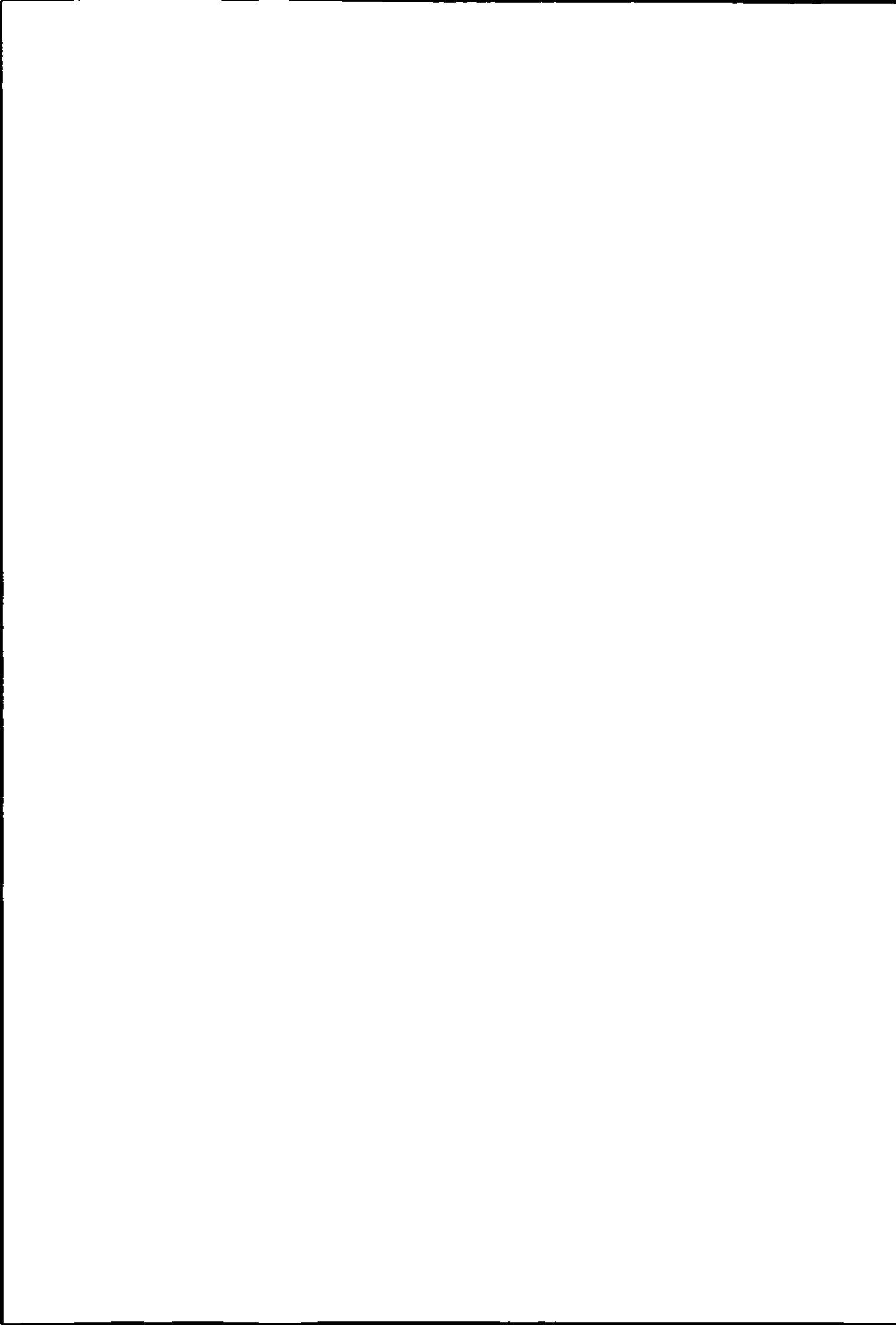


Figure 2: Modelled ammonia emissions over the study area at a 1 km grid resolution (Dragosits *et al.*, 1998), compared with the measured mean NH₃ concentrations at the 12 monitoring sites.



The emissions map shows much higher emissions in the intensively farmed valley areas with both sheep and cattle farming, against the very low background emissions over the extensive upland moorlands. Emissions from the feeding and housing of livestock, and the storage and disposal of their wastes are much larger than from grazing animals. As a result, although animals may graze hill areas at some time (e.g. sheep taken to higher pastures in summer), most of the NH_3 emissions are located within better agricultural land in the valley. The emission model of Dragosits *et al.* (1998) therefore provides realistic spatial NH_3 emissions estimates for the upland landscape, by relocating emission sources from the extensive upland areas to the more intensively farmed lowland areas within the grid square. This is a direct result of reallocation rules introduced into the emission model, which avoided the artificial location of housing and landspreading emissions in hill areas. Confidence in the accuracy of the emissions estimates is vital, since they are used as primary input into the LADD model to predict atmospheric NH_3 concentration and deposition.

Measured air NH_3 concentrations

The measured concentrations from the sampling sites also confirmed the spatial variability in relation to valley and hill locations, with concentrations typically a factor of 4 larger in the valley than on the hills (Figure 2). This provides support for the emission inventory approach developed by Dragosits *et al.* (1998).

Substantial temporal variability in ammonia concentration was observed at all the measurement sites (Figure 3).

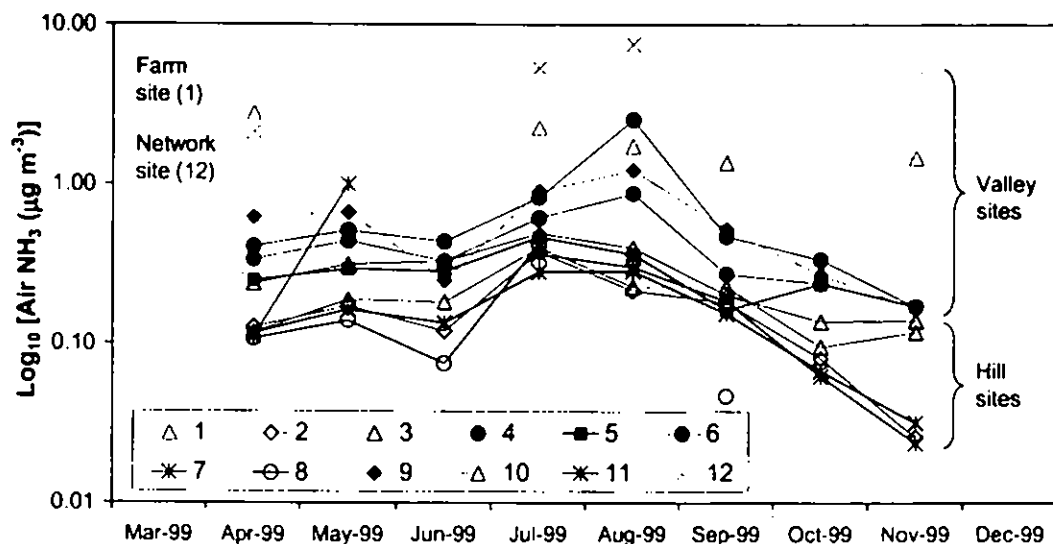
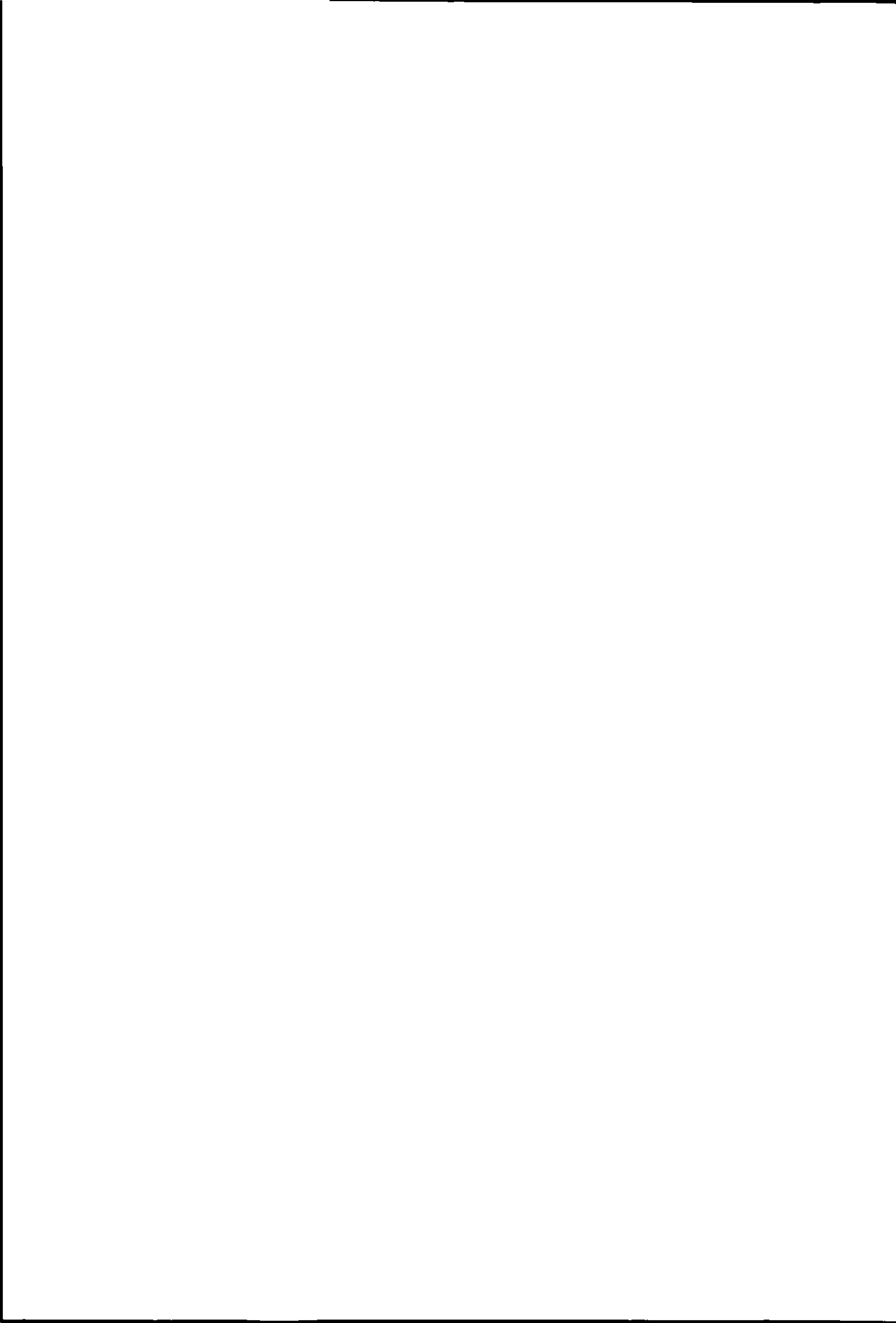


Figure 3: Temporal trends in measured NH_3 air concentrations over the 8 months study period.

At Site 1, peaks in ammonia concentrations were observed in the spring, coinciding with the usual time for land spreading of animal wastes. At all other sites, the highest concentrations occurred during the summer months, with values up to five times higher than during winter. This is due to increased potential for ammonia volatilisation in the warmer and drier conditions during the summer months. Temporal patterns for the hill sites are very similar and are typical of clean background sites (Sutton *et al.*, 1998b), where the variation in NH_3 concentration is mostly influenced by the seasonal effect on NH_3 emissions.



Ammonia concentrations at the network site (site 12) were very high for the study period, even compared with other sites in the valley area (Figure 3). The mean concentration of $4.2 \mu\text{g NH}_3 \text{ m}^{-3}$ for the study period is also larger than previous measurements prior to December 1998 (Figure 4).

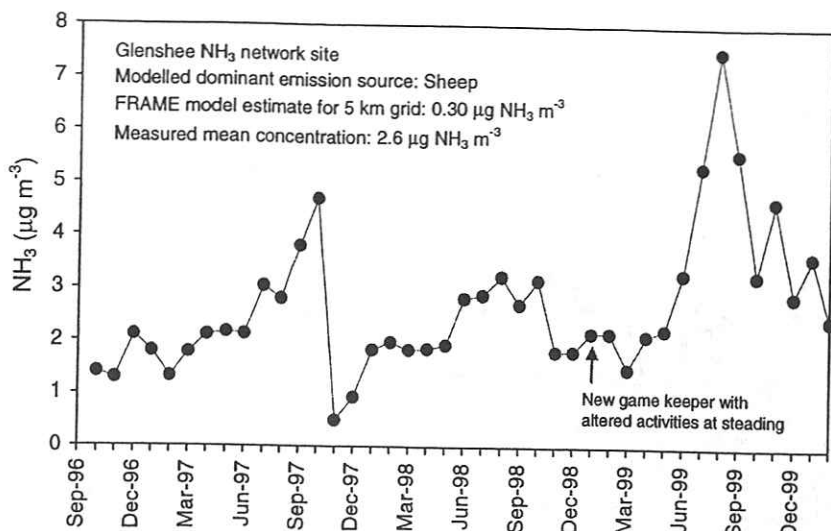


Figure 4: Long-term trend in NH_3 air concentrations at the main NH_3 network site for Glenshee from October 1996.

It transpires that this site is affected by very local sources of NH_3 (e.g. proximity of dog kennels, preparation of game and other game-keeping activities), since the concentrations decreased to $0.71 \mu\text{g NH}_3 \text{ m}^{-3}$ at site 6 over a distance of 200 m. Significant emission sources local to site 12 had not been expected, and the site location had originally been selected on the basis of being at the valley edge with mains electricity available for active sampling of both air NH_3 and aerosol NH_4^+ (Sutton *et al.*, 2001).

Modelled air NH_3 concentrations

The predicted NH_3 concentration field output from LADD at 500 m and 250 m grid resolutions are shown in Figures 5A and 5B.

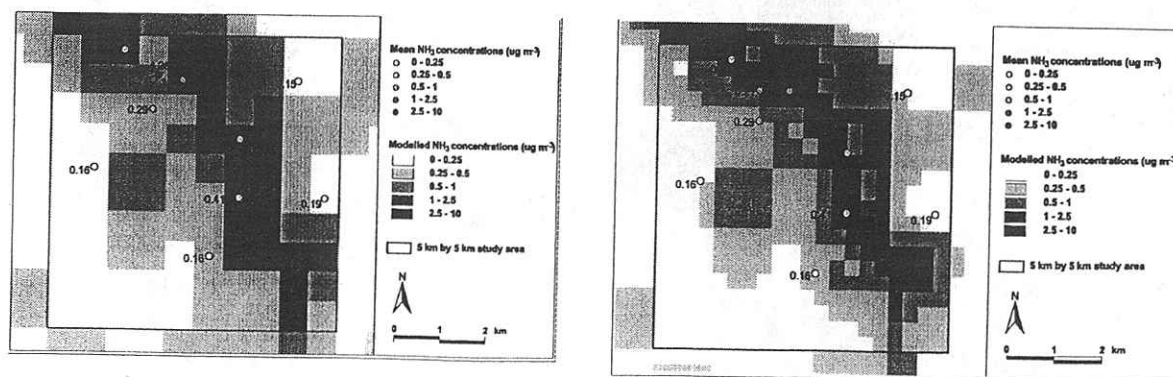
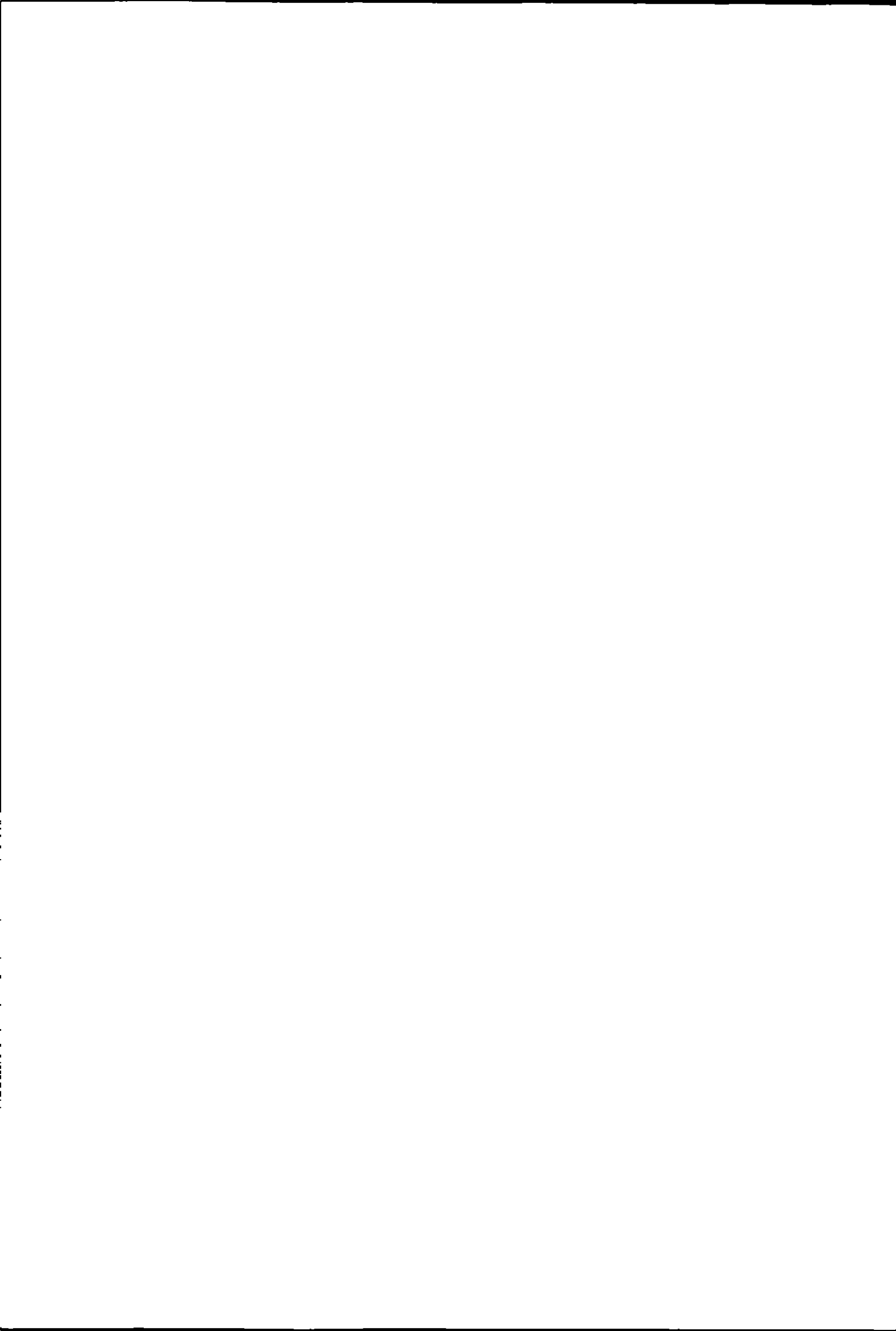


Figure 5: Modelled NH_3 air concentrations from the LADD model for the study area, with land cover data at (A) 500 m grid resolution and (B) 250 m grid resolution. The mean measured NH_3 concentrations for each sampling site are plotted on the map for comparison.



Both 500 m and 250 m estimates were made with land cover data at corresponding resolutions, to compare the difference in LADD model output when using the emissions inventory at the 1 km level. The estimates for both grid resolutions are generally similar (Figure 6), although at site 10, the LADD estimate at 500 m resolution for the grid square is about 60 % greater than at 250 m resolution. The difference between the estimates at site 10 is due to the resolution of the land cover data, which affects values of z_o and V_d .

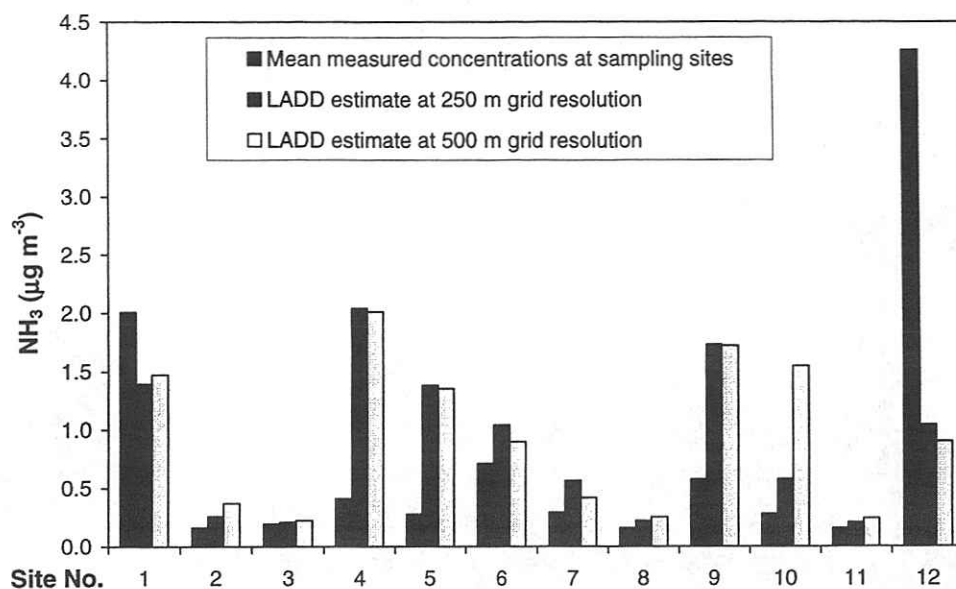


Figure 6: Comparison of measured and modelled air NH₃ concentrations at the 12 sampling locations around Glenshee.

3.4. Comparison of measured and modelled NH₃ concentrations

The local variability study at Glenshee provided data with which to test the performance of the LADD model. Good agreement was shown between the LADD model results (mean = 0.89 µg NH₃ m⁻³, range 0.21 - 2.04 µg NH₃ m⁻³) and field measurements for 11 of the 12 sampling sites (mean = 0.48 NH₃ µg m⁻³, range 0.15 - 2.01 µg NH₃ m⁻³) (Table 1).

	Mean (µg NH ₃ m ⁻³)	Min (µg NH ₃ m ⁻³)	Max (µg NH ₃ m ⁻³)
FRAME estimate for 5 km grid square	0.30	-	
LADD estimate for 5 km grid square: 250 m resolution	0.60	0.16	2.65
500 m resolution	0.62	0.18	2.46
LADD estimate for grid squares : 250 m resolution	0.89	0.21	2.04
with measurement sites 500 m resolution	0.95	0.22	2.01
Measurement data: All 12 sampling locations	0.79	0.15	4.26
11 sampling locations (excluding site 12)	0.48	0.15	2.01

Table 1: Comparison of measured and modelled air ammonia concentrations in the 5 km x 5km study area.

Overall, LADD is seen to overestimate ammonia concentrations compared with the measurements (Figure 6). This may be because of uncertainties in the diffusion processes, which are sensitive to surface roughness (z_o) and atmospheric stability, as well as the fact that this model does not describe wet deposition scavenging of ammonia. The local emission and



land cover data may also be limited by the resolutions used, which may not be sufficiently detailed to resolve the more complex landscape, especially in grid cells where semi-natural areas are integrated closely with improved grasslands. The locations of sites 4 and 5 are borderline semi-natural / improved grassland, whereas the grid cells in which site 9 is on is classified by the land cover dataset as improved grassland, when in actual fact the immediate area is interspersed with woodlands and semi-natural areas. Ammonia concentrations are also calculated within the 1 m vertical layer, whilst measurements were made at 1.5 m above ground. The vertical concentration profile of NH_3 in source regions (e.g. agricultural land in the valley) can vary by as much as a factor of 2 between heights of 1 m and 2 m, whereas the gradient is smaller in sink areas (e.g. moorland) (Sutton *et al.*, 2000). Work is currently in progress to refine the model to estimate concentrations at different vertical profiles. It is expected that this will result in better agreement with the measurements which are made at 1.5 m above ground, particularly in source areas.

Recognizing the uncertainties in the model, and the dependence of LADD on the emission inventory as a primary input, this comparison demonstrates that the Dragosits *et al.* (1998) model provides sound separation between source and sink areas in this study area. This is important to note, since this model is based on parish agricultural statistics and land cover data across Great Britain, and this study provides the first field testing of the inventory at a sub-5 km level.

The present study also provides information to assess the most representative sampling location in the 5 km grid square for future measurements. The measurements have shown that the original measurement site (Site 12) was unrepresentatively high, even compared with other sites in the valley area. Of the remaining sites, the question arises as to which is the most representative. The simplest estimate would be to calculate the mean concentration from the measurements ($= 0.48 \mu\text{g m}^{-3}$), but this is potentially biased by having too few measurements in the hill areas of the grid square. Therefore the model was used to calculate the most representative concentration, since by definition this covers the whole grid square.

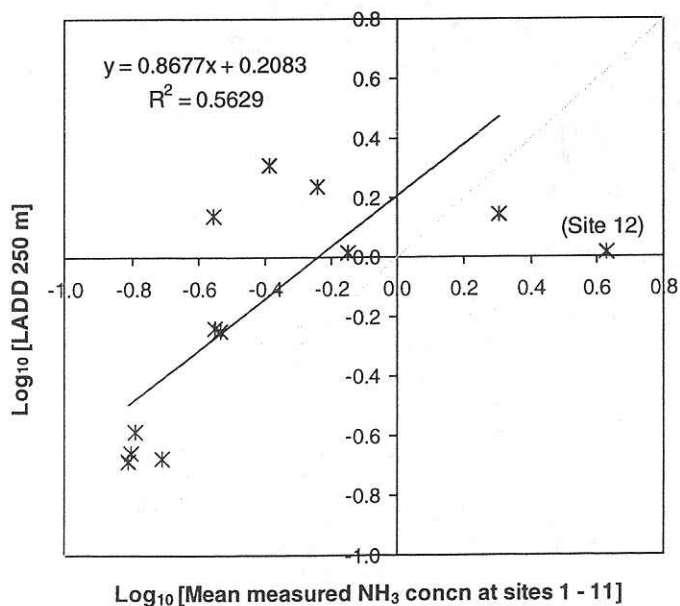


Figure 7: Regression plot of predicted NH_3 concentration ($\mu\text{g NH}_3 \text{ m}^{-3}$) from LADD at 250 m grid resolution versus the average of the field measurements from sites 1 to 11.



For this purpose the LADD estimates of NH_3 concentration at a 250 m grid resolution were used to gauge the most typical model concentration. Of the 400 250 m x 250 m estimates in the study area, the mean modelled concentration is $0.49 \mu\text{g m}^{-3}$. Applying this value to the regression of LADD using the emissions at a 250 m resolution on the average of the measurements at each monitoring site (Figure 7) would imply a mean measured concentration representative for the 5 km grid square of $0.29 \mu\text{g m}^{-3}$. LADD is taken as the independent variable in the regression, since the graph is used to estimate the most representative measured concentration. For the purpose of the regression, Site 12 has not been included, as this was established as being affected by very local sources of NH_3 . With this exception, there is a significant correlation between the model and the measurements ($R^2 = 0.56$, $P < 0.01$), once the data are transformed to a more normal distribution by taking the Log_{10} of concentration.

Three of the measurement locations provided measured concentrations close to the calculated representative concentration of $0.29 \mu\text{g m}^{-3}$: sites 5, 7 and 10. Of these, site 5 was selected for future long-term monitoring in the grid square because of the availability of a suitable site operator and the presence of electricity nearby to allow monitoring of ammonium aerosol. It may be noted that the national estimate of the FRAME model for the 5km grid square is $0.30 \mu\text{g m}^{-3}$, which is very close to the most representative measured concentration.

Modelled dry deposition of NH_3

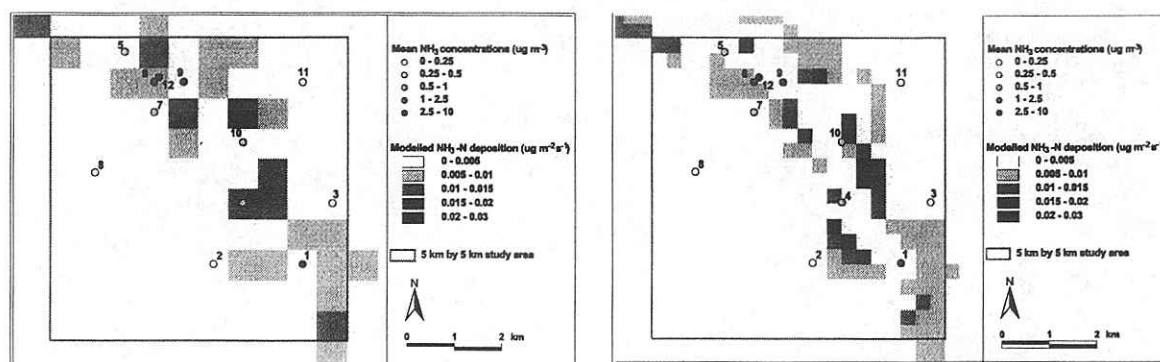
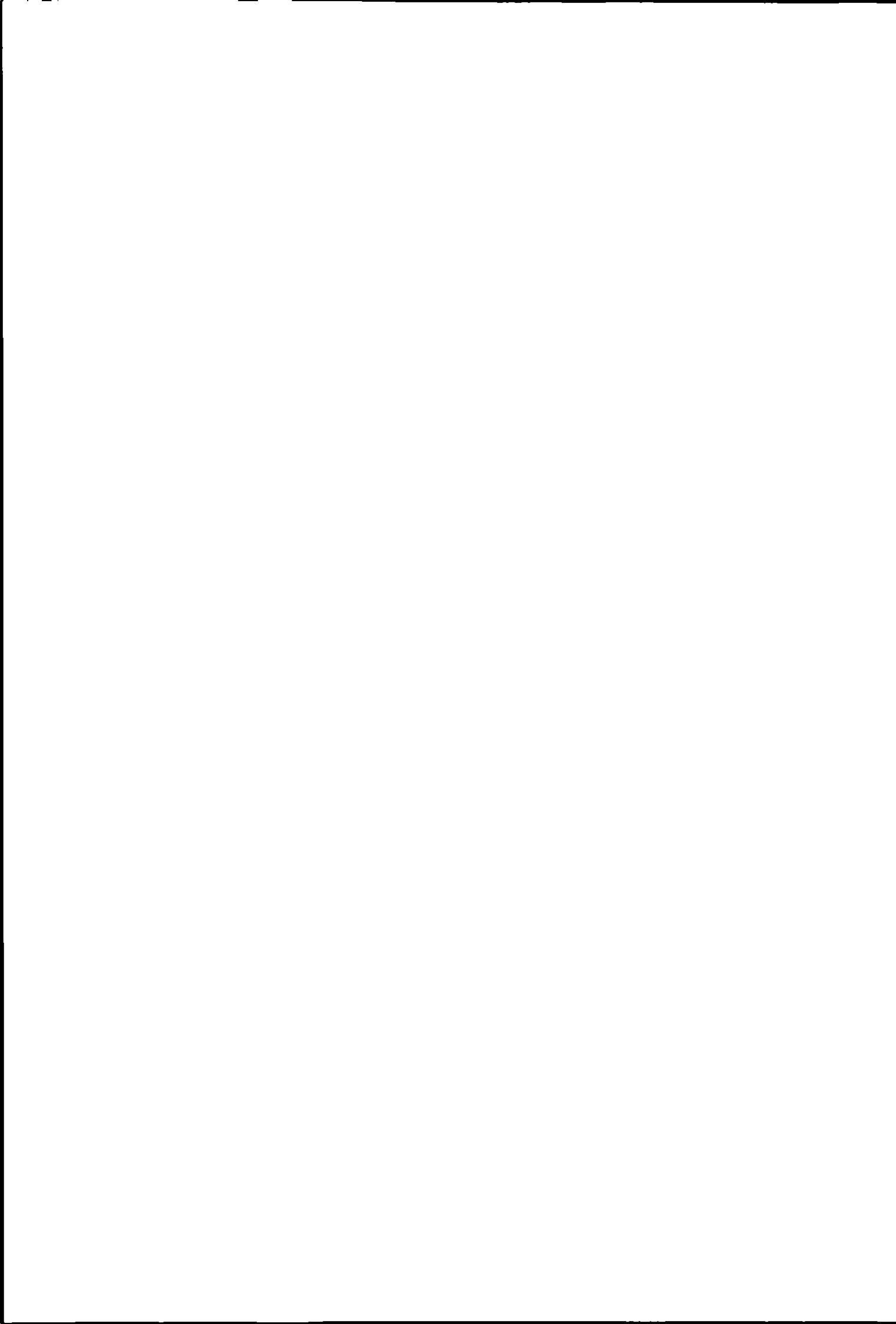


Figure 8: Modelled NH_3 -N dry deposition from the LADD model for the study area, with input data at (A) 500 m grid resolution, and (B) 250 m grid resolution.

Large spatial variability in NH_3 dry deposition was estimated within the study area (Figure 8), reflecting both the local patterns of ammonia concentration and the land-cover dependent differences in deposition velocity. Forests and moorland areas downwind of emission sources (wind direction from N / NW) received more NH_3 dry deposition on average, due to greater surface roughness (forests) and small values of R_c . Upland moorland areas further than 1 km from NH_3 sources were estimated to receive less dry deposition than moorlands adjacent to agricultural land. Although concentrations were highest over the agricultural land in the valley, dry deposition was small to these areas due to low deposition velocities. Hence the largest rates of dry deposition were to moorland and forest vegetation located along the edge of the valley bottom. The results highlight the importance of fine scale (sub-5 km) variability of NH_3 deposition in relation to impacts of N deposition.



Conclusions

Substantial variability in NH_3 air concentrations and dry deposition has been demonstrated within a 5 km x 5 km grid study area surrounding an NH_3 monitoring site in the Scottish Highlands. Ammonia concentrations were typically a factor of 4 larger in the valley (mean = $0.72 \mu\text{g m}^{-3}$, range = $0.28 - 2.01 \mu\text{g m}^{-3}$, excluding one outlier) compared with the hill areas (mean = $0.18 \mu\text{g m}^{-3}$, range = $0.13 - 0.29 \mu\text{g m}^{-3}$), and are seasonally variable, with peak concentrations in the summer. In the valley, peak concentrations were observed in the spring, coinciding with manure application to fields.

Good agreement was shown between the LADD model results and field measurements, lending support for the performance of the NH_3 emission model of Dragosits *et al.* (1998) for an upland landscape at 1 km resolution. Measured NH_3 concentrations were generally lower than LADD predictions. This may be attributed to limitations of the input data at the grid resolutions used, output of NH_3 concentrations within the 1 m vertical layer and uncertainties within the model. While the study provides measurement support for the 1 km national NH_3 emission inventory of Dragosits *et al.* (1998), further development of this approach is essential.

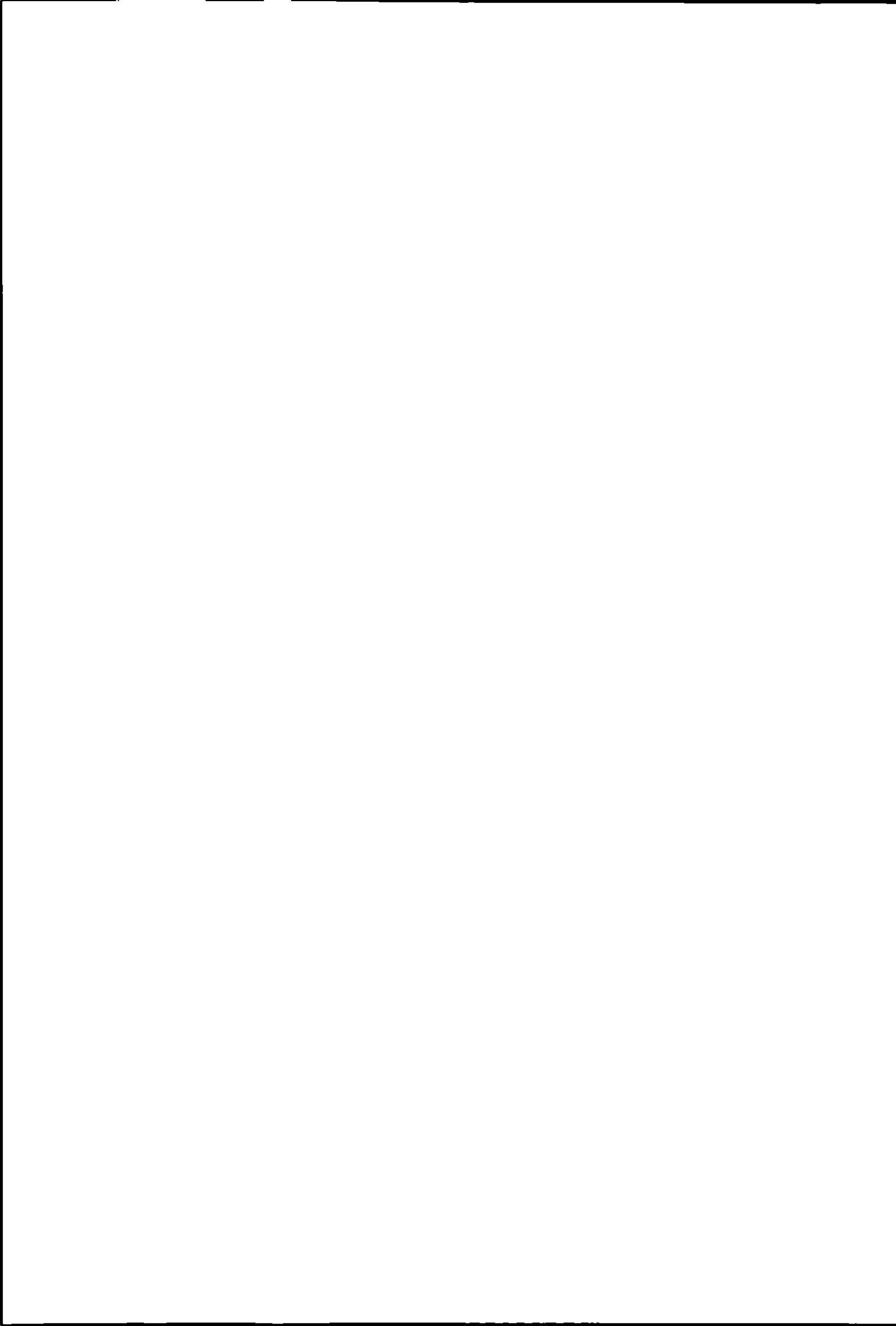
It has been established that the National Network site was an outlier influenced by very localised emission sources (e.g. gamekeeping activities), and that the monitoring location overestimated NH_3 concentrations compared with the national 5 km grid estimate due to the presence of such local sources. A more representative new sampling location for the area has been identified from this local variability study, by applying the relationship between modelled and measured concentrations for the grid square. While the previous monitoring location provided a long term mean of $2.6 \mu\text{g m}^{-3}$ (1996 - 1999), the most representative measured concentration for the grid square is $0.29 \mu\text{g m}^{-3}$. The latter compares favourably with the 5 km grid square average value of $0.30 \mu\text{g m}^{-3}$ estimated by the UK-scale FRAME dispersion model.

Acknowledgement

This work was carried out with funding from the Department of Environment, Transport and the Regions (DETR) and from supporting CEH programmes. We would like to thank the Invercauld estate, Finegand farm, Glenshee outdoor centre and Spittal of Glenshee hotel for permitting access to field sites for carrying out the monitoring work.

References

- Dragosits, U., Sutton, M.A., Place, C.J. & Bayley, A.A. (1998) Modelling the spatial distribution of agricultural ammonia emissions in the UK. *Environmental Pollution* **102**, S1, 195-203.
- Dragosits, U. (1999) *A spatially distributed ammonia emissions inventory for the UK*. Ph.D. thesis. University of Edinburgh.
- Dragosits, U., Theobald, M.R., Place, C.J., Lord, E., Webb, J., Hill, J., ApSimon, H.M. & Sutton, M.A. (2001) Ammonia emission, deposition and impact assessment at the field scale: a case study of sub-grid spatial variability. *Environmental Pollution* (in press).



- Hill, J. (1998) *Applications of computational modelling to ammonia dispersion from agricultural sources*. Ph.D. thesis, University of London.
- Singles, R.J. (1996) *Fine resolution modelling of ammonia dry deposition over Great Britain*. Ph.D. thesis, University of Edinburgh.
- Singles, R.J., Sutton, M.A. & Weston, K.J. (1998) A multi-layer model to describe the atmospheric transport and deposition of ammonia in Great Britain. *Atmospheric Environment* **32** (3) (Ammonia Special Issue), 393-399.
- Sutton, M.A., Milford, C., Dragosits, U., Place, C.J., Singles, R.J., Smith, R.I., Pitcairn, C.E.R., Fowler, D., Hill, J., ApSimon, H.M., Ross, C., Hill, R., Jarvis, S.C., Pain, B.F., Phillips, R., Harrison, R., Moss, D., Webb, J., Espenhahn, S.E., Lee, D.S., Hornung, M., Ulliyett, J., Bull, K.R., Emmett, B.A., Lowe, J. & Wyers G.P. (1998a) Dispersion, deposition and impacts of atmospheric ammonia: quantifying local budgets and spatial variability. *Environmental Pollution* **102**, S1, 349-361
- Sutton, M. A., Nemitz, E., Fowler, D., Wyers, G. P., Otjes, R. P., Schjoerring, J. K., Husted, S., Nielsen, K. H., San Jose, R., Moreno, J., Gallagher, M. W. & Gut, A. (2000) Fluxes of ammonia over oilseed rape - Overview of the EXAMINE experiment. *Agricultural and Forest Meteorology*. **105**, 327-349.
- Sutton, M.A., Tang, Y.S., Miners, B.P., Coyle, M., Smith, R. & Fowler, D. (1998b) Spatial and temporal patterns of ammonia concentration in the UK. Results of the National Ammonia Monitoring Network. Final Report to the Department of the Environment Transport and Regions (DETR), Air and Environmental Quality Division. (Contracts EPG 1/3/58). ITE Edinburgh, Penicuik.
- Sutton, M. A., Tang, Y.S., Miners, B. and Fowler, D. (2001) A new diffusion denuder system for long-term, regional monitoring of atmospheric ammonia and ammonium. *Water, Air and Soil Pollution* (in press).
- Tang, Y.S., Cape, J.N. & Sutton, M.A. (2001) Development and types of passive samplers for monitoring NO₂ and NH₃ concentrations. *The Scientific World* (under review).



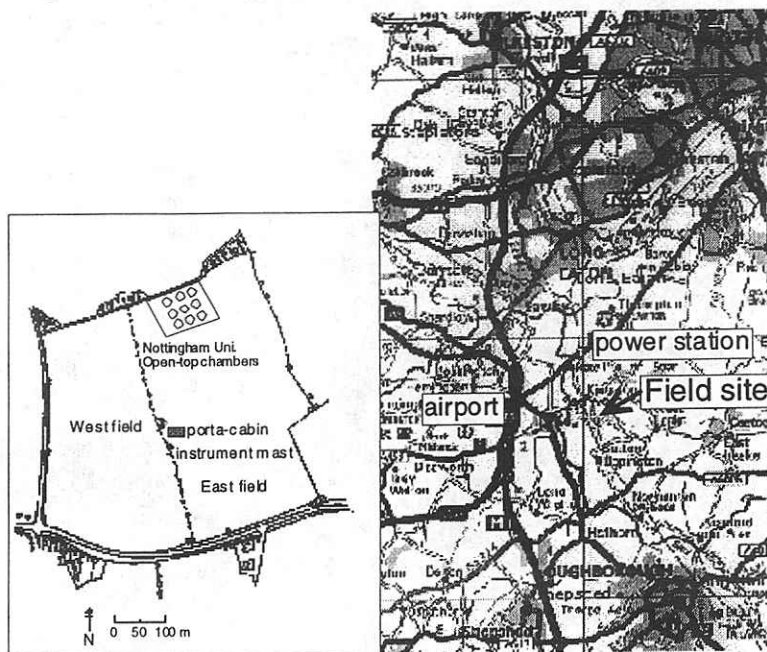
Ozone deposition at a polluted site in the English Midlands

M. COYLE, D. FOWLER, R. STORETON-WEST

Centre for Ecology and Hydrology, Edinburgh Research Station, Bush Estate, Penicuik, Midlothian, UK, EH26 0QB

Measurements of ozone deposition, using the aerodynamic flux/gradient method, started on the 1st of May 1998 at Sutton Bonnington in the English Midlands, and have been made continuously since then. The field is split into two halves from north to south, which are planted with different commercial crops, although they are not physically separated (Figure 1a). In 1998 the west field was planted with sugar beat and the east with wheat whereas during 1999 wheat was in the west field and oats in the east.

Fetch requirements are well met for wind directions in the ranges 190° to 300° and 70° to 170° of the measurement mast. The area is mainly agricultural, although the region is quite densely populated, and there are several sources of NO_x and SO₂ near to the field, such as: Ratcliffe coal fired power station 3 km north, the M1 motorway to the west and the East Midlands Airport about 4 km to the south west, see Figure 1b.



A, from Biscoe *et al* 1975

B, Bartholemews UK Road Map CD v 3 (50 km x 50 km grid)

Figure 1. Location of the Sutton Bonnington dry deposition monitoring site

The background concentration of NO_x is between 8 to 16 ppb. This level of NO_x and episodes of higher concentrations lead to significant reductions in the ozone concentration being observed at Sutton Bonnington, potentially causing errors in the calculated fluxes. Hence the NO_x concentration is also monitored to allow corrections to be made to the ozone flux.

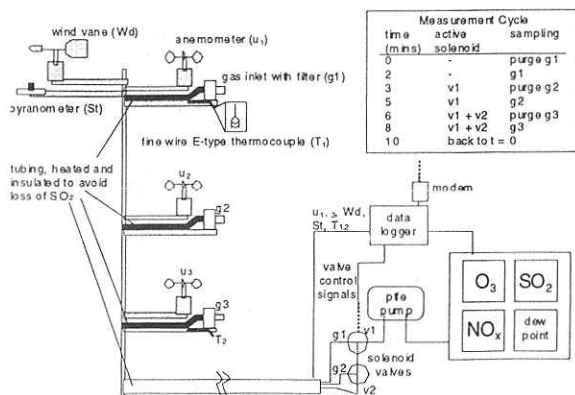
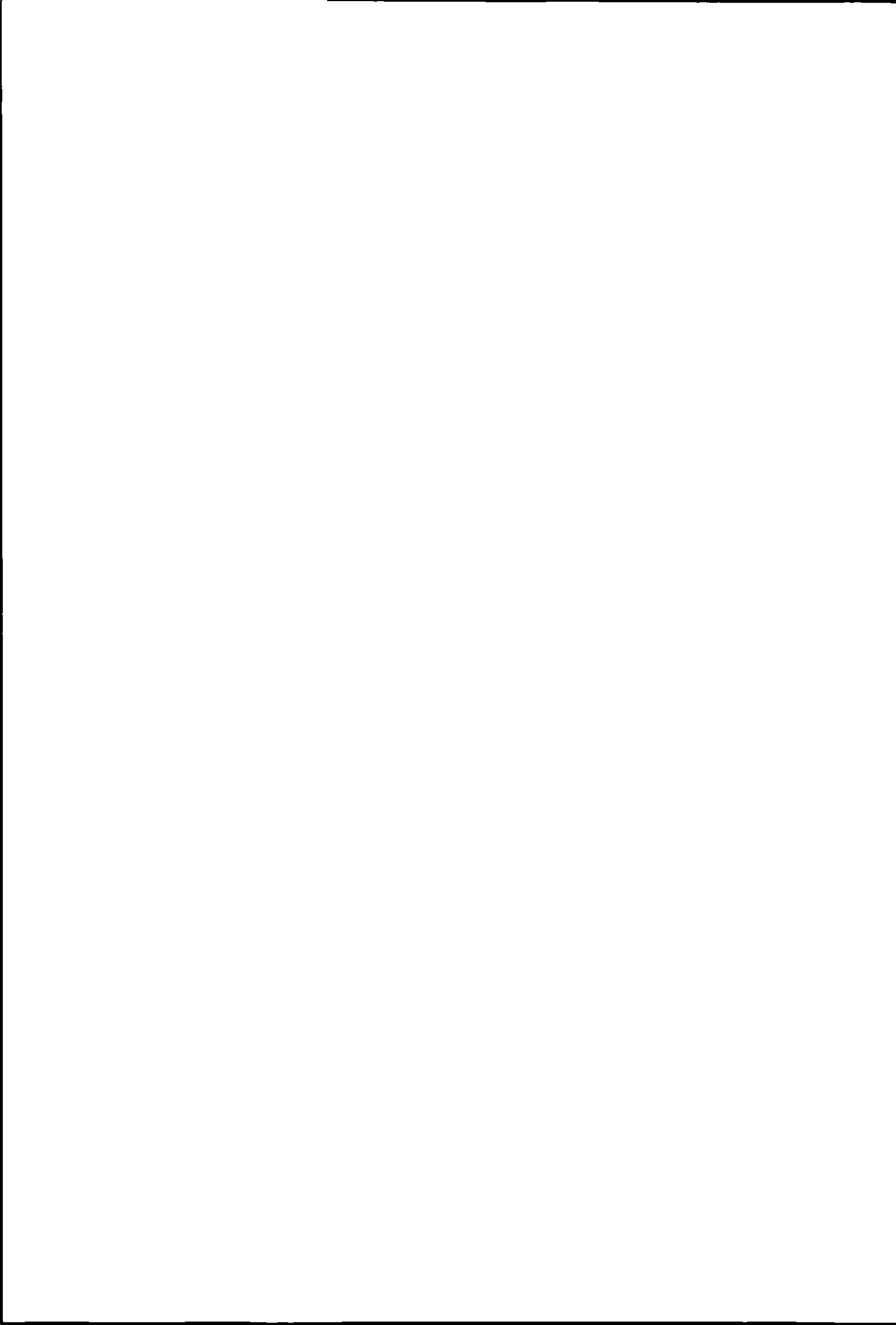


Figure 2. Configuration of the measurement mast.

Measurements of O₃ and NO_x concentration are made at the 3 heights in sequence, as described in Figure 2. The top height is fixed at ~3 m, the middle and bottom heights are moved so that log spacing is maintained with the bottom inlet just above the canopy, in the inertial sub-layer. The prevailing wind direction is from the west (Figure 3) and so the majority of measurements suitable for flux



analysis are obtained from the westerly fetch. Hence, only the ozone deposition measurements over sugar beet in 1998 and wheat in 1999 are considered here. Figure 4 shows the monthly data capture of ozone and NO_x in total and for the westerly fetch.

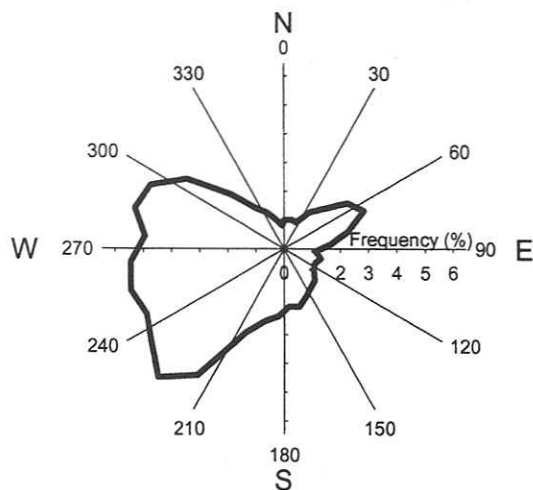


Figure 3. Wind rose of %frequency of wind direction (3/3/98 to 26/8/99).

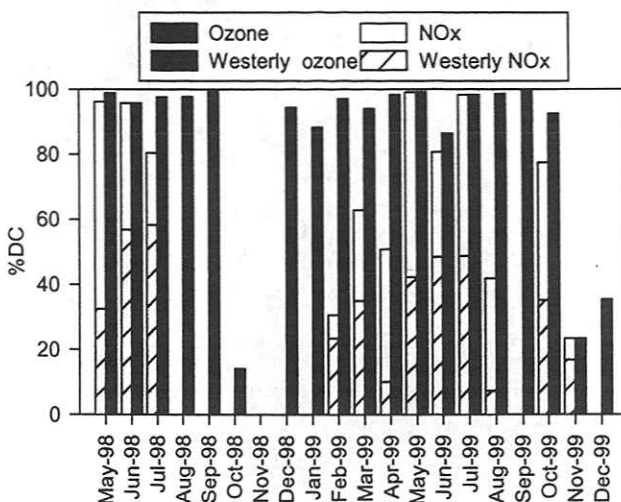
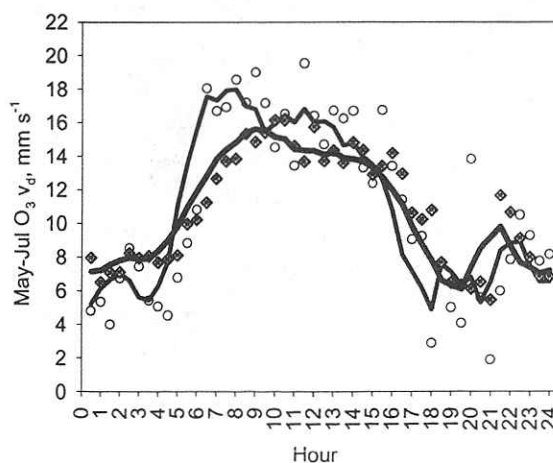
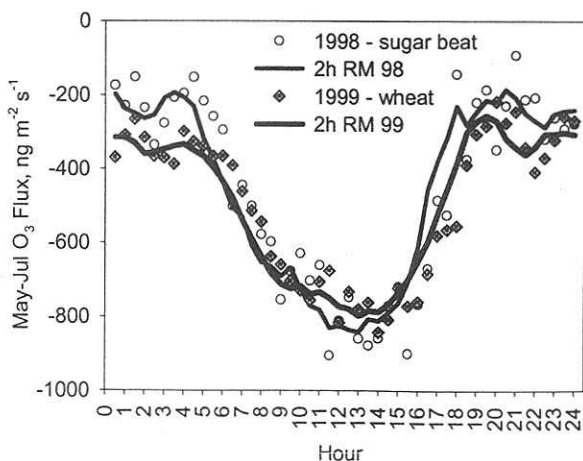


Figure 4. Monthly total and westerly % data capture.

The aerodynamic gradient method used to calculate the ozone flux is described in Sutton 1990 and Sutton *et al* 1993. Where coincident ozone and NO_x measurements have been made the calculated ozone fluxes are corrected for the O₃-NO-NO₂ and other reactions using the empirical method of Duyzer *et al* 1995. The corrections are typically between 0.1 to 2%. These are smaller than expected and further analysis, with different correction methods are in progress.

Figure 5 shows plots of the diurnal cycle in ozone flux and deposition velocity during the two growing seasons. Pronounced diurnal variations in ozone flux, deposition velocity and canopy resistance are evident in the measurements throughout the year. Diurnal patterns in flux and deposition velocity are similar for wheat and sugar beet. Nocturnal deposition to wheat is greater than that to sugar beet, 200 ng m⁻² s⁻¹ vs 300 ng m⁻² s⁻¹, due to differences in canopy resistance.



a.

b.

Figure 5 May to July (a) ozone flux and (b) deposition velocity at 1m. 1/2 hourly average and 2 hour running mean averages for sugar beet in 1998 and wheat in 1999.



Plots of average ozone flux, deposition velocity (v_d) and median canopy resistance (R_c) for both growing seasons and January to March 1999, when the field was practically bare, are shown in Figure 6. Nocturnal winter ozone deposition fluxes (average $-232 \text{ ng m}^{-2} \text{ s}^{-1}$) exceed summer nocturnal fluxes (average $-153 \text{ ng m}^{-2} \text{ s}^{-1}$) as a consequence of higher wind speeds during the winter. May-July daytime canopy resistances (average 34 sm^{-1}) are substantially smaller than those for Jan-March (average 175 sm^{-1}) as a consequence of the stomatal uptake of ozone. During May-July stomatal and non-stomatal ozone deposition fluxes are of similar magnitude. During the winter most of the ozone deposited is non-stomatal.

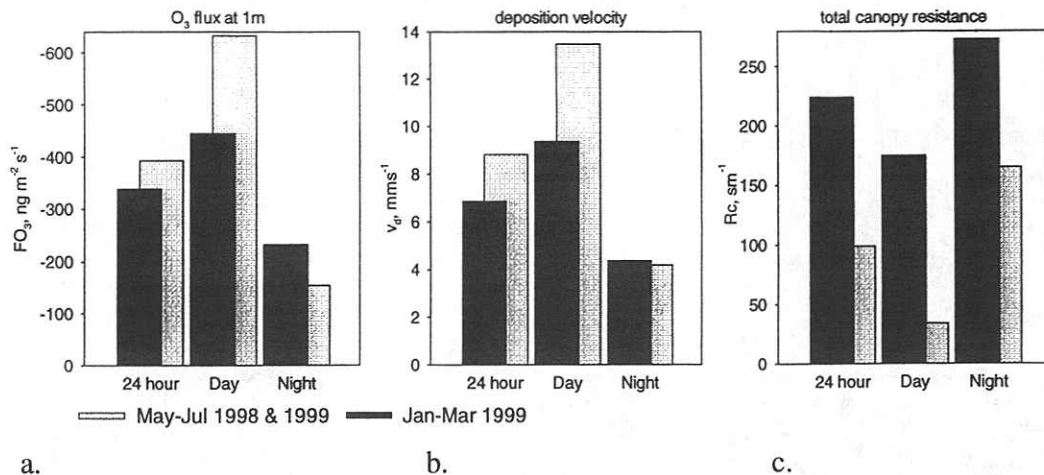
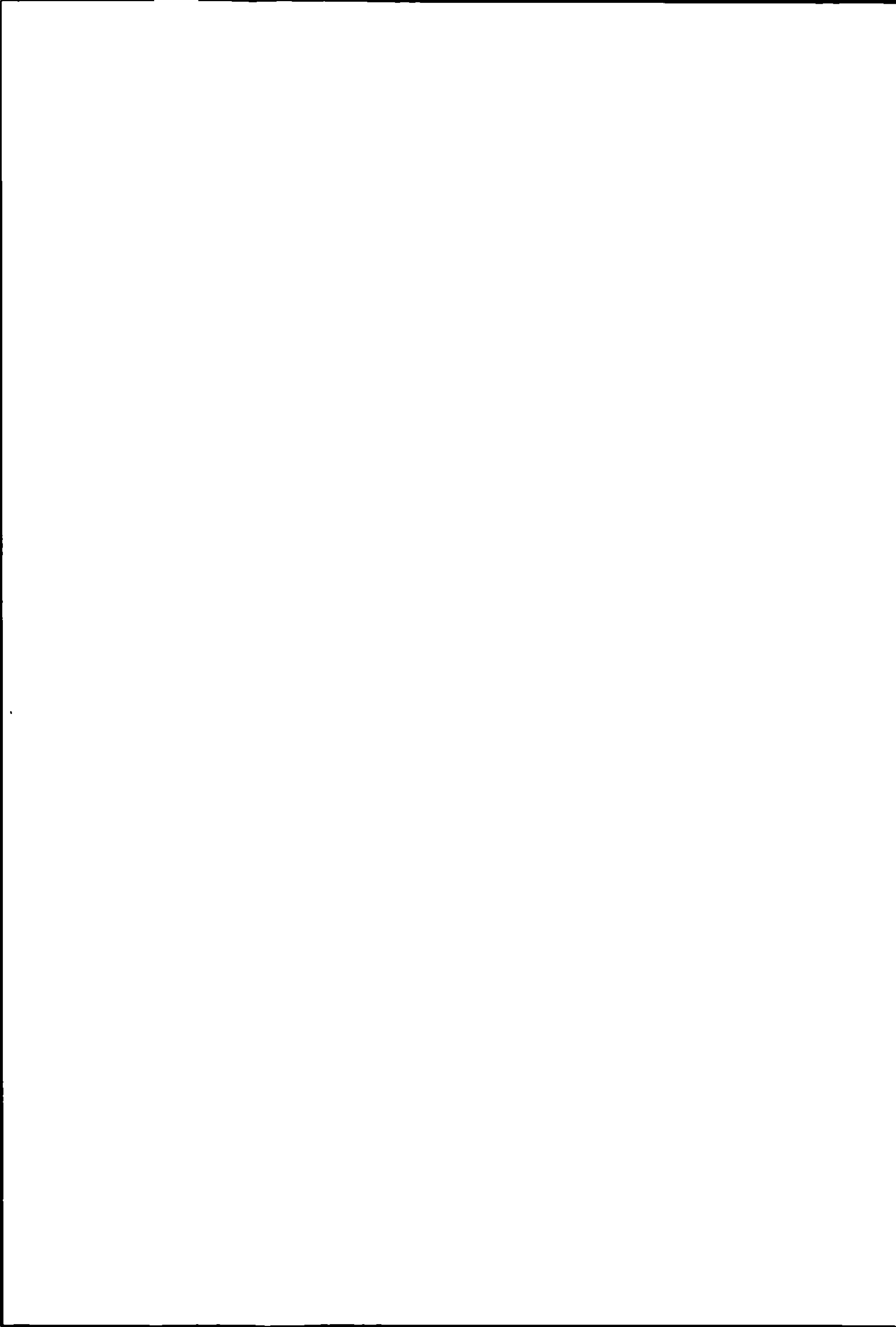


Figure 6. May to July 1998/1999 and January to March 1999 (a) average ozone flux, (b) average deposition velocity and (c) median canopy resistance. Daytime is taken to be when solar radiation $\geq 50 \text{ Wm}^{-2}$.

In conclusion, this initial analysis gives typical patterns of ozone deposition to arable crops, although the magnitude is slightly larger than has been reported from other field experiments. There are also indications that non-stomatal deposition makes up a significant fraction of the total throughout the year.

References

- Sutton MA. 1990. The surface-atmosphere exchange of ammonia. PhD Thesis The University of Edinburgh, Edinburgh, UK.
- Sutton MA, Fowler D, Moncrieff JB. 1993. The Exchange of Atmospheric Ammonia with Vegetated Surfaces .1. Unfertilized Vegetation., *Quarterly Journal of the Royal Meteorological Society*, **119**: 1023-1045
- Duyzer JH, Deinum G, Baak J. 1995. The interpretation of measurements of surface exchange of nitrogen- oxides - correction for chemical-reactions. *Philosophical Transactions of the Royal Society of London Series A-Physical Sciences and Engineering* **351**(1696), 231-248.



Ozone flux monitoring by shoot chambers

NURIA ALTIMIR

*Department of Forest Ecology, University of Helsinki, PO Box 24, FI-00014
e-mail: nuria.altimir@helsinki.fi*

Abstract

At the field SMEAR II monitoring station in Finland we have been measuring ozone flux into Scots pine canopy shoots by means of branch cuvettes over three years. These kind of direct, detailed, and continuous information can help the understanding on the dynamics and partition of shoot-mediated removal of ozone. This paper offers a technical description of the system methodology and some illustrative data.

Introduction

Micrometeorological techniques, which operate at whole-canopy level, seem to be the favoured way of measuring O₃ fluxes over vegetated surfaces. Insights into O₃ dry deposition phenomena have been deepening as research has gone from single layer to multilayered and phenomenological descriptions. As description, i.e., models, have increase in detail so demand for detail or compartmented measurements should arise at some point. Here comes the value of small scale gas exchange chamber.

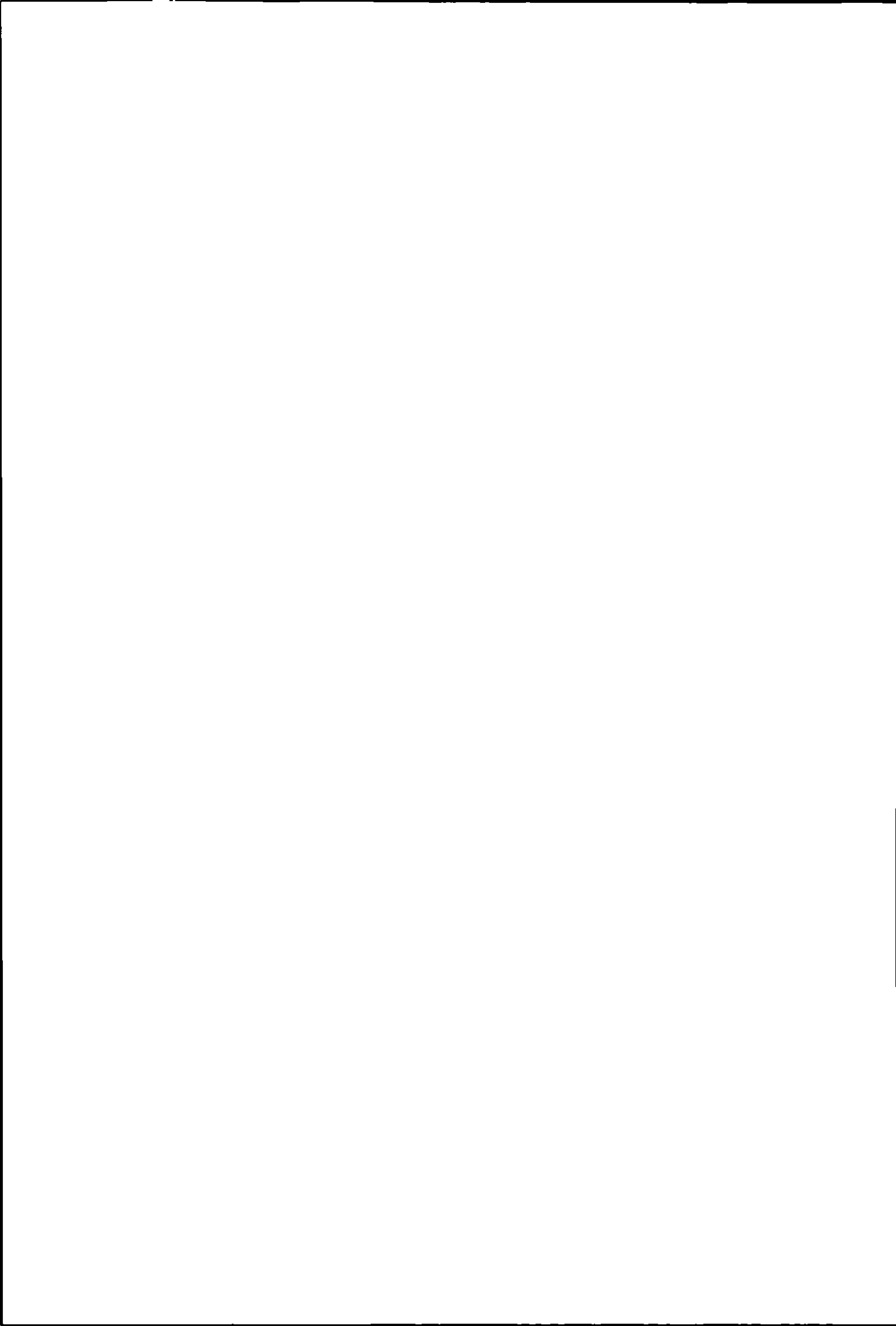
The use of chambers at the moment is accepted and extended in soil emissions research, and so it is in VOC research in plants. But comparatively few measurements on O₃ exchange is done. This might be due to the belief we already understand how the O₃ exchange happens, that is, the uptake and control by stomata. However, they might be more to it than stomatal control and so the validity of the surrogate approach and the relative importance of surface reactions are yet to be deciphered. Intensive and extensive measurements of simultaneous CO₂ water vapour and O₃ removal stomatal behaviour would prove valuable for the purpose. Such are the chambers operating at SMEAR II.

I present here the technical context of this gas exchange system and introduce the rational for calculations of O₃ removal.

System description

SMEAR II (Station for Measuring Forest Ecosystem-Atmosphere Relations) is a monitoring field station dedicated to the study of fluxes of mass and energy between soil, atmosphere and forest. It is located in Finland (61° 51'N, 24° 17'E) at a 34-year-old Scots pine stand (all-sided LAI 9) and has been operating since 1996. Vesala *et al.* 1998 offers an overview on the SMEAR II capabilities and research within.

The station features a gas exchange system that supports several shoot chambers which measure CO₂, water vapour, O₃ and NO_x exchange simultaneously. For the purpose of O₃ flux monitoring we have used chambers installed on shoots at the top of the canopy. Fig1 shows the gas circulation pathway and its components. It is an open system, where air ultimately



exhausts, and flow rates are measured and controlled. Following requirements of endurance, simplicity, and reliability small ventilated chambers and short closure times were favoured (instead of climatized cures). Chambers are most of the time open, and close intermittently for only 70 s to perform a measurements, being all the time ventilated with the aid of small fans. There are several versions of chambers operating at SMEAR II regarding to inner volume, shape, wall material and shoot positioning, but they all follow the same measurement principle. The chamber type used in the measurements reported here can be seen in Fig 2, together with the accompanying sensors.

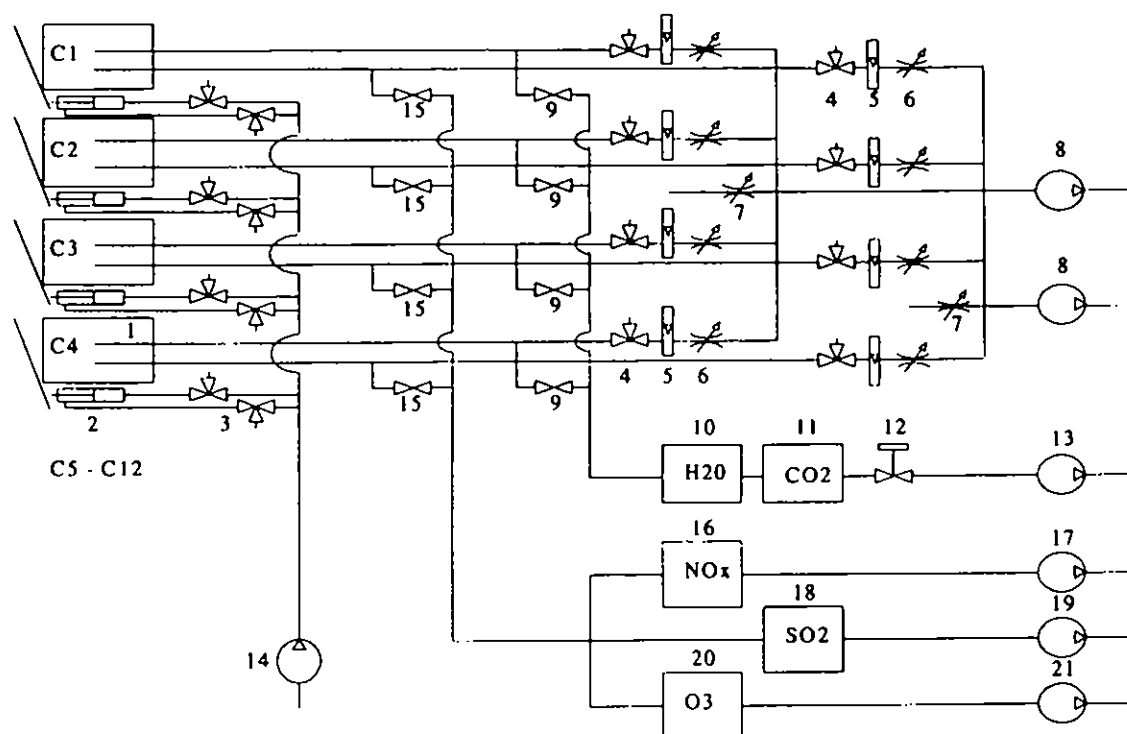


Fig.1. Details of the gas exchange system, NO_x and SO_2 analysers are also present. C1 - C12) shoot chambers, (2) pneumatic cylinder for opening and closing of cuvettes, (3) magnetic valves for operating of cuvette cylinders, (4) magnetic valve to select flush flow rate, (5) flow meter, (6) and (7) controllers of flush flow, (8), (13), (17), (19) and (21) air pumps, (9) magnetic valves to select the chamber for H_2O and CO_2 measurement, (10) IRGA for H_2O , (11) IRGA for CO_2 , (12) flow rate controller for IRGA, other analysers have critical orifice, (14) air compressor for cuvette pneumatics, (15) magnetic valves to select the chamber for NO_x and O_3 measurements, (16) NO_x analyser, (18) to SO_2 analyser and (20) to O_3 analyser. Flow within O_3 and NO_x analyser is controlled by critical orifice. Pipelines are made of Teflon (\varnothing 6/4, PTFE, GER) and kept warm by heating cable. Compressed air for the pneumatic system is dried to avoid water condensation problems in pneumatic pipelines with a PNEUDRI midi dryer (Domnic Hunter, UK). From Haataja & Vesala 1997.

Computer-controlled magnetic valves operate pneumatic cylinders that open and close the lids of the chambers in the programmed order. Similarly, a second system of magnetic valves selects the origin of the air to be led to the analysers and positions the rest of the pipelines in a flushing mode. CO_2 and water vapour concentrations are measured with infrared absorption analysers (Hartmann Braun URAS 4) and O_3 concentration by an ultraviolet absorption analyser (API 400, Advanced Pollution Instrumentation). All measurements are automatically recorded and stored every 5 s.



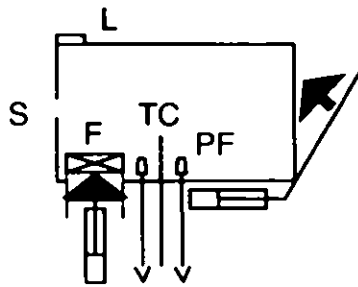


Fig 2. Schematic detail of one chamber version, a 3.5 l metacrylat cylinder, with one fan (F) and a big lid at opposite ends. The end of the sampling tube is restricted with a 7- μ m particulate filter (PF). L Li-Cor PAR sensor, S inserting point for the shoot, TC copper-constantane thermocouple. Bold arrows show moving for the closure, thin arrows show direction of sampling flow.

The gas exchange is calculated from the change of concentration inside the chamber during closure. The mass balance expression applied to the calculation of O_3 flux is

$$\frac{VdC(t)}{dt} = q(C_a - C(t)) - VKC(t) - Av_dC(t) \quad (1)$$

where left-hand term is the change of O_3 mass in time inside the chamber, and the right-hand terms are the mass flow produced by the sampling, the chamber walls, and the shoot respectively. q is the flow rate through the chamber ($m^3 s^{-1}$), C_a is ambient concentration ($g m^{-3}$), K is wall-loss rate constant (s^{-1}), A is total shoot needle area (m^2) and V_d is total shoot removal velocity ($m s^{-1}$).

Parameter values (K and V_d) are estimated from the best fit between the solution of equation 1 for $C(t)$ and the concentration chamber measurements, as computed by non-linear regression. $V_d = 0$ and empty chamber data solves the value of the wall-loss rate, K . Using this K and shoot chamber data solves the value of total shoot removal, V_d . O_3 flux can be then calculated as

$$F = V_d \cdot C(0) \quad (2)$$

where $C(0)$ is ozone concentration right before chamber closure.

Results and Discussion

Fig 3 provides averaged data from the same chamber during 5 sunny days. There were 120 measurement points per day, that is, one measurement every 12 minutes. These days render clear daily patterns easy to compare between them and to judge over the quality of measurements. When interpreting the values the reader should keep in mind that they are obtained on total (not projected) needle area basis and that they represent a one single shoot (not whole canopy) phenomena.

Being able to take into account the loss rate of O_3 to the chamber wall reactions was considered important. In fair weather conditions when the shoot activity is high the values of wall loss appear comparatively small to the total shoot removal (Fig 1a). Nevertheless, under less favourable conditions ignoring the wall loss produces a considerable overestimation of the shoot removal.



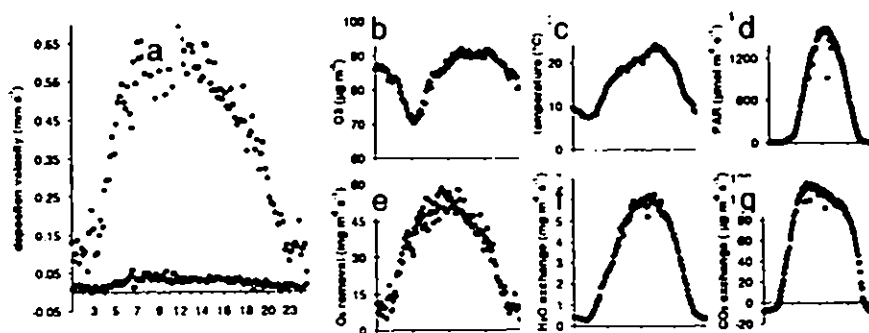


Fig 3. Five-day average of chamber measurements for 1st, 3rd, 4th, 5th and 7th of June 1997. All y-axis denote one 24-hour period, note the relative short night due to the location. In a) empty circles stand for empty chambers and full circles for chamber containing shoot, that is, total removal velocity of the shoot.; b, c, d) environmental conditions; e, f, g) calculated gas fluxes.

Taking this into account and considering the instrumentation noise (mainly analyser), the resolution of the system to measurements of O₃ removal has been estimated to be in the range of $10^{-2} \mu\text{g m}^{-2} \text{s}^{-1}$.

The V_d pattern with a maximum before midday and afternoon decline (Fig 3a) seems to match with the idea of stomata control of over O₃ removal. Further analysis of all the series should show to what extent or in what conditions this stomatal behaviour explains O₃ removal. Similarly, positive night time values are evident but it remains to be seen whether they can still be attributed to stomatal uptake or whether surface reactions would play a role. Analysis of the time series is under way.

Acknowledgements

Technical proficiency at SMEAR should be credited to Dr.Hc.Toivo Pohja.

References

- Haataja, J & Vesala, T.:1997. SMEAR II *University of Helsinki Department of Forest Ecology Publications* 17, 100pp.
- Vesala, T., Haataja, J., Aalto, P., Altimir, N., Buzorious, G., Garam, E., Hämeri, K., Ilvesniemi, H., Jokinen, V., Keronen, P., Lahti, T., Markkanen, T., Mäkela, J.M., Nikinmaa, E., Palmroth, S., Palva, L., Pohja, T., Pumpanen, J., Rannik, Ü., Siivola, E., Ylitalo, H., Hari, P., & Kulmala, M.: 1998. Long-term field measurements of atmosphere-surface interactions in boreal forest combining forest ecology, micrometeorology, aerosol physics and atmospheric chemistry. *Trends in heat, mass & momentum transfer* 4:17-35



Ozone dry deposition measurements over wheat in Central Spain

J. PLAZA[†], J.M. FERNÁNDEZ, D. DE LA TORRE, A. GONZÁLEZ^{*}, B.S. GIMENO AND B. ARTIÑANO

CIEMAT-Environmental Impact of Energy Dpt., Madrid (Spain) [†]javier.plaza@ciemat.es
^{*}"El Encín", Agricultural Research Institute of the Madrid Community

Summary

The eddy covariance technique has been implemented to measure ozone fluxes over a wheat crop during its growing season. The stationarity criteria used to filter 10-minute averaged raw data have revealed the mean features of ozone dry deposition process. Fluxes and related parameters (deposition velocity and surface resistance) obtained as well as preliminary results of stomatal resistance calculation from conductance measurements are presented, allowing discussion of the different sinking processes in ozone dry deposition.

Measurement Site and Experimental Set-Up

The measurement site is located 40 km east of Madrid, in "El Encín" research agricultural institute of the Madrid Community (fig. 1). A simple scheme of the experimental wheat crop (*Triticum durum* cv Camacho) is depicted in the same figure, showing its dimension (60x60 m²) and the location of ozone deposition mast, the meteorological tower and the data acquisition cabin. The canopy density was about 200 plants m⁻².

The sonic anemometer (GILL 3-axis research) and ozone sampling point were placed at a height of 2.5 m above the ground. Fast response ozone analyzer (LOZ-3, Scintrex Unisearch) was placed inside a sheltered box at the bottom of the tower. The analyzer was calibrated before and after short measurement periods (2-3 days). Additionally, a meteorological tower (10 m) close to ozone deposition mast was instrumented with standard wind, temperature, humidity and radiation sensors. On this site, fetch conditions ranged from 20 to 100 m (Grünhage et al., 2000) depending on wind direction, since only one side of the experimental crop was also a wheat plantation, and land use of the rest of sides corresponds to bare soil.

Stomatal conductance for H₂O_v (g_s) measurements were carried out on 18 wheat plants sampled randomly within the canopy using a portable photosynthesis system LICOR-6400. The measurements were performed on different dates following wheat phenology.



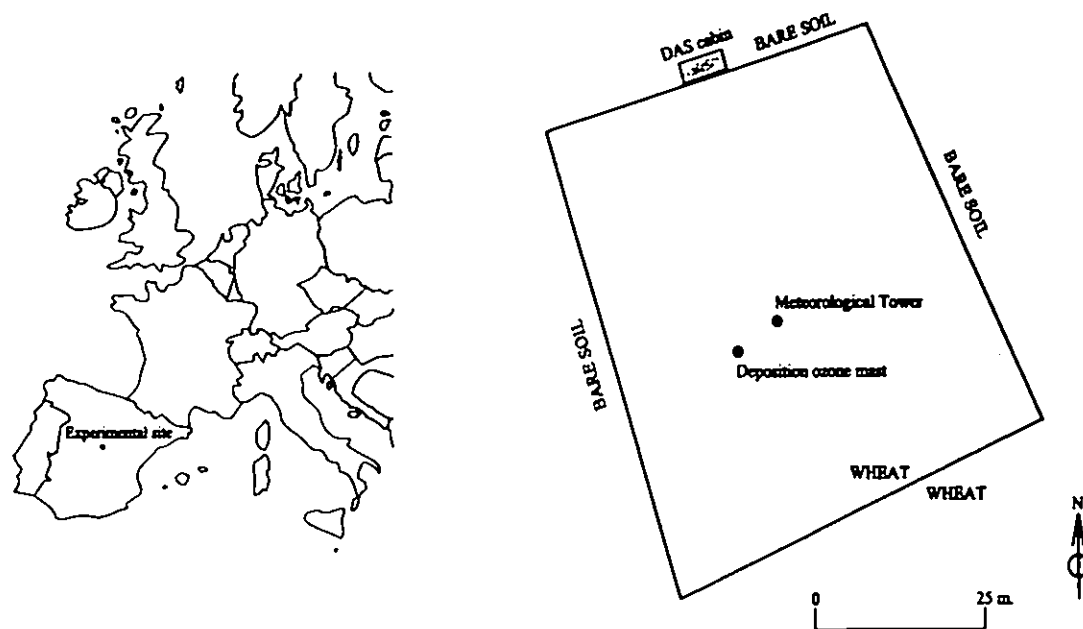


Fig. 1 Location and scheme of experimental crop

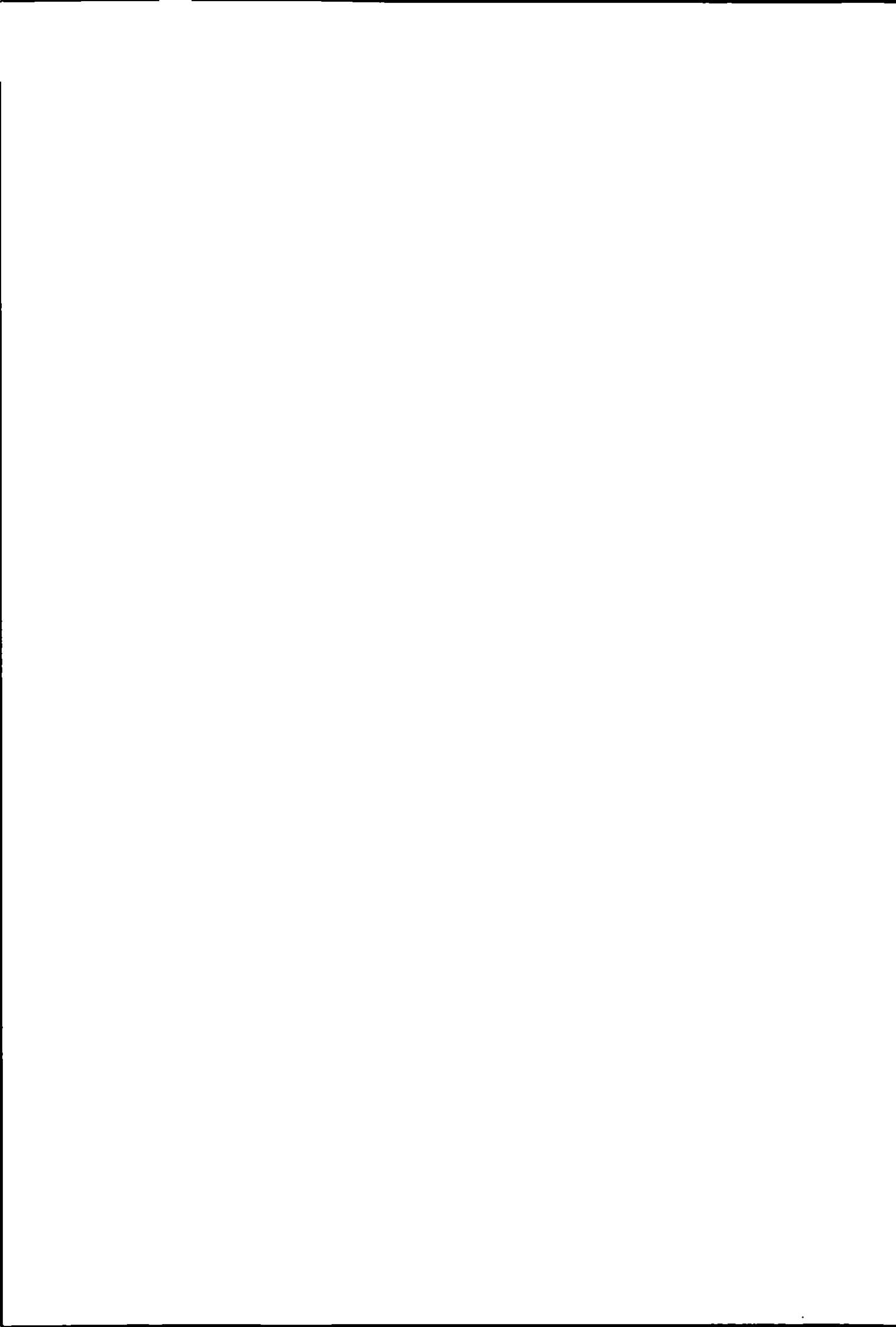
Data Processing

The ozone flux measurements were performed in short intensive periods during the last part of the wheat growing cycle (May-June) in 2000, corresponding to the anthesis, milk and dough development phenological states.

Sample frequency for eddy correlation technique was that corresponding to the fast response ozone analyzer (10 Hz). The instrumental response time of ozone analyzer including time residence of air inside the 2 m long teflon sampling line was calculated to correlate simultaneous vertical wind component and ozone concentration signals, and was fixed at 2.4 s. The chosen average time for flux calculation was 10 minutes, and ozone detrending was not applied to raw data. Fluxes were corrected by two-axis rotation to minimize aerodynamic effects (Güsten and Heinrich, 1996). The criteria for stationarity of ozone concentration and meteorological conditions to validate ten minute averaged flux data are shown in Table 1.

10-min interval	
Change in ozone concentration	< 5 %
Change in wind direction	< 45 °
Change in horizontal wind velocity	< 1 m/s
Change in air temperature	< 1 °C

Table 1. Criteria for stationarity



Results and Discussion

Figure 2 shows horizontal wind speed (sensor from the meteorological tower) and ozone concentration (UV-absorption analyzer) as recorded in the experimental site during two periods of eddy covariance flux measurements (17-19 and 22-25 May). These days were hot and cloudless, with prevailing thermal diurnal and nocturnal weak wind flows.

The proximity of the experimental site to a motorway (500 m) and the nocturnal atmospheric stability led to a significant ozone depletion during most part of the night, when the site is downwind of the motorway (W to NE wind directions). In addition, the site is usually downwind the metropolitan area of Madrid during daytime under meteorological conditions favouring the accumulation of ozone in the airshed. As can be observed in the figure, high ozone concentrations were reached during some of measurement days.

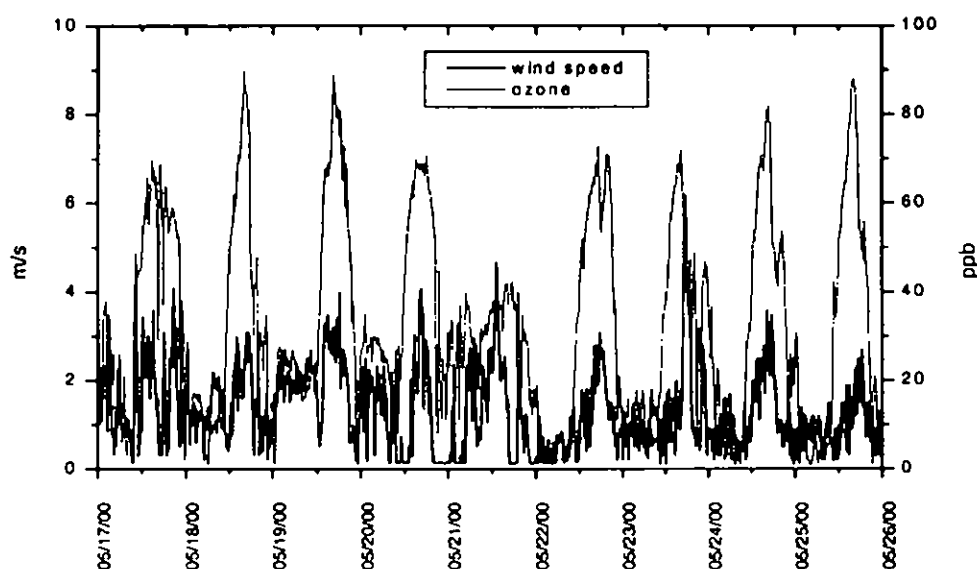


Fig. 2 Ozone and wind speed during the measurement days

After applying criteria for stationarity on all 10-minute averaged fluxes obtained in these two periods of measurements, 66% of these data were rejected, mainly during night and transition periods between the diurnal and nocturnal wind flows. The change in ozone concentration was by far the more unfulfilled criterion in this site.

Figure 3 upper presents one example of daily cycle of fluxes (19 May) after applying the criteria for stationarity. The presence of net downward fluxes during the night is remarkable. In the lower figure the same daily cycle for deposition velocity is presented, obtained from measured fluxes and ozone concentrations. The evolution of this parameter reveals a significant ozone deposition during morning hours, although measured fluxes are not yet high.



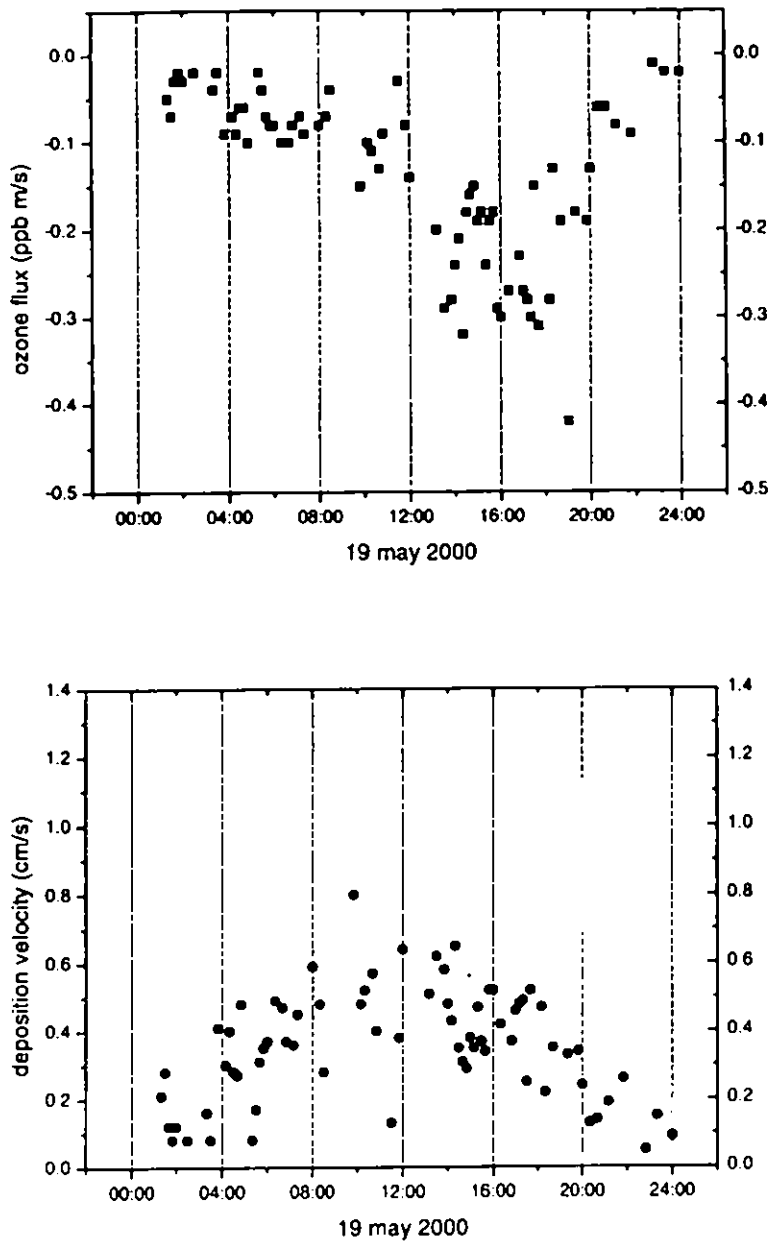


Fig. 3 10 min averaged ozone fluxes (upper) and deposition velocities (lower) after stationarity filtering on 19 May 2000

The eddy covariance technique allows the calculation of the surface or canopy resistance (r_c) following the classical dry deposition parameterization approach, in which the deposition velocity can be obtained by the addition of the inverse of three resistances, an atmospheric resistance r_a , a quasi-laminar layer resistance r_b and a canopy resistance r_c :

$$v_d = -\frac{F_{O_3}}{[O_3]} = \frac{1}{r_a + r_b + r_c}$$



From this expression, surface resistance (r_c) can be calculated from the measured ozone flux and concentration, and calculated deposition velocity and resistances r_a and r_b :

$$r_a = \frac{u}{u_*^2} \quad (\text{Fowler et al. 1986}), \quad r_b = \frac{2}{ku_*} \left(\frac{Sc}{Pr} \right)^{2/3} \quad (\text{Hicks et al, 1987})$$

A second filter was applied to 10-min interval data before calculating resistances (Pilegaard *et al.*, 1998). Only those periods with downward momentum flux ($u'w' < 0$) m^2/s^2) and enough friction velocity ($u_* > 0.05$ m/s) have been considered. The figure 4 presents resistances and r_c calculated for 19 May after data filtering. There is no diurnal trend in r_a and r_b , and their values are lower than r_c values. The canopy resistance appears to be the limiting factor in this parameterization during almost all the day.

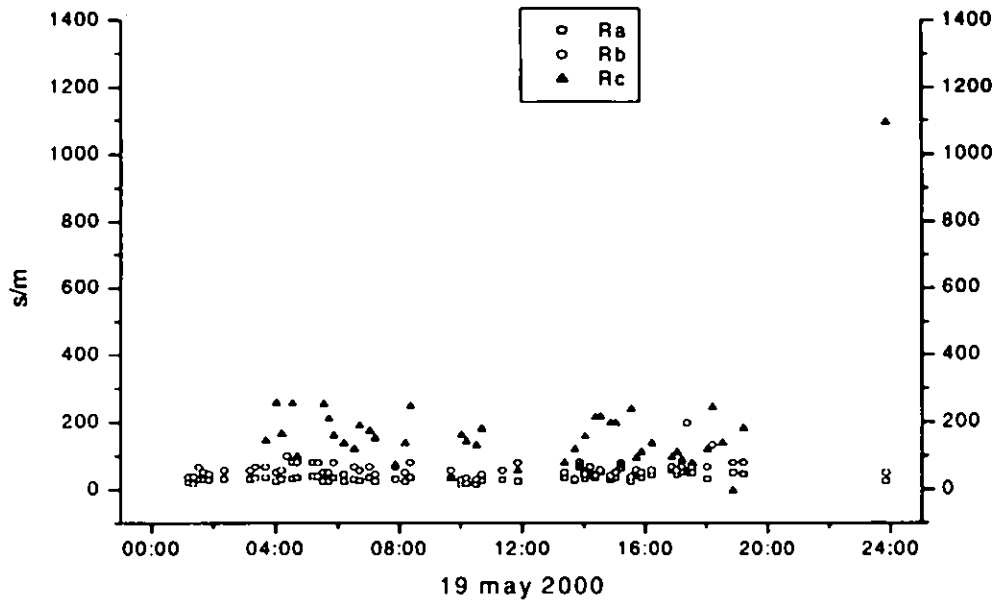


Fig 4 Daily cycle of 10 min-averaged resistances r_a , r_b and r_c

Figs. 5, 6 and 7 represent all valid ozone fluxes, deposition velocities and canopy resistances, respectively, obtained during these two measurement periods. A polynomial fit has been done to average the dispersion of data and to reveal the trend of these parameters. Similar features of the 19th May cycle can be observed.

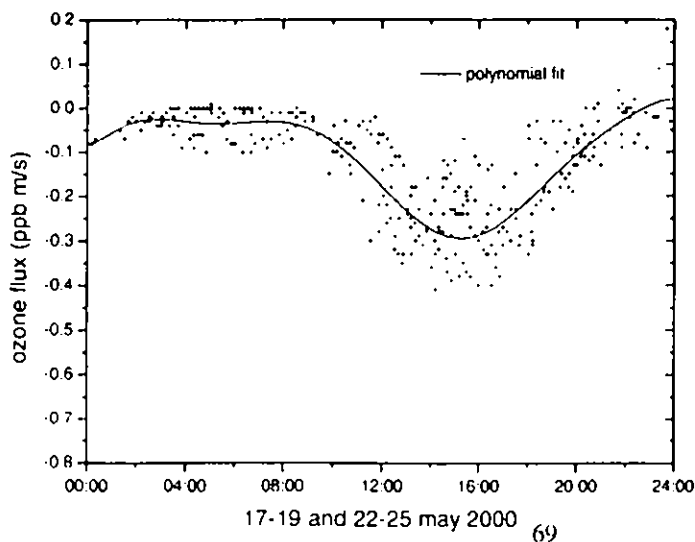


Fig. 5 Filtered 10 min averaged ozone fluxes



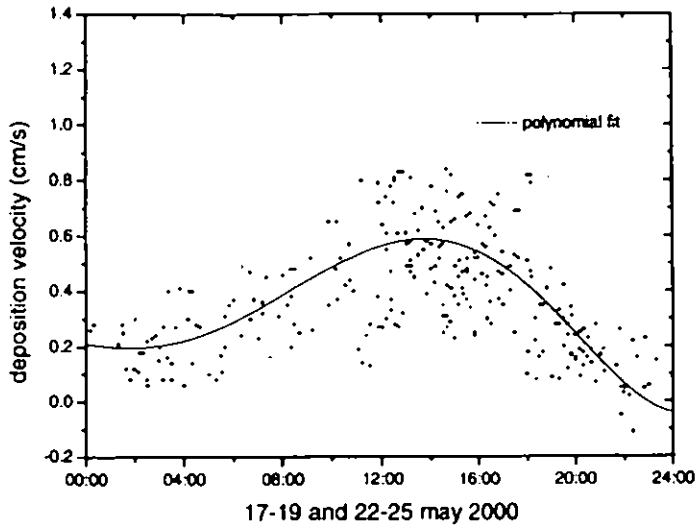


Fig. 6 Filtered 10 min averaged ozone deposition velocities

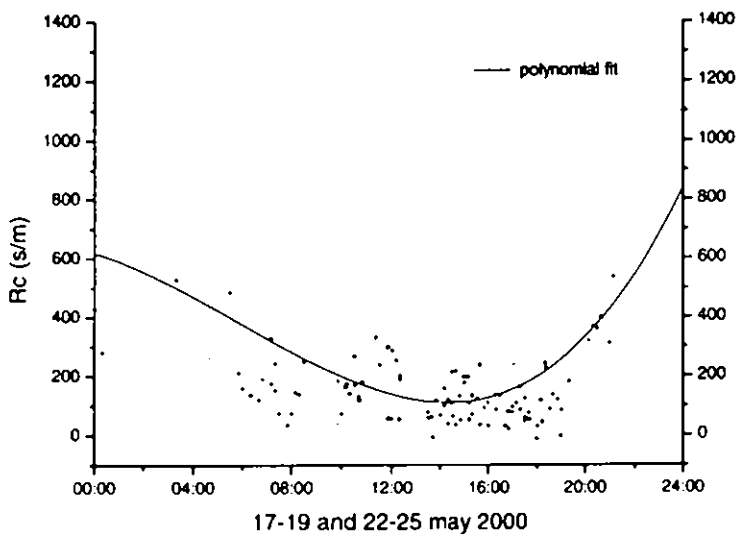


Fig. 7 Filtered 10 min averaged surface resistances

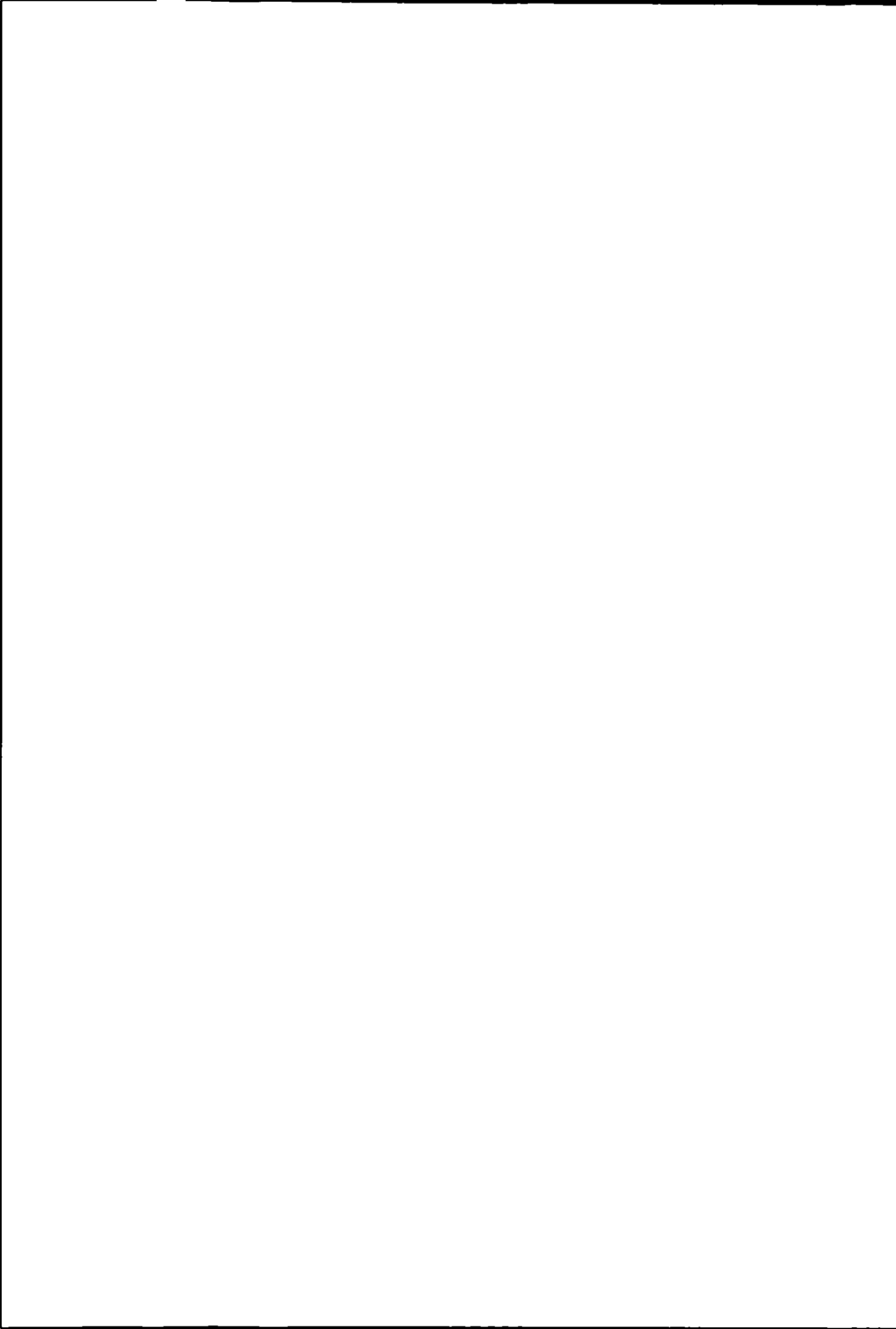
Surface resistances of Fig. 7 are in the same range as those calculated in Wesely (1989) parameterization for this type of surface and season of the year.

The aim of conductance measurements was to ascertain the influence of stomatal resistance (r_s) on ozone deposition, therefore r_c values derived from micrometeorological techniques were compared with ozone stomatal resistances. The stomatal resistance to ozone, $r_s(O_3)$ was estimated from $r_s(H_2O)$ taking into account the ratio of molecular diffusivities between water vapour and O_3 using the following equation derived from Wesely (1989):

$$r_s(O_3) = 0,613 r_s(H_2O)$$

The actual stomatal resistance ($s \cdot m^{-1}$) for ozone is calculated as the inverse of stomatal conductance for this pollutant ($m \cdot s^{-1}$).

The daily cycle of the calculated r_c and the actual $r_s(O_3)$ for May 18th 2000 is presented in Figure 8.



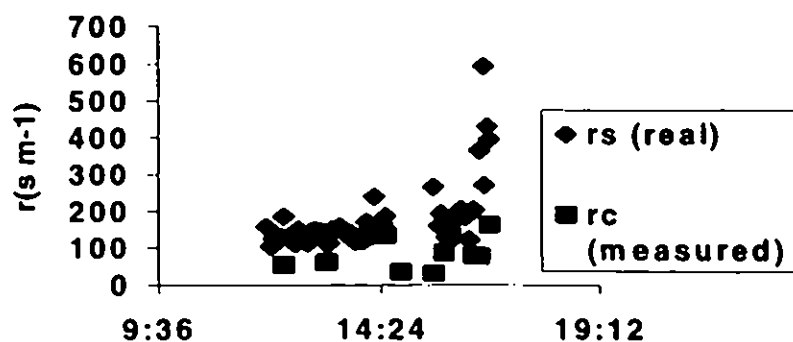


Fig. 8 Comparison between canopy resistances (r_c) and stomatal resistances for ozone $r_s(O_3)$ for May 18th 2000

Canopy resistance can be defined as a function of stomatal and non-stomatal resistance as,

$$r_c = (r_s + r_{ns}) / (r_s + r_{ns})$$

deriving from the following equation: $1/r_c = 1/r_s + 1/r_{ns}$, where non-stomatal resistance encompasses the resistance of ozone deposition over the cuticle and mesophyll of active vegetation and underlying soil (Grünhage *et al.*, 2000).

As can be seen in the graph, almost all r_c values calculated from experimental fluxes were lower than stomatal resistances, hence calculation of the non-stomatal resistance r_{ns} gave a value in the same range of r_s . This would indicate the presence of other surface sinks in addition to the stomatal pathway, which is predominant in the central hours of the day when fluxes are high. This non-stomatal sink would explain the measurement of significant fluxes during the night and during early evening hours when stomatal resistance is very high. The results obtained by Pilegaard *et al.* (1998) in an eddy correlation study over a harvested wheat crop also seem to reinforce the importance of non-stomatal sinks in ozone dry deposition over wheat, at least at its late phenological stages.

References

- Grünhage, L., H.D. Haenel and H.J. Jäger (2000), The exchange of ozone between vegetation and atmosphere: micrometeorological measurement techniques and models, *Environmental Pollution*, **109**, 373-392,
- Güsten H. and G. Heinrich (1996), On-line measurements of surface fluxes: Part I. Methodology and instrumentation, *Atmospheric Environment*, **30**, 6, 897-909
- Fowler D. (1986), The transfer of air pollutants to the ground by wet and dry deposition, *Regional and Long-Range Transport of Air Pollution*, S. Sandroni (Ed.), ISPRA, Italy
- Hicks, B.B., Baldocchi, D.D., Meyers, T.P., Hosker, R.P., and Matt, D.R. (1987), A preliminary multiple resistance routine for deriving dry deposition velocities from measured quantities, *Water Air Soil Pollut.* **36**, 311-330
- Pilegaard K., P. Hummelshøj and N.O. Jensen, Fluxes of ozone and nitrogen dioxide measured by eddy correlation over a harvested wheat field, *Atmospheric Environment*, **32** (1998):1167-1177
- Wesely M.L. (1989), Parameterization of surface resistances to gaseous dry deposition in regional-scale numerical models, *Atmospheric Environment*, **23**, 1293-1304



Development of a 1-km Vegetation Database for Modeling Biogenic Fluxes of Hydrocarbons and Nitric Oxide

THOMAS E. PIERCE*¹, ELLEN J. KINNEE² AND CHRISTOPHER D. GERON³

¹*Air Resources Laboratory, National Oceanic and Atmospheric Administration, Research Triangle Park, NC, USA*

²*DynTel Corporation, Research Triangle Park, NC, USA*

³*National Risk Management Research Lab., U.S. Environmental Protection Agency, Research Triangle Park, NC, USA*

Objective

Air quality simulation models must account for land surface characteristics when estimating biogenic emissions, dry deposition of gases and particles, and fluxes of moisture, heat, and momentum. The performance of most atmospheric models may be hampered, however, because they fail to consider the distribution of specific vegetation types. For example, the flux of isoprene can vary by several orders of magnitude depending on the distribution of tree species in a deciduous forest. Nitric oxide fluxes and stomatal resistance can also vary significantly between different crop types. Our objective here is to integrate the fine spatial resolution available with satellite-derived datasets with the detailed vegetation distributions available at a county-level. While the focus is on biogenic emissions, the resulting vegetation database should improve the handling of surface exchange and atmospheric chemical processes within models such as EPA's Community Multi-Scale Air Quality (CMAQ) modeling system.

Procedure

The current version of CMAQ uses the Biogenic Emissions Landuse Database (BELD2) (Kinnee et al., 1997), a county-based dataset with 156 different tree genera and crop species. We have developed a procedure and identified several datasets to build the next version of the Biogenic Emissions Landuse Database (BELD3). The following sets of data were used in this procedure:

USGS EROS North American land characteristics dataset is a widely-used 1-km dataset that contains a number of vegetation classification systems. None of them resolves tree species and crop types to the detail needed for estimating biogenic emission fluxes. The modified Anderson Level 2 classification system was selected as the basis for merging with the other datasets.

U.S. Census from 1990 provided geographical boundaries of urbanized areas across the United States.

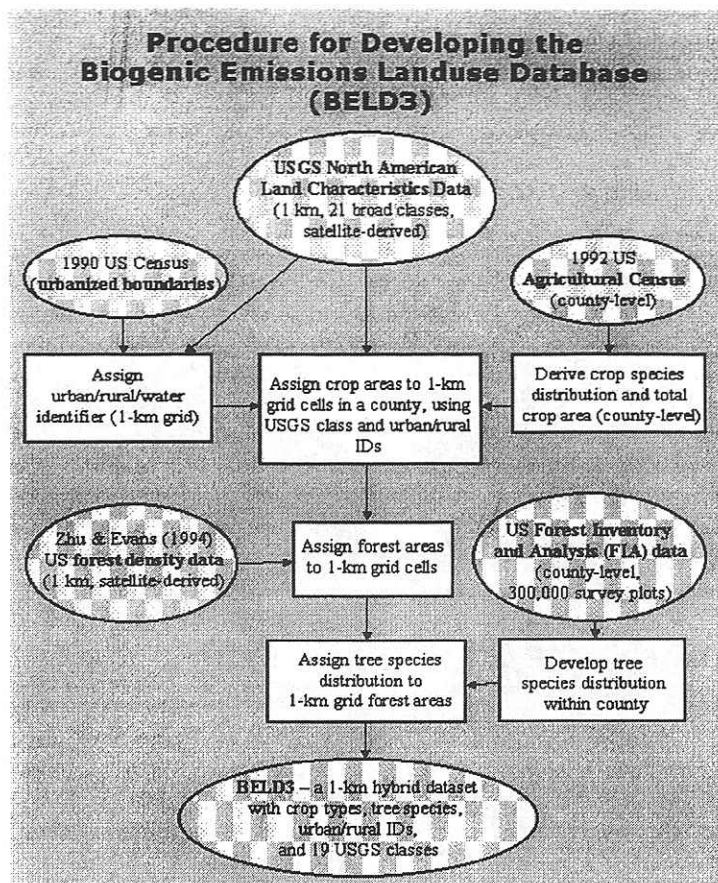
U.S. Agricultural Census for 1992 provided area coverage of specific crop types for each reporting county across the United States.

U.S. forest density dataset of Zhu and Evans (1994) is a 1-km dataset that was based on an analysis of AVHRR and LANDSAT satellite imagery.

U.S. Forest Service's Forest Inventory and Analysis (FIA) dataset, which we processed and resolved to the county-level, has tree species and tree diameters from over 300,000 ground-survey plots across the United States. Each plot could be resolved spatially only to the county-level because of confidentiality concerns.



The procedure shown below was used to create BELD3, which contains 259 vegetation types at a resolution of 1-km.



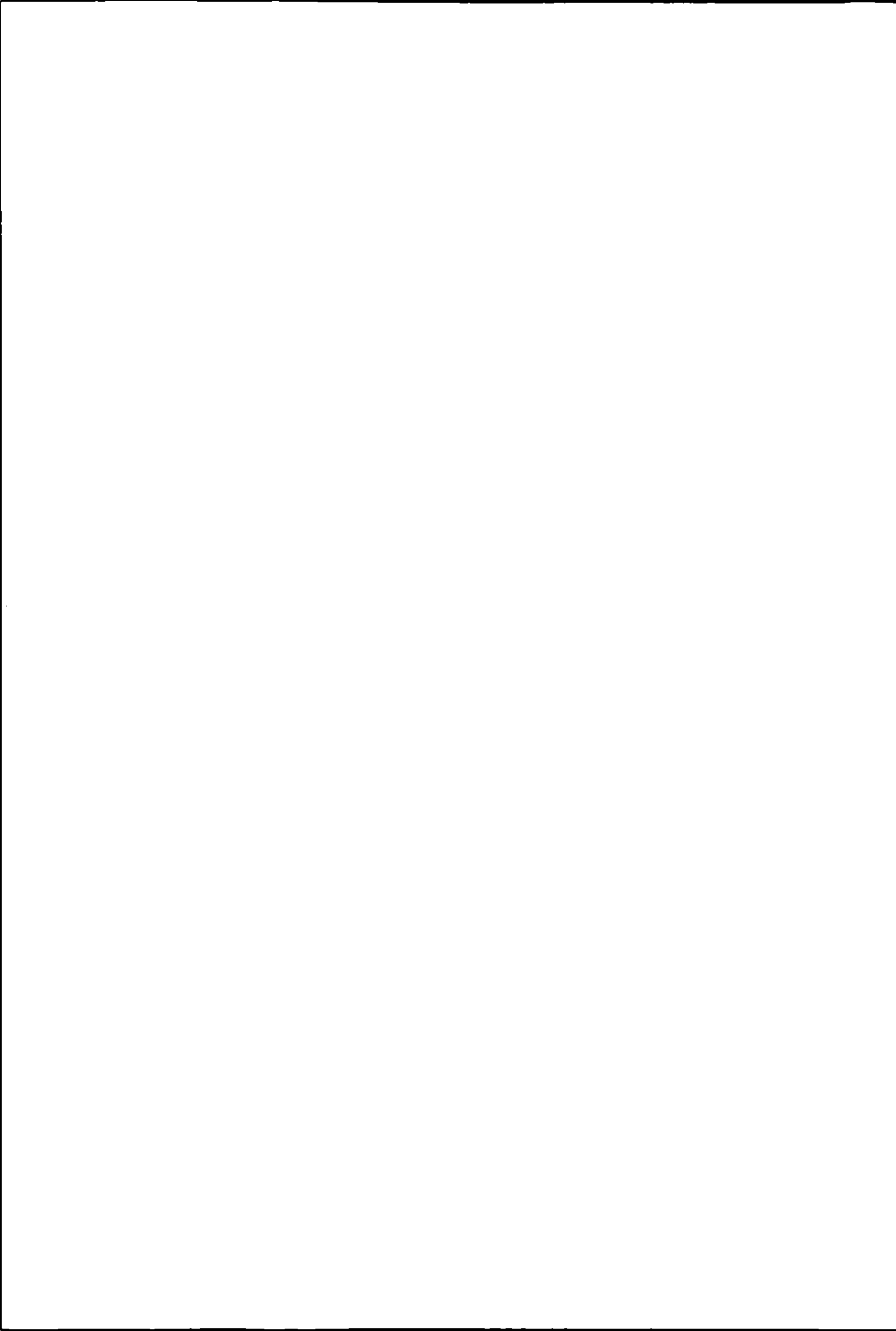
The percent coverage of *quercus alba* (white oak) developed with this procedure is shown below. White oak is prevalent in the eastern United States and is a high isoprene emitter. While oaks in BELD2 were aggregated at the county-level by genus (*quercus*), oaks in BELD3 have been separated into species at a 1-km resolution. The enhanced specificity should improve estimates of surface exchange processes such as isoprene emissions modeling.

Emissions Fluxes

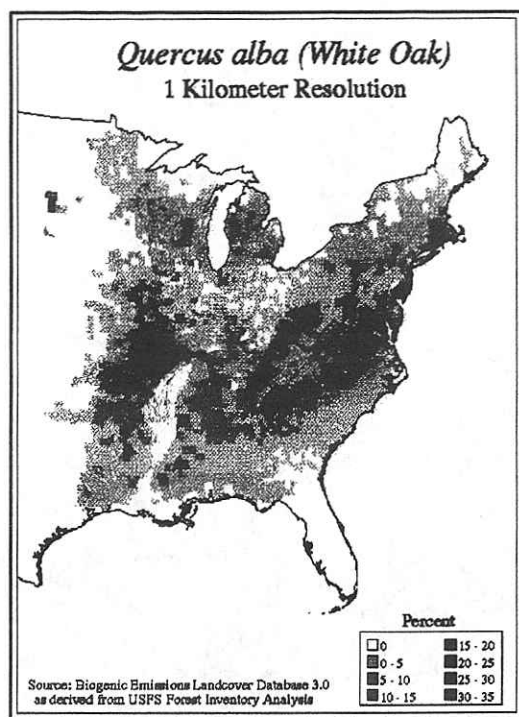
We demonstrate the utility of the 1-km vegetation database by comparing normalized isoprene fluxes computed at 1-km (BELD3) against county-level resolution (BELD2). Isoprene emission factors at standard conditions (leaf temperature=30°C and photosynthetically active radiation=1000 $\mu\text{mol}/\text{m}^2\text{-s}$) were obtained from Guenther et al. (2000), Pierce and Bender (1999), and Pierce et al. (1998) for 259 vegetation variable types.

References

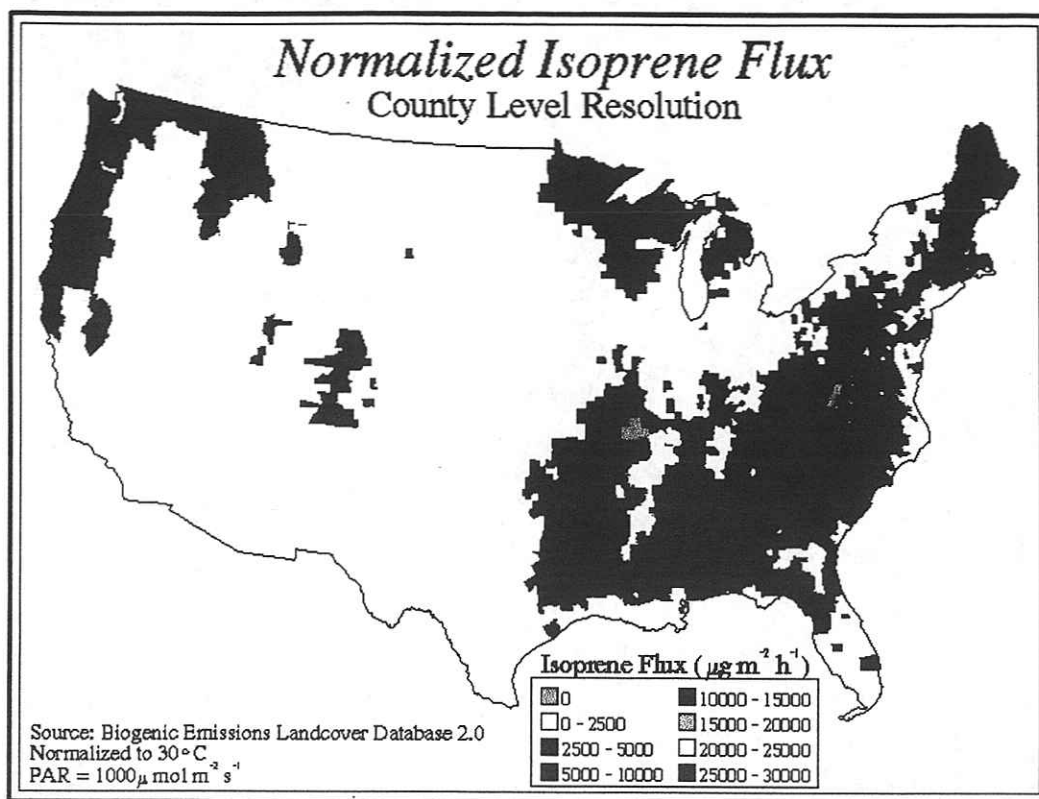
Guenther, A., C. Geron, T. Pierce, B. Lamb, P. Harley, and R. Fall (2000) Natural emissions of non-methane volatile organic compounds, carbon monoxide, and oxides of nitrogen from North America, *Atmospheric Environment*, 34, pp. 2205-2230.



- Kinnee, E., C. Geron, and T. Pierce (1997) United States land use inventory for estimating biogenic ozone precursor emissions, *Ecological Applications*, 7, pp. 46-58.
- Pierce, T., C. Geron, L. Bender, R. Dennis, G. Tonnesen, and A. Guenther (1998) Influence of increased isoprene emissions on regional ozone modeling, *Journal of Geophysical Research*, 103, pp. 25611-25629.
- Zhu, Z. and D. Evans (1994) U.S. forest types and predicted forest cover from AVHRR data, *Photogrammetric Engineering & Remote Sensing*, 60, pp. 525-531.







For further information: This Word document has been reformatted because of page limitations. The original, full-sized poster presentation is available for viewing and downloading at www.epa.gov/asmdnerl/biogen.html. For further information, please contact Thomas E. Pierce via email at pierce.tom@epa.gov.

Acknowledgements: The authors appreciate the help of Cliff Stanley (DynTel Corporation) in using SAS to process the USFS FIA data and the support of Sherry Brown (NOAA/EPA) in preparing the poster.

Disclaimer: *This poster has been reviewed in accordance with the U.S. Environmental Protection Agency's peer and administrative review policies and approved for publication and presentation. Mention of trade names or commercial products does not constitute endorsement or recommendation for use.*



AEROSOL PARTICLE FLUX MEASUREMENTS OVER THE RAINFOREST OF AMAZONIA

J BECK, C AMMANN, U RUMMEL, F X MEIXNER, M O ANDREAE, G HELAS

Max Planck Institute for Chemistry, Biogeochemistry Dept., Mainz, Germany
jbeck@mpch-mainz.mpg.de / Fax: + 49 (0) 6131 305487

Introduction

Project: LBA-EUSTACH 99

- European Studies on Trace gases and Atmospheric CHemistry within the Large scale Biosphere Atmosphere Experiment in Amazonia 1999

Why aerosol particle flux measurements in Amazonia?

- Amazonia is one of the major sources of aerosol particles to the global atmosphere. The export
- of only a small fraction of the aerosols could contribute significantly to their budgets in the free troposphere.
- In the context of budgets of aerosols the flux is a fundamental parameter of interest.

Aim of the aerosol flux study

- Determination of the aerosol particle exchange between the primary rainforest and the atmosphere in Rondônia, a southwestern part of the Amazon region in Brasil, using an eddy correlation (EC) method.

Method

Instrumentation

- The three wind-speed components were measured using an ultrasonic anemometer (Gill, UK).
- The particle concentration was determined with a condensational particle counter (CPC 3010/3762, TSI) which delivered a single particle count voltage output.
- The output of the ultrasonic anemometer was recorded via the serial port of a PC and the single particle voltage pulses were recorded with a counter on a PC card for data acquisition. Both outputs were coordinated by a Labview program (National Instruments, USA) and recorded with 20.8 Hz.
- Both instruments were installed on top of a measurement tower in a height of ~53 m above ground which corresponded to ~20 m above the canopy of a primary forest. The sonic anemometer was mounted at the end of a boom at the top segment of the tower (Fig. 1) which extended approximately 3 m away from the tower.
- The inlets for the aerosol particle measurements (and other trace gases) were installed in the height of the ultrasonic head at the horizontal distance of 15 cm (Fig. 1).



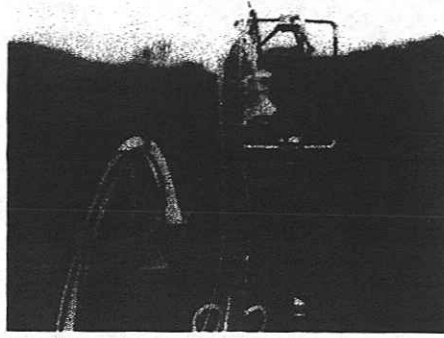


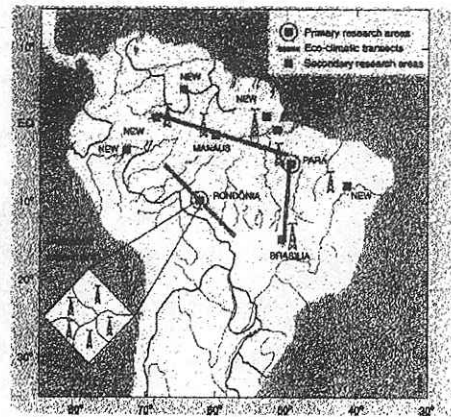
Fig.1 The ultrasonic anemometer was mounted at the end of a boom on the top segment of the measurement tower. The sample inlets for the aerosol particles were installed ~15 cm away from the anemometer.

Data Processing

- In order to reduce instationarities in the aerosol concentration, the raw data of the aerosol concentration was detrended using a running mean window filter with a width of 300 s.
- The power and co-spectra were calculated from half-hour datasets. The flux results represent half-hour means.

Location

- The measurement tower was located in Rondônia, Brasil, in the southwestern part of the Amazon (10° 5' S, 61° 55' W) in a region of primary rainforest.



Results

1 Aerosol particle concentration

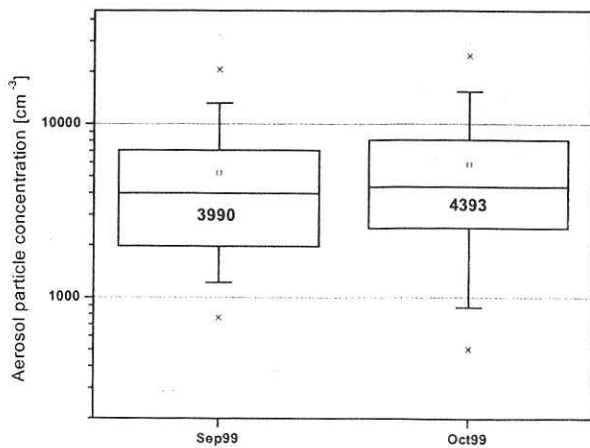


Fig.2 Distribution of aerosol concentrations in the dry season. The values inside the boxes give the median concentration.

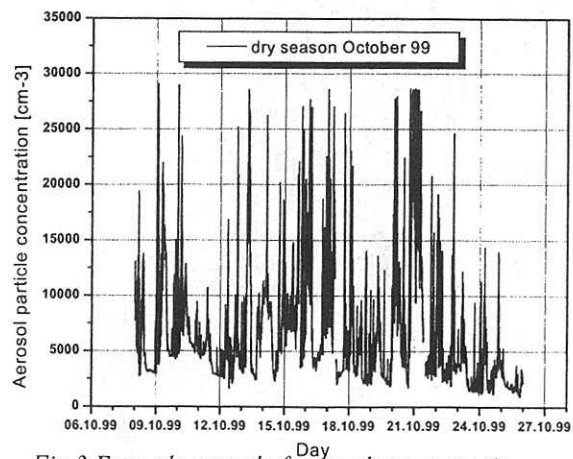
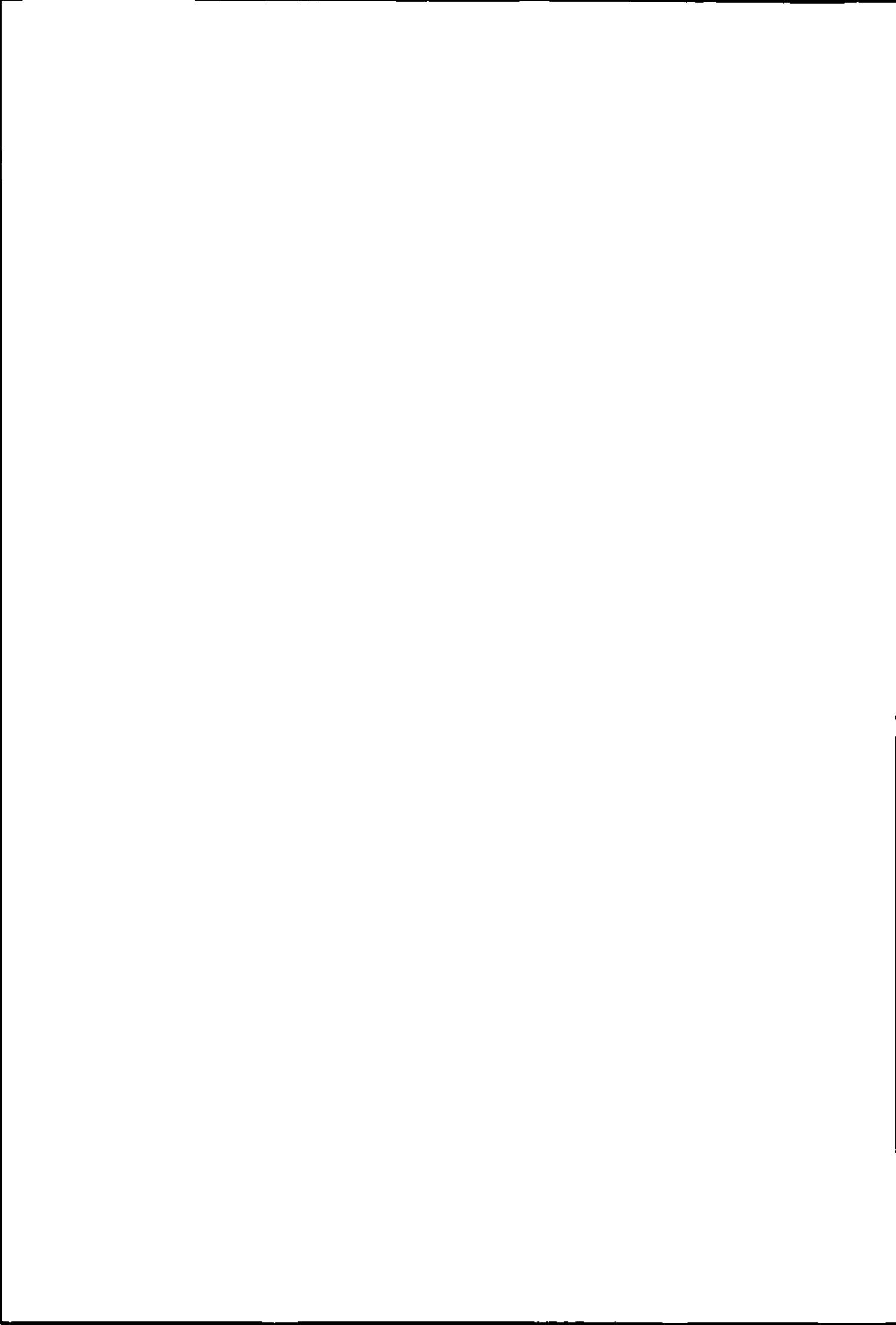


Fig.3 Example record of aerosol concentrations measured during 8-25 October.



II Power- and Co-Spectra

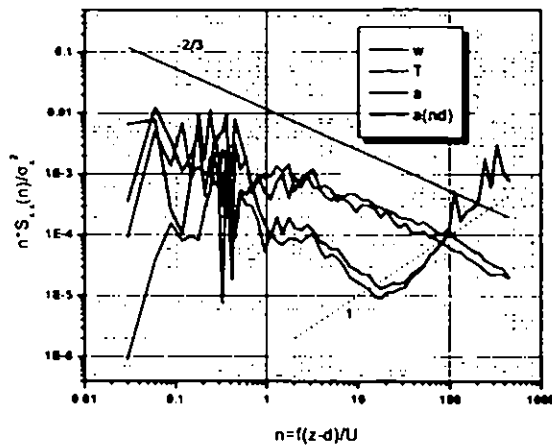


Fig.4 Normalised, frequency-weighted powerspectra of the detrended vertical wind speed (w), temperature (T), aerosol concentration (a) and the undetrended aerosol concentration ($a(nd)$).

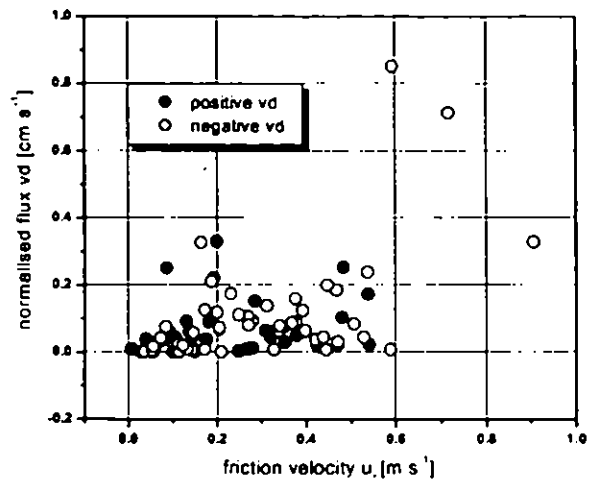


Fig.5 Normalised, frequency-weighted cospectra of the detrended windspeed u (wu), temperature (wT), aerosol concentration (wa) and the undetrended aerosol concentration ($wa(nd)$).

III Deposition velocity or normalised flux of aerosol particles

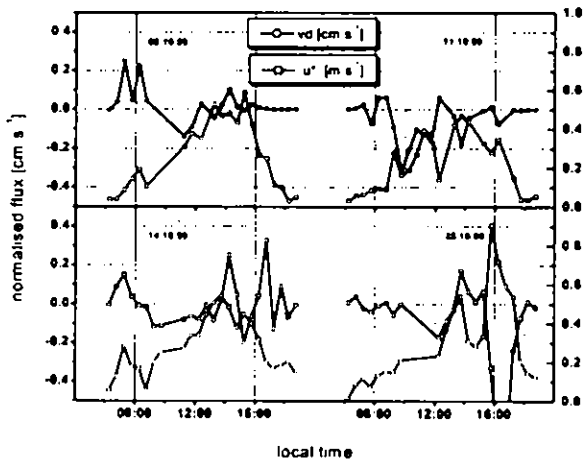


Fig.6 Daytime normalised flux (vd , deposition velocity) determined by eddy correlation and friction velocity (u^*). Positive values of vd denote deposition, negative values denote emission.

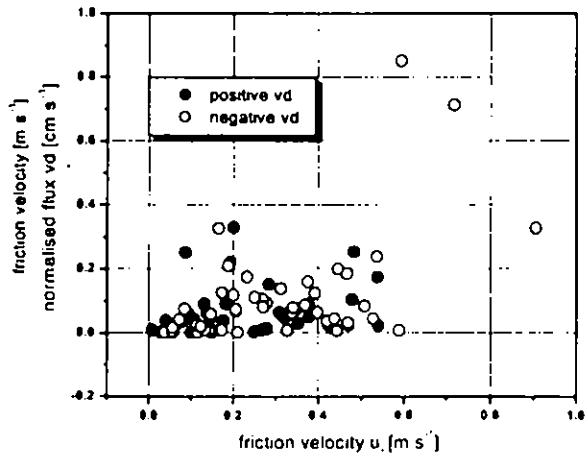


Fig.7 Daytime normalised flux (vd) versus friction velocity (u^*).

Discussion

Aerosol particle concentration

- An overview of the measured aerosol particle concentrations for the dry season during September/October is presented in Fig. 2. The aerosol concentrations were rather high due to biomass burning activity in the area close to the measurement site.
- The aerosol concentrations varied strongly on short timescales of a few minutes caused by advection which is shown in Fig. 3. These instationarities in the concentrations had to be removed for the eddy correlation determination of the particle flux by using a filter as described in the method.



Spectral Analysis

- The power spectra of all measured components are compared in Fig 4. The spectra follow the $-2/3$ slope in the inertial subrange. The spectra for the aerosol particles ran into a -1 slope above $n=20$ ($f=0.3$ Hz) caused by white noise underlying the particle counter signal. This spectral region did not contribute significantly to the flux of aerosol particles (Fig.5).
- The cospectrum of the raw aerosol particle concentration with vertical windspeed w ($w_a(nd)$) showed a large contribution at low frequencies compared to other cospectra (Fig.5). This was due to a low frequency contamination caused by the highly variable concentration due to advected plumes. The running mean filtering described in the method reduced that contribution and yielded cospectra that were comparable to the spectra of the sensible heat.

Deposition velocity or normalised flux of aerosol particles

- The normalised aerosol particle fluxes ($=vd$) determined by eddy correlation were generally below 1 cm s^{-1} (Fig.6). Deposition was observed as well as emission.
- The normalised fluxes compared to the friction velocity u_* are presented in Fig.7. The friction velocity is a measure for turbulence. It can be seen from Fig.7 that the turbulent flux increased with u_* although the scatter was large. The normalised fluxes observed for these example days were mainly in the range of $\pm 0.2 \text{ cm s}^{-1}$. This is within the range of $\pm 0.15 \text{ m s}^{-1}$ that is known from published investigations over forests using similar techniques (Buzorius et al., J.Aerosol Sci.(29), 1998).
- The observed aerosol particle emissions could have been due to photochemical production of aerosol particles within or close to the canopy top. The forest emitted hydrocarbons which are known to produce particles by photooxidative processes. On the other hand instationarities in the aerosol particle concentration could not be removed completely. They might have contributed artificially to the flux.

Conclusion

Preliminary results from the aerosol particle flux measurements above a primary rainforest in Amazonia using an eddy correlation method were presented. The spectral analysis showed that the variances follow the expected theoretical behaviour and that underlying white noise in the particle counter signal prevented the resolution of frequencies above 0.3 Hz. These did not contribute significantly to the flux. Deposition and emission were observed within the range reported in literature with normalised fluxes of mainly $\pm 0.2 \text{ cm s}^{-1}$. The aerosol particle emission could be caused by particle formation within the forest canopy but further investigations have to be done on the influence of the instationarities in the particle concentration on the calculated flux.

Acknowledgement

The author would like to thank Dr. Martin Gallagher (UMIST, Manchester) and Dr. Eiko Nemitz (CEH, Edinburgh) for the generous and friendly introduction to the determination of aerosol particle fluxes using the eddy correlation method.



Direct Measurements of the Long-Term Enhancement of Aerosol Deposition onto Woodland using a ^{210}Pb Tracer Method

¹F CHOUBEDAR, ¹D BRANFORD, ¹K J WESTON, ²D FOWLER, ²E NEMITZ, ³K GOULDING

¹Dept of Physics, University of Edinburgh, JCMB, Mayfield Road, Edinburgh EH9 3JZ.

²Centre for Ecology & Hydrology, Bush Estate, Penicuik, Midlothian EH26 0QB.

³IACR Rothamsted, Harpenden, Hertfordshire AL5 2TQ

Abstract

The dry deposition flux of atmospheric aerosols has been measured using a ^{210}Pb tracer method. Inventories of ^{210}Pb in soil which have been undisturbed for in excess of 100 years at Rothamsted provide long term coverage dry deposition fluxes in the range $34 \text{ Bq m}^{-2} \text{ y}^{-1}$ for grassland, $60 \text{ Bq m}^{-2} \text{ s}^{-1}$ for deciduous woodland and $68 \text{ Bq m}^{-2} \text{ s}^{-1}$ for a deciduous shelter belt. These fluxes are equivalent to long-term average deposition velocities respectively of 4.6 mm s^{-1} , 8.3 mm s^{-1} and 9.4 mm s^{-1} for aerosols in the size range $0.2 - 0.5 \mu\text{m}$ diameter. The deposition velocities for woodland are substantially larger than those obtained in wind tunnel studies but are similar to field measurements by eddy co-variance methods.

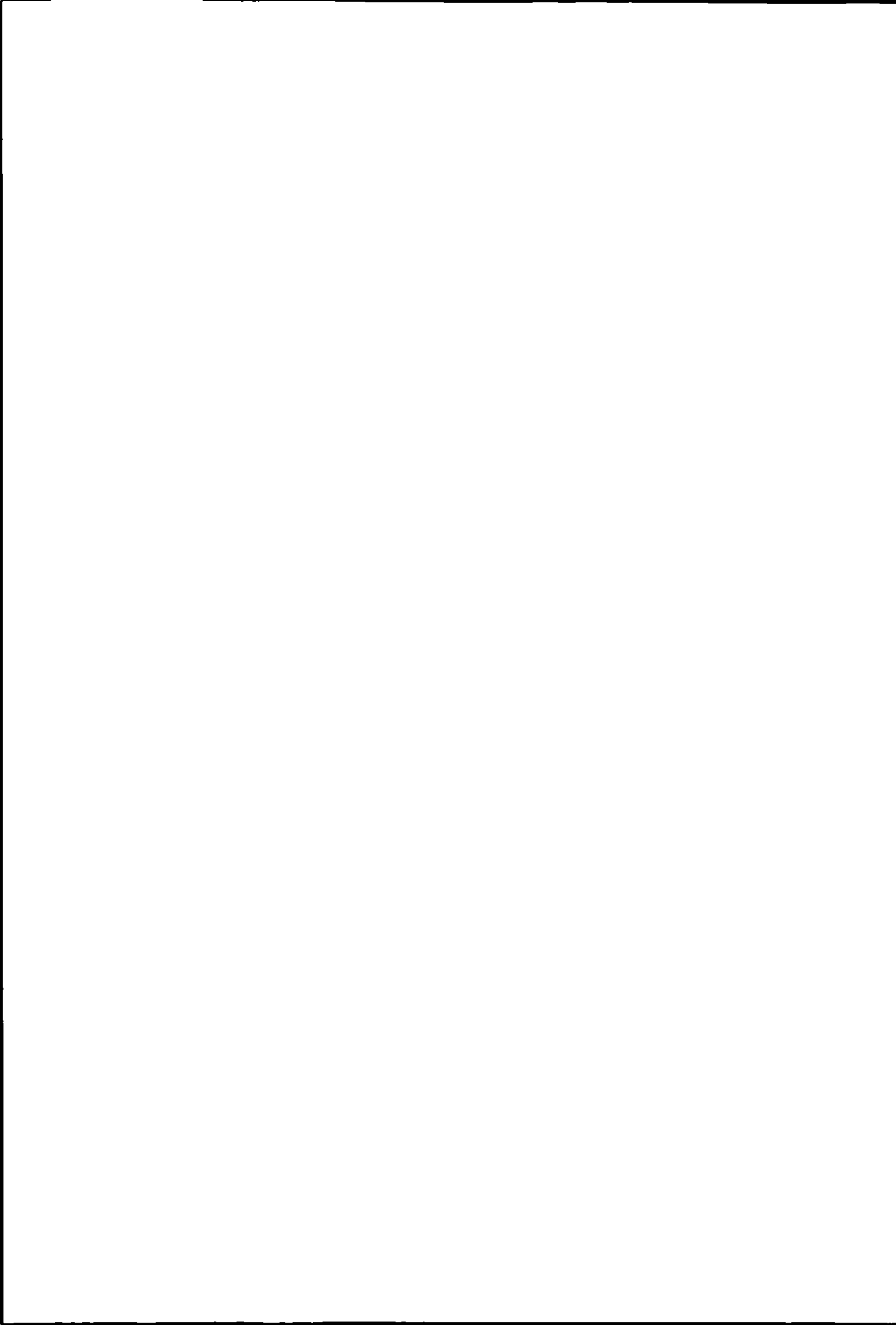
Introduction

The earth's crust contains the radioactive element ^{238}U which decays through ^{226}Ra to ^{222}Rn . This element emanates out of the earth's crust into the atmosphere. ^{222}Rn (mean radioactive lifetime of 5.52 days) is a water-insoluble inert gas which is lost from the atmosphere by radioactive decay to ^{210}Pb . The decay series of ^{238}U is shown in Figure 1. ^{210}Pb atoms (mean radioactive lifetime of 32.3 years) become quickly attached to aerosol particles, (the same size aerosols as SO_2 and NO_x) and are removed from the atmosphere primarily by dry and wet deposition. The mass median diameter of ^{210}Pb -containing particles both in continental and marine environments is in the range of 0.3-0.4 micrometres; typically, 90% or more is present on particles less than 1.0 micrometre (e.g. Turekian *et al.*, 1989, Knuth *et al.*, 1983).

A small proportion of ^{222}Rn emanated from the earth's surface is redeposited as short-lived decay products, but most decay in the atmosphere into ^{210}Pb . The mean residence time of ^{210}Pb is short (a few days) compared with its radioactive half-life (22.3 years), so the downwards flux of ^{210}Pb , in $\text{atoms m}^{-2} \text{ s}^{-1}$, should equal the upwards flux of ^{222}Rn .

Sampling methods

When scavenged from the atmosphere along with carrier aerosols, ^{210}Pb is retained by the organic-rich surface horizontal soil which acts as an efficient integrating collector (Lewis, 1977). Forest soils are generally well suited for ^{210}Pb deposition rate measurements (Graustein and Turekian, 1983). The excess ^{210}Pb (^{210}Pb - ^{214}Pb) in each section of the core were measured. Non-destructive gamma-spectroscopy was used to measure ^{210}Pb in each core. ^{210}Pb total inventory in undisturbed soils was used as a measure of total aerosol deposition averaged over about 30 years, approximately the mean nuclear life time (30.2 years).



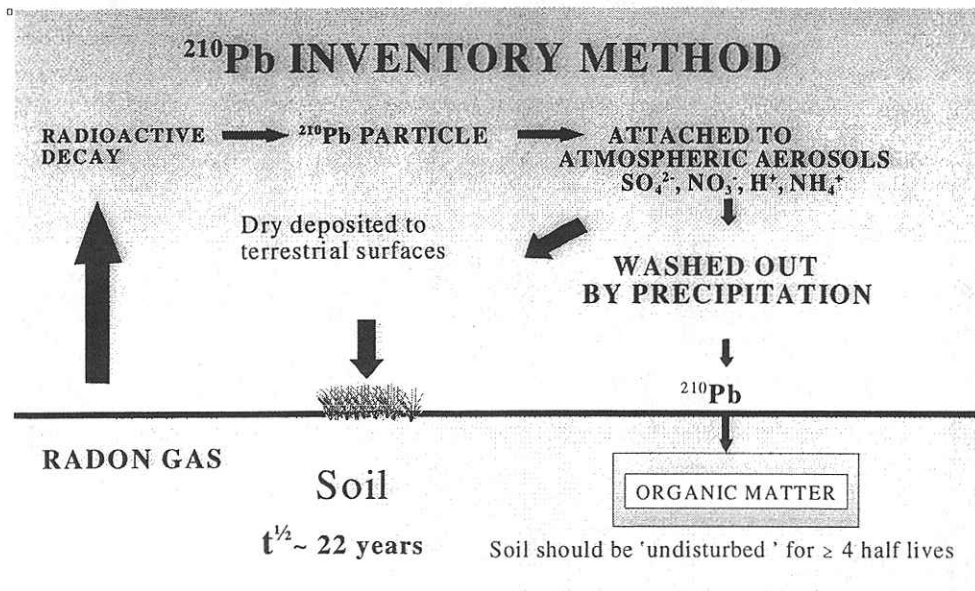
On the bases of the above criteria, soil samples were collected from locations in Rothamsted experimental station in Harpenden, Hertfordshire, England during February 1998.

In total from 10 sites, 50 samples were collected and divided to 150 sub-samples in 3 open areas and 2 woodlands. All of the samples were taken using a corer 10 cm diameter and 25 cm long.

Results and discussions

The ^{210}Pb isotope in the atmosphere is removed by precipitation and dry deposition and therefore provides a valuable tracer to study deposition processes. At a site which experiences little fog or orographic cloud, and where wet deposition is constant over different land uses, the measured inventory of ^{210}Pb in upper horizons of soil may be used to derive a mean annual deposition flux and to study the effect of the vegetation height and roughness length on the deposition flux and deposition velocity (V_{dd}).

The atmospherically derived ^{210}Pb inventory into the canopies exceed those in adjacent open areas, indicating that forest sites receive more atmospheric inputs. The mean ^{210}Pb inventories are $3753 \pm 139 \text{ Bq m}^{-2}$ for open grassland, $4607 \pm 135 \text{ Bq m}^{-2}$ for Geescroft canopy and $4844 \pm 124 \text{ Bq m}^{-2}$ for Broadbalk canopy, shown in figure 1.

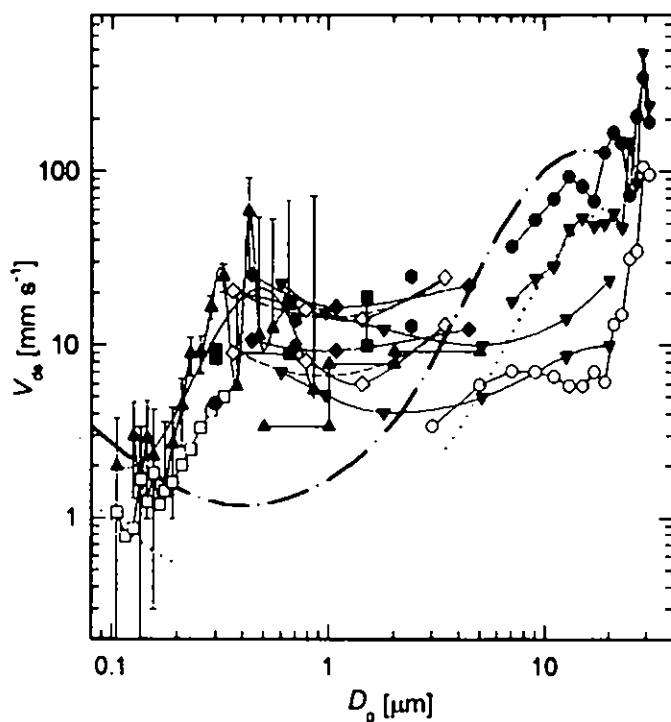


The results of these calculations together with the results from different studies and the wind tunnel results are plotted in Figure 2.

The inventories may be used to calculate the annual deposition fluxes directly. These fluxes may then be partitioned into dry and wet deposition by subtracting the much more readily measured wet deposition (which for this site was provided by measurements at Harwell). The dry deposition flux may be used to calculate deposition velocity using ambient aerosol ^{210}Pb concentration measurements (0.23 mBq m^{-3}).



The results of calculations from this study showed substantially larger dry deposition velocities (V_{dd}) in size range of ^{210}Pb carrier aerosols (sub-micron) than the wind tunnel prediction of dry deposition. The values of V_{dd} for this study were $4.7 \nabla 0.6 \text{ mm s}^{-1}$ for grassland, $8.4 \nabla 0.6 \text{ mm s}^{-1}$ for Geescroft woodland and $9.3 \nabla 0.5 \text{ mm s}^{-1}$ for Broadbalk woodland. These values are an order of magnitude larger than the wind tunnel results which imply that the wind tunnel measurements do not simulate the full range processes occurring in the field.



- | | |
|---|--|
| ◇ Höfken and Gravenhorst (1983) | ▲ Lorenz and Murphy (1989) |
| ◆ Grosch and Schmitt (1988) | Gradient Loblolly Pine, $h_c = 9 \text{ m}$ |
| ■ Brückman (1988) | ● Höfken <i>et al.</i> (1983) TF Beech |
| □ Joutsenoja (1992) $u^* = 0.68 \text{ m s}^{-1}$,
$u = 5.6 \text{ m s}^{-1}$, $z_0 = 0.08 - 0.13 \text{ m}$ | ● Höfken <i>et al.</i> (1983) TF Spruce |
| ▼ Waraghai and Gravenhorst (1989) | · Slinn (1982), $u^* = 0.65 \text{ m s}^{-1}$ |
| ▼ Gallagher <i>et al.</i> (1992) | — Unmodified Model Result |
| $u_* = 0.71 \text{ m s}^{-1}$, $z_0 = 15.7 \text{ cm}$ | — Slinn (1982), $u^* = 1.30 \text{ m s}^{-1}$ |
| ● Gallagher <i>et al.</i> (1992) | Unmodified Model Result |
| $u_* = 0.75 \text{ m s}^{-1}$, $z_0 = 18.6 \text{ cm}$ | ● Choubedar and Fowler (2000) |
| ○ Beswick <i>et al.</i> (1991) | ^{210}Pb grassland Rothamsted ($u_* = 0.14 \text{ m s}^{-1}$) |
| $u_* = 0.37 \text{ m s}^{-1}$, $z_0 = 30.1 \text{ cm}$ | ■ Choubedar and Fowler (2000) |
| ▲ Gallagher <i>et al.</i> (1997a) | ^{210}Pb forests Rothamsted ($u_* = 0.36 \text{ m s}^{-1}$) |
| $u_* = 0.5 \text{ m s}^{-1}$, $z_0 = 3.5 \text{ m}$ | |

Furthermore, the measurements from this study show that V_{dd} may be measured directly by knowing the soil inventory, rain flux and air concentration of the isotope.

Conclusions

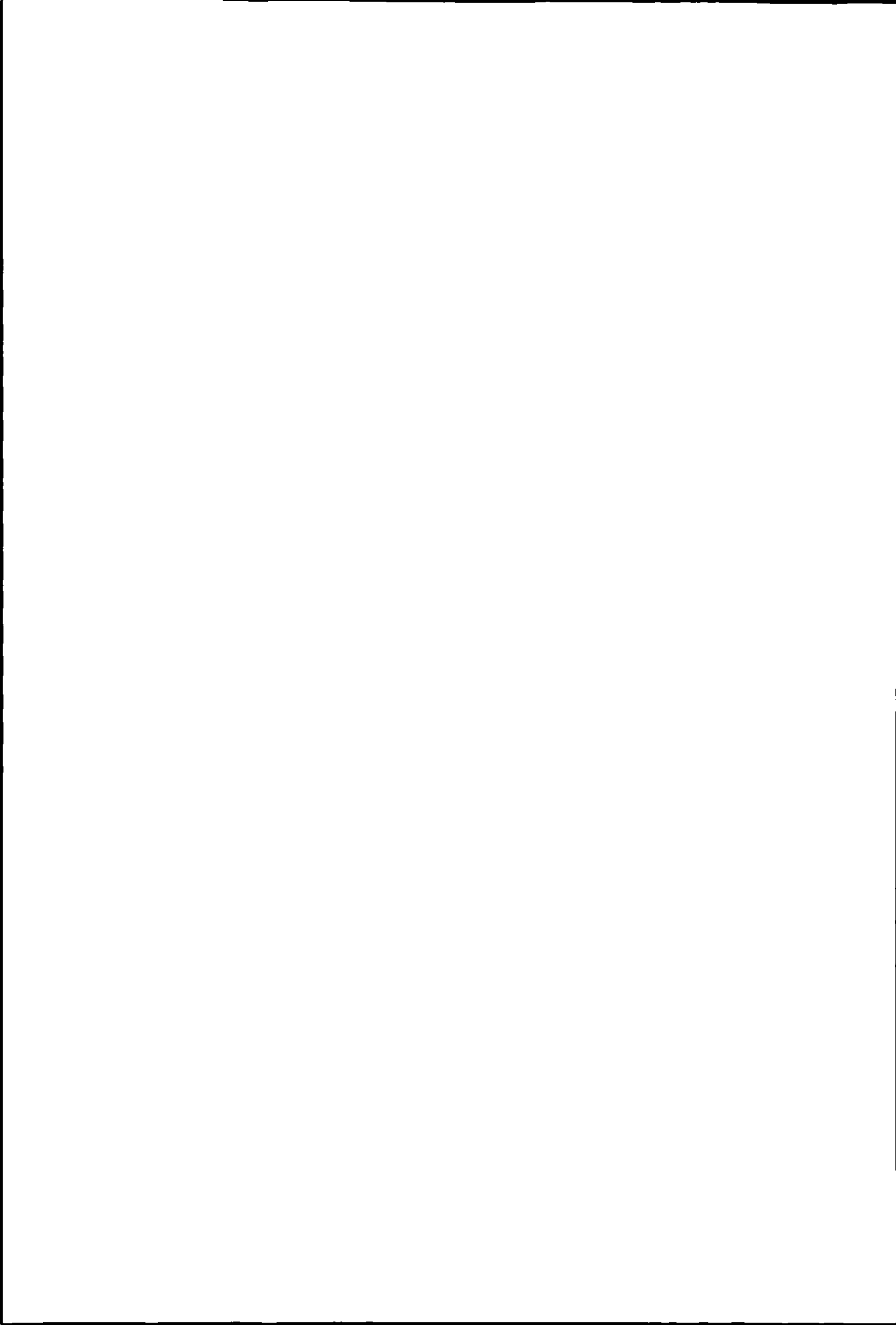
Long-term average aerosol dry deposition fluxes and deposition velocities onto terrestrial



surfaces may be obtained from ^{210}Pb inventories in soils. Measurements of ^{210}Pb inventories in soils within the long-term Rothamsted experiments show annual dry deposition inputs into woodland larger than those into grassland by approximately a factor of 2. Deposition velocities for ^{210}Pb carrier aerosols in the size range 0.2 to 0.5 μm diameter were 4.7 mm s^{-1} for grass, 8.4 mm s^{-1} for deciduous woodland and 9.3 mm s^{-1} for a shelter belt deciduous woodland.

References

- Gallagher M.W., Beswick, K.M., Duyzer, J., Westrate, H., Choularton, T.W. and Hummelshoj, P.: 1997, 'Measurements of aerosol to Speulder forest using a micrometeorological technique', *Atmos. Environ.* **31**(3), 359-373.
- Graustein, W.C. and Turekian, K.K.: 1983, ' ^{210}Pb as a tracer of the deposition of sub-micrometre aerosols', in *Precipitation scavenging, dry deposition, and resuspensions*, pp. 1315-1324.
- Knuth, R.H., Knutson, E.O., Feely, H.W. and Volchok, H.L.: 1983, 'Size distribution of atmospheric Pb and ^{210}Pb in rural New Hersey', in *Precipitation scavenging, dry deposition, and resuspensions*, pp. 1325-1335.
- Lewis, D.M.: 1977, 'The use of ^{210}Pb as a heavy metal tracer in the Susquehanna River system', *J. Geochemica et cosmochimica Acta.* **41**, 1557-1564.
- Turekian, K.K., Graustein, W.C. and Cochran, J.K.: 1989, ' ^{210}Pb in SEAREX program: An aerosol tracer across the Pacific'. *J. Chem. Oceanography* **10**, 51-81.



Eddy Correlation Measurements of Urban Aerosol Fluxes

J.R. DORSEY¹, E.G. NEMITZ², M.W. GALLAGHER¹, K.N. BOWER¹, P.I. WILLIAMS¹ & D. FOWLER²

¹ Physics Dept, UMIST, P.O. Box 88, Sackville Street, Manchester, M60 1QD, UK

² Centre for Ecology and Hydrology, Edinburgh Research Station, Penicuik, Midlothian, EH26 0QB

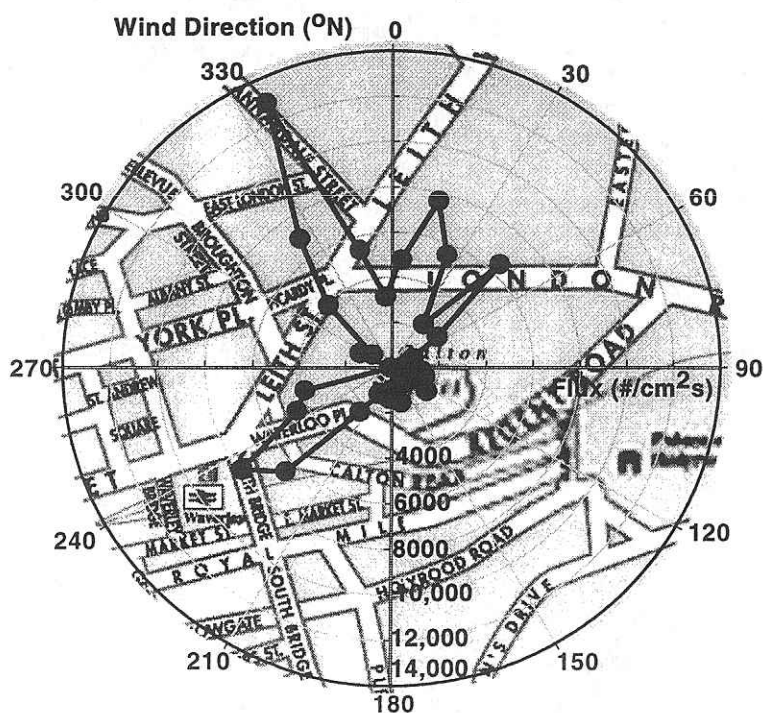
Introduction

Urban aerosols have a variety of effects, including direct impacts on human health. They can be transported large distances downwind of their city of origin, and deposited to potentially sensitive ecosystems. SASUA is an ongoing project aimed at quantifying the Sources and Sinks of Urban Aerosol.

Measurements

We have measured total and size segregated aerosol fluxes in the size range $11 \text{ nm} < D_p < 25 \mu\text{m}$ within Edinburgh City centre, using the eddy correlation technique. The city was treated as a tall canopy, with measurements being made above it. The Nelson Monument (70 m above street level) was used to achieve the required height. Size segregated concentrations were also measured for $D_p > 3 \text{ nm}$. Along with supporting trace gas and traffic activity measurements, this allows identification of the main pollution sources in the city.

Figure 1, (below) shows the particle flux distribution with wind direction.





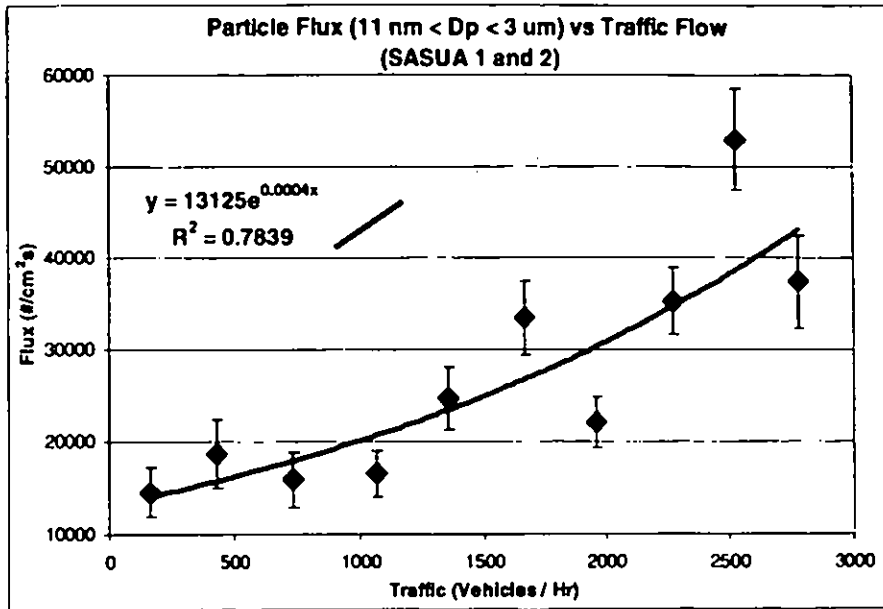
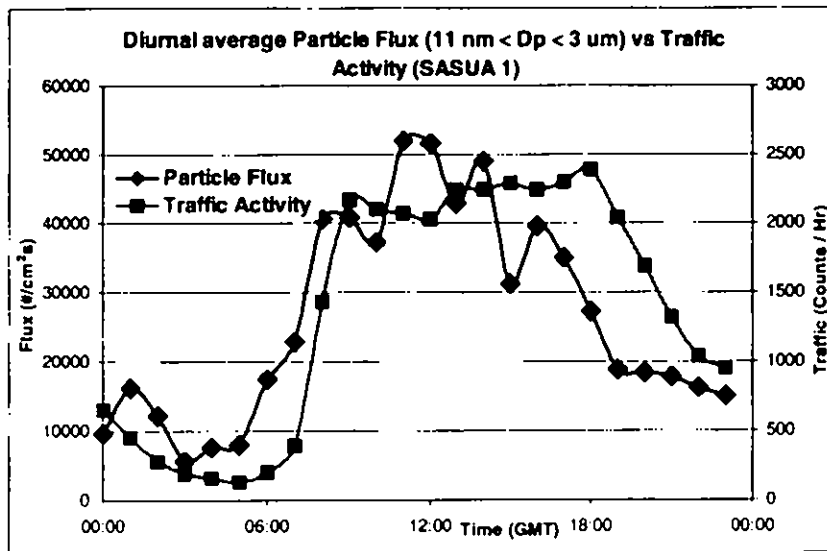


Figure 2, (above) shows the relationship between traffic activity and total particle flux



(production)

Figure 3, (above) shows the relation between fine and accumulation mode aerosol fluxes measured in the city.

The particle flux distribution shown in Figure 1 has a number of interesting features. The large values to the NW and SW are caused by the busy northern one way system including Queen Street, and the main road through the city, Princes Street respectively.



The effect of traffic is shown in Figure 2, with a clear increase in particle flux with traffic activity in the city. Scatter is introduced by inclusion of data from different regimens and wind directions. Particulates produced by traffic are thought to peak at around 20 nm. This is borne out in Figure 3, a comparison of fine and accumulation mode fluxes.

Traffic activity appears to dominate the particle flux in the city, as shown in the preceding figures. However the imperfect correlation between traffic activity and total particle flux shown in Figure 4 may suggest there are also other mechanisms producing particles. These may include space heating, biogenic emissions and non-road transport sources, as well as unaccounted-for background.

These results will be used to develop and test parameterisations for urban aerosol concentrations and fluxes, in terms of anthropogenic activity and meteorological conditions.

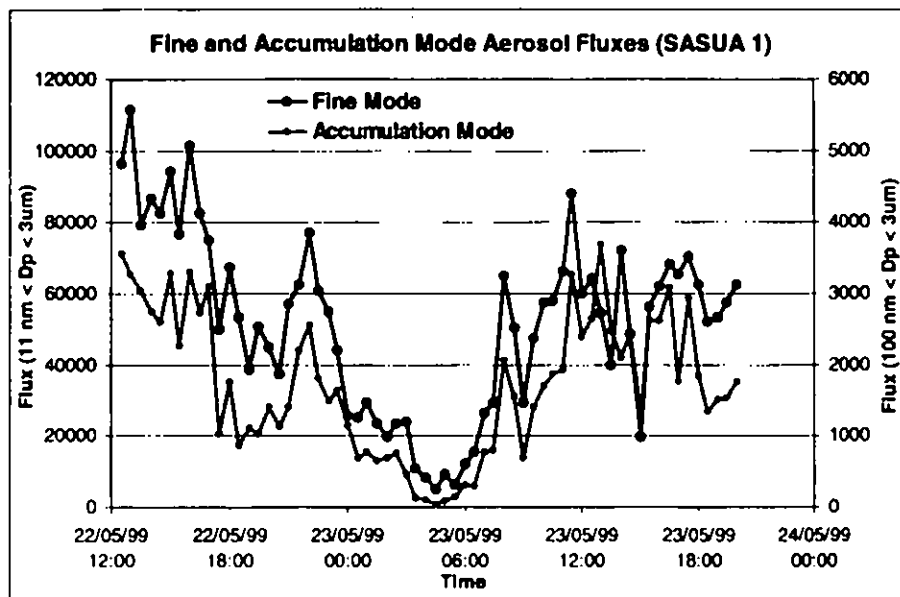


Figure 4, (above) shows the traffic activity and total particle flux, diurnally averaged over the first project (May 1999).

Acknowledgements

The help of Edinburgh City Council in providing infrastructure and additional data is gratefully acknowledged. This work was supported under NERC grant 022244.



UNCERTAINTIES IN MASS BALANCE OF U.S. ATMOSPHERIC MERCURY EMISSIONS

¹LEONARD LEVIN*, ²STEVE LINDBERG, ³MAE SAXAUER GUSTIN

¹*Electric Power Research Institute, 3412 Hillview Avenue, Palo Alto, California 94303 USA*

²*Oak Ridge National Laboratory, Oak Ridge, TN USA*

³*University of Nevada, Reno, NV USA*

Corresponding author: llevin@epri.com

Introduction

The primary source of current mercury input to many US water bodies is believed to be atmospheric deposition (Engstrom & Swain, 1998). Of this deposition, an unknown portion is made up of regional and local atmospheric emissions from US point sources, and the balance from globally-circulating mercury from both US and international atmospheric sources. These proportions may be about 60 and 40% respectively, at least for northern tier US states. Speciation of emitted mercury is similarly uncertain; a common default assumption is that 50% each is in ionic and elemental form when emitted from combustion sources (US EPA, 1998). That speciation is likely to impact the fraction that is transported beyond local scale. Calculations indicate that, for a combustion source stack height of 300m, less than 20% of the emitted mass of mercury will deposit within a radius of 50km even under the assumption that it is all ionic when emitted.

The control on a mass balance of US-emitted mercury is the extent of data on ground-level atmospheric concentrations and deposition nationally. Monitoring and sampling networks are only now beginning to reach spatial density and time extent that allow patterns and trends to begin to be discerned (NADP, 1999). These are still inadequate to provide good closure on goodness-of-fit for regional or local models of atmospheric mercury transport and deposition, and so these tools remain highly uncertain for purposes of assessing source-receptor relationships.

Recent measurements in Ontario, California, Nevada, and Tennessee have begun to quantify an additional source of mercury long included in global mass balances, but to date not incorporated in regional mercury inventories (Rasmussen, 1997; Gustin, 1999; Lindberg, 1999). Field measurements of emission rates from natural and anthropogenically-impacted background areas show wide variability in rates of emission of total gaseous mercury with terrain characteristics, the occurrence of precipitation onto the surface, and other factors. Extension of these point measurements in time and space is highly speculative, since no general scheme for assigning rates to terrain characteristics is yet available. One extrapolation to the area of the continental US yields background emission rates roughly equal to the total of current US industrial emissions. Another extrapolation from Ontario measurements of mercury emissions from black shale yielded rates sufficient to explain a good portion of station-monitored atmospheric concentrations in north-eastern states (Pai *et al.*, 1999).

Nonetheless, inclusion of these new point readings in regional and continental inventories is not yet possible. In addition to their low density of coverage, basic characteristics of these emissions are unknown, including their ionic form and the mechanism for their transport. Diffusive vertical mixing is possibly dominant, but episodic large-volume vertical transport



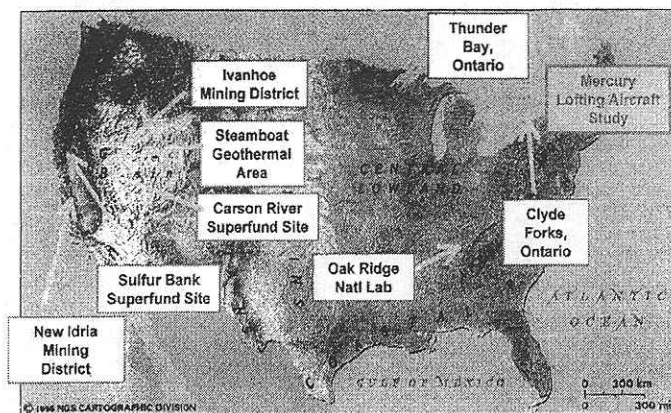
by wildfires and meteorological events may also play a role. Current research is investigating these potential mechanisms in order to a low inclusion of the background term in future

Measurements of Background Mercury Emissions

Field studies have been carried out in a variety of North American settings, including Nevada (Fig. 1), California, Tennessee and Ontario. Two primary methods have been employed to measure mercury

emissions from these areas. One, the flux chamber method, employs a bottomless surface enclosure, typically transparent, fixed over the surface of interest. Two tubes are attached, one at each end of the dome, with one serving as an outlet to which an exhaust pump is attached. Mercury is measured at the inlet and outlet tubes, with the flow adjusted to attain a stable mercury concentration difference over time.

Fig. 1. North American mercury emissions field study sites



The second method is the vertical flux method. An instrumented tower is erected, with two levels of measurement of temperature and turbulent wind velocity. Mercury fluxes are calculated indirectly from measurements of concentration at the two levels using a modified Bowen ratio to calculate vertical fluxes. In this, the two instrumenting levels are used to measure fast-response sensible heat fluxes and slower latent heat fluxes, as well as fast - response concentrations of a passive atmospheric constituent such as CO₂. These values are used to derive a vertical diffusivity coefficient for passive constituents, then applied to mercury concentrations measured at one level to derive vertical mercury fluxes (Fig. 2).

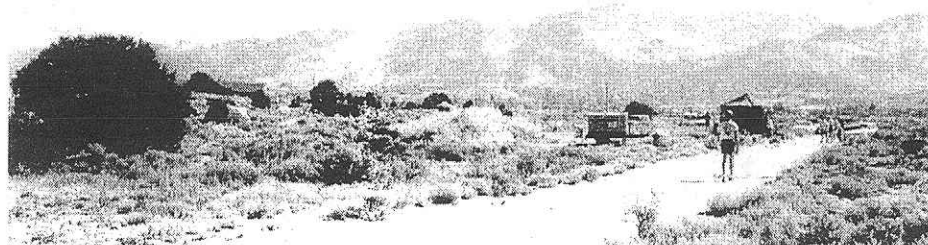


Fig. 2. Flux chamber developed by Oak Ridge National Laboratory, US, for use in the Nevada methods intercomparison experiment



Field comparisons among the two methods at the Nevada Study and Test of the Release of Mercury from Soils

Field measurements in mid-2000 are expected to help clarify in particular the role of wildfires in lofting surficial emissions of mercury to the free atmosphere.

(SToRMS) Experiment, 1997, at the Steamboat (Nevada) Geothermal Area showed that the flux chamber consistently predicted lower fluxes than those derived from the micromet towers (Fig. 3) by about a factor of 3 (Gustin *et al.*, 1999). This systematic bias is probably due to insufficient volume flow rate through the flux chambers, even though the devices were designed and operated independently by investigators.

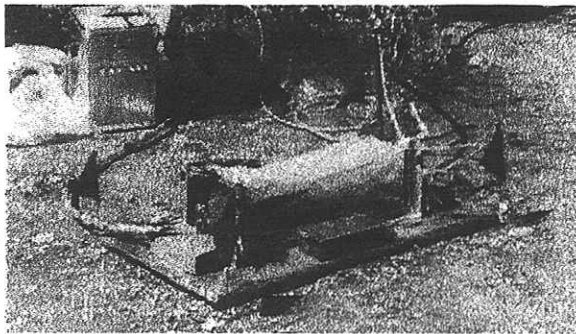


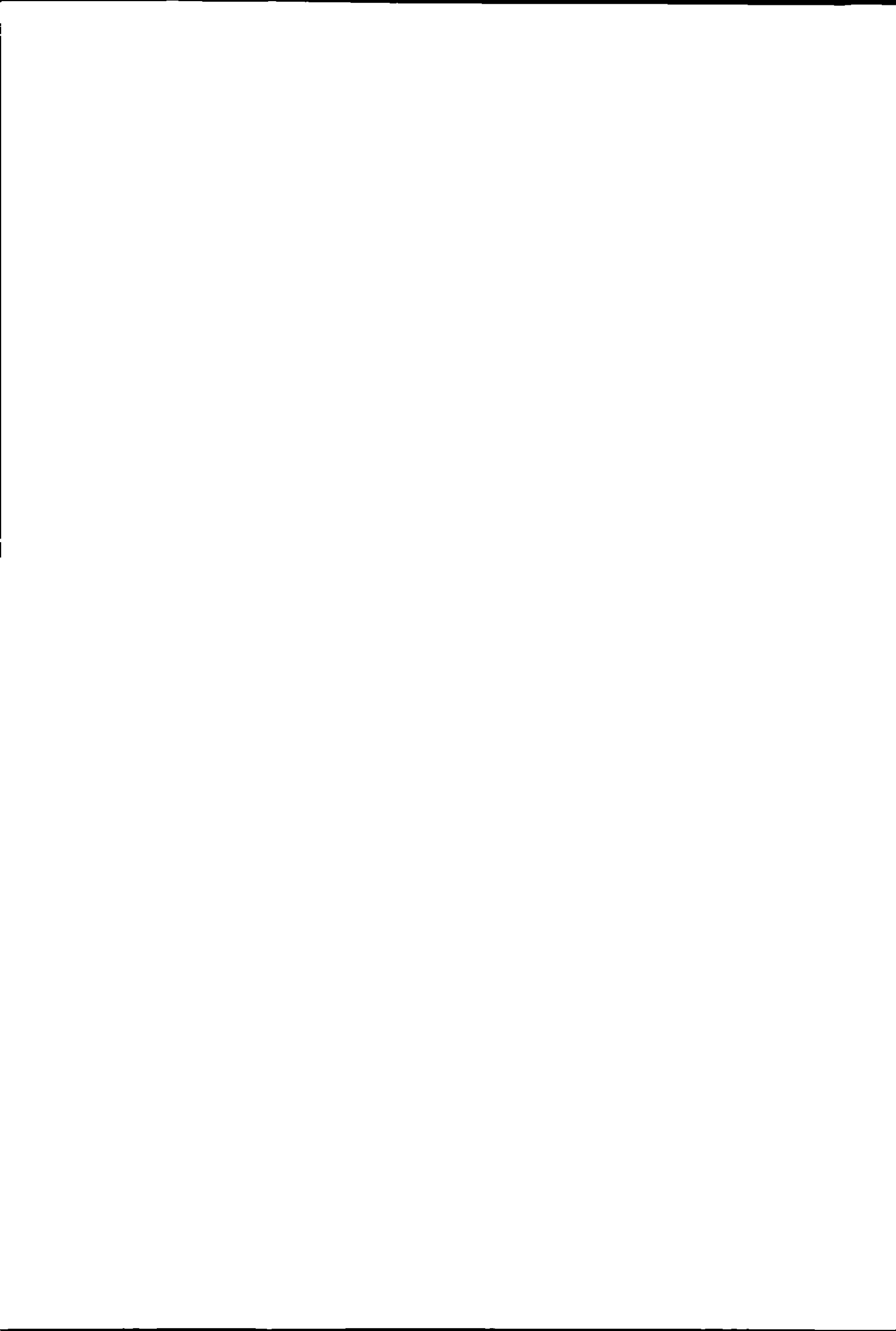
Fig. 3. Profiling towers deployed by US Geological Survey at Nevada methods intercomparison experiment. Meteorological arms are placed at logarithmic spacing to capture fluxes.

Initial Model Results, Background Mercury “Signal to Noise Ratio”

A simplified box model was developed for the continental United States to carry out initial estimates of the expected contribution of background mercury emissions to regional surface fluxes (fluxes far removed from deposition due to nearby elevated atmospheric point sources of total mercury), that is, fluxes at distances greater than about 50-100 km from such point sources.

For the model, an atmospheric mixing height of 6 km was assumed. Measurements of surface background emissions at this time consist of total mercury only; no information is yet available on valence state of the emissions, either at the surface or through transformations aloft. Since the estimates were carried out to evaluate the potential signal of background emissions in regional deposition patterns, a maximum ratio of Hg^{+2}/Hg^0 of 10/90 was assumed, with no reduction or oxidation occurring at regional scales under consideration.

A uniform surface emission rate of $18 \text{ ng/m}^2\text{-h}$ was assumed. The portion that is emitted as ionic mercury was assumed to follow the deposition behaviour of ionic mercury emitted from elevated point sources, analyzed using a Monte Carlo deposition model by Levin (1996); the median fraction deposited was found to be 17% within 50 km, and that rate was assumed to hold within the borders of the US. When these emission and deposition rates were compared with patterns of deposition from current measurement networks, and the US divided laterally at longitude 100W, a distinct difference was found between the eastern and western sectors in how much was contributed by natural emissions. For the western US sector, background emissions were found to be contributed (under the stated assumptions) between 10 and 15% to deposition at western sites. East of 100W, however, contributions were found to be in the 4 to 8% range.



Given these levels, it is likely that a discernible “signal” from background emissions is present in data from western sites, but not at eastern sites. The method is limited by the limited observations of deposition to date, apparently varying more in response to interannual patterns of precipitation than changes in source terms. As well, the assumption of a nationally uniform emission rate is limiting. It is likely that emissions are concentrated in the Basin and Range province of the western US, rather than uniformly distributed nationally. The effect of this would be to increase the signal in western stations and further decrease it at eastern sites.

Regional Fluxes of Background Mercury

Measurements in the eastern and western continental United States (Ebinghaus *et al.*, 1999) have demonstrated mercury emission rates from both natural crustal zones and from zones impacted by earlier human disturbance, such as mining sites, ranging from about 8 up to over 10^4 ng/m²-h (Gustin *et al.*, 1999). Using measurements in the vicinity of Medicine Lake, California, Gustin scaled these emissions by surface type, arriving at a total emission rate of mercury of 5,640 g/y over an area of 244 km². This yielded an average flux of 2.64 ng/m²-h in the region, based on the relationship derived between soil mercury content and emission flux (Fig. 5).

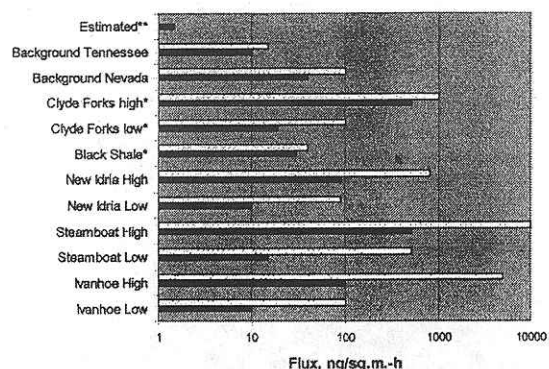


Fig. 5. Mercury emissions as a function of soil mercury concentration

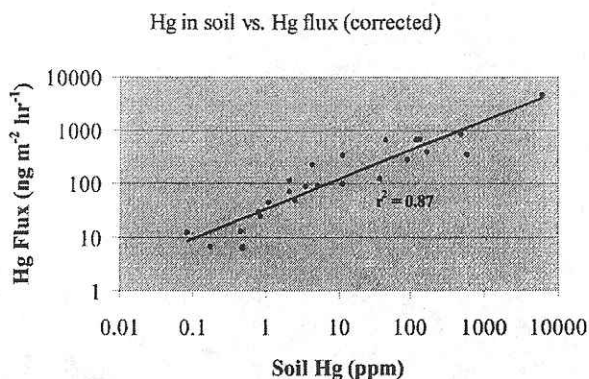


Fig. 6. Effect of incident radiation on mercury emissions, New Idria region, California

Measured fluxes vary greatly, apparently in a gradient away from disturbed mining sites; measured values at the Steamboat, Nevada, exercise ranged over 3 orders of magnitude. Scaling over mill sites near Virginia City, Nevada, by Gustin *et al.* (unpub. data) was used to estimate emissions from mill tailing piles, based on mercury content of the tailings wastes. When scaled to milling sites near Reno, Nevada, an estimate of 94.5 kg/y total mercury emissions to air is arrived at. This estimate accounts for the probable semidiurnal rise in mercury emissions (Fig. 6).



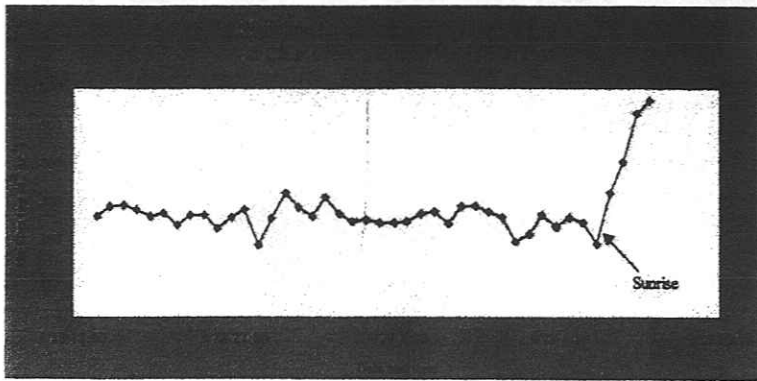


Fig. 6. Hypothesized continental-scale mercury emissions profile for United States, unweighted areal scaling

When these figures are scaled up by areal extent to the land area of the continental United States, a number approximating that of known anthropogenic emissions is derived (Fig. 6). This is recognised to be an oversimplification, since mid-continental areas are subject to both lower levels of mercury emission from crustal activity and vulcanism, and to a history of less mining activity than areas to the west. Eastern US areas may be subject to re-emission of surface-deposited mercury due to prevailing winds carrying atmospheric emissions from current and former industrial sources over that region. Nonetheless, to an order of magnitude, mercury emissions may be significant from these background areas of the US.

Current deposition measurements (Figs. 7-9) are still insufficient to act as a quantitative control on these estimates. Major portions of the US, such as the Mississippi River Valley, are essentially unmeasured. Recent additions to the network in northern California and in Colorado have the potential to establish some data on background deposition, representing global background plus regional contributions. An extended time series from this network is needed to clarify any patterns that may emerge.

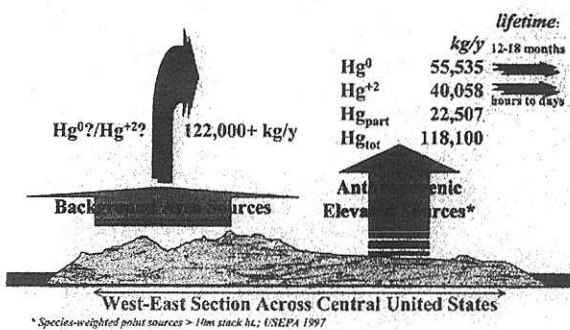


Fig. 7. US Mercury Deposition Network station data for wet deposition, 1996 (:g/m²/y)

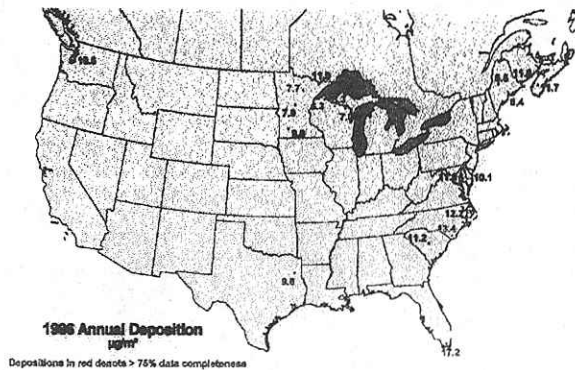
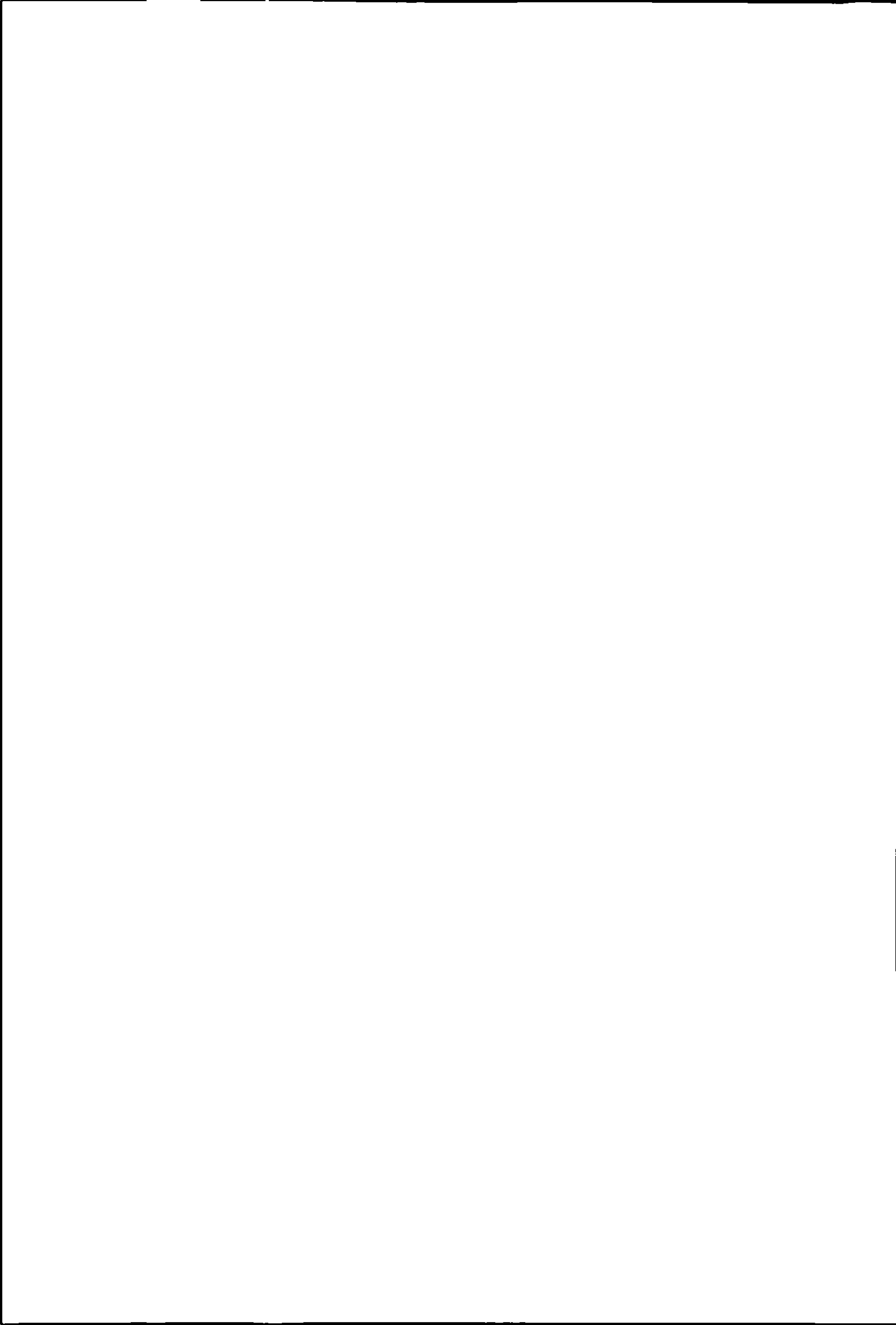


Fig. 8. US Mercury Deposition Network station data for wet deposition, 1997 (:g/m²/y)



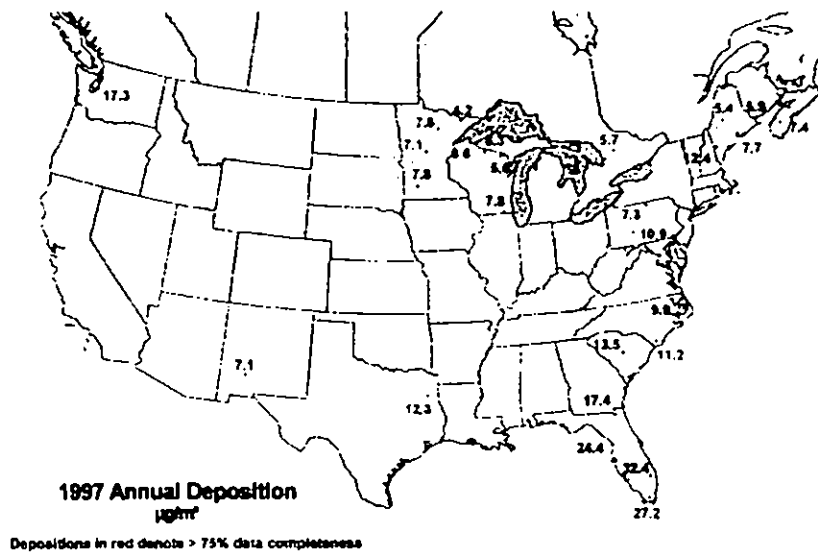
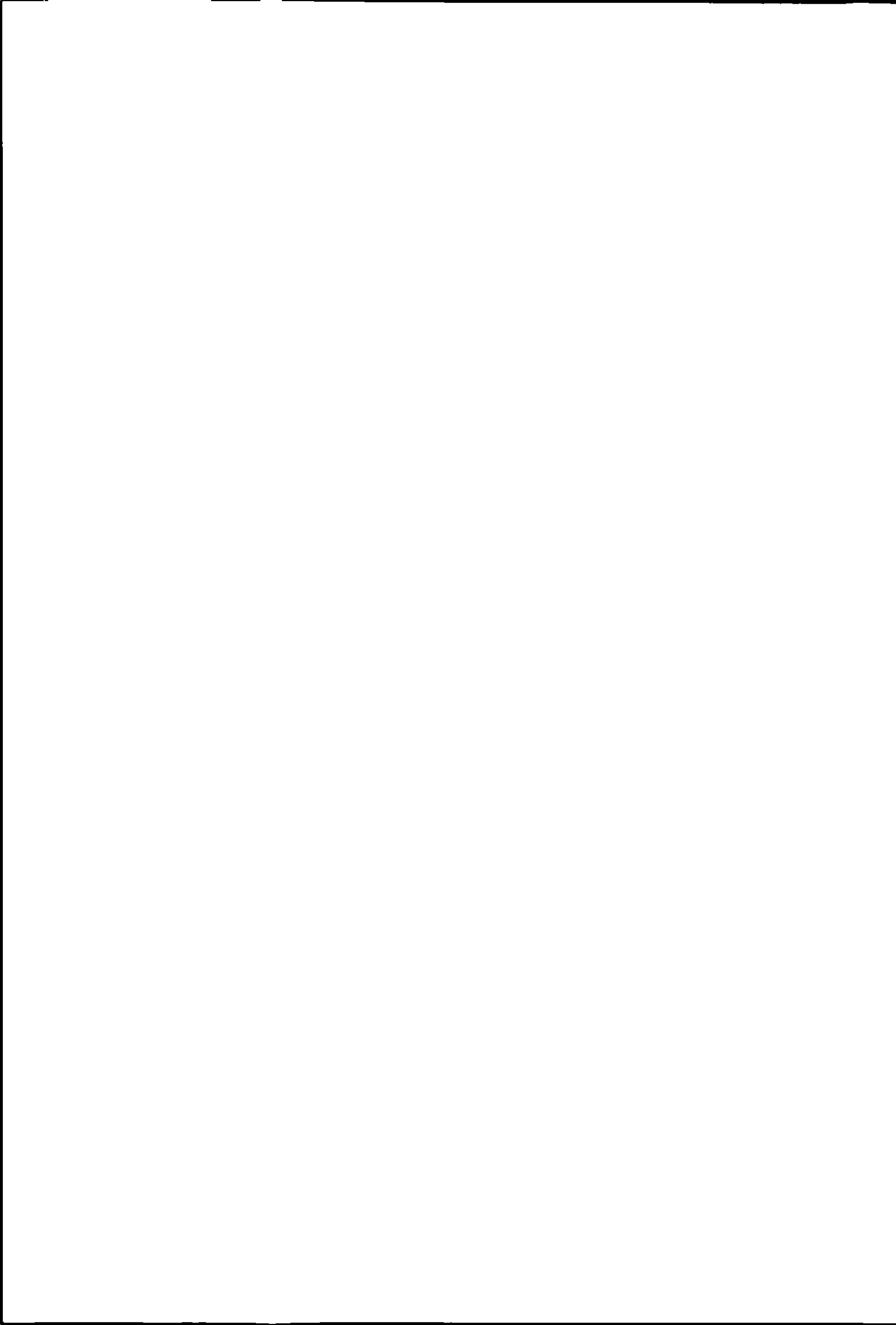


Fig. 9. US Mercury Deposition Network station data for wet deposition, 1998 ($\mu\text{g}/\text{m}^2/\text{y}$)

References

- Ebinghaus, R., Tripathi, R.M., Wallschlaeger, D. and Lindberg, S.E., "Natural and Anthropogenic Mercury Sources and Their Impact on the Air-Surface Exchange of Mercury on Regional and Global Scales," *Mercury -Contaminated Sites* (ed. Ebinghaus *et al.*), Springer-Verlag, Berlin, 1999.
- Gustin, M.S., Lindberg, S., Marsik, F., Casimir, A., Ebinghaus, R., Edwards, G., Hubble-Fitzgerald, C., Kemp, R., Kock, H., Leonard, T., London, J., Majewski, M., Montecinos, C., Owens, J., Pilote, M., Poissant, L., Rasmussen, P., Schaedlich, F., Schneeburger, D., Schroeder, W., Sommar, J., Turner, R., Vette, A., Wallschlaeger, D., Xiao, Z. and Zhang, H., "Nevada STORMS Project: Measurement of Mercury Emission from Naturally Enriched Surfaces." *J. Geophys. Res.*, 104: 21, 821-831, 844, September 1999.
- Gustin, M.S., Lindberg, S.E., Austin, K., Collbaugh, M., Vette, A and Zhang, H., "Assessing the Contribution of Natural Sources to Regional Atmospheric Mercury Budgets," submitted to *Science of the Total Environment*, 1999.
- Levin, L., "Mercury in the Environment: A Research Update", EPRI Report TR-104694, 1996.



Size Dependent Particle Concentration And Deposition Measurements With Filterpacks - A Five Year Study In Germany

G. SPINDLER¹⁾, TH. GNAUK, H. HERRMANN, K. MÜLLER, U. TEICHMANN

Institut für Troposphärenforschung e.V. (IfT), Permoserstr. 15, D-04318 Leipzig, Germany

Abstract

During a period of seven years (1993 to 2000) daily and since 1995 weekly filter pack samples (PM 10, PM 2.5, and additionally in 1999/2000 two packs for PM1) were collected at the IfT-research station Melpitz (altitude 87 m, latitude 51°32' N, longitude 12°54' E) in the downwind plume of the Leipzig conurbation. Teflon-filters used for the determination of ion concentration (analyzed by ion chromatography) and were since 1999 quartz-filters were used for the characterization of the carbon fraction (analyzed by thermographic technique). The particle mass concentration shows a decreasing trend, with different distributions in the size fractions over the year. Maxima for the mass ratios (PM10 – PM 2.5)/PM2.5 were observed in summer indicating more coarse material particles with higher aerodynamic diameter during relatively dry periods. Using a simple model and results from micrometeorological measurements, the proportion of the ions containing in PM 2.5 and PM 10 and the total deposition are estimated for Melpitz for 1995, 1996 and 1997.

Key words: Dry deposition, elemental carbon, filter pack, organic carbon, particles

Measurements and experimental set-up

During seven years (1993 to 2000) daily and, since 1995, weekly, filter pack samples (PM 10, PM 2.5, and additional in 1999/2000 also two packs for PM1) were collected by virtual impactors high volume (HV) and low volume sampling (LV) using Teflon-filters for the determination of ion concentration (analyzed by ion chromatography) and especially in 1999 quartz-filters for the characterization of the carbon fraction (analyzed by thermographic technique using a Ströhlein carbon analyzer). The daily samples were taken with a modified Sierra-Andersen-PM 10 high volume sampler since 1993 (Andersen Samplers Inc.). The weekly samples were collected using a low flow "Partisol 2000" Air Sampler (Römer and Veldkamp, 1994) (Rupprecht and Patashnik Co. Inc.) at the IfT-research station Melpitz in the downwind plume of the Leipzig conurbation (Brüggemann and Spindler, 1999). The sampling schedule started every day at 8:00 CET for daily samples and every Tuesday at 12:00 CET for weekly samples. The two sampling systems deliver corresponding results. The total mass concentration shows a decreasing trend from 1993 to 2000 for all size fractions, Figure 1. The highest values have been observed in the winters 93/94, 95/96 and 96/97. In the following winters no pronounced concentration peaks were found. A possible reason is the decreasing number of coal heating systems in the Leipzig conurbation and its surroundings. Additionally, in the last winters high pressure systems with transport of dry continental air masses and small mixing height relatively seldom occurred.

1) Tel 0341 235 2865 Fax. 0341 235 2325 e-mail: spindler@tropos.de



Mass concentration and ionic components in different size classes

In Figure 1 the ratio $(PM_{10} - PM_{2.5})/PM_{2.5}$ (coarse/fine mode) is plotted together with the mass concentrations. The mass ratio of coarse to fine mode gives a typical variation seasonal variation. In the summer more coarse mode particles exist. The cause for a pattern between different summers can be found in a fluctuation of the amount and distribution of precipitation. Summers which are continuously wet have smaller pronounced peak values (95 and 96, mostly wet surfaces) compared to summers with a high precipitation value in short time (97 and 98) or a relatively dry summer (99). Also for May 2000 (extremely warm and dry) this result is found. The main part of the water soluble ions was found in the fine mode (Figure 2). The sulfate content was higher in the fine mode in summer. Most of the nitrate and ammonium was detected in the fine mode. The mass concentration especially for nitrate is higher in the winter. This may be caused by (i) a different distribution between gas phase and particles, (ii) different intensity of chemical nitrate-chloride exchange on particle surfaces during long range transport from the sea to the sampling site, (iii) different mixing layer heights in winter and summer and finally, (iv) by sampling artifacts. Chloride was also found mainly in the fine mode, with higher concentration levels in winter. Possible reasons are the faster transport with higher wind speeds from the sea and a slower nitrate-chloride exchange during winter. Calcium was emitted from coal burning and building trade and is included in resuspended particles, therefore it was found mostly in the coarse mode. The somewhat higher summer concentrations are in agreement with the resuspension of coarse particles (Heintzenberg et al., 1998; Spindler et al., 1999). The percentage of total mass of PM 1 indicates that most of the fine particles were smaller than 1 μm .

Figure 1: Course of mass concentration PM 10, PM 2.5 and PM 1 (HV and LV) and ratio coarse/fine mode (LV)

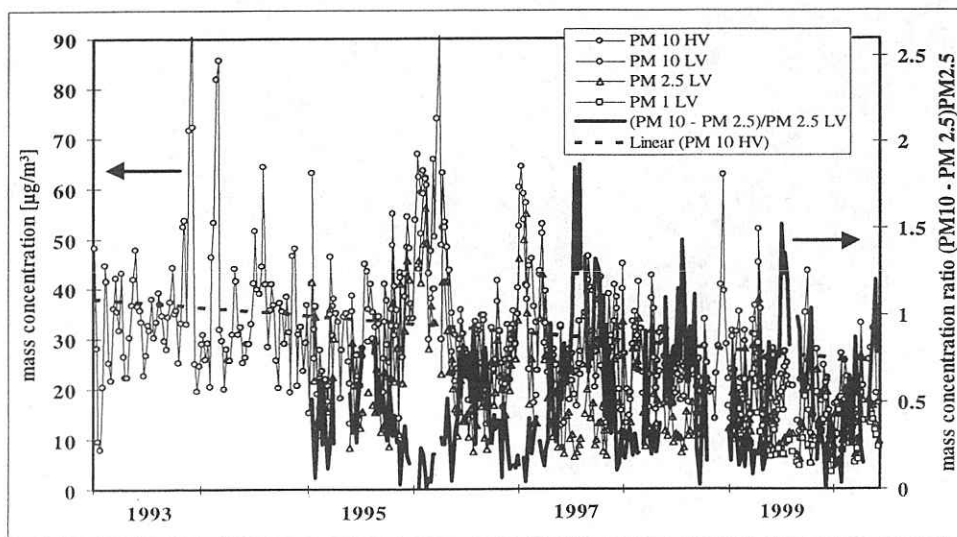
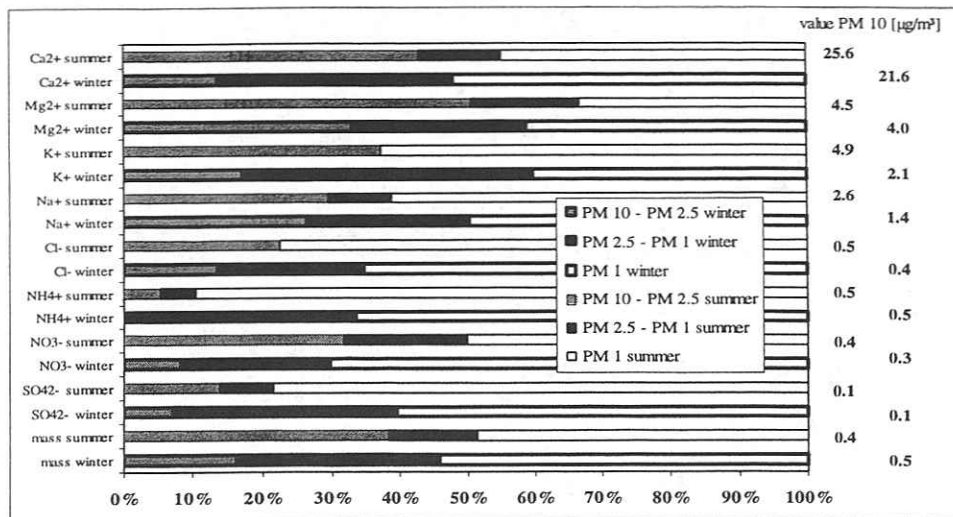




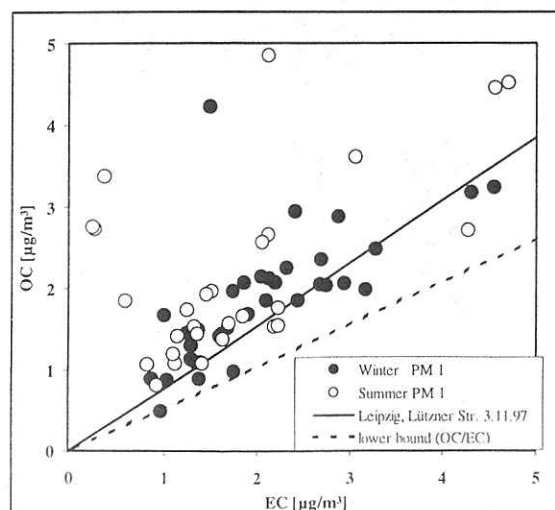
Figure 2: Percentage of ions in the different particle size fractions in 1999 for summer (May-October) and winter (January-April, November-December)



Carbon content in particle size fraction PM 1

The carbon content of the PM 1 fraction from quartz filters was determined with a thermographic method using a Ströhlein C-mat 5500 carbon analyzer separating the OC (590°C, nitrogen) and EC (650 °C, oxygen) part. Figure 3 is a scatter plot corresponding to Castro et al., 1999, with all identified OC/EC-ratios in PM 1, distinguished between summer and winter. The lower bound line for all ratios was found for a fraction of 52 % OC of the sum of OC and EC (total carbon, TC). In the summer the ratio is often larger as in winter. The straight line an example for the OC/EC ratio from a street canyon in the city of Leipzig. The mean ratio for Melpitz as a remote site is larger, possibly indicating a modification of particles by an addition of organic carbon i.g. by condensation of low vapour pressure compounds from the gas phase.

Figure 3: Scatter plot for all weekly means of the absolute OC and EC mass concentration in the particle size fraction PM 1 measured in 1999. The dotted line is the lower bound line for this scatter.





Deposition of particles

Figure 4 contains an example of the estimated diurnal annual deposition velocities of particles using the turbulent atmospheric resistance R_a and the friction velocity u^* following Slinn (1982). The deposition velocity follows in the mean strongly the daily course of turbulence, for the coarse mode particles the deposition velocity is higher than for the fine mode particles resulting from the stronger influence of the gravitation. The deposition levels (sum of fluxes PM 10 - PM 2.5 and PM 2.5) in the Table were calculated as the product of the mass concentration and the estimated deposition velocities. The wet deposition was quantified with a wet only sampler and, for the quantification of the dry deposition fluxes of gaseous species, micrometeorological methods (gradient method and eddy correlation) were used, see Erisman et al. (1998) and Hensen et al. (1999). The results show the influence of the location and the character of the measuring site. For the Speulder Forest a higher percentage of the particle impact was detectable. The reason is a much higher roughness than at the low vegetation sites Melpitz and Auchencorth Moss.

The absolute value of chloride deposition in Melpitz is low, because the site is far away from the sea. The higher level for the dry deposition in particles for calcium and sulphate in Melpitz is an indication of anthropogenic influence. An indicator for agricultural activities in the surroundings is the higher N impact at Speulder Forest and Melpitz compared with the rural site Auchencorth Moss.

Figure 4: Example for diurnal annual deposition velocities of different water soluble ions containing coarse and fine mode particle.

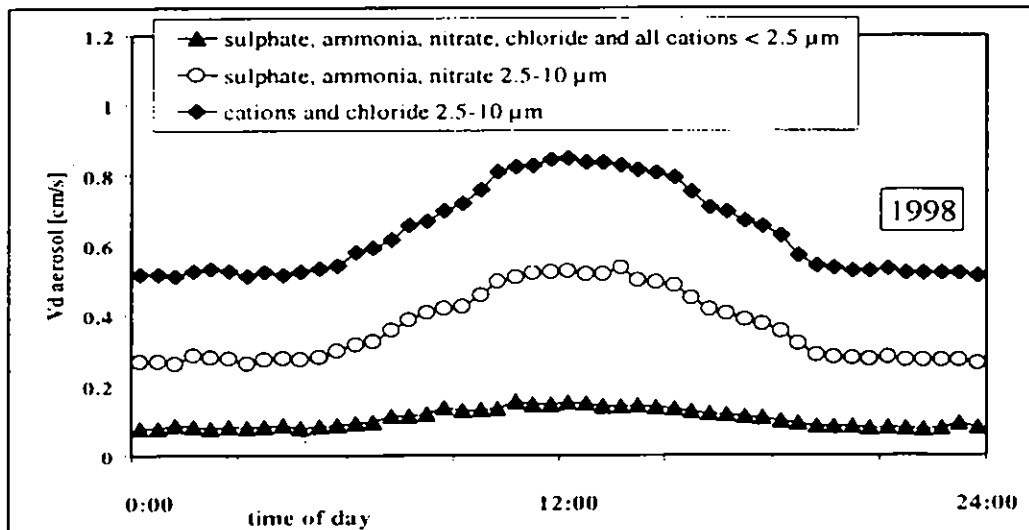




Table 1: Deposition level (mol/(ha*a)) and percentage of total deposition (bold numbers) for the impact of ion containing particles PM 10 and ions in rain water (wet deposition), Hensen et al., 1999

Ion	year	Auchencorth Moss, UK (open moorland) 55° 47' N 3° 14' W			Speulder Forest, NL (Douglas forest) 52° 14' N 5° 14' E			Melpitz, D (grassland) 51° 32' N 12° 54' E		
		Deposition			Deposition			Deposition		
		Dry PM 10	Wet	[total]	Dry PM 10	Wet	[total]	Dry PM 10	Wet	[total]
SO ₄ ²⁻ [total S ^{a)}	1995	11 (5.2)	128 (61)	210 (100)	106 (14)	291 (39)	742 (100)	35 (3.5)	209 (21)	995 (100)
	1997	-	122	-	-	214	-	19 (4.2)	144 (32)	455 (100)
	1998	-	153	-	81 (13)	283 (46)	615 (100)	15 (3.8)	129 (33)	392 (100)
NO ₃ ⁻ [total N ^{b)}	1995	14 (2.4)	133 (23)	586 (100)	267 (7.8)	374 (11)	3430 (100)	20 (1.6)	233 (19)	1241 (100)
	1997	-	136	-	-	289	-	29 (2.1)	223 (17)	1345 (100)
	1998	-	164	-	189	369	-	23 (2.9)	244 (31)	797 (100)
NH ₄ ⁺ [total N ^{b)}	1995	24 (4.1)	173 (30)	586 (100)	337 (9.8)	806 (23)	3430 (100)	47 (3.8)	336 (27)	1241 (100)
	1997	-	171	-	-	697	-	49 (3.6)	355 (26)	1345 (100)
	1998	-	200	-	240	752	-	40 (5.0)	335 (42)	797 (100)
Cl ⁻ [total Cl ^{c)}	1995	48 (10)	395 (86)	460 (100)	214 (19)	855 (75)	1139 (100)	12 (10)	75 (64)	118 (100)
	1997	-	394	-	-	436	-	11 (6.5)	90 (53)	169 (100)
	1998	-	474	-	177	884	-	10 (6.7)	103 (69)	150 (100)
Ca ²⁺ [total Ca]	1995	3 (7.7)	36 (92)	39 (100)	37 (44)	46 (56)	83 (100)	32 (40)	49 (60)	81 (100)
	1997	-	-	-	-	31	-	17 (21)	65 (79)	82 (100)
	1998	-	-	-	-	37	-	15 (16)	63 (84)	93 (100)

- a) Sum dry deposition of SO₄²⁻ and SO₂
b) Sum dry deposition of NH₃, NH₄⁺, NO₃⁻, NO, NO₂, HNO₃ and HNO₂
c) Sum dry deposition of Cl⁻ and HCl

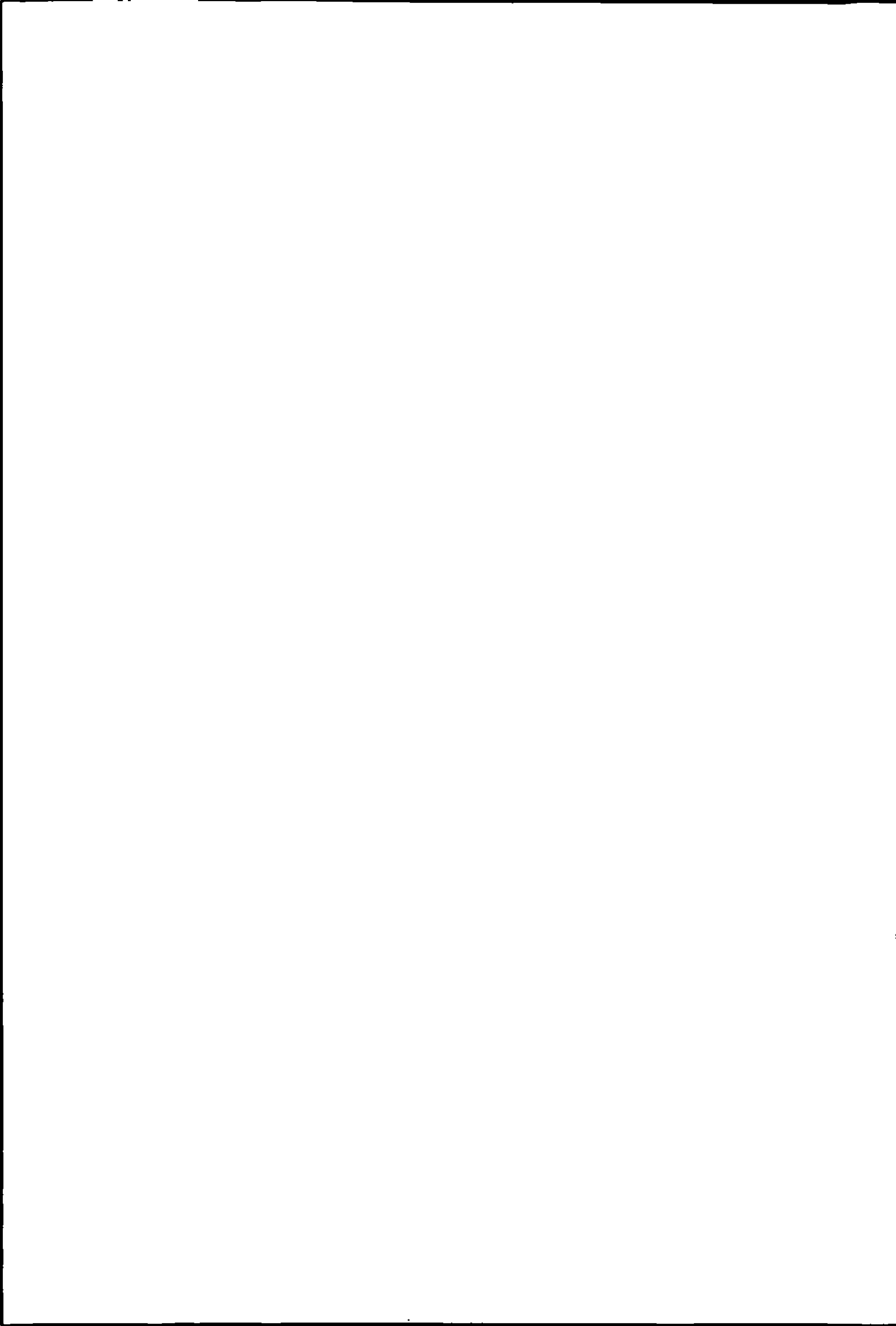


Acknowledgements

We wish to thank the European Community within the LIFE programme (1995-96, 722108 and 1998-99, ENV/NL/215). We are greatly indebted to J. Hanß and A. Grüner for the reliable measurements, for the numerous analysis we thank E. Neumann, A. Thomas, E. Brüggemann and B. Gerlach.

References

- Brüggemann, E. and Spindler, G.: 1999, 'Wet and Dry Deposition of Sulphur at the Site Melpitz in East Germany', *Water, Air, and Soil Pollut.* **109**, 81-99.
- Castro, L.M., Pio, C.A., Harrison, R.M. and Smith, D.J.T.: 1999 'Carbonaceous aerosol in urban and rural European atmospheres: estimation of secondary organic carbon concentrations' *Atmospheric Environment* **33**, 2771-2781.
- Erisman, J.W., Mennen, M.G., Fowler, D., Flechard, C.R., Spindler, G., Grüner, A., Duyzer, J.H., Ruigrok, W. and Wyers, G.P.: 1998. 'Deposition Monitoring in Europe' *Environmental Monitoring and Assessment* **53**(2), 279-295.
- Heintzenberg, J., Müller, K., Birmili, W., Spindler, G. and Wiedensohler, A.: 1998, 'Mass-related aerosol properties over the Leipzig Basin' *J. Geophys. Res.* **103D**, 13.125-13.135.
- Hensen, A., Erisman, J.W., Fowler, D., Flechard, C.R., Grüner, A., Spindler, G., Duyzer, J.H., Weststrate, H., Römer, F.G., Vonk, A.W. and van Jaarsveld, H.: 1999, 'Towards development of a deposition monitoring network for air pollution in EUROPE - Low-cost monitoring methods' *Final Technical Report 'LIFE' 96/ENV/NL/215*, 69 pages, Netherlands Energy Research Foundation ECN, report: ECN--C-99--075
- Römer, F.G. and Veldkamp, A.A.: 1994, 'Test results of a selected aerosol sampler to be applied in the CEC LIFE Project', *Report 63944-KES/MLU 94-3231*, KEMA, The Netherlands.
- Slinn, W.G.N.: 1982, 'Predictions for particle deposition to vegetation surfaces' *Atmos. Environ.* **16**, 1785-1794
- Spindler, G., Müller, K. and Herrmann, H.: 1999, 'Main Particulate Matter Components in Saxony (Germany)'
ESPR - Environ. Sci & Pollut. Res **6**, 89-94.



Validation Experiments for Wet Deposition Estimates at 5 km x 5 km in Complex Topography

I.D. LEITH¹, D. FOWLER¹, B. REYNOLDS², A.J. DORE³, T.W. CHOULARTON³, M. MOUSAVI³,
J.A.H. LOWE², D. NORRIS² AND M. J. ROSSALL⁴

¹CEH Edinburgh, Bush Estate, Penicuik, Midlothian EH26 0QB, UK

²CEH Bangor, University of Wales, Deiniol Road, Bangor, Gwynedd, LL57 2UP, UK

³Physics Department, UMIST, PO Box 88, Manchester, M60 1QD, UK

⁴CEH Merlewood, Grange-over-sands, Cumbria, LA11 6JU, UK

Introduction

Monitoring wet deposition in remote upland areas of the UK is difficult because of accessibility and harsh terrain. These high rainfall areas of the UK however, provide some of the largest inputs of acidity and nitrogen in Europe. To validate current estimates of wet deposition at 5 km x 5 km and determine the influence of complex topography on orographic enhancement a series of field measurements were made in Snowdonia, N. Wales, an area with the largest estimated wet deposition in the UK.

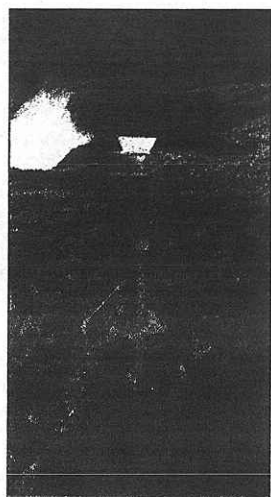


Figure 1a. Rain gauge

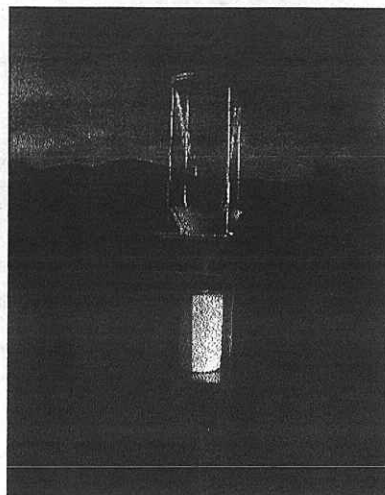
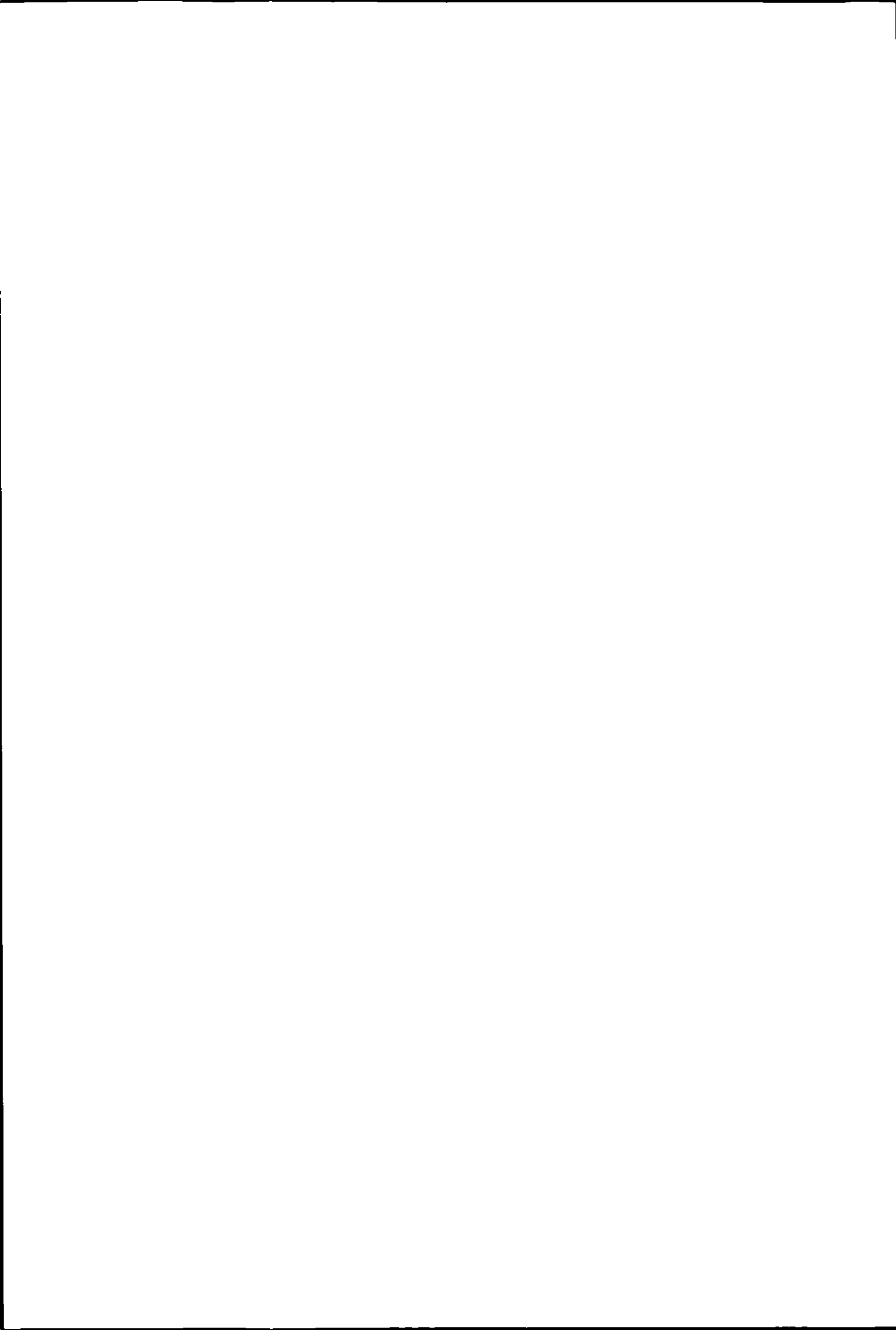


Figure 1b. Cloud gauge

Methods

Field measurements of wet deposition (October 1996 and November 1998) were made along two transects using a series of rain and cloud collectors (fig.1a & b). The two transects, each 20 km long (Snowdon (NW-SE and Moel Hebog SW-NE) were along altitudinal gradients. The Llyn Llydaw sites were at a fixed altitude providing precipitation chemistry data for both transects. Prior to the start of each rain event all gauges were washed with de-ionised water. The precipitation from that rain event was then collected simultaneously from both transects. The duration of the sampling period was dependent on weather patterns. Automatic weather stations provided wind speed, wind direction, temperature and precipitation rate and amount.



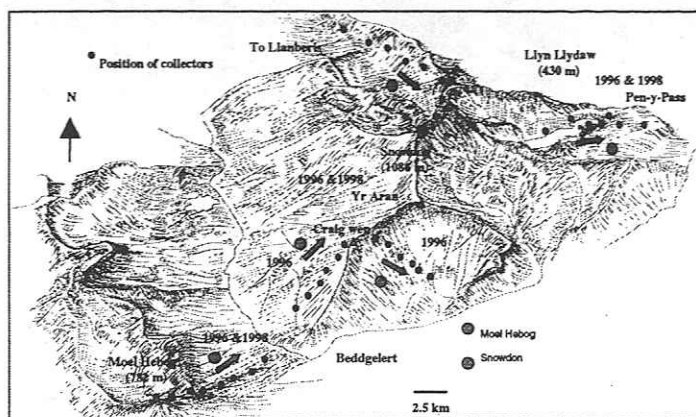


Figure 2. Schematic diagram of the two transects

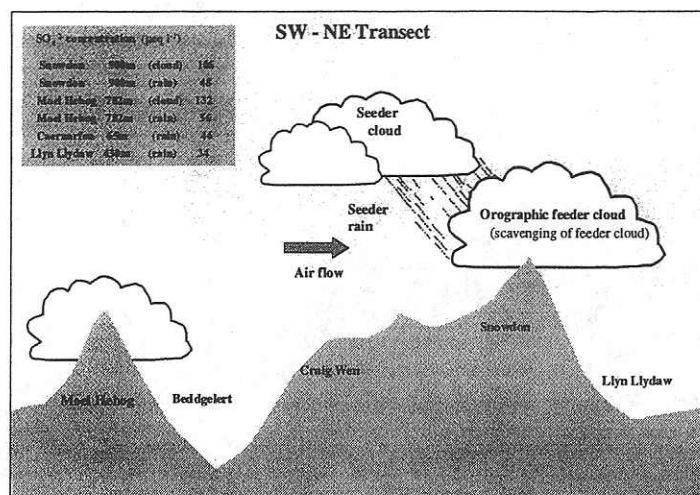


Figure 3. Orographic enhancement of mean SO_4^{2-} concentrations

Results and Conclusions

The concentration of ions in rainfall at hill summits were approximately twice that of low altitude sites (Table 1). The mean concentration of ions within hill cloud scavenged by falling rain were larger than those in low level rain by a factor of 1.4 to 2.5 depending on ion. In complex topography, figure 4 shows that the second and third hills to receive less orographic enhancement than the first hill.

NH_4^+	NO_3^-	SO_4^{2-}	Cl^-
x 2.1	x 1.8	x 1.5	x 1.6

Table 1: Mean orographic enhancement in rainfall concentrations (2 transects, 1998)

NH_4^+	NO_3^-	SO_4^{2-}	Cl^-
1.8	2.5	1.4	1.9

Table 2: The mean ratio of scavenged hill cloud 1996 and 1998

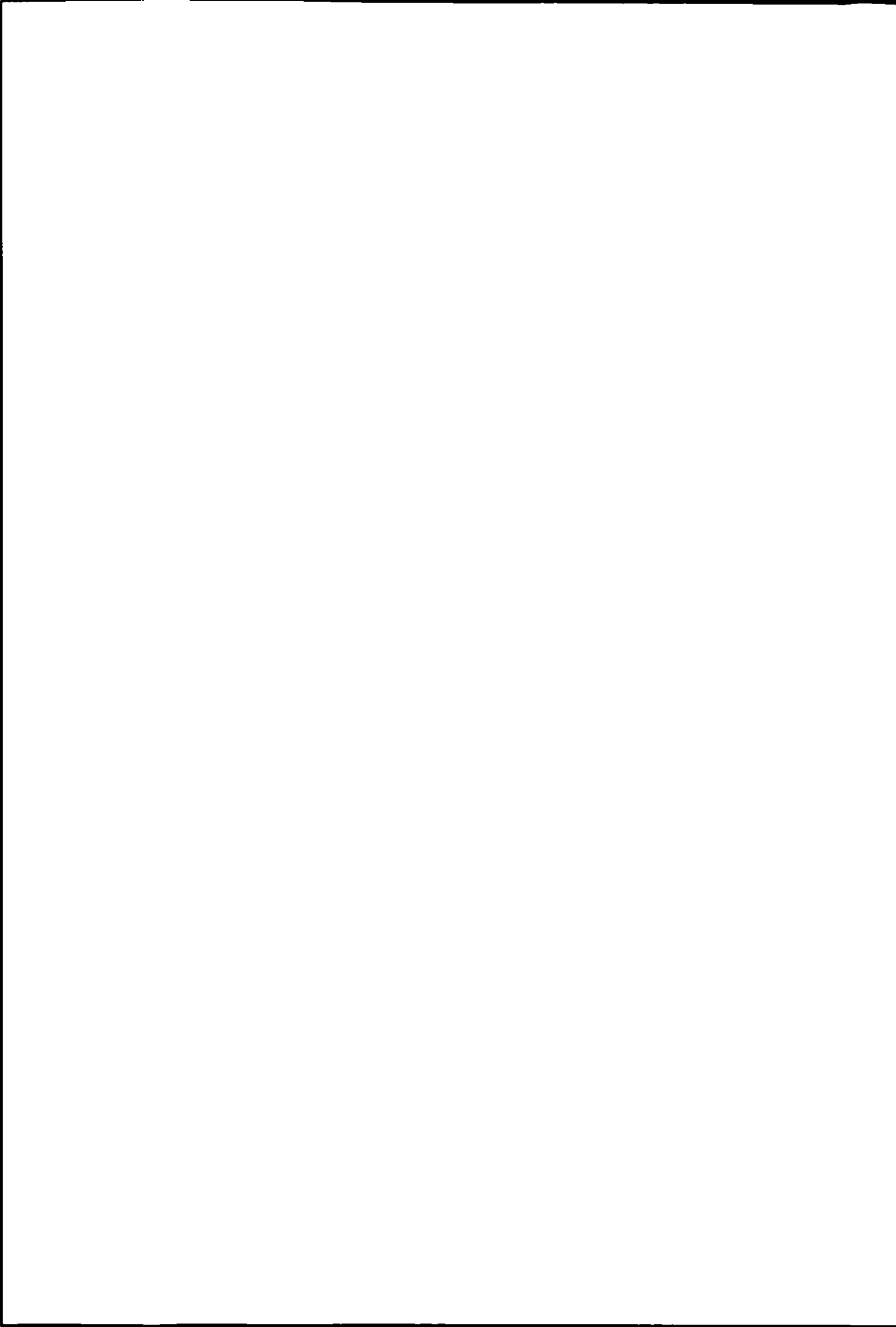


Figure 4

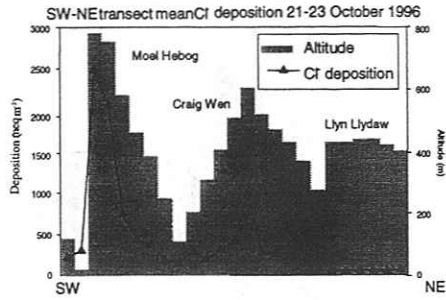


Figure 5 shows the measured orographic enhancement in NO_3^- deposition to be broadly similar to the model output for Snowdon using annual rainfall data.

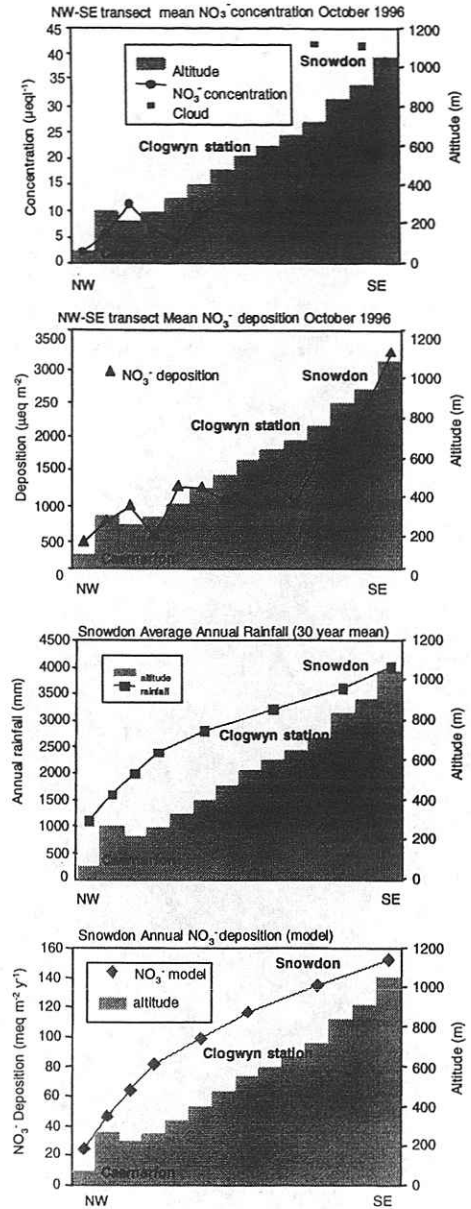


Figure 6 shows annual wet deposition of SO_4^{2-} -S (kg ha^{-1}) modelled at $1 \text{ km} \times 1 \text{ km}$ resolution for the $20 \text{ km} \times 20 \text{ km}$ grid square centred on Snowdon.



SO₄²⁻ Deposition (kg S ha⁻¹)

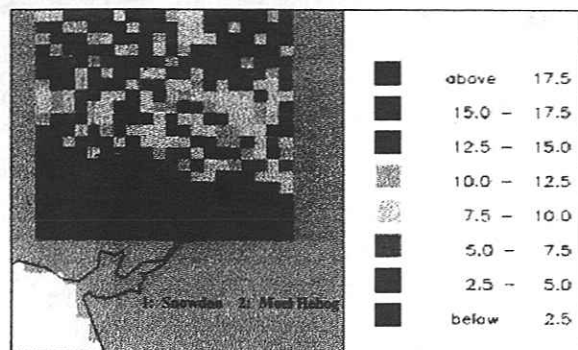
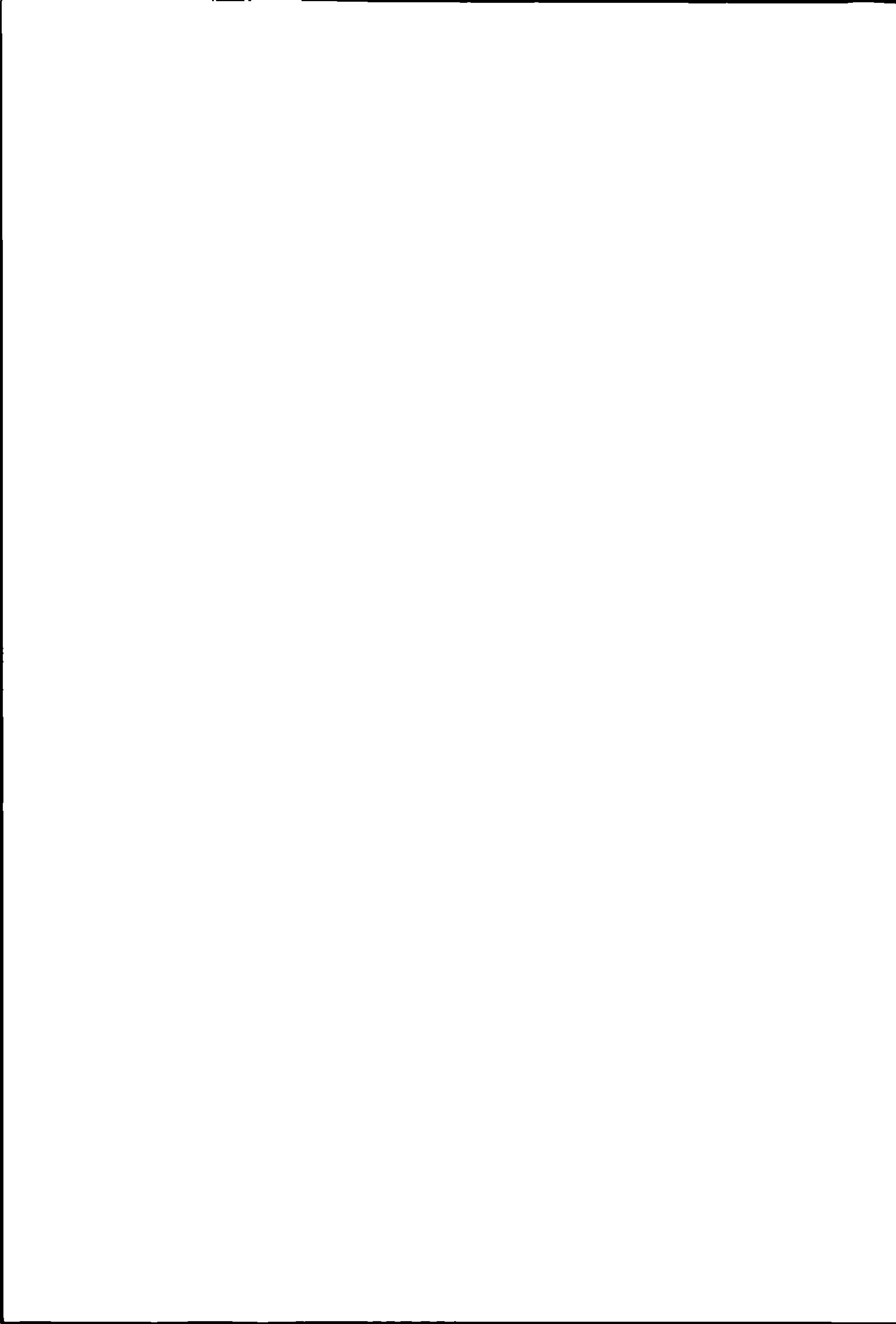


Figure 6

Acknowledgements

The authors wish to thank The Department of the Environment, Transport and the Regions for their financial support.



N₂O Flux from a Solid Dairy manure Pile Determined with a Micrometeorological Mass Balance Technique

C. WAGNER-RIDDLE, H. A. BROWN, G.W. THURTELL, AND R. WENZEL

Dept. Land Resource Science, University of Guelph, Guelph, Ontario, Canada, N1G 2W1

Abstract

Animal waste management systems may represent a significant proportion of agriculture's contribution to the increase in atmospheric nitrous oxide concentration. The objective of this study was to quantify short-term nitrous oxide flux from a solid dairy manure pile with *in situ* measurements using the integrated horizontal flux (IHF) method. Emissions were two orders of magnitude larger during June 1998 when compared to the fall 1999 period. These results have important implications for the calculation of greenhouse gas emissions for countries in cold climates.

Introduction

Several sources acknowledge that the storage of manure may represent a significant proportion of agriculture's contribution to the increase in atmospheric nitrous oxide concentration (Hartung and Phillips, 1994; Berges and Crutzen, 1996). However, only a few studies have estimated nitrous oxide flux from stored slurries and stored solid manure. These estimates range from <0.01 to >15% of total N (Mosier *et al.*, 1998). The global N₂O budget currently includes a 2% emission factor for solid manure storage, but because this estimate is based on a limited number of studies, it requires updating and improvement (IPCC, 1996).

Our objective in this study was to quantify the *in situ* nitrous oxide flux from a solid dairy manure pile using a micrometeorological mass balance method.

Materials and Methods

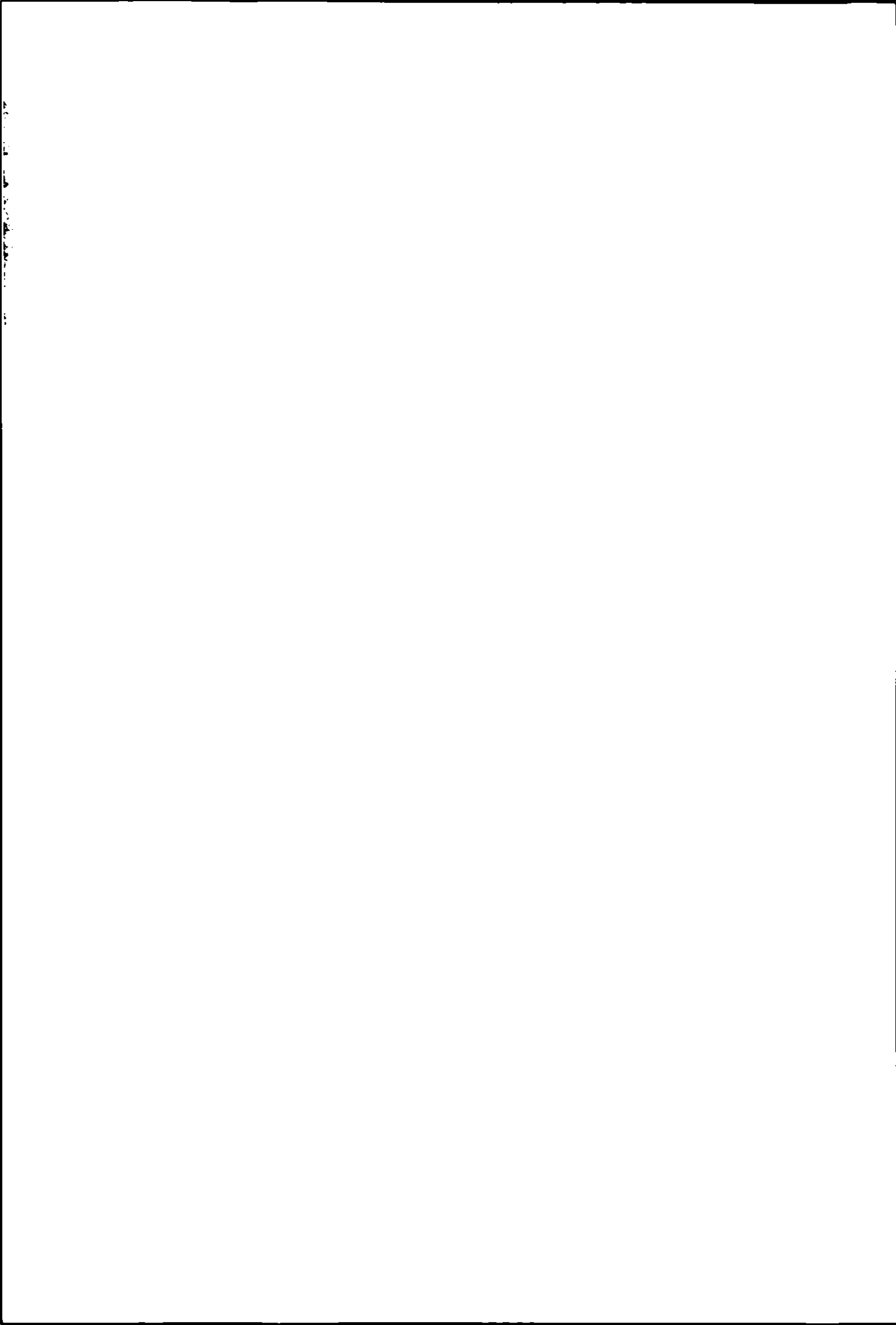
Experimental Site

Nitrous oxide fluxes from a solid dairy manure storage pile were measured from June 10 to June 19, 1998 (days 161 to 170), and from November 22 to December 10, 1999 (days 326 to 346) at the Elora Research Station (43°49'N, 80°35'W), Ontario, Canada.

The manure stored in this facility was supplied by approximately 310 cattle, of which about half are milking cows. These animals are confined throughout the year, and straw is the material used for bedding. The manure pile was contained in a concrete curbed slab (37 x 37 m), and was loaded once a day from above using a mechanical stacker. Samples of manure taken in June 1998 indicated a dry matter content of 19%, nitrate and ammonium concentrations of 0.25 and 246 (mg L⁻¹), respectively.

Micrometeorological Measurements

In 1998, one mast was attached to the inside of the storage area's concrete wall, which was oriented in the northeast to southwest direction, and used for installation of four cup



anemometers and seven gas sampling intakes (Figure 1). To improve the frequency of data collection, a mast was installed on each of the four sides of the storage area, for a total of four masts in 1999.

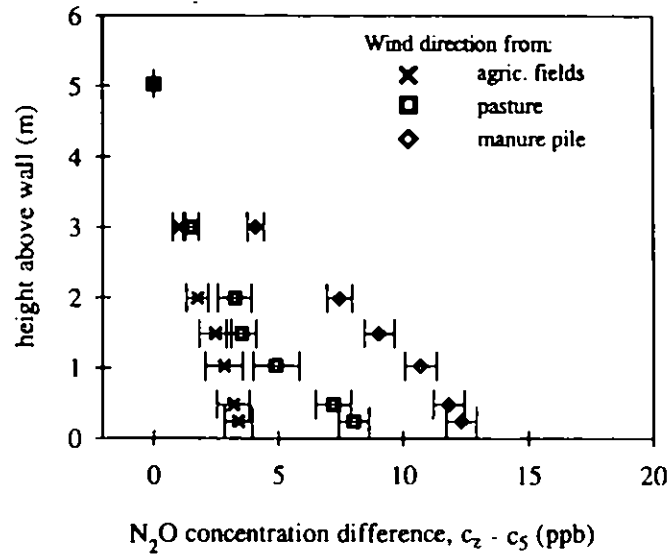


Fig. 1 – Mean nitrous oxide hourly concentration difference between measurements at several heights and the background concentration (at $z = 5$ m) in June 1998. Data have been grouped according to wind direction.

The vertical flux of nitrous oxide was calculated using the integrated horizontal flux method, where the flux from a source is given by the difference in the horizontal flux at an upwind and downwind position of the source area:

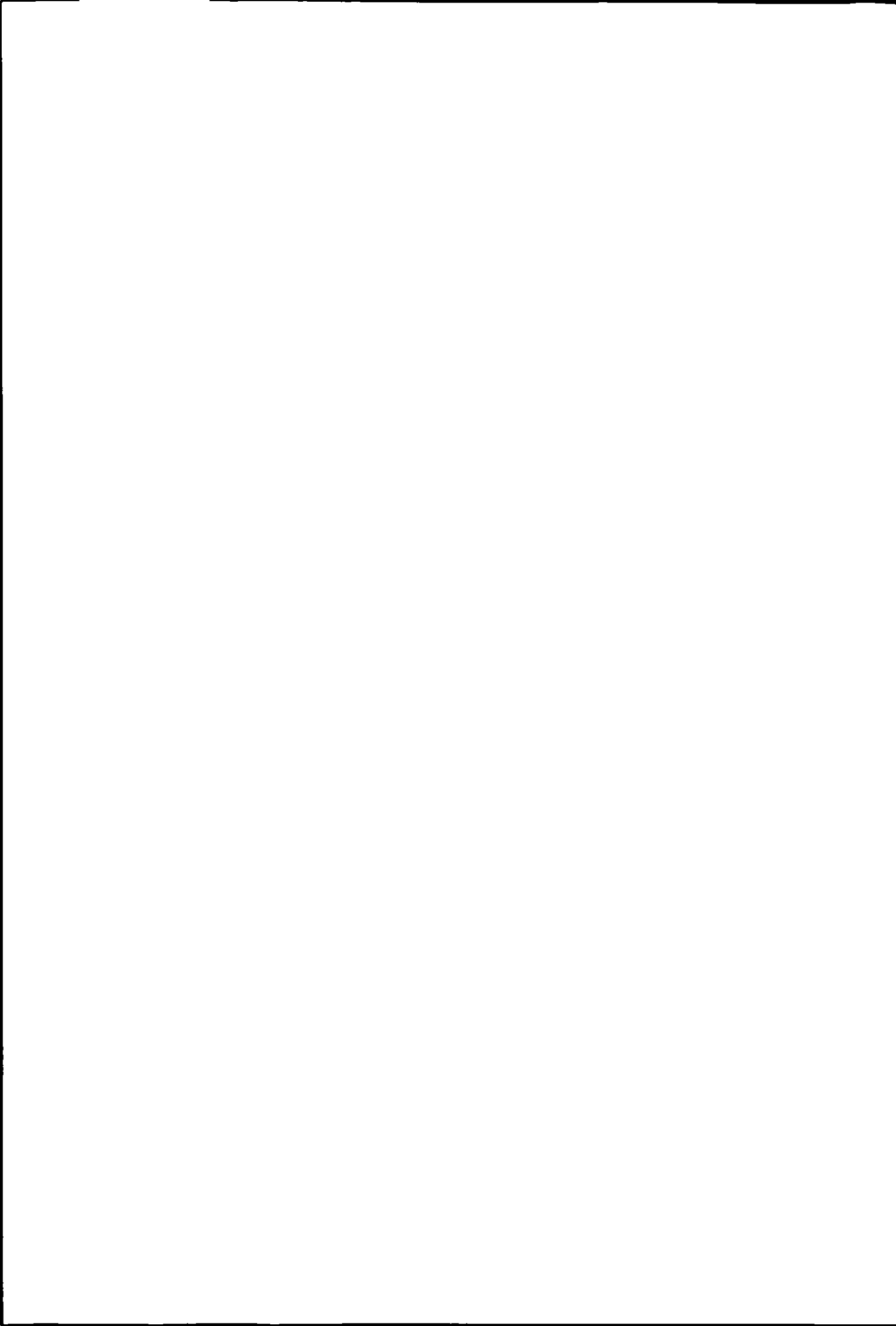
$$\text{Flux} = \frac{1}{L} \int_{z=0}^{z_{\text{max}}} (\bar{u}_z \bar{c}_{z,\text{out}} - \bar{u}_z \bar{c}_{z,\text{in}}) dz \quad (1)$$

where L is the horizontal distance (m) the flow of air travels over the manure pile, \bar{u}_z and \bar{c}_z are mean hourly values of wind speed (m s^{-1}) and N_2O concentration (g m^{-3}) at height z , respectively. The subscript 'out' indicates the gas concentration in the air after it moves over the manure pile, and the subscript 'in' indicates the gas concentration in the air before it moves over the manure pile. The integration limits were the heights at which gas intakes were setup (7 intakes in 1998 and 4 in 1999). Because only one mast was set-up in 1998, $c_{z,\text{in}}$ for all heights was assumed to be equal to the concentration of N_2O measured at 5 m.

Hourly N_2O concentration averages were determined using a tunable diode laser trace gas analyzer (TGA 100, Campbell Scientific, Logan, UT), which provided high precision concentration difference measurements (resolution = ± 10 ppt for hourly means).

Flux Calculations

In 1998, an hourly flux was calculated when the average hourly wind direction indicated that the air plume had travelled directly over the manure pile (235 to 340°). Only those hours when the wind direction was within the boundaries of the manure pile for more than 2 consecutive hourly averages were included in the nitrous oxide flux calculations. In 1999, only those



periods over which the 5-minute wind direction did not vary more than 30° from the orientation of paired masts were used for the calculations.

Results

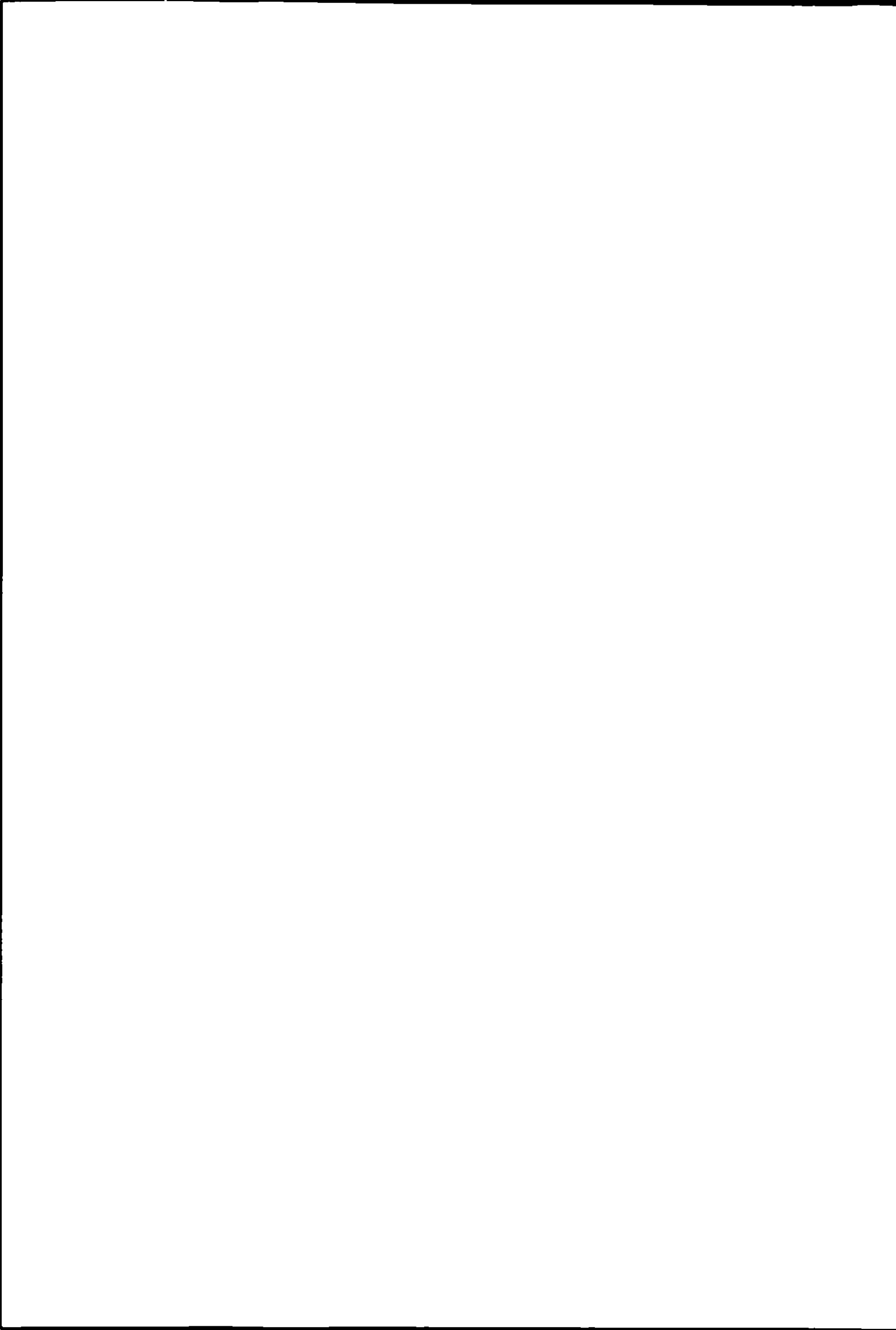
Profiles of Nitrous Oxide Concentration

Three profiles of N₂O concentration were produced from data averaged for different ranges of wind direction in 1998 (Figure 1). When the direction of the prevailing wind indicated that the plume of air was approaching from the agricultural fields, and not the manure pile (0 to 135°, or N to SE), the concentration profile showed a small increase of nitrous oxide at heights close to the surface. An average concentration difference of 6 ppb was detected at the lowest height, 0.25 m (Figure 1). This can be explained by the fact that these wind directions provided air samples which could have passed over the NE corner of the manure storage area before approaching the mast. Therefore, the 6 ppb difference was probably due to some influence of the manure storage area, and the agricultural fields. Figure 2 also illustrates the concentration profile when the wind direction was in the range between the SE and SW (136 - 225°). The average concentration difference was 14 ppb at the same 0.25 m height. Within this region, there were grazing cattle, an exercise pen and a covered underground liquid storage. Flessa *et al.* (1996) studied pastures under the influence of droppings of grazing cattle and concluded that such areas are an important source of N₂O. The concentration profile in the airflow passing over the manure pile had the greatest concentration difference of the directions we investigated (Figure 1), yielding a 20 ppb mean concentration difference at the lowest height, $z = 0.25$ m.

Nitrous Oxide Flux

During the summer of 1998 the mean hourly air temperature was 18.5 °C and during the November to December 1999 mean hourly air temperature fluctuated between 16 and -10.5 °C (Figure 2).

In June 1998, fluxes never fell below 200 ng N₂O-N m⁻² s⁻¹ (Figure 2). The mean hourly N₂O flux during the measurement period was 4865 ng N₂O-N m⁻² s⁻¹ ($n = 65$, $SD = 2493$ ng m⁻² s⁻¹) can be extrapolated to a 3% N loss as N₂O. Preliminary analyses of the fall 1999 data gave a mean of 40 ng N₂O-N m⁻² s⁻¹.



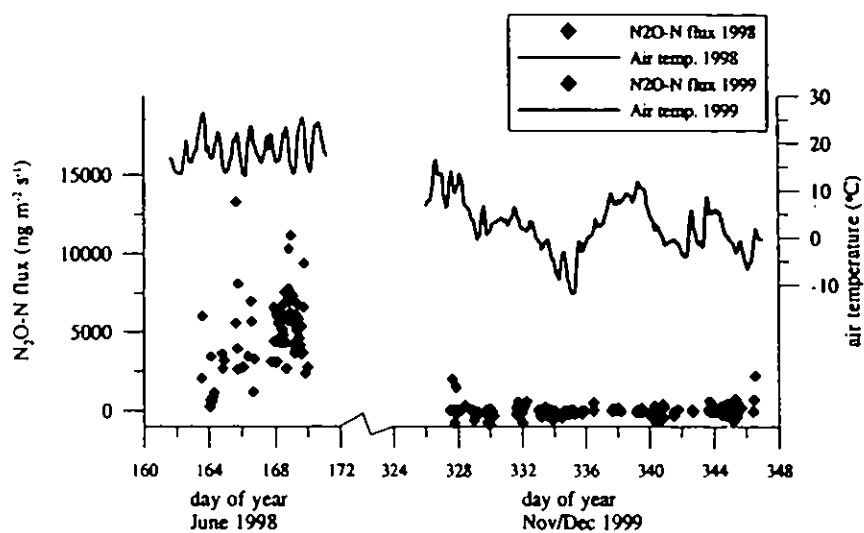


Fig. 2 – Hourly nitrous oxide fluxes measured during June 1998 and November to December 1999. Hourly air temperature is also shown.

Conclusions

Nitrous oxide flux was successfully quantified using a micrometeorological mass balance method during two contrasting periods of the year. Emissions were two orders of magnitude larger during June 1998 when compared to the November to December 1999 period. A previous laboratory study (Brown et al., 2000) showed that N_2O fluxes were negligible at negative redox potentials (E_h). N_2O emission from these samples was limited by low NO_3^- -N levels in samples with high WC and low E_h . Samples taken from the manure pile in November 1999, when conditions were wet and cool, showed that E_h values were always negative, which presumably would not allow for nitrate formation and subsequent denitrification. Prevalence of such conditions over a significant portion of a year has important implications for the calculation of greenhouse gas emissions from stored manure. Monitoring over a longer period, possibly year-round would provide more information regarding the variability of emissions and enable the recommendation of improvements in manure management in order to reduce N_2O emissions.

Acknowledgments

This research project was funded by the Ontario Ministry of Agriculture, Food and Rural Affairs, and the Natural Science and Engineering Research Council of Canada.

References

- Berges MG & Crutzen PJ 1996. Estimates of global N_2O emissions from cattle, pig and chicken manure, including a discussion of CH_4 emissions. *J Atmos Chem* **24**: 241-269
- Brown HA, Wagner-Riddle C and Thurtell GW 2000. Nitrous oxide flux from solid dairy manure in storage as affected by water content and redox potential. *J Environ Qual* **29**: 630-638
- Flessa H, Dorsch P, König H & Bouwman AF 1996. Influence of cattle wastes on nitrous oxide and methane fluxes in pasture land. *J Environ Qual* **25**: 1366-1370
- Hartung J & Phillips VR 1994. Control of gaseous emissions from livestock buildings and manure stores. *J Agric Engng Res* **57**: 173-189.



- IPCC 1996. Climate Change 1995. Impacts, adaptations and mitigation of climate change: scientific-technical analysis. Contribution of working group II to the second assessment report of the IPCC. Watson RT, Marufu CZ & Moss RH (eds) Cambridge University Press, Cambridge, UK
- Mosier A, Kroeze C, Nevison C, Oenema O, Seitzinger S & van Cleemput, O, 1998. Closing the global N₂O budget: nitrous oxide emissions through the agricultural nitrogen cycle. OECD/IPCC/IEA phase II development of IPCC guidelines for national greenhouse gas inventory methodology. *Nutr Cycl in Agroecosys* 52: 225-248.



Stochastic Properties of Micrometeorological Parameters

ULRICH DÄMMGEN & CATHLEEN FRÜHAUF

Federal Agricultural Research Centre Braunschweig, Institute of Agroecology
Bundesallee 50, 38116 Braunschweig, Germany

Representativity of measurements of stochastic entities

Eddy covariance and gradient measurements of fluxes of sensible heat, momentum and matter presuppose that the entities measured in a confined volume or column of air above a given plant/soil system are representative of the extensive source or sink above which they have been obtained. However, the properties of the turbulent atmosphere are stochastic. Stochastic entities can only be used for flux determinations if their deviation from the means and the respective averaging times are known and adequate. Replicated measurements of wind velocities, fluxes of momentum, vertical temperature gradients and fluxes of sensible heat were performed at the centre of a large homogeneous winter barley field (fetch 200 m, for details see Weigel & Dämmgen 2000) from March to May 2000 with an arrangement of sensors as shown in Fig. 1. The intention was to get detailed information about the errors of the results obtained and the applicability of the methods involved.

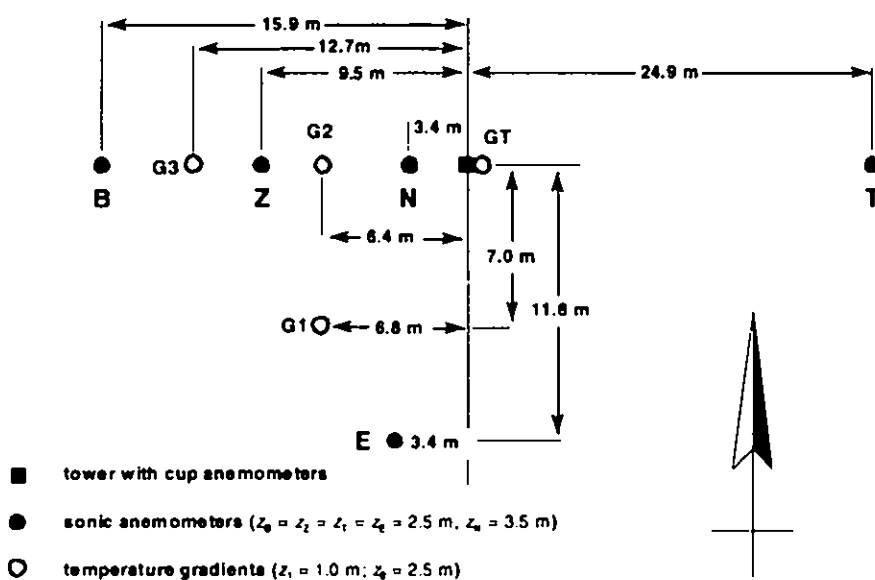


Fig. 1.: Position of sensors above the winter barley field. General arrangement see Frühauf et al. (this volume).

Instrumentation:

- Ultrasonic anemometers Boreas (B), Notos (N), Tycho (T) and Zephyros (Z): Gill Solent R2
- Ultrasonic anemometer EdiSol (E) Gill Solent R3
- Cup anemometer attached to tower (CT) Thies 4.3303
- Vertical air temperature gradients (G1 to G3) and at tower (GT) using 2 aspirated and intercalibrated Thies Pt100 sensors
- Data reported here were collected over 30 min to form half-hourly means.

Not all sensors could be operated in parallel at a time.



Convergence

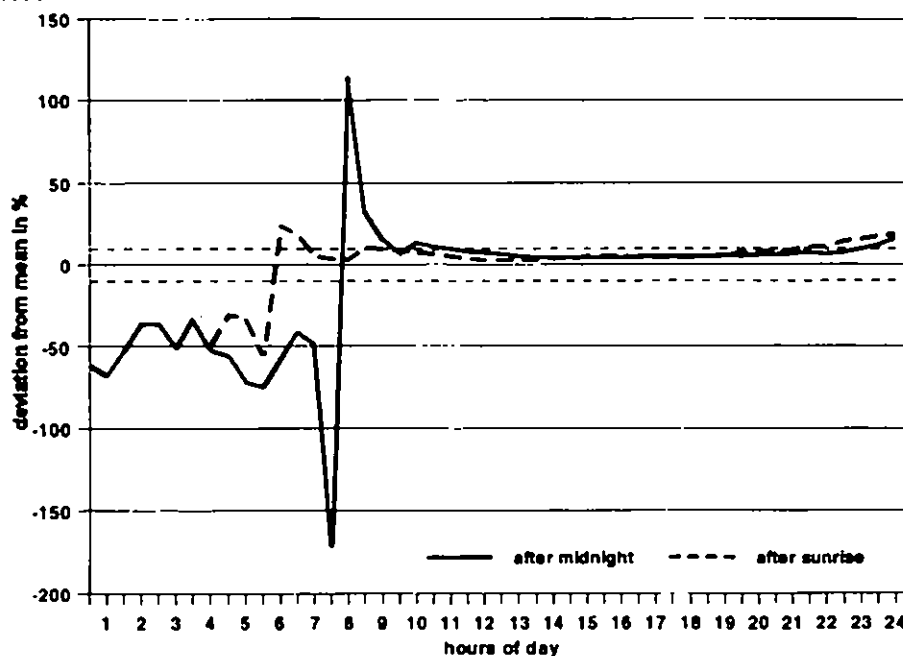


Fig. 2:
Exemplary convergence of the sums of sensible heat fluxes. Dotted lines near zero indicate the acceptable margins of convergence ($\pm 10\%$).

The convergence of relative standard deviations (i.e. standard deviation / mean * 100 of the sums of wind distances and sensible heat and of averages of temperature gradients and fluxes of momentum) was used as main quality criterion for the assessment of the likely standard errors and the obtainable resolutions in time. Exemplary times to convergence were calculated (1) for hours from midnight and (2) for hours after sunrise (Fig. 2).

Wind velocities

Of the 75 days evaluated, relative standard deviation of 10 % was achieved almost immediately at all times. Measurements after sunrise yielded immediate convergence only. Standard deviations of u were normally between 3 and 4 %.

Fluxes of momentum scatter considerably. They rarely converge in the time scale needed for micrometeorological measurements (Fig. 3). Their daily means deviate considerably for great fluxes.

Air temperature gradients

Although we cared for intercalibration, the temperature gradients obtained did not coincide in the way we expected. For our convergence calculations the readings were transformed to yield equal means. The results shown in Fig. 5 do not resolve the region of small gradients, i.e. gradients $\Delta T < 0.1$ K. For these, convergence cannot be calculated. For larger gradients, convergence can normally be observed after a few hours.



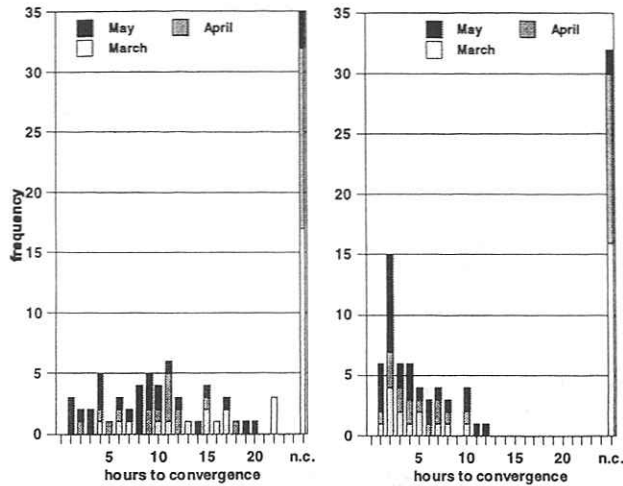


Fig. 3: Frequency distribution of periods, after which convergence of momentum fluxes was achieved after midnight and after sunrise.

n.c.: no convergence.

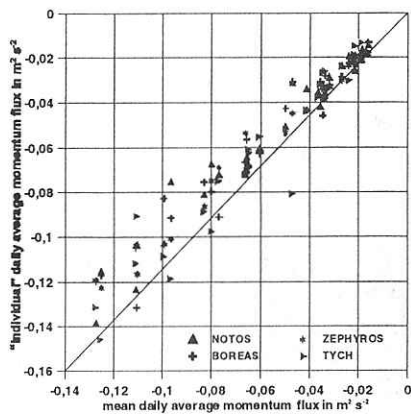


Fig. 4: Daily mean fluxes of momentum. (April 2000)

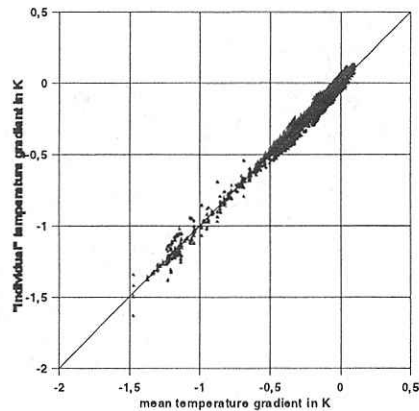


Fig. 5: Scattering of vertical temperature gradients (March 2000).

Fluxes of sensible heat

Sensible heat fluxes converge much faster than momentum fluxes and scatter less (Figs. 6 and 7). However, most of the fluxes measured at night-time reveal that turbulent fluxes in the stably stratified atmosphere cannot be dealt with as stochastic entities which add up to equal sums after a while. Sums of these fluxes converged at day-time.



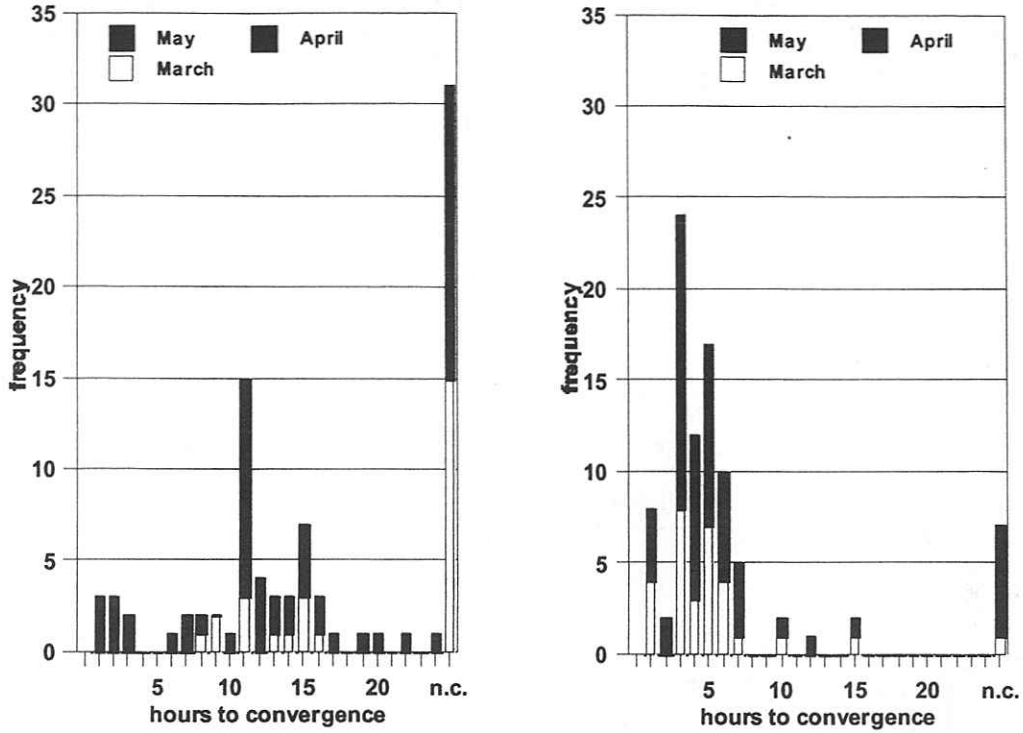


Fig. 6: Frequency distribution of periods, in which convergence of fluxes of sensible heat fluxes was achieved after midnight and after sunrise.

n.c.: no convergence

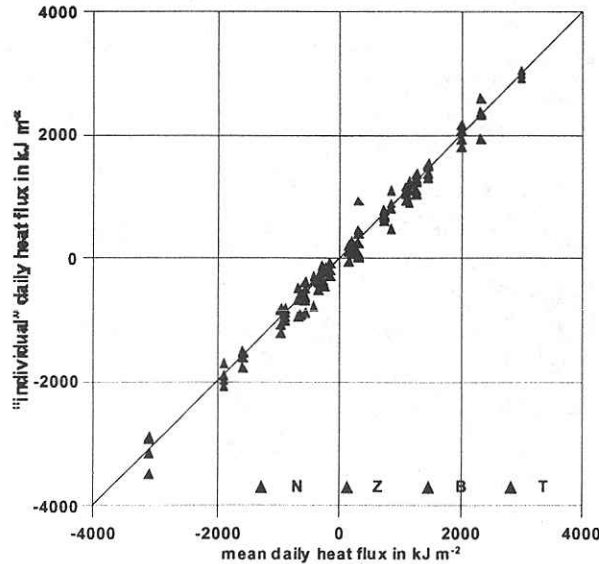
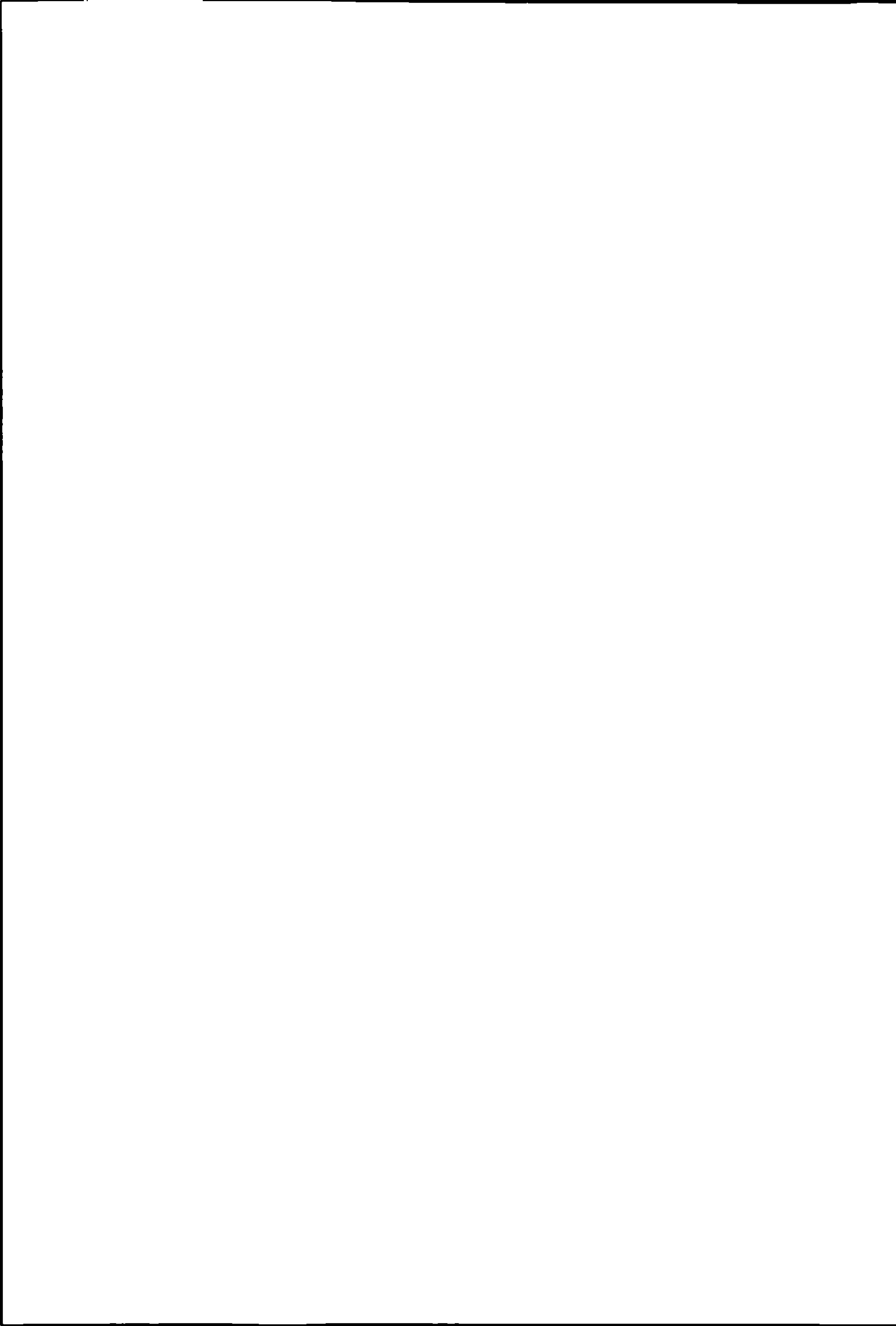


Fig. 7: Daily mean sums of sensible heat fluxes. April 2000.

Discussion of the results

Stochastic entities can be used in micrometeorology if they converge in reasonable periods of time. Of the entities considered here, only wind velocities can be measured with single instruments to produce representative results. Air temperature gradients prove to be difficult to measure. Their representativity is small, convergence can hardly be stated, as gradients at day-time often cannot be resolved adequately. The resolution in time of fluxes of sensible heat for day-time measurements cannot be less than approx. 3 hours. Days without



convergence have to be identified and be dealt with separately. Night-time measurement of vertical fluxes fail to be representative of the system, even if comparatively many sensors are involved. As atmospheric resistivities for fluxes of matter are closely related to those of sensible heat, the same restriction should apply for fluxes of matter.

Reference

Weigel, H.J., Dämmgen, U. (2000): The Braunschweig Carbon Project: Atmospheric Flux Monitoring and Free Air Carbon Dioxide Enrichment (FACE). *J. Appl. Bot.* **74**, 55-60.



Sharpening the Regional Picture of N₂O Emissions from Agricultural Land

R.L. DESJARDINS¹, J.I. MACPHERSON², C.R. FLECHARD¹, E. PATTEY¹, T. ZHU¹, R. RIZNEK¹,
D. DOW¹

¹ Agriculture and Agri-Food Canada, Ottawa, Canada

² National Research Council of Canada

Introduction

Atmospheric N₂O is an important contributor to the greenhouse effect. It accounts for almost 2/3 of the agricultural greenhouse gas emissions (Desjardins and Keng, 1999; Desjardins and Riznek, 2000). Although there is a strong need for accurate N₂O budgets with respect to the Kyoto protocol and for meeting our emission reduction targets, estimates of N₂O emissions from agricultural soils on regional, national and global scales are subject to very large uncertainties, due to the high spatial and temporal variability of N₂O emissions. In this poster, we show N₂O emissions for Eastern Ontario / Western Quebec for the spring-thaw period based on the IPCC methodology. We present the instrumentation recently developed to measure the flux of N₂O as well as the first set of measurements of N₂O fluxes obtained over two agricultural regions.

Theoretical Considerations

The release of nitrous oxide is sporadic, often occurring in bursts (Grant and Pattey, 1999). Excess water causes anaerobic conditions that, coupled with adequate nitrate, available carbon, and favourable temperatures, allow for denitrification and the formation of nitrous oxide. During the winter, nitrous oxide is trapped under the frozen soil and as the soil thaws, nitrous oxide escapes (Fig. 1). Emissions of nitrous oxide are very variable across space because of different moisture conditions and soil nitrogen content. The release may be minimal in certain areas but high where conditions are ideal for nitrous oxide production. Tower-based measurements have demonstrated that about 50-75% of the annual emissions of nitrous oxide in Eastern Canada occur in early spring (Wagner-Riddle et al., 1997).

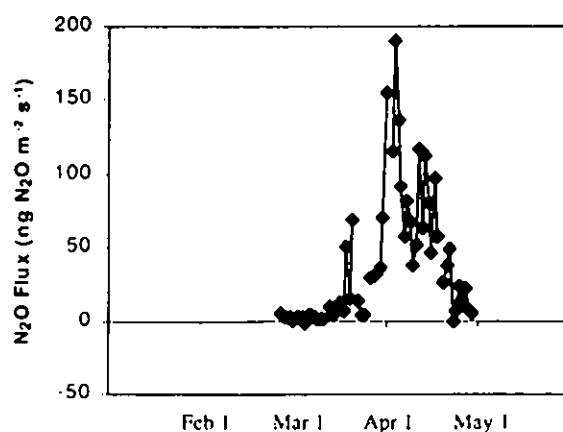


Figure 1. Nitrous oxide emissions measured in 1996 over a soybean field in Ottawa using a tower-based system



Materials and Methods

An aircraft-based system, which relies on the relaxed-eddy accumulation technique (Zhu et al., 1999), was developed and used to measure N_2O fluxes. This system controls a conditional sampler that collects air associated with upward and downward moving air in teflon bags (Fig. 2). The difference in N_2O concentration in each pair of bags is then measured using a Campbell N_2O tunable diode laser analyzer. It is possible to measure the difference in the N_2O concentration of the air collected in such bags with an accuracy better than 10 pptv about 9 times out of 10. This resolution provides flux measurements of N_2O with an accuracy of about $3 \text{ ng } N_2O \text{ m}^{-2} \text{ s}^{-1}$.

Two transects of about 9 km in length were selected for flux measurements. These transects are plotted on a map showing N_2O emission estimates (Fig. 3). These transects were flown around midday at a mean altitude of about 65 m on six different days during the spring thaw of 2000.

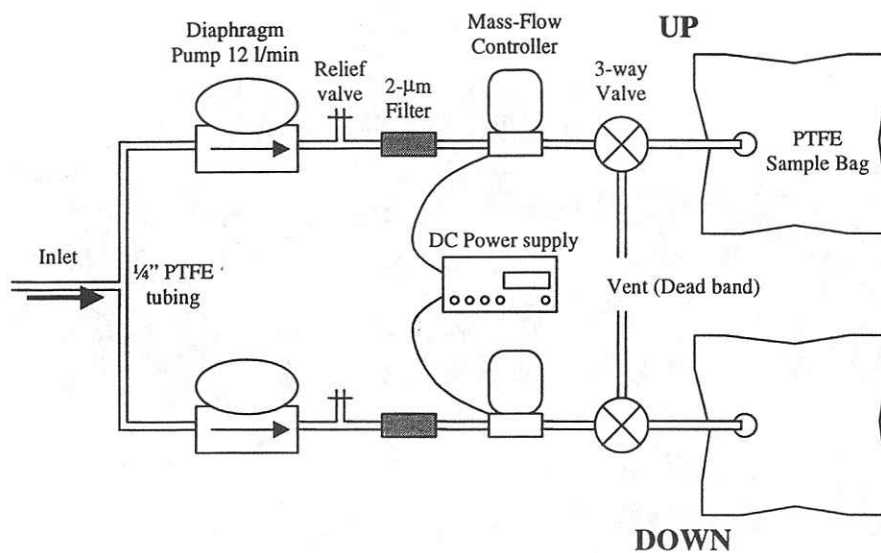


Figure 2: Relaxed Eddy Accumulation System

Results and Discussion

The estimated N_2O emissions for Eastern Ontario associated with spring thaw are presented. These estimates are based on the revised IPCC methodology (Monteverde et al., 1998). The Census data available for each soil landscape polygon was used to produce this map. It assumes that about 50% of the N_2O emissions occur during the three week period associated with spring thaw (Wagner-Riddle et al., 1997).

The observed N_2O emission estimates were significantly larger over the transect near Casselman than over the one near Morewood. The two areas selected were expected to be substantially different, the Casselman area being more intensively farmed. This difference is not reflected on the IPCC-based map.



These results confirm that more detailed information is required in order to sharpen the regional picture of N₂O emissions from agricultural land.

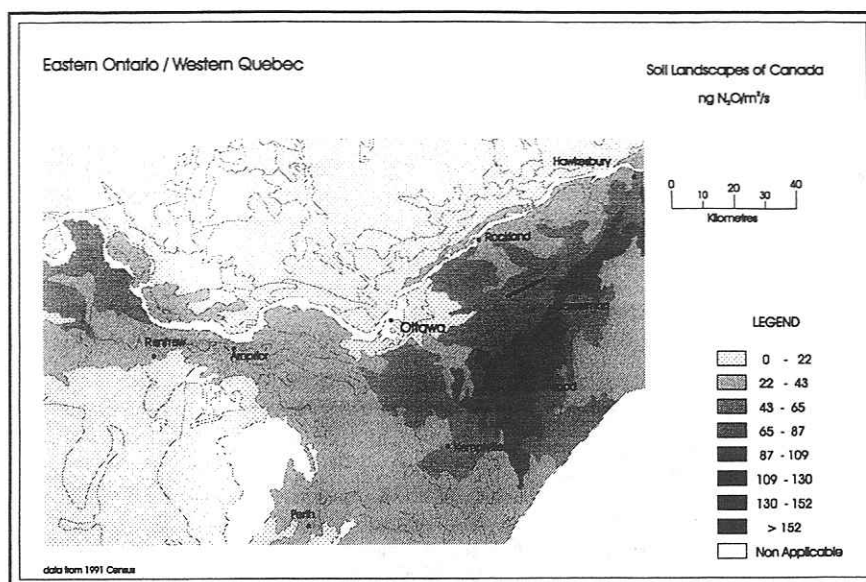


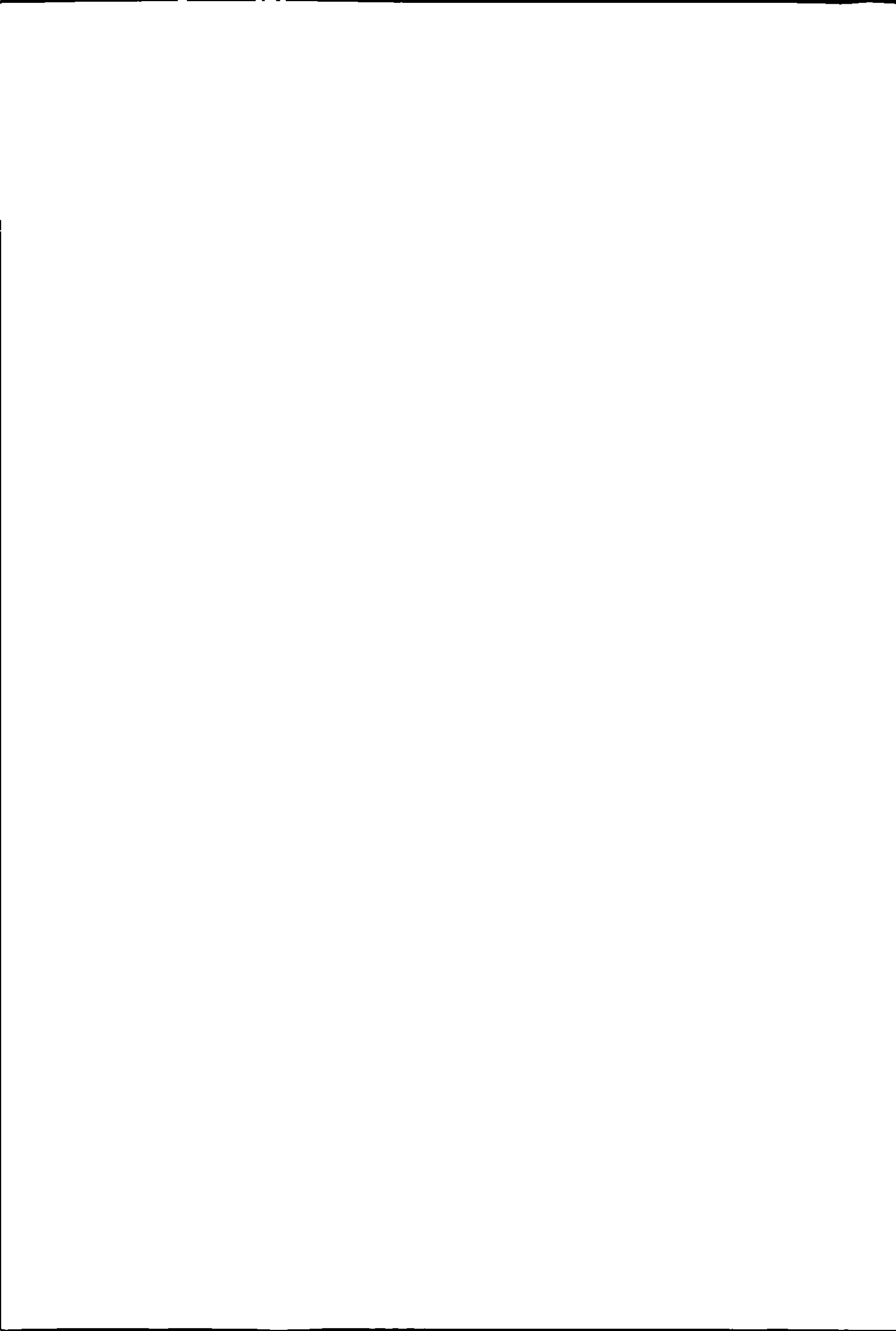
Figure 3. N₂O emissions during the spring-thaw period

References

- Desjardins, R.L. and J.C.Keng. 1999. Nitrous oxide emissions from agricultural sources in Canada. pp 51-56. In Desjardins, R.L., J.C. Keng, and K. Haugen-Kozyra (eds.). International Workshop on Reducing Nitrous Oxide Emissions from Agroecosystems. Agriculture and Agri-Food Canada; Alberta Agriculture, Food and Rural Development. Banff, Alberta, Canada. March 3-5 1999. 256 pp.
- Desjardins, R.L. and R. Riznek. 2000. Agricultural greenhouse gas budget. Pages 133 – 142 in McRae, T., C.A.S. Smith and L.J. Gregorich (eds.) Environmental Sustainability of Canadian Agriculture: Report of the Agri-Environmental Indicator Project. Catalogue No. A22-201/2000E. Agriculture and Agri-Food Canada, Ottawa, Ont.
- Grant, R.F. and E. Pattey. 1999. Mathematical modeling of nitrous oxide emissions from an agricultural field during spring-thaw. *Global Biogeochem. Cycles*. **13**: 679-694.
- Monteverde, C.A., Desjardins, R.L. and E. Pattey. 1998. Agroecosystem greenhouse gas balance indicator: nitrous oxide component. Agri-Environmental Indicator Project. Agriculture and Agri-Food Canada, Report No. 20. 29 pp
- Wagner-Riddle, C., G.W. Thurtell, G.E. Kidd, E.G. Beauchamp and R. Sweetman. 1997. Estimates of N₂O emissions from agricultural fields over 28 months. *Can. J. Soil Sci.* **77**: 135-144.
- Zhu, T., Wang, D., Desjardins, R.L., and J.I. MacPherson. 1999. Aircraft-based volatile organic compounds flux measurements with relaxed eddy accumulation. *Atmos. Env.* **33**: 1969-1979.

Acknowledgements

The assistance of Daniel E. Sabourin for producing the N₂O map and the financial support of the Climate Change Action Fund (CCAF) and the Program for Energy Research and Development (PERD) are gratefully acknowledged.



CO₂ Fluxes At Regional Scales From Profile Measurements Through The Convective Boundary Layer

C.R. FLECHARD¹, R.L. DESJARDINS¹, E. PATTEY¹, W.S. REID¹, A.S. DENNING², P.J. SELLERS³
AND J.A. BERRY⁴

¹*Agriculture and Agri-Food Canada, Ottawa, Canada*

²*Department of Atmospheric Science, Colorado State University, Fort Collins, Colorado, USA*

³*NASA Goddard Space Flight Center, Greenbelt, Maryland, USA*

⁴*Department of Plant Biology, Carnegie Institution of Washington, Stanford, California, USA*

Introduction

Convective Boundary Layer (CBL) budget techniques (Denmead et al., 1996) may provide regional (10^2 - 10^3 km²) estimates of turbulent trace gas fluxes of conserved species such as CO₂ or CH₄. Such methods are based on measurements of concentration profiles up to 3 km in the atmosphere, and on the fact that the CBL may be considered a natural integrator of surface-atmosphere fluxes over time and space.

Changes in CO₂ concentrations between two successive vertical soundings of the CBL may be directly attributed to surface processes if either:

- 1° there is no advection or horizontal concentration gradient, or;
- 2° the two soundings are performed over the same air column.

Corrections for advection errors are theoretically possible but practically difficult to implement and fairly uncertain. On the other hand, tracking down an air column as it moves across the landscape in response to the mean wind presents logistic challenges, but nonetheless remains the most elegant and attractive option of the two. The time elapsed between the two soundings must be long enough for concentration changes to be detectable, yet short enough to prevent dispersion and loss of "memory" of the air column due to large-scale turbulence and Ekman processes.

Theory

The average surface flux $F_{S_1S_2}$ over the time period t between two soundings S_1 and S_2 of the same air column (Fig. 1) may be calculated from:

(1)

where χ is trace concentration (mg m⁻³) and, z_0 is the roughness length of the canopy, and z_S is the top height of the profile.



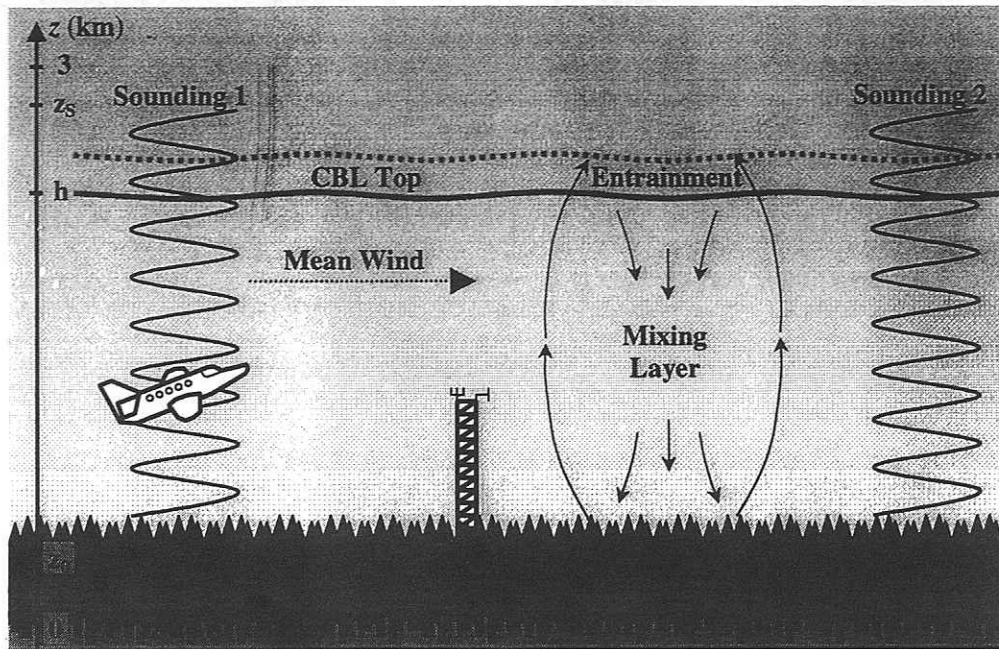


Figure 1. Convective Boundary Layer sampling strategy.

Materials and Methods

An instrumentation package was developed at Agriculture and Agri-Food Canada, Ottawa, to measure concentration profiles of CO_2 with an accuracy of 0.1 ppmv over the first 3 km of the troposphere using a LI-6262 infrared gas analyzer (LI-COR Inc, Lincoln, Nebraska).

The self-contained unit may be installed easily on board a small commercial aircraft and flown to measure concentration profiles above various ecosystems. Reference gas cylinders and switching valves are also included for in-flight calibrations (Fig. 2), and a Global Positioning System provides Earth coordinates in order to track down air masses.

As LI-COR concentration readings vary with pressure and temperature (LI-COR, 1996), sample and reference gas pressure and temperature are maintained at 85 kPa and 40°C, respectively, throughout soundings and in-flight calibrations. This alleviates the need for post-flight pressure and temperature corrections that are normally necessary and which normally provide an additional source of uncertainty.

CO_2 profiles are corrected during post-flight analysis for cross-sensitivity due to H_2O , dilution corrections due to H_2O (LI-COR, 1996), and zero and span adjustments. Profiles are then divided into pressure and/or height bins, from which average surface fluxes between two consecutive soundings may be calculated using Eq. (1).



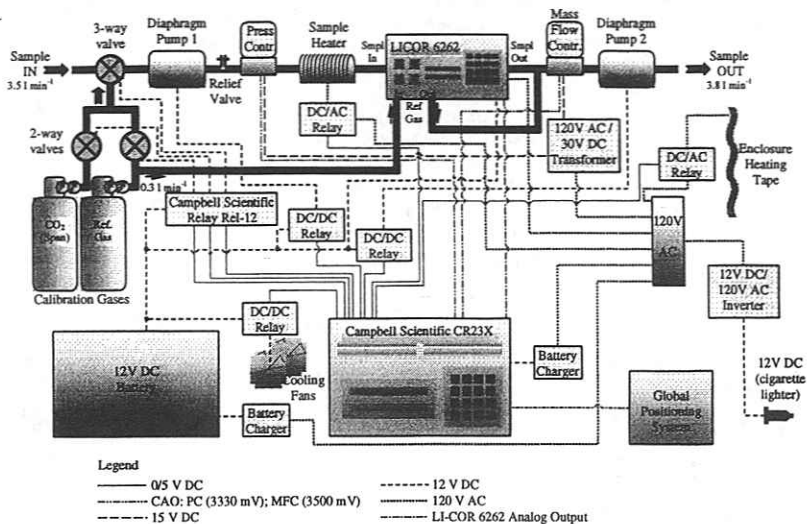


Figure 2. Schematic of the instrumentation package used to measure CO_2 profiles through the CBL.

Results and Discussion

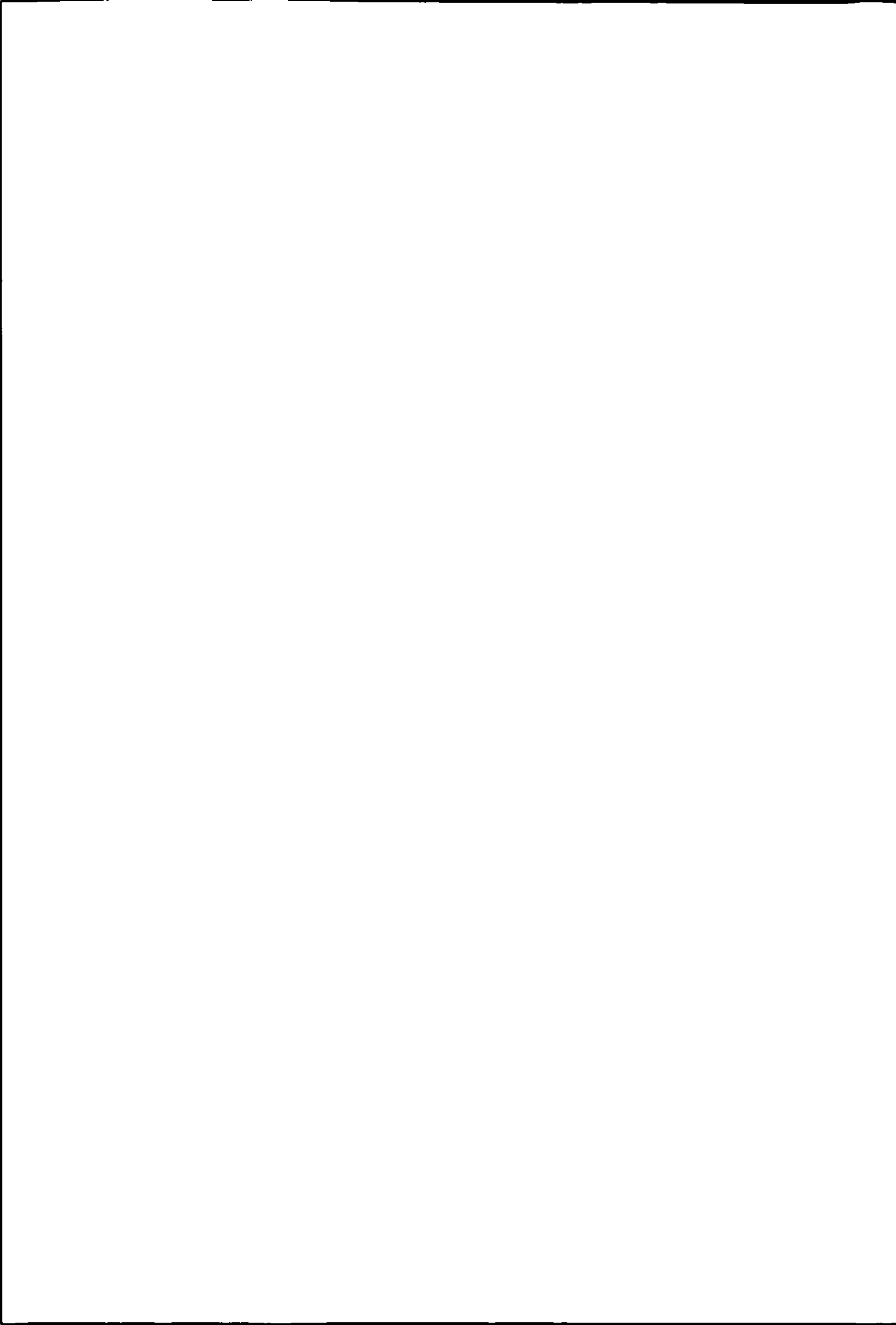
Example CO_2 profiles measured on two days in spring and summer during the Boreal Ecosystem-Atmosphere Study (BOREAS) (Sellers et al., 1995), are presented in Fig. 3. These measurements were obtained using an earlier version of the instrument package described above, which did not control sample temperature or pressure and thus offered less accuracy. The time elapsed between the two soundings S_1 and S_2 was typically 1.5 hours.

Sharp increases or decreases with height in CO_2 concentration graphically show the top of the CBL, while its growth between S_1 and S_2 is clearly visible on both days presented. Water vapour and temperature profile data (not shown) offer similar information on the vertical structure of the CBL. In springtime mixing ratios were larger within the boundary layer than in the free atmosphere, indicating a net CO_2 emission by the forest. By contrast, reversed profiles occur in the summer due to a net downward flux through photosynthesis.

CO_2 fluxes calculated from CBL profiles during BOREAS 1996 were generally in poor agreement with tower-based eddy covariance measurements, although differences in footprint between tower and aircraft soundings may have added to existing discrepancies due to instrumental and methodological difficulties.

Numerical simulations show that a 0.1 ppmv error in CO_2 concentration integrated up to about 2 km over a time period of 1.5 hours amounts to a maximum error in the CO_2 flux of about $0.05 \text{ mg m}^{-2} \text{ s}^{-1}$; a 0.5 ppmv error may amount to an error of up to $0.3 \text{ mg m}^{-2} \text{ s}^{-1}$. Bearing in mind the magnitude of CO_2 uptake by the boreal forest, typically -0.25 to $-0.75 \text{ mg m}^{-2} \text{ s}^{-1}$ in summer sunny conditions, the need for CO_2 -measuring instrumentation capable of 0.1 ppmv resolution clearly becomes crucial. On-going tests on the new version of the instrumentation package indicate that this may be achieved through controlled sample pressure and temperature.

In addition to instrumentation challenges there are difficulties associated with following an air mass across the landscape, while the air column is liable to disperse under the influence of turbulence and change of wind direction and speed with height. The combined effects of



cloud and entrainment processes at the top of the CBL may result on many occasions in unclear vertical profiles from which regional fluxes cannot be derived.

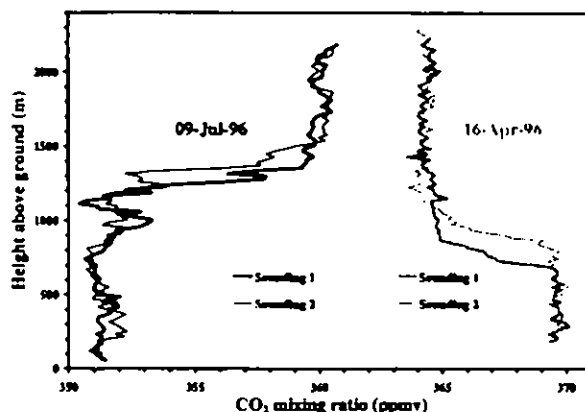


Figure 3. CO_2 profiles through the convective boundary layer above boreal forest during the BOREAS experiment, Saskatchewan, Canada.

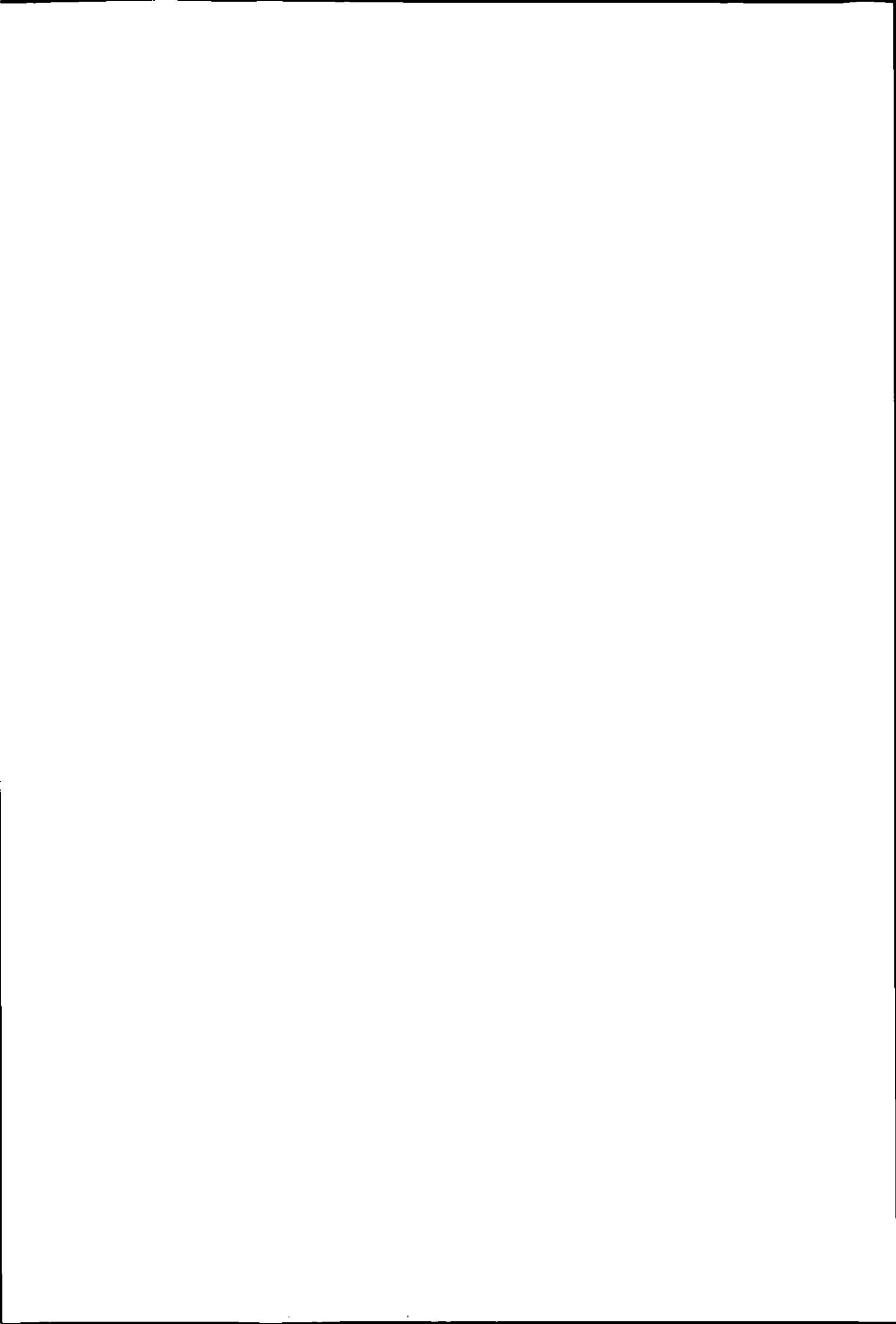
Further testing and experimentation are required to demonstrate the technical and methodological feasibility of CBL budgeting for CO_2 using profile data. The instrument package will be used in the Large Scale Biosphere-Atmosphere (LBA) experiment above the Amazon Forest in Brazil in 2001, which should provide opportunities for bridging the gap between local scale (chamber, tower) and regional scale flux measurements.

References

- Denmead, O.T., Raupach, M.R., Dunin, F.X., Cleugh, H.A. and Leuning, R. (1996). Boundary layer budgets for regional estimates of scalar fluxes. *Global Change Biology* 2 : 255-264.
- LI-COR (1996). LI-6262 $\text{CO}_2/\text{H}_2\text{O}$ Analyzer - Operating and Service Manual. LI-COR Inc., Lincoln, Nebraska.
- Sellers, P.J., Hall, F.G., Margolis, H., Kelly, R.D., Baldocchi, D., den Hartog, G., Cihlar, J., Ryan, M.G., Goodison, B., Crill, P., Ranson, K.J., Lettenmaier, D. and Wickland, D. (1995). *The Boreal Ecosystem-Atmosphere Study (BOREAS): An Overview and Early Results from the 1994 Field Year*. *Bulletin of the American Meteorological Society*, Vol. 76, No. 9, September 1995.

Acknowledgements

The authors wish to thank Dave Dow and the technical staff of Agriculture and Agri-Food Canada for assistance during the development work and testing of the instrument package. Funding for this research was provided by the Program for Energy Research and Development (PERD).



Footprint Estimates Using Analytical and Numerical Methods

ROBERT KORMANN¹, NATASCHA KLJUN², FRANZ X. MEIXNER¹, MATHIAS W. ROTACH²

¹*Max-Planck-Institut für Chemie, P.O. Box 3060, 55020 Mainz, Germany*

²*Institute for Atmospheric and Climate Science, ETH, Winterthurerstr. 190, 8057 Zürich, Switzerland*

Contact: Robert Kormann (kormann@mpch-mainz.mpg.de) for the analytical model,
Natascha Kljun (kljun@geo.umnw.ethz.ch) for the numerical model

Abstract

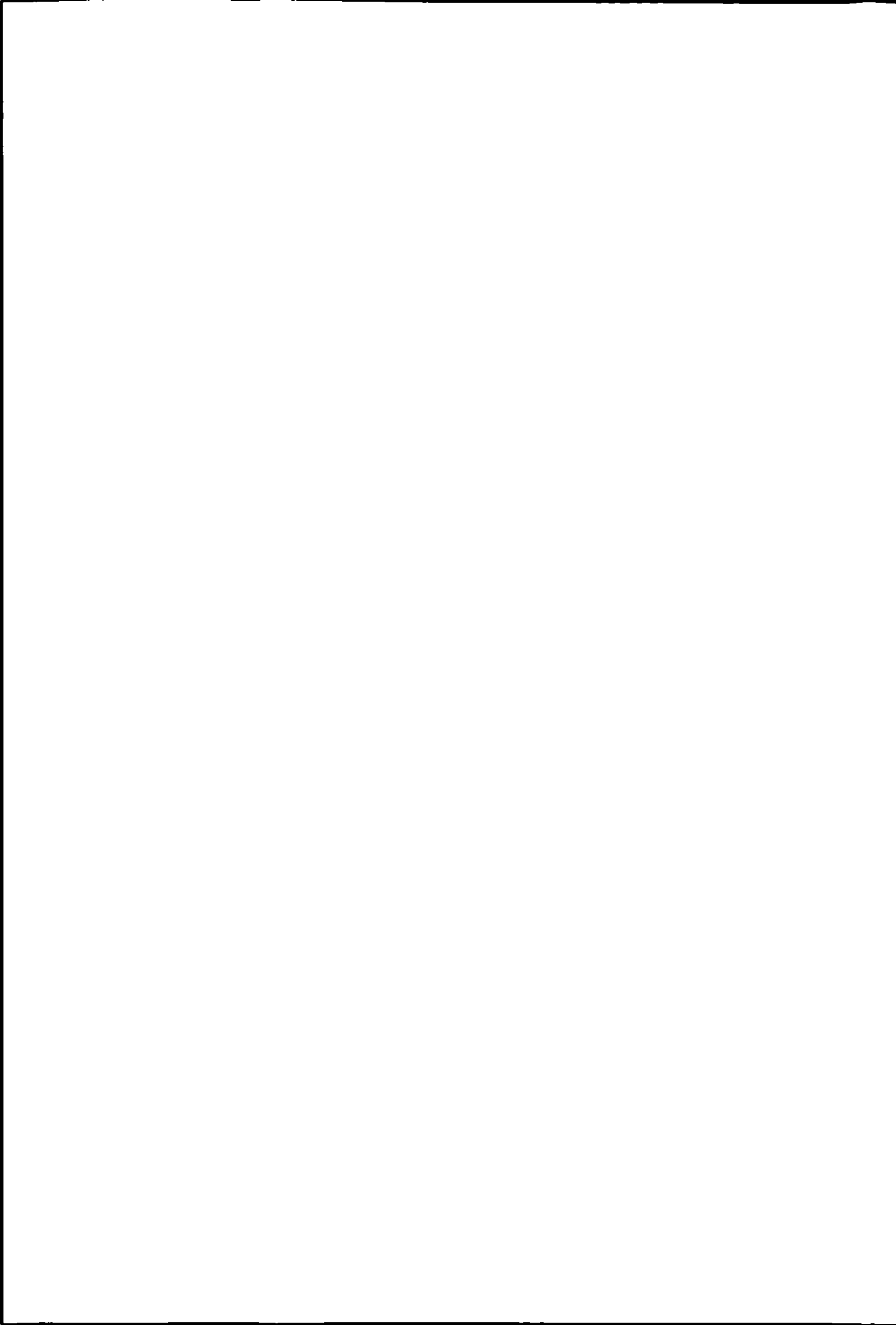
We briefly present general concepts of an analytical and a numerical technique to estimate the source area or footprint of surface-layer eddy covariance measurements. An exemplifying intercomparison of both methods is performed on the basis of observational data. The analytical model is a generalization of a model already published in literature. It uses the solution of the two-dimensional advection-diffusion equation for power law profiles of the horizontal wind velocity and the eddy diffusivity. The numerical model is of the Lagrangian type and employs a recently established approach using backward trajectories of particles. It is based on a 3-dimensional Lagrangian stochastic particle dispersion model satisfying the well-mixed condition continuously for stable to convective stratification, as well as for receptors above the surface layer.

Introduction

From the viewpoint of the experimenter, methods for the measurement of the exchange of scalars (e.g., gases, heat, aerosols) between the earth's surface and the atmosphere can be distributed into two different groups: chamber and micrometeorological techniques. The first are typically easy to realize, but suffer from several serious drawbacks. The system of transfer resistances can be disturbed [5]. Possible reactions on the chamber surfaces restrict the method to chemically inert gases. Chambers probe usually only a small surface area. Observations with adjacent chambers show that alleged identical surfaces on an experimental plot can exhibit remarkably different fluxes. Statistically reliable results therefore require numerous measurements at different locations of the same biotope [6], which is normally not tractable. This problem is usually referred to as the "upscaling problem" in the literature.

Micrometeorological methods, especially the eddy covariance method, avoid these difficulties, but the dimension of the probed area is not immediately obvious. In recent years, several models have been proposed to estimate the size of this upwind surface area of influence (i.e., the footprint). These models can be roughly classified in analytical, Lagrangian stochastic numerical approaches and large eddy simulations. Analytical models are based on solutions of the diffusion equation (e.g., [16], [15], [7], [9]), while Lagrangian models describe the diffusion of a scalar by a stochastic differential equation (e.g., [11], [7], [4], [8]). An example of footprint predictions using large eddy simulations can be found in [10].

The intended application of the two approaches used here differ from each other. The analytical approach extends an existing model [16] for thermally neutral stratification into non-



neutral situations. It is intended to be routinely applied for the estimation of footprints, even for continuous long-term measurements. In fact, the development of the introduced analytical model was motivated by the homogeneity restrictions of the measurement area shown in this work. The Lagrangian stochastic approach is intended to give quantitative descriptions of the surface flux budgets of atmospheric trace gases on a regional scale under various environmental and experimental conditions. In contrast to the analytical approach, it is not restricted to the surface layer.

The data used here was taken during the "Riceotopes" measurement campaign. Funded by the European Union, the main objective of the project was to study methane emissions from rice paddies and the emission pathways over two growing seasons. The measurements were performed at the "Istituto Sperimentale per la Cerealicoltura" near Vercelli, Italy. Enclosure-based measurements were compared to eddy covariance measurements. The fast methane measurements were performed by R. Kormann, using a fast tunable diode laser instrument developed at the Max-Planck-Institut für Chemie. The micrometeorological data is gathered by ultrasonic anemometry.

The motivation of this study was to intercompare the presented numerical and analytical model, on the basis of experimental results. The results of this intercomparison are intended to serve as starting point for a more systematic investigation.

Analytical Footprint Estimation

As already mentioned, several assumptions concerning the observation conditions have to be made to keep the analytical treatability. The model assumes homogeneous and stationary flow conditions over homogeneous and isotropic terrain. The vertical turbulent transport is represented by a gradient diffusion process. Longitudinal turbulent diffusion along the mean wind is neglected compared to advection processes. The assumption of a height-independent crosswind dispersion allows the reduction of the continuity equation to a two-dimensional advection-diffusion equation,

$$u \frac{\partial c}{\partial x} = - \frac{\partial f}{\partial x}, \quad (1)$$

where c describes the crosswind-integrated concentration and f the crosswind-integrated flux, which corresponds to the crosswind-integrated flux footprint. Although not necessary for the analytical treatment, we restrict ourselves to Gaussian crosswind dispersion,

$$D_y(x, y) = \frac{1}{\sqrt{2\pi} \sigma(x)} \exp\left(-\frac{y^2}{2\sigma(x)^2}\right). \quad (2)$$

We assume further power law profiles for the horizontal wind velocity and the eddy diffusivity,

$$u(z) = U z^m \quad \text{and} \quad K(z) = \kappa z^n, \quad (3)$$

which leads to the following solution of eq. (1) for a ground level point source,



$$c(x, z) = \frac{A}{\bar{u} \bar{z}} \exp \left[- \left(\frac{Bz}{\bar{z}} \right)^r \right] \quad (4)$$

\bar{z} is the mean height of the plume, \bar{u} its effective velocity, and the shape factor $r = 2 + m - n$ gives the vertical extent, see, e.g., [12] or [17]. The coefficients A and B depend on the shape factor. Taking $\mu = (1 + m)/r$ and introducing the length scale

$$\xi(z) = \frac{U z^r}{r^2 \kappa}, \quad (5)$$

we find for the crosswind integrated flux footprint f ,

$$f = \frac{1}{\Gamma(\mu)} \frac{\xi^\mu}{x^{1+\mu}} e^{-\xi/x}. \quad (6)$$

Eq. (6) includes the solution given by [16], when using the eddy diffusivity power $n = 1$ for neutral stratification and its conjugated wind velocity power $m = 0$. The maximum of f is

$$f_{\max} = \frac{(1 + \mu)^{1+\mu}}{\Gamma(\mu)} e^{-1-\mu}, \quad \text{found at } x_{\max}^{(f)} = \frac{\xi}{1 + \mu}. \quad (7)$$

Eqs. (6) and (2) lead to the three-dimensional footprint

$$\phi(x, y, z) = D_y(x, y) f(x, z). \quad (8)$$

The equation

$$y^2 = 2\sigma^2 \ln \left(\frac{1}{\sqrt{2\pi} \phi_0} \frac{f}{\sigma} \right) \quad (9)$$

describes the isopleths of ϕ at the level ϕ_0 , see the examples below. Taking the short range limit of the statistical turbulence theory, $\sigma = \sigma_v x/\bar{u}$, with σ_v being the constant crosswind fluctuation, we find the maximum of ϕ at

$$x_{\max}^{(\phi)} = \frac{r \xi}{2r + 1} \quad (10)$$

A more detailed discussion of the model, which also relates the power law profiles, eq. (3), to the Monin-Obukhov profiles, can be found in [9].



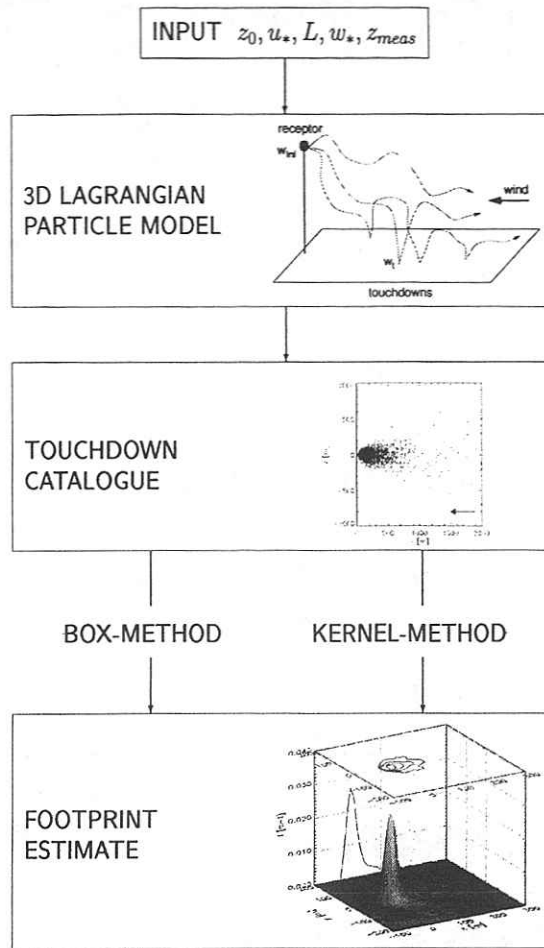


Fig. 1: Calculation scheme of the numerical model.

Numerical Footprint Estimation

The numerical footprint model is based on the 2-dimensional Lagrangian stochastic particle dispersion model developed by [13] and extended to three dimensions by [2]. This model satisfies the well-mixed condition continuously for stable to convective conditions, as well as for receptors above the surface layer (e.g., for use in connection with aircraft measurements).

With given input of the turbulence statistics at a given measurement location (z_0, u_*, L, w_*, z_i , and, if available, $\bar{u}, \sigma_v, \sigma_w$), particles are tracked backwards in time, from the measurement location to the surface source, employing a recently established approach using backward trajectories of particles ([4], see Fig. 1). For each particle, release velocity, as well as touchdown locations and velocities are collected in a touchdown catalogue. Using this output, the flux footprint for a given receptor is determined according to [3].



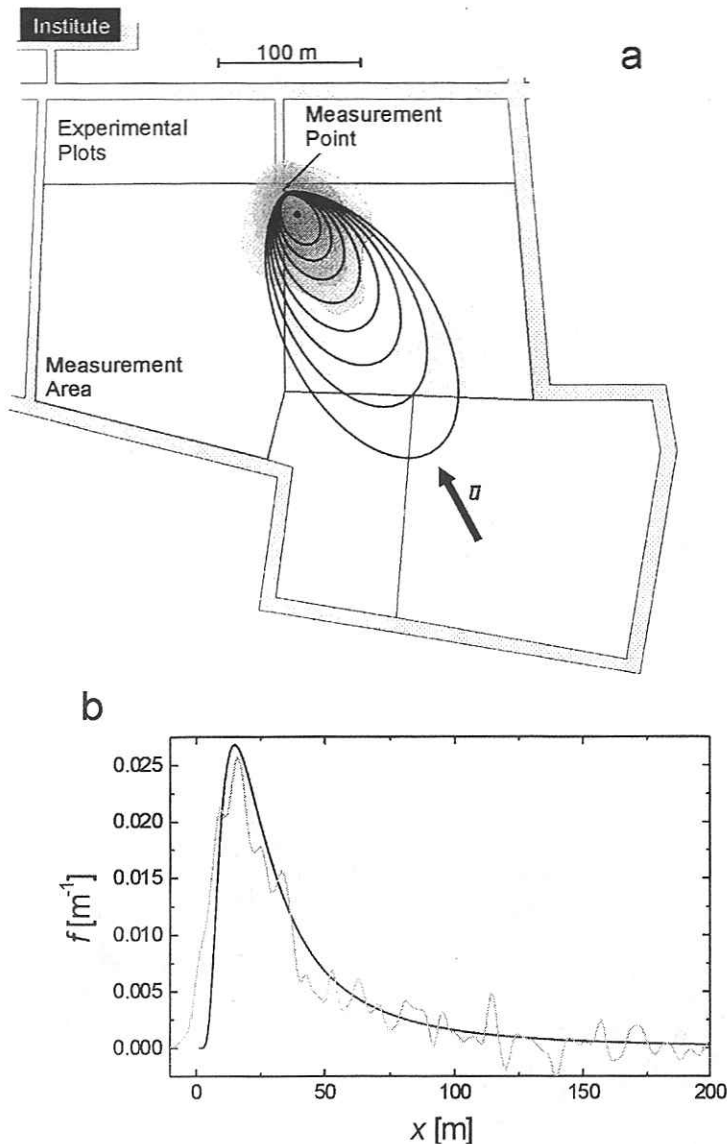
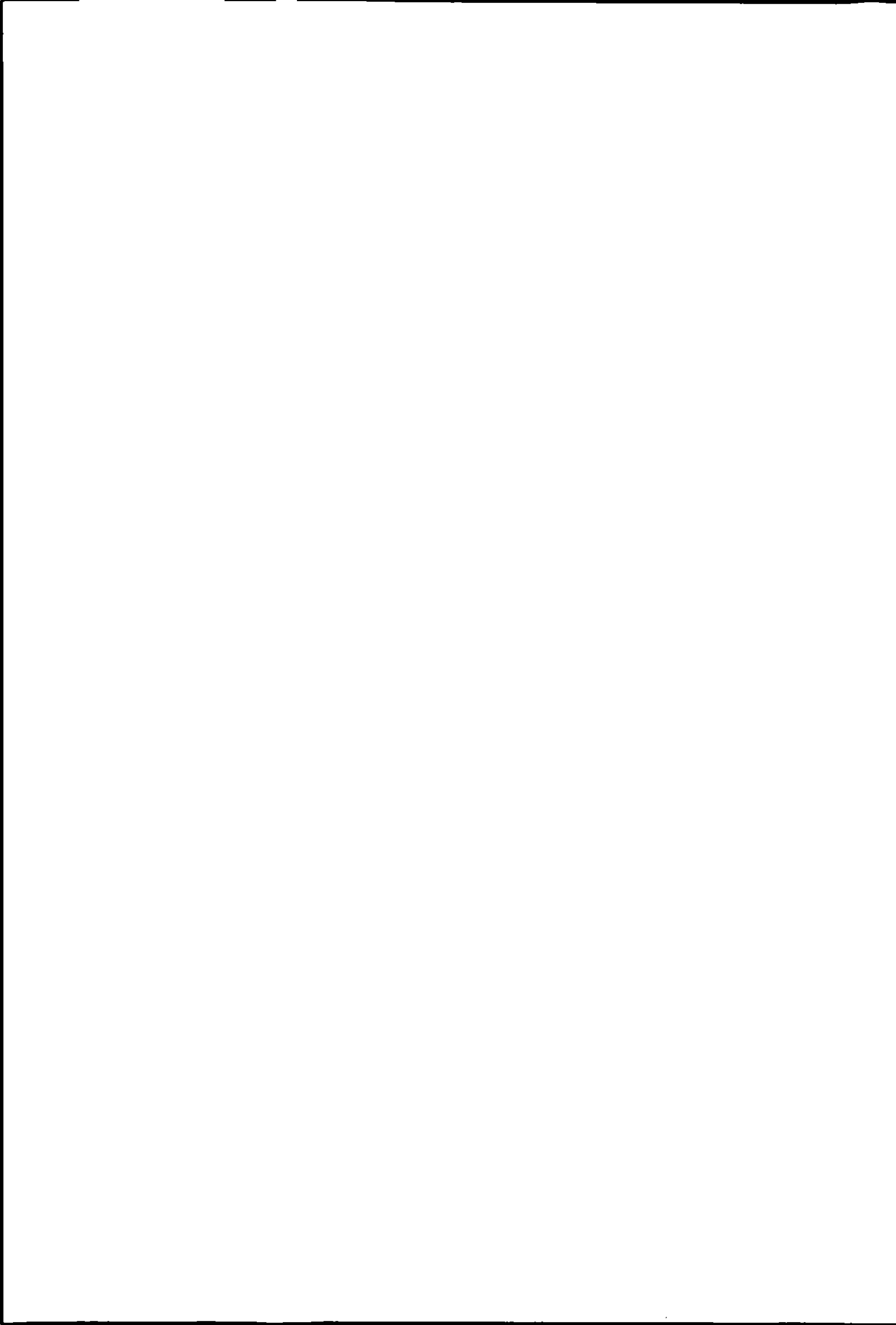


Fig 2: Top view of (a) the footprint ϕ and (b) the crosswind-integrated footprint f for the unstable case. The micrometeorological parameters were $z_m/L = -0.888$, $\bar{u} = 1.20 \text{ m s}^{-1}$, $u_* = 0.129 \text{ m s}^{-1}$ and $\sigma_v = 0.35 \text{ m s}^{-1}$. The measurement height was $z_m = 3.00 \text{ m}$, the roughness length $z_0 = 0.03 \text{ m}$. The results of the numerical models are depicted in grey (applying the grid-box method), the analytical results in black. The black dot indicates the maximum of the analytical solution. The lowest isopleth corresponds to $\phi = 2 \times 10^{-5} \text{ m}^{-2}$, doubling at each level for both models. The numerical data is slightly smoothed.

Fig. 3: Same as Fig. 2, but for the nearly neutral situation. The micrometeorological parameters are: $z_m/L = -0.039$, $\bar{u} = 2.33 \text{ m s}^{-1}$, $u_* = 0.220 \text{ m s}^{-1}$ and $\sigma_v = 0.40 \text{ m s}^{-1}$. The measurement conditions are the same as in Fig. 2.



The footprint estimates can be evaluated using either the traditional way of the grid-box average, where the upwind area of interest is overlaid with a grid, and the footprint function is then calculated for each grid cell (see e.g. the footprints in Figs. 2b and 3b), or by applying the density kernel method following the suggestions of [1]. This statistical treatment of the particle touchdowns applies locally optimized bandwidths for appropriate smoothing, depending on the particle touchdown density, and results in a significant reduction of CPU-time by more than an order of magnitude.

For a complete description of the model development, the reader is referred to [8].

Footprint Intercomparison

Figs. 2 and 3 show the (a) crosswind-dispersed and (b) crosswind-integrated footprints of the two examples under investigation. As mentioned above, these two cases are based on methane emission measurements performed at the Istituto Sperimentale per la Cerealicoltura. We refer to the first example as the "unstable case", the second one as the "nearly neutral case". Both cases exhibit southeasterly wind on average. The measurement height was $z_m = 3.0$ m and the roughness length estimated to be $z_0 = 0.03$ m.

Differences occur in the vicinity of the measurement point (receptor), especially in downwind direction. Since the analytical model neglects longitudinal turbulence, only the upwind area contributes to the footprint. In contrast, the numerical model predicts a contribution from the receptor location itself, especially for the low wind (unstable) case. Moreover, the source area predicted by the analytical model is more elongated due to differences in the shape of the crosswind dispersion. Nevertheless, the crosswind-integrated footprints of the two models coincide excellently. However, the crosswind-integrated flux footprint f typically exhibits a slower roll-off at large upwind distances for the analytical model. Of course, this is also reflected in the source area, which is again larger in the estimates of the analytical model (nearly neutral case). Theoretical considerations [9] anticipate this observation. The analytical model of [14] shows a similar behavior.

From several cases with different stability (not shown), the correspondence between the two approaches appears to be highly dependent on z_m/L . The reason for this is presently under investigation.

Summary and Outlook

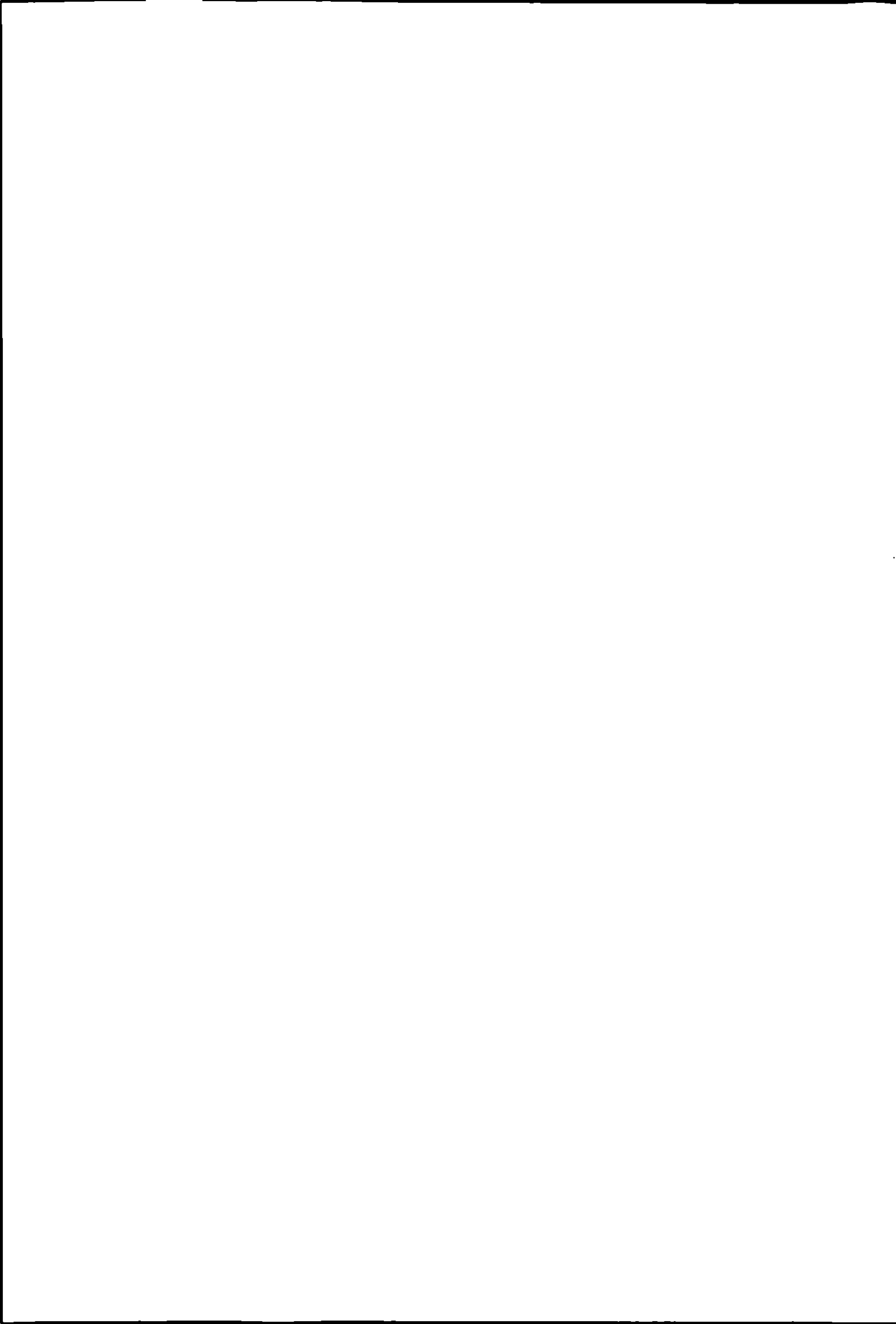
We present first results of an intercomparison between a numerical (Lagrangian stochastic) and an analytical flux footprint model by means of experimental data. Although we observed some differences, the general agreement is very promising. The present exemplifying investigation will be followed by a systematical intercomparison. We expect to clarify the role of the necessary simplifying assumptions in the analytical model. The analytical model seems to be a valuable tool to investigate the behavior of the numerical approach in the idealized case of the surface layer.

Furthermore, we intend to combine both techniques to optimize the choice of the power law parameters for the analytical footprint estimation.



References

1. de Haan, P., (1999) On the use of density kernels for concentration estimations within particle and puff dispersion models. *Atmos. Environ.* **33**: 2007-2021.
2. de Haan, P. and M.W. Rotach, (1998) A novel approach to atmospheric dispersion modelling: The puff-particle model. *Quarterly Journal of the Royal Meteorological Society*, **124**: 2771-2792.
3. Flesch, T.K., (1996) The footprint for flux measurements, from backward Lagrangian stochastic models. *Boundary-Layer Meteorology*, **78**: 399-404.
4. Flesch, T.K., J.D. Wilson, and E. Yee, (1995) Backward-time Lagrangian stochastic dispersion models and their application to estimate gaseous emissions. *Journal of Applied Meteorology*, **34**: 1320-1332.
5. Foken, T., R. Dlugi, and G. Kramm, (1995) On the determination of dry deposition and emission of gaseous compounds at the biosphere-atmosphere interface. *Meteorologische Zeitschrift*, **4**: 91-118.
6. Folorunso, O.A. and D.E. Rolston, (1984) Spatial variability of field-measured denitrification gas fluxes. *Soil Sci. Soc. Am. J.*, **48**: 1214-1219.
7. Horst, T.W. and J.C. Weil, (1992) Footprint estimation for scalar flux measurements in the atmospheric surface layer. *Boundary-Layer Meteorology*, **59**: 279-296.
8. Kljun, N., M.W. Rotach, and H.P. Schmid, A 3D backward Lagrangian footprint model for a wide range of boundary layer stratifications. *Boundary-Layer Meteorology*, submitted.
9. Kormann, R. and F.X. Meixner, (2001) An analytical footprint model for non-neutral stratification. *Boundary-Layer Meteorology*, **99**: 207-224.
10. Leclerc, M.Y., S.H. Shen, and B. Lamb, (1997) Observations and large-eddy simulation modeling of footprints in the lower convective boundary layer. *Journal of Geophysical Research*, **102**: 9323-9334.
11. Leclerc, M.Y. and G.W. Thurtell, (1990) Footprint prediction of scalar fluxes using a Markovian analysis. *Boundary-Layer Meteorology*, **52**: 247-258.
12. Pasquill, F., (1974) Atmospheric diffusion. 2nd edition. New York: J. Wiley & Sons.
13. Rotach, M.W., S.E. Gryning, and C. Tassone, (1996) A two-dimensional Lagrangian stochastic dispersion model for daytime conditions. *Quarterly Journal of the Royal Meteorological Society*, **122**: 367-389.
14. Schmid, H.P., (1994) Source areas for scalars and scalar fluxes. *Boundary-Layer Meteorology*, **67**: 293-318.
15. Schmid, H.P. and T.R. Oke, (1990) A model to estimate the source area contributing to turbulent exchange in the surface layer over patchy terrain. *Quarterly Journal of the Royal Meteorological Society*, **116**: 965-988.
16. Schuepp, P.H., M.Y. Leclerc, J.I. MacPherson, and R.L. Desjardins, (1990) Footprint prediction of scalar fluxes from analytical solutions of the diffusion equation. *Boundary-Layer Meteorology*, **50**: 355-373.
17. van Ulden, A.P., (1978) Simple estimates for vertical diffusion from sources near the ground. *Atmospheric Environment*, **12**: 2125-2129.



FLUXES OF ENERGY, WATER VAPOUR AND CARBON DIOXIDE ABOVE A WINTER BARLEY FIELD

CATHLEEN FRUHAU, ULRICH DAMMGEN, STEFAN BURKART, REMY MANDERSCHIED AND HANS-JOACHIM WEIGEL

*Federal Agricultural Research Centre Braunschweig, Institute of Agroecology
Bundesallee 50, 38116 Braunschweig, Germany*

The task

Fluxes of energy, water vapour and carbon dioxide have been measured above an arable crop field (see Fig. 2) in the context of the Braunschweig Carbon Project (Weigel and Dämmgen, 2000). The project combines micrometeorological flux measurements of air constituents (CO_2 , H_2O) and Free Air Carbon Dioxide Enrichment (FACE) which are related to soil, physiological, meteorological and agronomic variables.

Materials and methods

The FACE facility has 6 rings with a diameter of 20 m each:

- 2 rings with CO_2 enrichment and blowers (FACE, set point $550 \mu\text{mol mol}^{-1}$),
- 2 rings only with blowers (control) and
- 2 rings without CO_2 enrichment and without blowers (ambient).

Fluxes of sensible heat, latent heat and carbon dioxide have been measured using eddy covariance (EC), eddy covariance energy balance (ECEB), a gradient technique (Grünhage et al., 1994) and with $\text{CO}_2/\text{H}_2\text{O}$ gas exchange chambers (Burkart et al., 1997) with ambient and increased CO_2 concentrations (see Fig. 1).

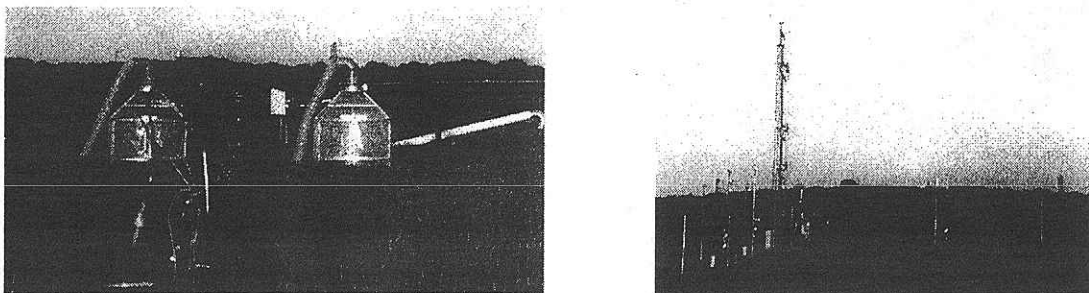


Fig. 1: (a): Micrometeorological tower with temperature sensors (Thies, aspirated PT100) and cup anemometers in 5 respectively 6 heights, 3 additional masts for additional temperature gradient measurements and 5 ultrasonic anemometers (Gill, Solent R2 (4x), EdiSol system: Solent R3 (1x) in combination with an IR gas analyzer Li-Cor 6262). (b): Gas exchange chambers in one FACE ring

Gas exchange chambers have been used in the FACE and its control rings and the CO_2 flux data did not include soil respiration from roots and microbial decomposition because of the slight overpressure in the chambers. Net radiation have been measured with a net radiometer (Thies) and the soil heat flux with soil heat flux plates.



Foot print areas

Foot print areas were calculated after Schuepp et al. (1990) to decide whether the fluxes measured were representative for the area under consideration. Under day-time conditions 90 % of the measured fluxes of the several ultrasonic anemometers (measuring height $z_m = 2.5$ m) originate from distances of less than 200 m from the instruments and thus are coined by the winter barle field (Fig. 2).

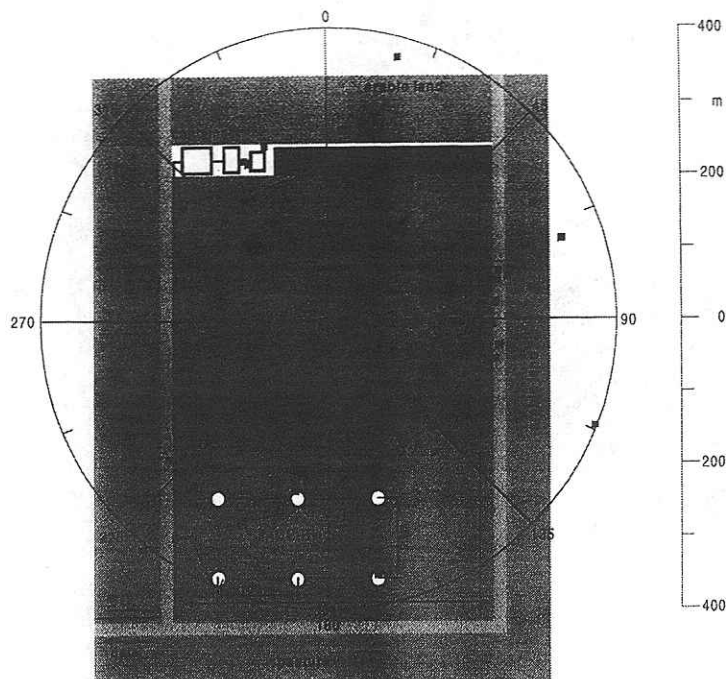


Fig. 2: Positions of most distant points of the 90 % contours of the foot print areas of the measured fluxes; day-time conditions ($R_n > 10 \text{ Wm}^{-2}$); May 2000, one ultrasonic anemometer (half hourly means)

Carbon dioxide and water vapour fluxes

Fluxes from EC respectively ECEB were compared to fluxes obtained from gradient measurements and to the results of canopy $\text{CO}_2/\text{H}_2\text{O}$ gas exchange chambers with ambient and increased CO_2 concentrations.

Fig. 3 shows the diurnal variation of the flux of carbon dioxide (F_c) from different methods for a number of days during the growing. CO_2 fluxes measured with the gas exchange chamber were in good agreement with CO_2 fluxes from the eddy covariance system (EdiSol) despite the different footprint areas of 0.8 m^2 (gas exchange chamber) and up to several 100 m^2 (EdiSol system). During daytime the amount of the CO_2 flux by EC is lower and during night higher than the CO_2 flux by canopy gas exchange chamber. Soil respiration from roots and microbial decomposition have been capture by EC and so the resulting net CO_2 flux between soil-plant-atmosphere must be lower than only the CO_2 flux between plant and atmosphere during daytime and higher during nights.



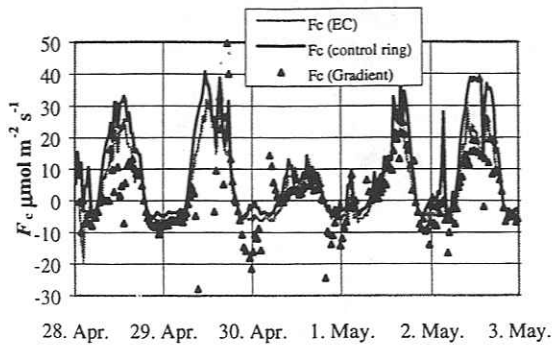


Fig. 3: Comparison of CO₂ flux measured by the EdiSol system, by a gradient technique and with the gas exchange chamber in one control ring of the FACE system (April 28th to May 2nd, 2000, half hourly means)

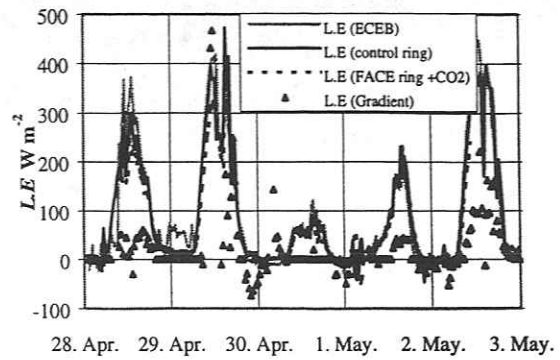


Fig. 4: Comparison of latent heat flux: *L.E* measured with the gas exchange chamber in one control ring and in one ring with CO₂ fumigation, by gradient technique and calculated with ECEB (April 28th to May 2nd, 2000, half hourly means)

The fluxes of CO₂ calculated from the gradient technique show mostly the same pattern, but in several hours the gradient technique deviates considerably. The latent heat fluxes displayed in Fig. 4 show agreement between the measurements of the gas exchange chamber and the calculations from the energy balance. The fluxes obtained by the gradient technique are mostly too low. Under higher CO₂ level (550 μmol mol⁻¹) the measured latent heat is somewhat lower than in the control ring due to the fact that CO₂ enrichment reduces stomatal conductance (water use efficiency of the plants increases).

Energy balance of the winter barley field

Fluxes of sensible heat are assessed by several sonic anemometers at different positions and in different heights as well as by gradient techniques (see Poster Dämmgen and Frühauf). Fig. 5 shows the diurnal variation of the components of the energy balance net radiation (*R_n*), soil heat flux (*G*), sensible heat flux (*H*) and latent heat flux (*L.E*) for 5 days.

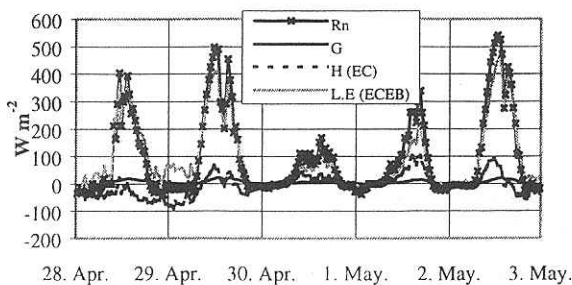


Fig. 5: Components of the energy balance (April 28th to May 2nd, 2000) (half hourly means)

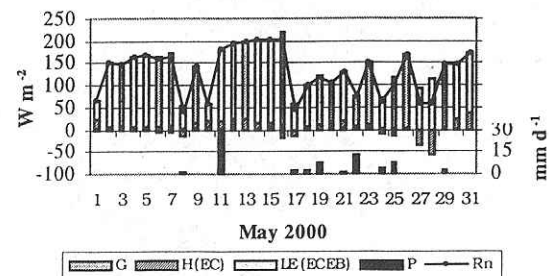


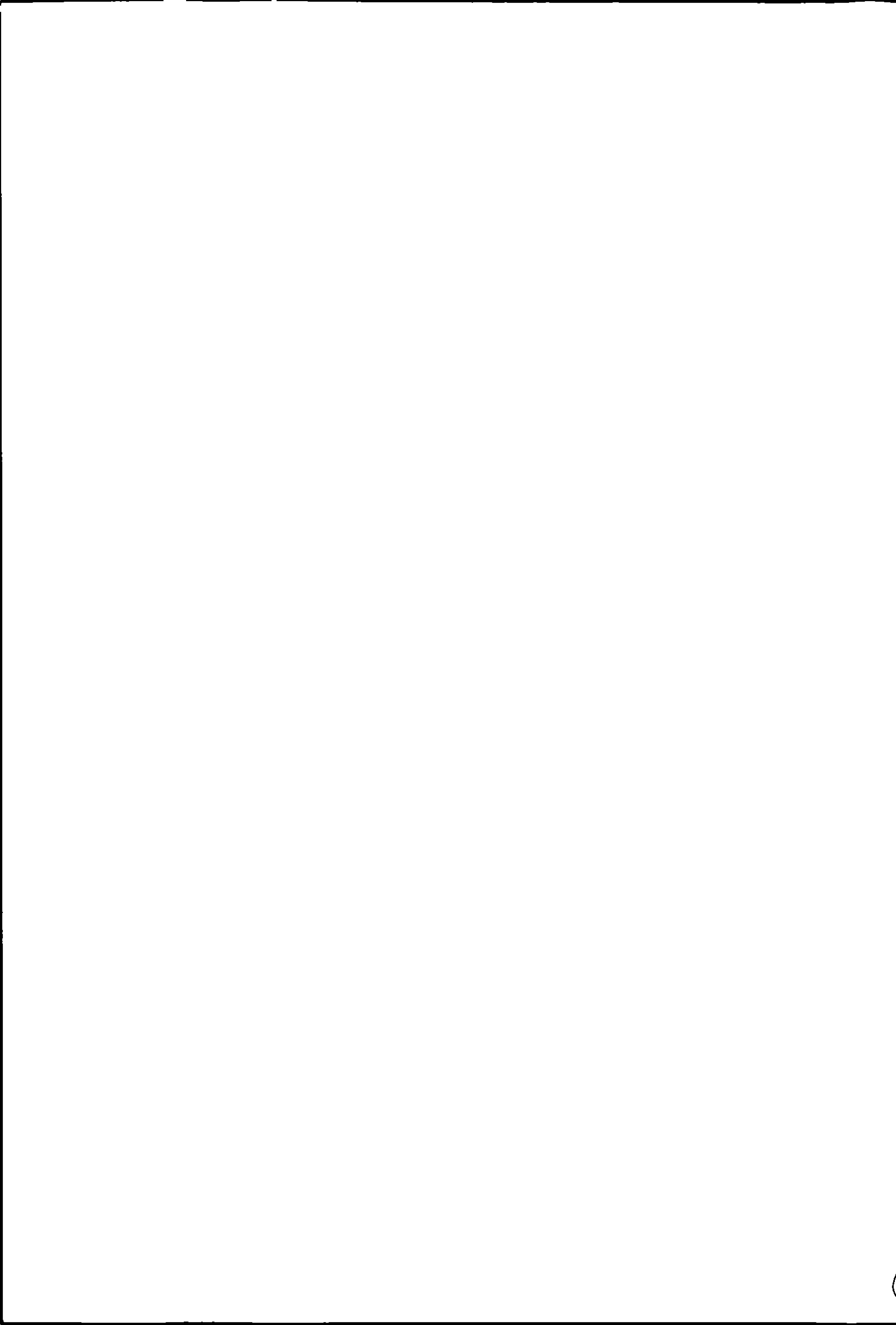
Fig. 6: Daily energy balances components and precipitation *P* for May 2000

The latent heat flux is the dominating part of the available energy *AE* ($AE = R_n - G = H + L.E$) (Fig. 6). The sensible heat flux contributes little. Negative daily means of sensible heat flux occur on 9 days in May 2000. This sensible heat fluxes are downwards to the plant canopy and so the latent heat flux can exceed the available energy.



References

- Burkart, S., Mejer, G.J., Weigel, H.-J. (1997): Ein Gaswechselsystem zur Erfassung des $\text{CO}_2/\text{H}_2\text{O}$ -Austausches von Pflanzenbeständen. In: *Übertragbarkeit ökophysiologischer Messergebnisse von Pflanzenteilen auf Pflanzenbestand*, Kappen L. (Ed.), *EcoSys Suppl.* 20, 59-69.
- Grünhage, L., Dämmgen, U., Haenel, H.-D., Jäger, H.-J. (1994): Response of a grassland ecosystem to air pollutants: – The chemical climate: Vertical flux densities of gaseous species in the atmosphere near the ground. *Environ. Pollut.* 85, 43-49.
- Schuepp, P.H., Leclerc, M.Y., MacPherson, J.I., Desjardins, R.L. (1990): Footprint prediction of scalar fluxes from analytical solution of the diffusion equation *Boundary-Layer Meteorol.* 50, 355-373.
- Weigel, H.-J., Dämmgen, U. (2000): The Braunschweig Carbon Project: Atmospheric Flux Monitoring and Free Air Carbon Dioxide Enrichment (FACE). *J. Appl. Bot.* 74, 55-60.



Airborne Observations of Surface-Atmosphere Energy and CO₂ Exchange over the Northern Mackenzie River Basin in Canada

¹J. I. MACPHERSON, ²P. H. SCHUEPP, ³R. L. DESJARDINS

¹ National Research Council, Ottawa, Ontario, Canada

² McGill University, Montreal, Quebec, Canada

³ Agriculture and Agri-Food Canada, Ottawa, Ontario, Canada

Abstract

This paper describes the operation of the NRC Twin Otter atmospheric research aircraft in the 1999 Mackenzie GEWEX Study. The aircraft was instrumented to measure the vertical fluxes of sensible and latent heat, momentum and CO₂ and supporting meteorological and radiometric data. Twenty-five project flights were flown from Inuvik NWT (68 N, 133 W) over tundra, forest and the Mackenzie Delta during two periods covering the spring snowmelt and early summer. Absolute energy exchange (particularly sensible heat flux) differed very significantly between forested and non-forested areas at the time of full and partial snow cover. The data also showed the importance of non-turbulent fluxes (melting processes and surface heating) for accurate modeling of this ecosystem.

Introduction

The Mackenzie GEWEX Study (MAGS, Stewart *et al.*, 1998) was a major Canadian contribution to the Global Energy and Water Cycle Experiment (GEWEX). MAGS was a comprehensive study of the hydrologic cycle and energy fluxes of the Mackenzie River Basin, which is the largest North American source of fresh water to the Arctic Ocean. This area has experienced one of the most pronounced warming trends in the world over the last few decades (Stewart *et al.*, 1998).

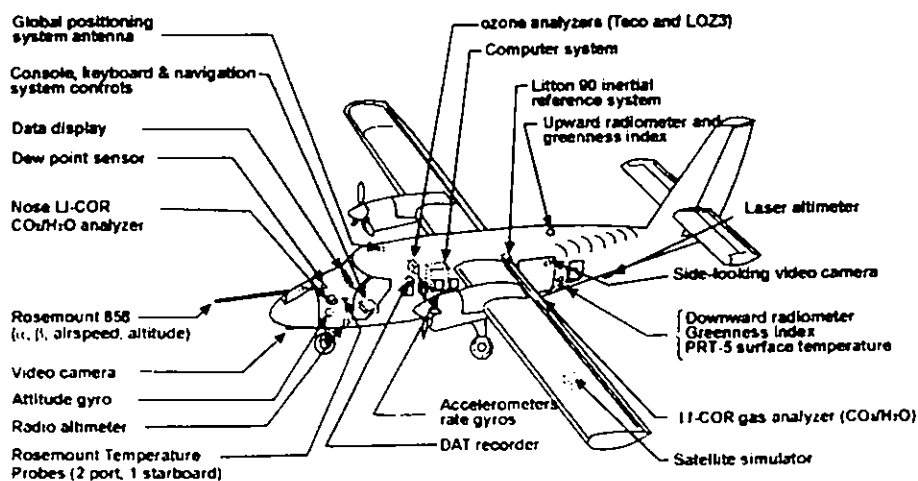


Fig. 1: NRC Twin Otter atmospheric research aircraft as configured for MAGS

An improved understanding of this ecosystem will contribute significantly to the coupled atmospheric-hydrologic-land surface models used for predicting the climate for many decades into the future.



The role of the NRC Twin Otter atmospheric research aircraft in MAGS was to provide measurements of surface-atmosphere exchange of sensible and latent heat and CO₂ at temporal and spatial scales suitable for testing models based on remote sensing and numerical simulation (MacPherson *et al.*, 1999). The instrumentation configuration for MAGS is shown schematically in Fig. 1. Flux estimates were made by the eddy-covariance technique by statistically correlating 32-Hz fluctuations of the vertical turbulent air motion with those of potential temperature, moisture and CO₂.

Twenty-five project flights were operated from Inuvik, NWT (68 N, 133W) in two 'windows'; May 21 to June 8, 1999 (calendar days 141-159) and July 5 to July 14 (days 186-195). The former covered the critical snowmelt period and the latter was representative of early summer conditions. Repeated flux runs were flown over several tracks representative of the different ecosystems in the northern Mackenzie Basin. This paper will present data from three of these sites: (1) a grid pattern over tundra 50 km north of Inuvik, (2) a 20-km run over the Delta, and (3) a sparse black spruce forest in the Havikpak Creek basin near the Inuvik Airport.

Grid Study on Tundra

The plotted flight track in Figure 2 represents the tundra grid pattern, which consisted of a series of nine lines 16 km in length separated by approximately 2 km. The pattern was flown twice in opposite directions to minimize temporal effects (i.e., each pair of lines was flown at approximately the same mean time). The average flight altitude was 60 m. This flight pattern is used to map flux distributions over an area and in scaling-up flux estimates from tower footprint scales to regional dimensions. A flux tower system operated by the National Hydrology Research Centre of Environment Canada was located near the east end of Line 8 of the grid. The grid area was located about 50 km north of Inuvik.

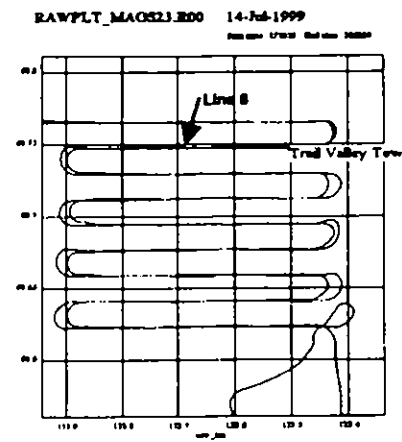


Fig. 2: Grid flight track

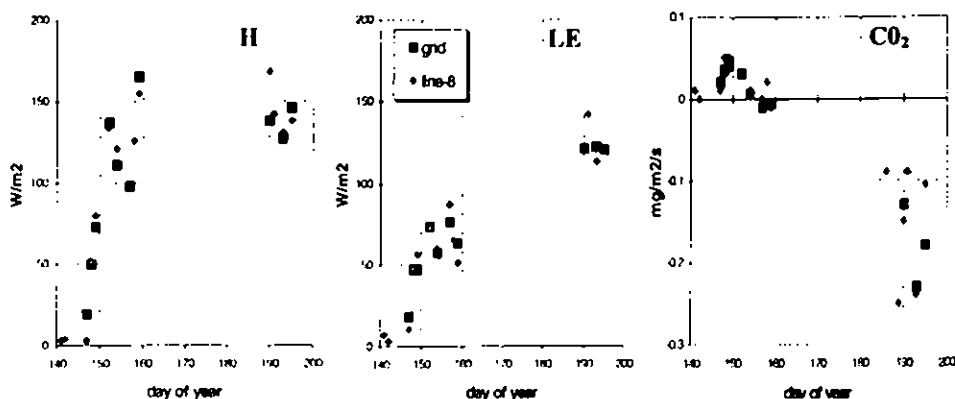


Fig. 3: Fluxes measured over the grid (squares) and line-8 of the grid (diamonds)



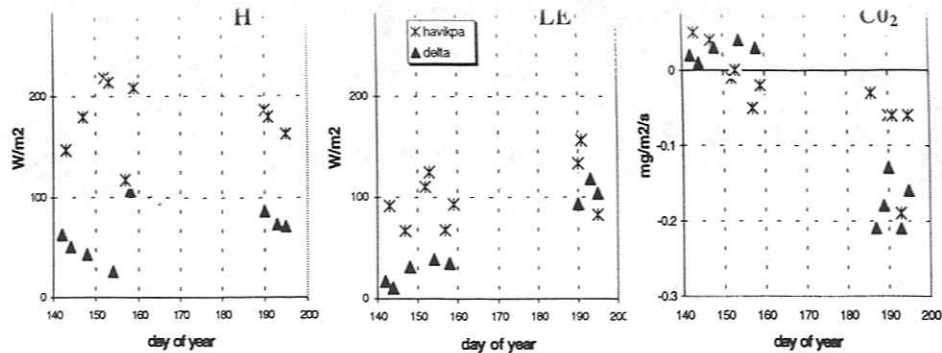


Fig. 4: Fluxes measured over the Delta (triangles) and Havikpak Forest (asterisks)

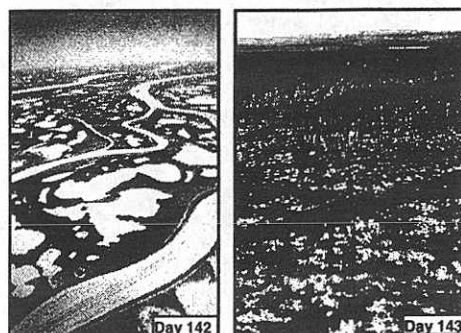
Figure 3 shows the aircraft-measured sensible heat flux H , latent heat flux LE , and the CO_2 flux averaged over the grid (18 runs) and for repeated passes over line-8 of the grid. The H and LE plots are restricted to clear or almost clear conditions, whereas that for the CO_2 flux includes overcast or broken conditions (Days 187-189). The data for Line-8 where the tower was located did not systematically differ in flux characteristics from the overall grid.

The dramatic increase in H over the snowmelt period is evident (Day 141-154, May 21 to June 3). LE over the grid exhibits a much more gradual approach to summertime values. It appears that, even though the surfaces are wet during snowmelt, there is sufficient aerodynamic resistance to convective moisture loss from the vegetation to suppress LE in favour of H until the rootzone is thawed sufficiently for transpiration to become significant.

As the snow melts, the CO_2 flux initially shows a small upward flux indicating respiration from the newly exposed surface, and then negative values as the vegetation greens and photosynthesis increases.

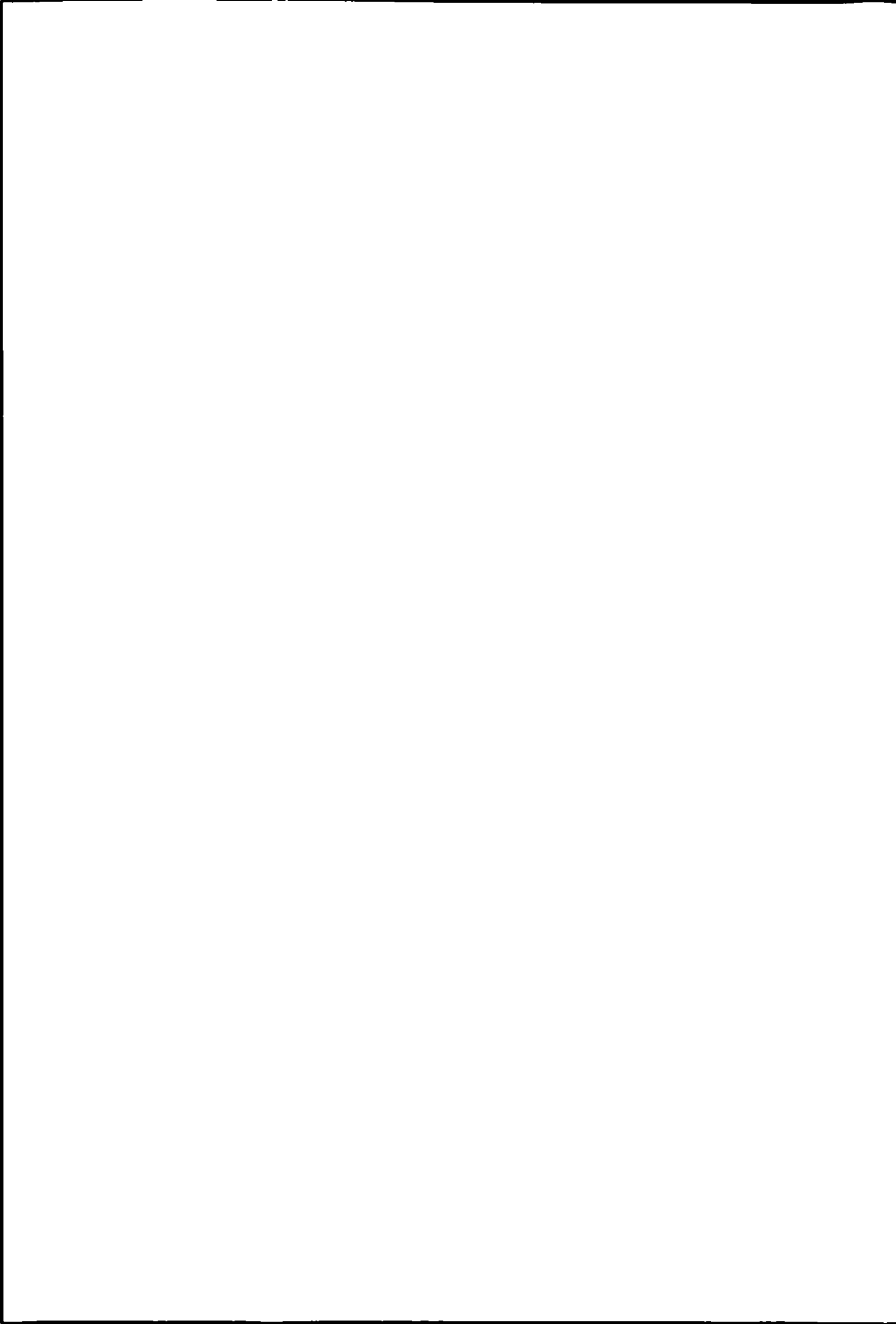
1. Delta and Forest

Repeated flux runs were flown over a 20-km track on the Mackenzie Delta (left photo) and a 3-km track over the Havikpak surface flux site located in a black spruce forest (right). Flight altitude was 60 m over the Delta, but lowered to 30 m over the smaller Havikpak site to reduce the flux footprint for flux tower comparison.



The largest sensible heat fluxes were measured over the forested sites, such as for Havikpak shown above (asterisks). The fluxes were significant even at the start of the observation period due to the warmth of the melted hummocks and lichen (right photo). As was the case for the tundra (grid), H reached summertime levels over both the Delta and forest by the end of the first observation period (June 8). For the latent heat flux LE , the second observation period (July), with melt in the root zone, showed higher moisture exchange due to root uptake in transpiration.

As was the case for the tundra, initial CO_2 fluxes were small and positive (upward). The Havikpak site was the first to become snow free and the first with downward fluxes signifying CO_2 uptake by the vegetation. As was observed over coniferous forests in the BOREAS project (MacPherson *et al.*, 1999), the largest CO_2 uptake usually occurred in cloudy conditions, as seen



above on Days 187 and 192. In the summer period, the CO₂ uptake was larger over the Delta than over the forested sites, despite the significant proportion of water surfaces on the Delta run. This unanticipated observation requires further study. Certainly, the vegetation on the Delta (forest, reeds and grasses) was well watered and appeared to be very lush.

Energy Closure

Eddy-covariance flux estimates have traditionally been plagued by non-closure, i.e., the fact that sensible (H) and latent (LE) heat fluxes, when added to the measured or estimated ground heat flux (G), do not add up to the measured net radiation, R_n. A 'residual' of the order of 10-20% has been hypothetically attributed to factors such as insufficient sampling of low frequency contributions, regional advection, or large-scale transport associated with a non-zero vertical velocity. Figure 5 shows the Residual Energy Flux computed from the equation:

$$R = [R_n - (H+LE)]/R_n.$$

The MAGS project differed from any previous Twin Otter flux program by: (a) the unusually large part of the available energy that was dissipated by non-turbulent fluxes (primarily snow and ice melting and heat storage in the gradually warming soil and water bodies), and (b) the fact that on some runs H+LE nearly equaled (or even exceeded) R_n. Such a case is indicated for the Delta on Day 192, for which clear sky conditions had just become overcast. The waterlogged surface systems exhibited a thermal inertia (or possibly a sign change in G) which delayed the expected drop in energy fluxes (particularly that of sensible heat).

Concluding Remarks

Absolute energy exchange (particularly sensible heat flux) differs very significantly between forested and non-forested areas at the time of full and partial snow cover, due to low albedo of coniferous trees for shallow sun angles. The delineation between tundra and 'forest' in land cover classification schemes based on remote sensing, which is not easy in this transition landscape, is important for the extrapolation of findings to the larger scale. The overwhelming importance of the non-turbulent energy fluxes (the 'residual' above) for the tundra and Delta during the snowmelt period is obvious and its correct representation in models will be a challenge to modelers.

Future analysis efforts will focus on the comparison of fluxes measured by the aircraft and the two flux towers. The generally good agreement between the grid averages and Line8 (where one of the flux towers was located) is a promising start to scaling up the tower data to regional scales.

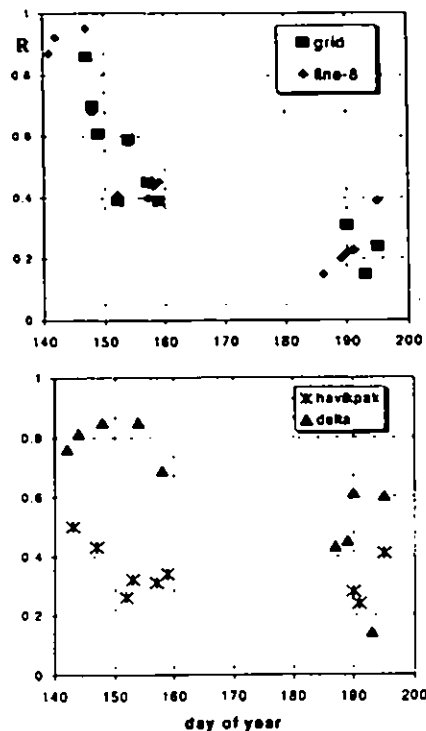


Fig. 5: Residual energy flux



Acknowledgments

Twin Otter operations in MAGS were funded by the Natural Sciences and Engineering Research Council of Canada, the National Research Council of Canada, the Meteorological Service of Canada, Agriculture and Agri-Food Canada, and NASA.

References

- MacPherson, J. I., M. Bastian, P. H. Schuepp, S. Ogunjemiyo, R. L. Desjardins, and R. Riznek, 1999: 'Relating Boundary Layer Flux Measurements to Remote -Sensed Radiometric Data'. *Proceedings of the Fourth International Airborne Remote Sensing Conference/21st Canadian Symposium on Remote Sensing*, Ottawa, June 21-24, 1999, pp. 605-614.
- Stewart, R.E., H.G. Leighton, P. Marsh, G.W.K. Moore, H. Ritchie, W.R. Rouse, E.D. Soulis, G.S. Strong, R.W. Crawford, and B. Kochtubajda, 1998: 'The Mackenzie GEWEX Study: The Water and Energy Cycles of a Major North American River System'. *Bull. Amer. Meteor. Soc.*, **79**, 2665-2683.



Soiling of Buildings Caused by Pollutant Deposition and its Removal by Rain

WEI TANG¹, CLIFF I. DAVIDSON¹, SUSAN FINGER¹ AND MARY F. STRIEGEL²

¹Department of Civil and Environmental Engineering, Carnegie Mellon University,
Pittsburgh, PA 15213, USA

²National Center for Preservation Technology and Training, NSU Box 5682,
Natchitoches, LA 71497, USA

Introduction

Deposition of air pollutants is known as the primary cause of surface soiling of calcareous stone buildings (Sherwood, et al., 1990), which involves several sequential processes. First, SO₂ and other acid gases react with the stone when the surface is moist, e.g., SO₂ reacts with CaCO₃ to form CaSO₄, or gypsum. Gypsum is more soluble in rainwater than the original stone, and thus pits and cracks develop as the gypsum is washed away. The rough surface then serves as a site for deposition of soot carbon and other particles, which can subsequently be bound to the stone by chemical reactions. If air quality later improves, the soiled areas can gradually become white through erosion of surface layers where rain-washing occurs. Therefore, changes in soiling patterns on buildings over long periods of time are apparently determined largely by two competing processes: deposition of air pollutants and rain-washing of the surface.

Background and Methods

The effects of the two competing processes on soiling of calcareous stone buildings have been investigated at the Cathedral of Learning, a 42-story limestone building on the University of Pittsburgh campus. In earlier work (Etyemezian, et al., 1998; Davidson, et al., 2000), we found that under highly polluted conditions, soiling of the Cathedral occurred within a few years after construction in the 1930's, and it was relatively uniform on the entire building. In contrast, removal of the soiling after air pollutant levels decreased has taken several decades, and the removal rate varies significantly at different elevations and on different faces of the building. Measurement results suggest that the complexity of soiling patterns on the Cathedral is not related to differences in pollutant concentrations and deposition rates, but rather to variability in wind-driven rain delivered to the building walls. Here we examine this hypothesis.

In this study, wind-driven rain fluxes to the walls of the Cathedral of Learning were estimated using a Computational Fluid Dynamics (CFD) method, similar to the approach proposed by Choi (1993). First, the steady-state airflow field around the Cathedral was solved in three dimensions using the Reynolds-averaged Navier-Stokes and continuity equations. The Re-Normalization Group $k-\epsilon$ (RNG) equations were used to achieve numerical closure, where k is the turbulent kinetic energy and ϵ is the turbulent kinetic energy dissipation. Second, trajectories of raindrops, subjected to each flow field obtained in the first step, were simulated and the locations where the raindrops strike the building walls were recorded. Finally, measurements of rain intensity, wind speed and wind direction were obtained at a location near the Cathedral. The collected data, combined with results from the first two steps, were used to estimate wind-driven rain delivered to individual sections of the building walls. The results allowed for comparison with observed soiling patterns at the Cathedral. The first two steps were conducted using FLUENT 5.3, a



commercially available computational fluid dynamics software package (FLUENT Inc, Lebanon, NH). A geometry including most large-scale architectural characteristics of the building was used in the numerical modeling.

Results and Discussion

Airborne concentrations and dry deposition of pollutants to building walls are strongly influenced by the airflow patterns around the building. The lack of vertical gradients of pollutant concentrations and deposition fluxes measured at the Cathedral (Etyemezian, et al., 1998) suggests a well-mixed atmosphere around the building, which is consistent with the modeling results. Characteristic flow patterns around a bluff body, such as recirculation in the wake region, vertical movement of airflow near the windward faces, and upward vertical movement of airflow on the leeward faces of the building, can all contribute to the lack of vertical gradients.

Based on the results of raindrop trajectory simulation, the Local Effect Factor (LEF) was calculated for every section on the building walls, under each discrete wind condition and for each raindrop size. The LEF, defined as the ratio of the flux/m² of rainwater volume on a vertical building wall to the flux/m² of rainwater volume on the ground, allows for calculation of wind-driven rain fluxes based on the amount of rainfall. LEF profiles for the four faces of the building are shown in Figure 1 for SW winds at a windspeed of 10 m/s (height of 30 m) and raindrops with a diameter of 2.5 mm. The calculated LEF profiles indicate that the upwind face of the building receives a much greater amount of wind-driven rain flux. This flux increases with height, and is more likely to be greater on corners than the center area of the building wall. The calculations are in agreement with the observed soiling patterns at the Cathedral, where walls on the upper floors are less soiled and the corners are normally whiter (i.e., more eroded), even on a heavily soiled face. Meteorological data collected during year 2000 indicate that W and SW are the most frequent wind directions during rain events. Therefore, the westerly faces of the Cathedral are expected to receive more driving rain than the other two faces and thus have less soiled area. This is consistent with the observed soiling patterns at the Cathedral (Davidson et al., 2000).

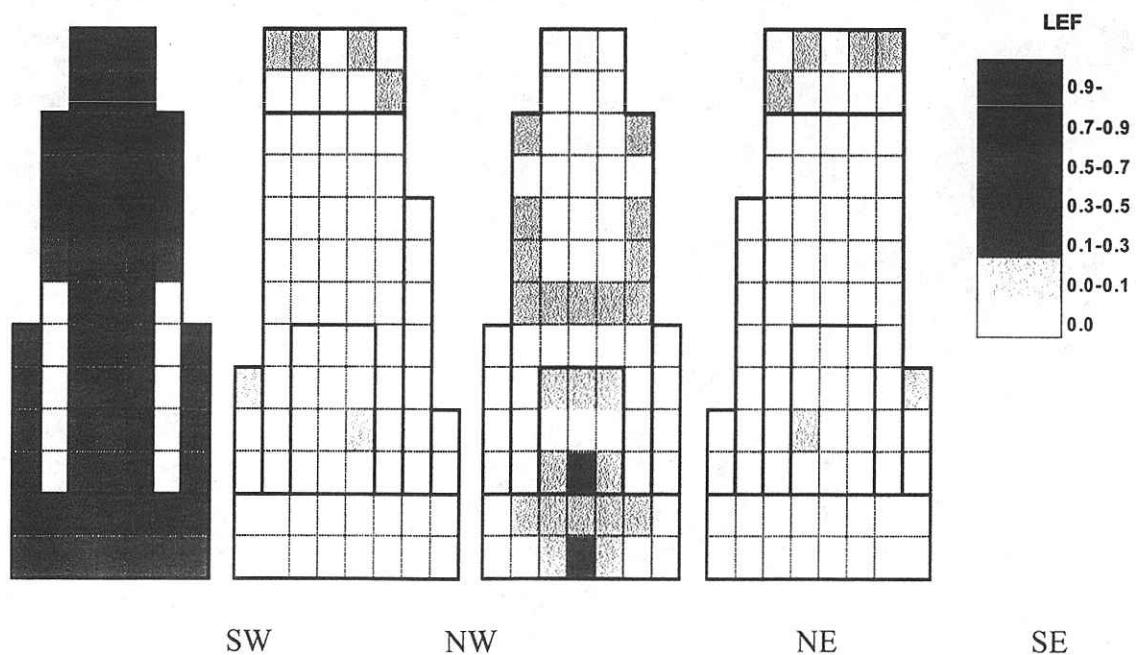
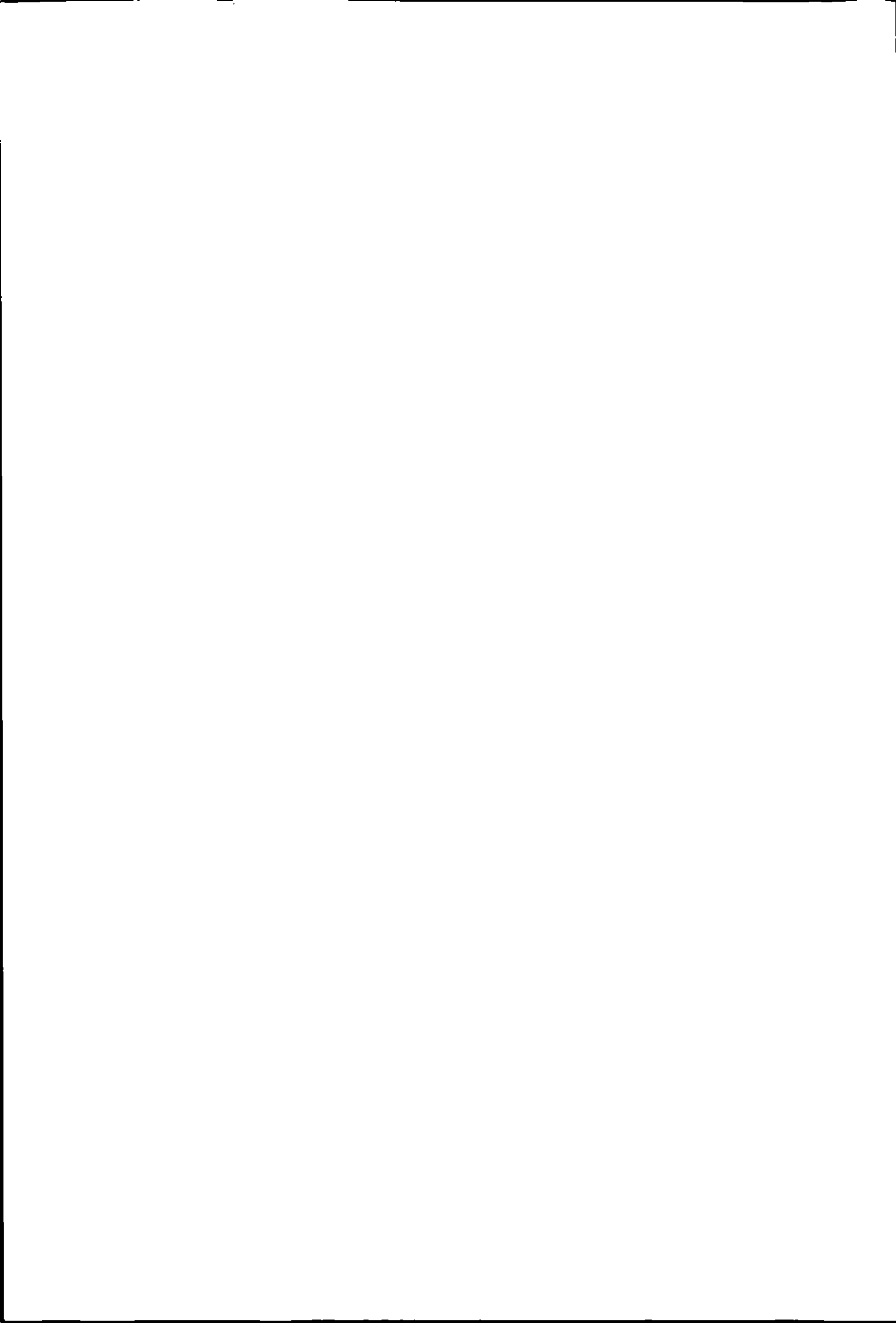


Figure 1. LEFs on each side of the building (SW wind at $U_{30m} = 10$ m/s Raindrop diameter = 2.5 mm)



Acknowledgments

This research is funded by U.S. National Park Service Cooperative Agreement 1443CA00196035. We would like to acknowledge the University of Pittsburgh for granting us access to the sampling sites at the Cathedral of Learning. We highly appreciate the contribution of several undergraduat students with data collection and processing: K. Vance, A. Pathak, and L. Urbschat. Thanks are due to C.P. Yeske for providing technical support. We also acknowledge S. Pandis, A. Robinson, and N. Donahue for their insightful suggestions on this work. Special thanks are given to L. Cartwright for his assistance with construction of field equipment.

References

- Choi, E.C.C. (1993) Simulation of wind-driven rain around a building. *Journal of Wind Engineering and Industrial Aerodynamics* **46**, 721-729.
- Davidson, C.I.; W. Tang; S. Finger; V. Etyemezian; M.F. Striegel and S.I. Sherwood. (2000) Soiling patterns on a tall limestone building: changes over 60 years. *Environmental Science & Technology* **34**, 560-565.
- Etyemezian, V.; C.I. Davidson; S. Finger; M. Striegel et al. (1998) Vertical gradients of pollutant concentrations and deposition fluxes on a tall limestone building. *Journal of the American Institute for Conservation* **37**, 187-210.
- Sherwood, S.I.; D.F. Gatz; R.P., Hosker, Jr.; et al. (1990) *National Acid Precipitation Assessment Program, Acidic Deposition: State of Science and Technology*, Report 20, Vol III.



Directory of Delegates

Nuria Altimir

Dept of Forest Ecology, University of Helsinki, PO Box 24, Helsinki FIN-00014, Finland

Tel: 00 358 9 191 7714

Fax: 00 358 9 191 7605

Email: altimir@LadyBird.helsinki.fi

Dr Christof Ammann

Max Planck Institute for Chemistry, Biogeochemistry Dept., PO Box 3060, 55020 Mainz, Germany

Tel: 00 49 6131 305 308

Fax: 00 49 6131 305 487

Email: ammann@mpch-mainz.mpg.de

Elizabeth Anderson

Glen Spectra Ltd., 2/4 Wigton Gardens, Stanmore, HA7 1BG, UK

Professor Viney P Aneja

North Carolina State University, Dept. of MEAS, NC 27695-8208, Raleigh, USA

Tel: 00 1 919 515 7808

Fax: 00 1 919 515 7802

Email: viney_aneja@ncsu.edu

Professor S. Pal Arya

North Carolina State University, Dept of MEAS, Box 8208, Raleigh, NC 27695-8208, USA

Tel: 00 1 919 515 7002

Fax: 00 1 919 515 7802

Email: pal_arya@ncsu.edu

Professor Mike Ashmore

Department of Environmental Science, University of Bradford, West Yorkshire BD7 1DP, UK

Tel: 00 44 1274 235695

Fax: 00 44 1274 235699

Email: m.r.ashmore@bradford.ac.uk

Dr Jens Beck

Max Planck Inst. for Chemistry, MPI f. Chemistry, Mainz, Germany

Tel: 00 49 6131 305 486

Fax: 00 49 6131 305 487

Email: jbeck@mpch-mainz.mpg.de

Mrs Jillian Binnie

CEH Edinburgh, Bush Estate, Penicuik, Midlothian, EH26 0QB, UK

Tel: 00 44 131 445 4343

Fax: 00 44 131 445 3943

Email: jillb@ceh.ac.uk

Dr. Jurgen Burkhardt

Rheinische Friedrich-Wilhelms-Universitat Bonn, Agrikulturchemisches Institut, Karlrobert-Kreiten-Str. 13, D-53115 Bonn, Germany

Tel: 00 49 228 732 186

Fax: 00 49 228 732 489

Email: j.burkhardt@uni-bonn.de



Dr J Neil Cape

CEH Edinburgh, Bush Estate, Penicuik, Midlothian, EH26 0QB, UK

Tel: 00 44 131 445 4343

Fax: 00 44 131 445 3943

Email: jnc@ceh.ac.uk

Dr F Choubedar

Dept. of Physics, University of Edinburgh, Mayfield Road, Edinburgh, UK

Tel:

Fax:

Email:

Professor T W Choularton

UMIST, Physics Dept., PO Box 88, Manchester, M60 1QD, UK

Tel: 00 44 161 200 3950

Fax: 00 44 161 200 3951

Email: t.w.Choularton@umist.ac.uk

Dr Jeffrey Collett

Atmos. Science Dept., Colorado State University, Fort Collins, CO 80523, USA

Tel: 00 1 970 491 8697

Fax: 00 1 970 491 8449

Email: collett@lamar.colostate.edu

Ellen Cooter

Atmospheric Sciences Modelling Division, NOAA/Air Resources Lab., Mail Drop 80, Research Triangle Park, NC 27711, USA

Tel: 00 1 919 541 1334

Fax: 00 1 919 541 1379

Email: cooter.ellen@epa.gov

Miss Mhairi Coyle

CEH Edinburgh, Bush Estate, Penicuik, Midlothian, EH26 0QB, UK

Tel: 00 44 131 445 4343

Fax: 00 44 131 445 3943

Email: mcoy@ceh.ac.uk

Professor Dr. Ulrich Dammgén

Institute of Agroecology, Federal Agricultural Research Centre, Bundesallee 50, D38116, Braunschweig, Germany

Tel: 00 49 596 837

Fax: 00 49 596 366

Email: ulrich.daemmgén@fal.de

Cliff Davidson

Carnegie Mellon University, Dept. of Civil & Environmental Engineering, 5000 Forbes Avenue, Porter Hall, 119 Pittsburgh, PA 15213-3890, USA

Tel: 00 1 412 268 2951

Fax: 00 1 412 268 7813

Email: cliff@cmu.edu

Ebba Dellwik

RISO National Laboratory, PO Box 49, DK-4000, Roskilde, Denmark

Tel: 00 45 4677 5032

Fax: 00 45 4677 5970

Email: ebba.dellwik@risoe.dk

Dr Jan Dick

CEH Edinburgh, Bush Estate, Penicuik, Midlothian, EH26 0QB, UK
Tel: 00 44 131 445 4343
Fax: 00 44 131 445 3943
Email: jand@ceh.ac.uk

Dr Anthony Dore

UMIST, P.O.Box 88, Manchester, M60 1DQ, UK
Tel: 00 44 161 200 3905
Fax: 00 44 161 200 3951
Email: Anthony.dore@umist.ac.uk

Mr James Dorsey

UMIST, P.O.Box 89, Manchester, M60 1DQ, UK
Tel: 00 44 161 236 3311
Fax: 00 44 161 200 3951
Email: mccphjd2@fs2.ee.umist.ac.uk

Dr Jan Duyzer

TNO-MEP, Postbus 342, 7300 AH, Apeldoorn, The Netherlands
Tel: 00 31 55 549 3944
Fax: 00 31 55 549 3252
Email: j.h.Duyzer@mep.tno.nl

Professor Grant Edwards

University of Guelph, School of Engineering, Guelph, Ontario, CANADA N1G 2W1
Tel: 00 1 519 824 4120
Fax: 00 1 519 836 0227
Email: gedwards@uoguelph.ca

Dr Jan Willem Erisman

ECN, Department of Air Quality, Box 1, 1755 ZG Petten, The Netherlands
Tel: 00 31 224 564 155
Fax: 00 31 224 563 488
Email: erisman@ecn.nl

Dr. Peter Finkelstein

U.S. EPA/NOAA, MD-80, Research Triangle Park, NC 27711, USA
Tel: 00 1 919 541 4553
Fax: 00 1 919 541 1379
Email: finkelstein.peter@epa.gov

Dr. Chris Flecharde

Agriculture and Agri-Food Canada, 960 Carling Avenue, KW Neatby Building, Ottawa ON K1A 0C6, Canada
Tel: 00 1 613 759 1542
Fax: 00 1 613 759 1432
Email: flecharde@em.agr.ca

Professor David Fowler

CEH Edinburgh, Bush Estate, Penicuik, Midlothian, EH26 0QB, UK
Tel: 00 44 131 445 4343
Fax: 00 44 131 445 3943

Email: dfo@ceh.ac.uk

Dr Cathleen Fruhauf

Federal Agricultural Research Centre, Institut of Agroecology, Bundesallee 50, D-38116
Braunschweig, Germany
Tel: 00 49 531 596 209
Fax: 00 49 531 596 366
Email: cathleen.fruhauf@fal.de

Dr. Martin Gallagher

UMIST, Physics Dept., P.O.Box 88, Manchester, M60 1QD UK
Tel: 00 44 161 200 3937
Fax: 00 44 161 200 3951
Email: martin.Gallagher@umist.ac.uk

Barry Gardiner

Forestry Commission Research Agency, Roslin, Midlothian EH25 9SY, UK
Tel: 00 44 131 445 2176
Fax: 00 44 131 445 5124
Email: b.a.gardiner@forestry.gov.uk

Dr John Garland

48 Priory Orchard, Wantage, Oxfordshire, OX12 9EL, UK
Tel: 00 44
Fax: 00 44
Email:

Laurie Halfpenny-Mitchell

University of Guelph, School of Engineering, Guelph, Ontario, CANADA, N1G 2W1
Tel: 00 1 519 824 4120
Fax: 00 1 519 836 0227
Email: laurieha@uoguelph.ca

Mr Max Hansson

Karlstad University, Division for Env. Sciences, Universitetsgatan 1, S-65188 Karlstad, Sweden
Tel: 00 46 54 700 2403
Fax: 00 46 54 700 1462
Email: max.hansson@kau.se

Dr Aryan Hensen

ECN, Department of Air Quality, Box 1, 1755 ZG Petten, The Netherlands
Tel: 00 31 22 45 64 203
Fax: 00 31 22 45 63 488
Email: hensen@ecn.nl

Professor Bruce Hicks

NOAA/Air Resources Lab., R/E/AR, SSMC3, Rm. 3151, 1315 East West Highway, Silver Spring,
MD 20910, USA
Tel: 00 1 301 713 1811
Fax: 00 1 301 713 0119
Email: bruce.hicks@noaa.gov

Dr. Peter Hofschreuder

Meteorology and Air Quality Group, Wageningen University, Duivendaal 2, 6701 AP Wageningen,
Netherlands

Tel: 00 31 317 482 104
Fax: 00 31 317 482 811
Email: peter.hofschreuder@user.metair.wag-ur.nl

Professor T M Holsen

Dept. of Civil & Env. Engineering, W J Rowley Laboratories Box 5710, Clarkson University,
Potsdam,
NY 13699-5710, USA
Tel: 00 1 315 268 3851
Fax: 00 1 315 268 7985
Email: holsen@clarkson.edu

Asst. Professor Keri Hornbuckle

Dept. of Civil & Env. Engineering, University of Iowa, Iowa City 2130 , SC 52242 , USA
Tel: 00 1 319 384 0789
Fax: 00 1 319 335 3337
Email: keri-hornbuckle@uiowa.edu

Dr Laslo Horvath

Hungarian Meteorological Service, Dept. for Analysis of Atmospheric Environment, PO Box 39, H
1675 Budapest, Hungary
Tel: 00 36 1 346 4817
Fax: 00 36 1 250 4174
Email: lhovath@met.hu

Dr. Husain

Wadsworth Center, New York State Department of Health, Empire State Plaza, Albany, New York
12201-0509, USA
Tel: 00 1 518 473 4854
Fax: 00 1 518 486 5699
Email: lhusain@wadsworth.org

Dr David Inglis

UMIST, PO Box 88, Sackville Street, Manchester, M60 1QD UK
Tel: 00 44 161 200 3954
Fax: 00 44
Email: david.inglis@umist.ac.uk

Dr. Svetlana Jagovkina

Main Geophysical Observatory, St. Petersburg, 194021, Russia
Tel:
Fax:
Email: svetlana@main.mgo.rssi.ru

Dr Andrew Jarvis

IENS, Lancaster University, Lancaster, LA1 4YQ UK
Tel: 00 44 1524 593894
Fax: 00 44 1524 843854
Email: a.jarvis@lancaster.ac.uk

Dr. Per Erik Karlsson

Swedish Environmental Research Institute, Box 47086, 402 58 Goteborg, Sweden
Tel: 00 46 31 725 6200
Fax: 00 46 31 725 6290
Email: pererik.karlsson@ivl.se

Dr Gerhard Kersteins

Dept of Biological Sciences, Lancaster University, Lancaster LA1 4YQ, UK

Tel: 00

Fax: 00

Email: g.kerstiens@lancaster.ac.uk

Dr Otto Klemm

Universitat Bayreuth, BITOK Klimatologie, PO Box 10 1251, D95440 Bayreuth, Germany

Tel: 00 49 921 55 5674

Fax: 00 49 921 55 5799

Email: klemm@bitoek.uni-bayreuth.de

Dr Robert Kormann

Max Planck Institut für Chemie, J J Becher Weg 27, 55128 Mainz, Germany

Tel: 00 49 6131 305 495

Fax: 00 49 6131 305 436

Email: kormann@mpch-mainz.mpg.de

Dr Andrew Kowalski

Dept. of Biology, University of Antwerp, Universiteitsplein1, B-2610 Wilrijk, Belgium

Tel: 00 32 3 820 2255

Fax: 00 32 3 820 2271

Email: andyk@uia.ac.be

Dr Uwe Kuhn

Max Planck Inst. for Chemistry, Biogeochemistry Dept., PO Box 3060, D-55020 Mainz, Germany

Tel: 00 49 6131 305 486

Fax: 00 49 6131 305 487

Email: kuhn@mpch-mainz.mpg.de

Dr. Victor Lagun

Arctic and Antarctic Research Institute, St. Petersburg, 199397, Russia

Tel:

Fax:

Email:

Dr. Patricia Laville

INRA, Unite de Recherche EGC, 78550 Thiverval-Grignon, France

Tel: 00 33 1 30 81 55 30

Fax: 00 33 1 30 81 55 63

Email: laville@begn.grignon.inra.fr

Mr Ian Leith

CEH Edinburgh, Bush Estate, Penicuik, Midlothian, EH26 0QB, UK

Tel: 00 44 131 445 4343

Fax: 00 44 131 445 3943

Email: idl@ceh.ac.uk

Dr Ray Leuning

CSIRO, FC Pye Laboratory, PO Box 1666, Canberra, 2601 ACT, Australia

Tel: 00 61 2 6246 5557

Fax: 00 61 2 6246 5560

Email: leu005@taipan.cbr.ciw.csiro.au

Dr Leonard Levin

EPRI, 3412 Hillview Avenue, Palo Alto, California 94303, USA
Tel: 00 1 650 855 7929
Fax: 00 1 650 855 1069
Email: llevin@epri.com

Dr. Steven Lindberg

Oakridge National Laboratory, Bldg. 1505, MS 6038, 37831 6038, Oak Ridge, Tennessee, USA
Tel: 00 1 865 574 7857
Fax: 00 1 865 576 8646
Email: lindbergse@ornl.gov

Mr Benjamin Loubet

INRA, Unite de Recherche EGC, 78550 Thiverval-Grignon, France
Tel: 00 33 130 81 55 33
Fax: 00 33 130 81 55 63
Email: loubet@bcgn.grignon.inra.fr

Ian Macpherson

Twin Otter Facility Manager, NRC Flight Research Laboratory, Building U-61, National Research .
Council of Canada, Montreal Road, Ottawa, CANADA K1A 0R6
Tel: 00 1 613 998 3014
Fax: 00 1 613 952 1704
Email: ian.macpherson@nrc.ca

Tarek Madhour

Helwan University, Department of Chemistry, 11 Abdel Khalek Sarwet St., Suite #21, Cairo, Egypt
Tel:
Fax:
Email:

Selma Maggiotto

Dept. of Land Resource Science, University of Guelph, Guelph, Ontario, ON N1G 2W1, Canada
Tel: 00 1 519 824 4120
Fax: 00 1 519 824 5730
Email: srmaggio@lrs.uoguelph.ca

Alexander Mangold

Universitat Bayreuth, BITOK Klimatologie, D95444 Bayreuth, Germany
Tel: 00 49 921 55 5672
Fax: 00 49 921 55 5799
Email: alexander.mangold@bitock.uni-bayreuth.de

Miss Celia Milford

CEH Edinburgh, Bush Estate, Penicuik, Midlothian, EH26 0QB, UK
Tel: 00 44 131 445 4343
Fax: 00 44 131 445 3943
Email: cmil@ceh.ac.uk

Dr J Mosquera

Postbus 1, A55 ZG Petten, The Netherlands
Tel: 00 31 224 564 203
Fax: 00 31 224 563 488
Email: mosquera@ccn.nl

Mr. Duncan Mounsor

Enviro Technology Services plc, Environment House, Dudbridge Road, Stroud, Glos. GL5 3EE, UK
Tel: 00 44 1453 751641
Fax: 00 44 1453 757596
Email: sales@et.co.uk

Dr Albrecht Neftel

Swiss Federal Research Station for Agroecology and Agriculture, Environment Department,
Schwarzenburgstrasse 155, CH-3003 Bern, Switzerland
Tel: 00 41 31 323 83 43
Fax: 00 41 31 323 84 15
Email: albrecht.neftel@mbox.iul.admin.ch

Mr Johan Neiryck

Institute for Forestry and Game Management, Gaversstraat 4, B-9500 Geraardsbergen, BELGIUM
Tel: 00 32 54 43 71 19
Fax: 00 32 54 41 08 96
Email: johan.neiryck@lin.vlaanderen.be

Dr Eiko Nemitz

CEH Edinburgh, Bush Estate, Penicuik, Midlothian, EH26 0QB, UK
Tel: 00 44 131 445 4343
Fax: 00 44 131 445 3943
Email: en@ceh.ac.uk

Dr Sue Owen

Institute of Environmental and Biological Sciences, Lancaster University, Lancaster, LA1 4YQ, UK
Tel: 00 44 1524 65201
Fax: 00 44 1524 593985
Email: s.owen@lancaster.ac.uk

Professor Nicolai Panikov

Stevens Institute of Technology, Dept. of Chemistry & Chemical Biology, Castle Point on Hudson,
Hoboken, NJ 07030, USA
Tel: 00 1 201 216 8193
Fax: 00 1 201 216 8196
Email: npanikov@stevens-tech.edu; panikov@mail.ru

Mr Thomas Pierce

Atmospheric Sciences Modeling Division, Air Resources Laboratory, MD-80, Research Triangle Park
, NC 27711, USA
Tel: 00 1 919 541 1375
Fax: 00 1 919 541 1379
Email: pierce.tom@epa.gov

Dr. Kim Pilegaard

Risoe National Laboratory, PO Box 49, DK-4000 Roskilde, Denmark
Tel: 00 45 4677 4677
Fax: 00 45 4677 4160
Email: kim.pilegaard@risoe.dk

Dr. Hakan Pleijel

Applied Environmental Science, PO Box 464, 405 30 Goteborg, Sweden
Tel: 00 46 31 773 25 32
Fax: 00 46 31 773 25 30
Email: hakan.pleijel@miljo.gu.se

Dr Jonathan Pleim

Atmospheric Sciences Modeling Division, Air Resources Laboratory, NOAA, Research Triangle Park,
NC 27711, USA
Tel: 00 1
Fax: 00 1 919 541 1379
Email: pleim@hpec.epa.gov

Dr Sara Pryor

Atmospheric Science Program, Dept. of Geography, Indiana University, Bloomington, IN 47405,
USA
Tel: 00 1 812 855 5155
Fax: 00 1 812 855 1661
Email: spryor@indiana.edu

Dr Andrew Quinn

Silsoe Research Institute, Wrest Park, Silsoe, Bedfordshire MK45 4HS, UK
Tel: 00 44 1525 860 000
Fax: 00 44 1525 861 735
Email: andrew.quinn@bbsrc.ac.uk

Dr David Reay

Dept of Biological Sciences, University of Essex, Wivenhoe Park, Colchester, Essex CO4 3SQ, UK
Tel: 00 44 1206 872818
Fax: 00 44 1206 873416
Email: dsreay@essex.ac.uk

Dr Nils Reinke

Department for Nuclear and New Energy Systems (NES), Ruhr University Bochum (RUB), D-44780
Bochum, Germany
Tel: 00 49 234 32 25984
Fax: 00 49 234 32 14158
Email: reinke@nes.ruhr-uni-bochum.de

Dr. Markus Reuther

EUROTRAC 2-/ISS, GSF-Forschungszentrum, Kuhbachstrasse 11, D-81543 Munich, Germany
Tel: 00 49 89 65 10 88 11
Fax: 00 49 89 65 10 88 19
Email: reuther@gsf.de

Dr. Udo Rummel

Max Planck Inst. for Chemistry, PO Box 3060, Mainz 55020, Germany
Tel: 00 49 6131 305 438
Fax: 00 46 6131 305 487
Email: rummel@mpch-mainz.mpg.de

Mr. Steven Sargent

Campbell Scientific Inc., 815 W. 1800 N, Logan, Utah 84321-1784, USA
Tel: 00 1 435 753 2342
Fax: 00 1 435 750 9639
Email: ssargent@campbellsci.com

Dr Jan Schjoerring

Royal Vet. and Agric. University, Plant Nutrition Laboratory & Centre for Ecology & Environment,
Thorvaldsvej 40, DK 1871 Fredriksberg, Denmark
Tel: 00 45 35 28 34 95

Fax: 00 45 35 28 34 60

Email: jks@kvl.dk

Martin Schmid

Swiss Federal Research Station for Agroecology and Agriculture, Environment Department,
Schwarzenburgstrasse 155, CH-3003 Bern, Switzerland

Tel: 00 41 31 323 83 76

Fax: 00 41 31 323 84 15

Email: martin.schmid@iul.admin.ch

Dr. M D J Schreuder

University of Montana, Missoula, MT, 59812, USA

Tel:

Fax:

Email:

Professor Stephen Schwartz

Env. Chemistry Division, Brookhaven National Laboratory, Bldg. 815E (75 Rutherford Drive), PO
Box 5000, Upton NY 11973-5000, USA

Tel: 00 1 631 344 3100

Fax: 00 1 631 344 2887

Email: ses@bnl.gov

Dr. Donna Schwede

Atmospheric Sciences Modeling Division, Air Resources Laboratory, NOAA, Research Triangle Park
NC 27711, USA

Tel:

Fax:

Email:

Mr Tanver Shah

Glen Spectra Ltd., 2/4 Wigton Gardens, Stanmore, HA7 1BG, UK

Tel: 00 44

Fax: 00 44

Email:

Dr Joseph Sickles

US EPA, NERL-ESD-LCB, MD-56, Research Triangle Park, NC 27711, USA

Tel: 00 1 919 541 2446

Fax: 00 1 919 541 1486

Email: sickles;joseph@epa.gov

Mr David Simpson

c/o IVL, Dagjammingsgatan 1, Box 470 86 Gothenburg, SE40258 Sweden

Tel: 00 46 31 725 6200

Fax: 00 46 31 725 6290

Email: david.simpson@ivl.se

Dr Ute Skiba

CEH Edinburgh, Bush Estate, Penicuik, Midlothian, EH26 0QB, UK

Tel: 00 44 131 445 4343

Fax: 00 44 131 445 3943

Email: ums@ceh.ac.uk

Professor Michael Smith

School of the Environment, University of Leeds, Leeds LS2 9JT, UK

Tel: 00 44 113 233 1595
Fax: 00 44 113 233 6716
Email: m.h.smith@env.leeds.ac.uk

Mr Ron Smith

CEH Edinburgh, Bush Estate, Penicuik, Midlothian, EH26 0QB, UK
Tel: 00 44 131 445 4343
Fax: 00 44 131 445 3943
Email: ris@ceh.ac.uk

Dr Gerald Spindler

Institut für Troposphärenforschung, Permoserstrasse 15, 07050 Leipzig, Germany
Tel: 00 49 341 235 2865
Fax: 00 49 341 235 2325
Email: spindler@tropos.de

Mr James Squires

BIRAL, PO Box 2, Portishead, Bristol BS20 7JB, UK
Tel: 00 44 1275 847787
Fax: 00 44 1275 847303
Email: j_squires@biral.com

Dr Rainer Steinbrecher

Fraunhofer-Institute für Atmos. Umweltforschung, Kreuzteckbahnstr. 19, D-82467 Garmisch-Partenk., Germany
Tel: 00 49 8821 183 217
Fax: 00 49 8821 73573
Email: steinbrecher@ifu.fhg.de

Professor Georgiy Stenchikov

Rutgers University, Dept. of Env. Sciences, 14 College Farm Road, New Brunswick, NJ 08901 8551, USA
Tel: 00 1 732 932 3637
Fax: 00 1 732 932 8644
Email:

Mr Robert Storeton-West

CEH Edinburgh, Bush Estate, Penicuik, Midlothian, EH26 0QB, UK
Tel: 00 44 131 445 4343
Fax: 00 44 131 445 3943
Email: rls@ceh.ac.uk

Dr Mark Sutton

CEH Edinburgh, Bush Estate, Penicuik, Midlothian, EH26 0QB, UK
Tel: 00 44 131 445 4343
Fax: 00 44 131 445 3943
Email: ms@ceh.ac.uk

Miss Y Sim Tang

CEH Edinburgh, Bush Estate, Penicuik, Midlothian, EH26 0QB, UK
Tel: 00 44 131 445 4343
Fax: 00 44 131 445 3943
Email: yst@ceh.ac.uk

Mr Bertrand Tanner

Campbell Scientific Inc., 815 W. 1800 N, Logan, Utah 84321-1784, USA

Tel: 00 1 435 753 2342
Fax: 00 1 435 750 9540
Email: bert@campbellsci.com

Dr Robert Tate

Dept. of Environmental Sciences, Rutgers University, 14 College Farm Road, New Brunswick, NJ
08901 8551, USA
Tel: 00 1 732 932 9810
Fax: 00 1 732 932 8644
Email: tate@aesop.rutgers.edu

Dr. Juha-Pekka Tuovinen

Finnish Meteorological Inst., Sahaajankatu 20E, FIN 00810 Helsinki, Finland
Tel: 00 358 9 1929 5515
Fax: 00 358 9 1929 5405
Email: juha-pekka.tuovinen@fmi.fi

Miss Saskia van Dijk

Max Planck Inst. for Chemistry, Becherweg 27, Mainz 55128, Germany
Tel: 00 49 6131 305 307
Fax: 00 49 6131 305 487
Email: svd@mpch-mainz.mpg.de

Dr Lambert W A van Hove

Wageningen University, Environmental Sciences, Meteorology and Air Quality Group, Duivendaal 2,
6701 AP Wageningen, The Netherlands
Tel: 00 31 317 482 808
Fax: 00 31 317 482 811
Email: bert.vanHove@pf.wau.nl

Dr Robert Vet

Environment Canada, Meteorological Service of Canada, Air Quality Research Branch, 4905 Dufferin
Street,
Toronto, Ontario, Canada M3H 5T4
Tel: 00 1 416 739 4853
Fax: 00 1 416 739 5704
e-mail: robert.vet@ec.gc.ca

Dr Claudia Wagner-Riddle

Dept. of Land Resource Science, University of Guelph, Guelph, Ontario, ON N1G 2W1, Canada
Tel: 00 1 519 824 4120
Fax: 00 1 519 824 5730
Email: criddle@lrs.uoguelph.ca

Dr Andreas Wahner

Institut für Atmosphärische Chemie ICG-3, Forschungszentrum Juelich, D-52425 Juelich, Germany
Tel: 00 49 2461 61 5932
Fax: 00 49 2461 61 5346
Email: a.wahner@fz-juelich.de

Miss Denise Welch

Silsoe Research Institute, Wrest Park, Silsoe, Bedfordshire MK45 4HS, UK
Tel: 00 44 1525 860 000
Fax: 00 44 1525 861 735
Email: denise.welch@bbsrc.ac.uk

Dr Marvin Wesely

Argonne National Laboratory, Bldg 203, ER, Argonne 60439, USA

Tel: 00 1 630 252 5827

Fax: 00 1 630 252 5498

Email: mlwesely@anl.gov

Dr. Tanja Winterrath

Institute for Physics of the Atmosphere, Johannes Gutenberg University, Becherweg 21, D-55099 Mainz, Germany

Tel: 00 49 6131 392 3532

Fax: 00 49 6131 392 3532

Email: winterra@mail.uni-mainz.de

Thomas Wrzesinsky

Universitat Bayreuth, BITOK Klimatologie, D95444 Bayreuth, Germany

Tel: 00 49 921 55 5673

Fax: 00 49 921 55 5799

Email: thomas.wrzesinsky@bitock.uni-bayreuth.de

Dr. Yee-Lin Wu

Department of Environmental Engineering, National Cheng Kung University, Tainan, Taiwan

Tel:

Fax:

Email:

Dr Leiming Zhang

ARQI, MSC, Environment Canada, 4905 Dufferin St., Downsview, Ontario M3H 5T4, Canada

Tel: 00 1

Fax: 00 1

Email: leiming.zhang@ec.gc.ca

